ResearchOnline@JCU

This file is part of the following reference:

Ali, Safaa Hussein (2017) *Syntheses, structures and reactivity of organolanthanoid complexes*. **PhD thesis, James Cook University.**

Access to this file is available from:

JAMES COOK
UNIVERSITY
AUSTRALIA

Syntheses, Structures and Reactivity of Organolanthanoid Complexes

A thesis submitted for the degree of

Doctor of Philosophy

by

Safaa Hussein Ali

M. Sc.

College of Science and Engineering

James Cook University

March 2017

"O my Lord! Increase me in knowledge"

Dedication

To the loyal and pure spirits…

To those brave, humble and merciful men…

To the peace and humanity fighters…

To those who left their dreams, future and life's goals,

just to keep us safe and happy…

To the Iraqi forces martyrs, both young and old…

To your unlimited sacrifices and giving…

This simple work is dedicated.

Table of Contents

Abstract

The focus of this thesis is divided into two directions. The first explores the pseudo-Grignard reaction involving the oxidative addition of aryl halide to lanthanoid metals (Yb, Eu) (Chapter two). The second aspect details the synthesis and reactivity of a series of lanthanoid biphenolate {2,2′-methylenebis(6-*tert*-butyl-4-methylphenolate)} complexes (Chapters three and four).

Chapter 1 gives an overall introduction to lanthanoid chemistry. This chapter details the general properties, extracting and separating techniques and applications of lanthanoid elements. In addition to highlighting the diverse range of the synthetic methods of lanthanoid formamidinate and lanthanoid phenolate complexes.

Chapter 2 explores the oxidative addition of aryl halide to lanthanoid metal (Yb, Eu) as a synthetic route to prepare different species of pseudo-Grignard reagents involving formamidinates such as $[Yb(RForm)(thf)_nX]_2$ (Form = ArNCHNAr; R = 2,4,6-Me$_3$; 2,6-Me$_2$; 2,6-Et$_2$; 2,6-^{i}Pr$_2$; X = Br, I) (see Figure below).

X = Br, I; R = 2,4,6-Me$_3$; 2,6-Me$_2$; 2,6-Et$_2$; 2,6-^{i}Pr$_2$
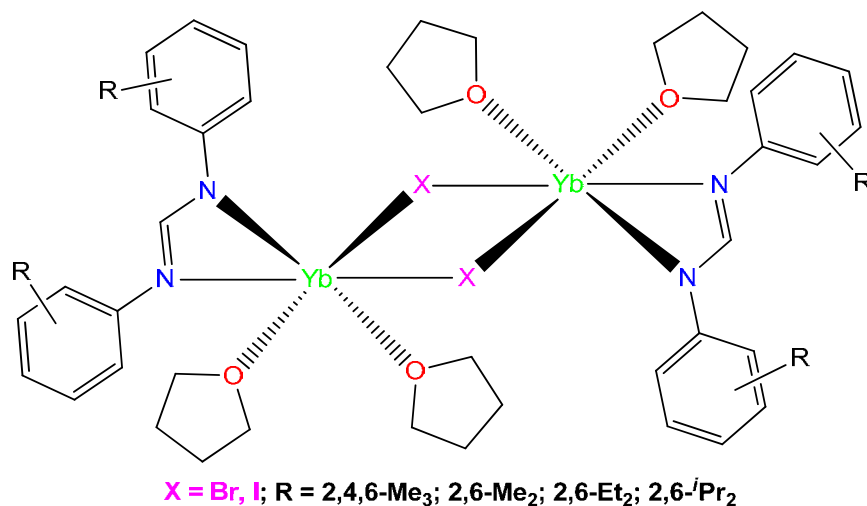
In addition, the reactivity of these pseudo-Grignard reagents [Yb(RForm)(thf)$_n$X]$_2$ towards a range of ketones with different polar functionalities such as 9-fluorenone, 1,4-benzoquinone and benzil is discussed.

Chapter 3 discusses the synthesis and characterisation of a series of lanthanoid biphenolate {2,2′-methylenebis(6-*tert*-butyl-4-methylphenolate)} complexes. Redox transmetallation protolysis reactions between the lanthanoid metals and the biphenol in the presence of Hg(C$_6$F$_5$)$_2$ yielded mononuclear [Ln(BPO$_2$)(BP(OH)O)(thf)$_3$] (Ln = Y, Gd, Er) or dinuclear [Ln$_2$(BPO$_2$)$_2$(thf)$_n$] (Ln = Sm, Tb n = 3, Ho, Yb n = 2) complexes depending on the extent of phenol deprotonation. When the biphenolate ligand was partially deprotonated the mononuclear form was produced and yielded the dinuclear form when it was doubly deprotonated described below.
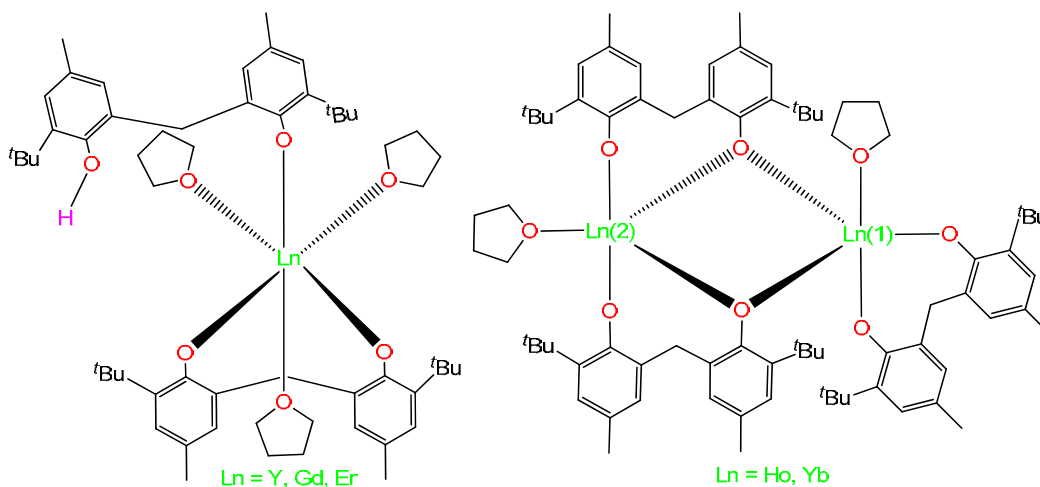
Chapter 4 details the synthesis and characterisation of a series of heterobimetallic complexes. Lanthanoid biphenolate complexes [Ln(BPO$_2$)(BP(OH)O)(thf)$_3$] have been metallated with different metal alkyls/amides such as (*^{n}*BuLi, KN(SiMe$_3$)$_2$, AlMe$_3$, ZnEt$_2$) and led to ionic and non-ionic heterobimetallic complexes, for example, [Li(thf)$_2$Ln(BPO$_2$)$_2$(thf)$_2$] (Ln = La, Pr) described below, [Li(thf)$_n$][Ln(BPO$_2$)$_2$(thf)$_n$]

(Ln = Y, Ho), [K(thf)$_3$Gd(BPO$_2$)$_2$(thf)$_2$], [ZnEtYb(BPO$_2$)$_2$(thf)],
[La(BPO$_2$)(thf)$_5$][AlMe$_2$(BPO$_2$)], [AlMe$_2$Ln(BPO$_2$)$_2$(thf)$_n$] (Ln = Sm, Tb).
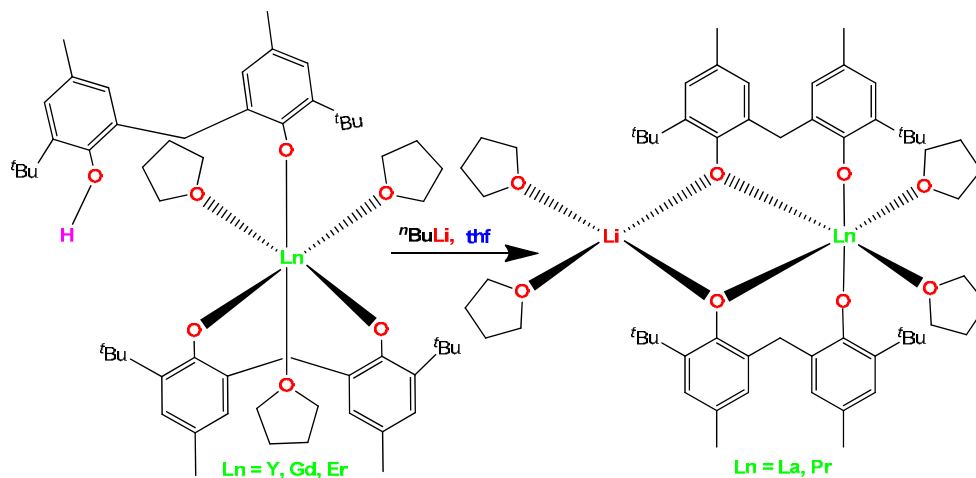
Overall, this thesis presents a significant contribution to pseudo-Grignard reagents. Formamidinate ligands can form stable and structurally interesting pseudo-Grignard reagents with divalent lanthanoid metals (Sm, Eu, Yb) as they can be readily modulated sterically and electronically in addition to their anionic, chelating features. Additionally, this thesis demonstrates the ability of the biphenolate ligand to stabilise lanthanoid in all readily known oxidation states (+2, +3, +4) for these metals. Additionally, the biphenolate ligands are able to stabilise a range of heterobimtallic complexes.

Abbreviations

Ar = aryl

BP(OH)$_2$ = 2,2′-methylenebis(6-*tert*-butyl-4-methylphenol)
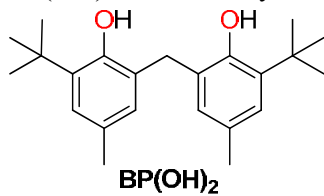
Bu = *n*-butyl

CN = coordination number

Cp = cyclopentadienyl

dme = 1,2-dimethoxyethane
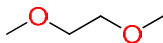
DippFormH = N,N′-bis(2,6-diisopropylphenyl)formamidine
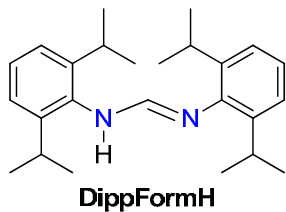
EtFormH = N,N′-bis(2,6-diethylphenyl)formamidine
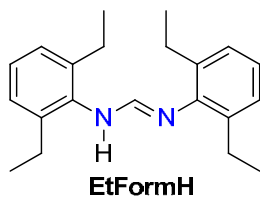
Et$_2$O = diethyl ether
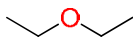
EDTA = ethylenediaminetetraacetic acid
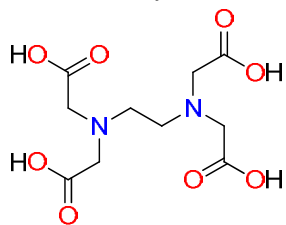
hmpa = hexamethylphosphoramide
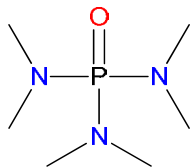
h = hour

IR = infrared

Ln = lanthanoid

MesFormH = N,N′-bis(2,4,6-trimethylphenyl)formamidine

MesFormH
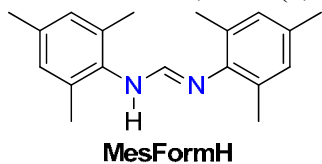
Me = methyl

m. p. = melting point

NMR = nuclear magnetic resonance

ArO = aryloxide

Ph = phenyl

ppm = parts per million

RTP = redox transmetallation/protolysis

RT = redox transmetallation

REEs = rare earth elements

r.t. = room temperature

thf = tetrahydrofuran

XylFormH = N,N′-bis(2,6-dimethylphenyl)formamidine

XylFormH
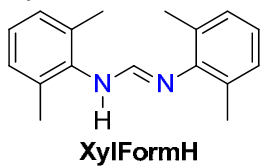
Declaration

To the best of the author's knowledge, this thesis contains no material which has been accepted for the award of any other degree or diploma at any university or other institution, and contains no material previously published or written by another person except where due reference is made in the text.

Safaa Hussein Ali

College of Science and Engineering

James Cook University

March 2017

Acknowledgements

First I would like to thank the lord of the universe to help me finish this study while I am away from my home. Secondly, I would to express deep thanks to my supervisors Prof. Peter Junk and Dr Murray Davies, for the continuous help, support and encouragement they have provided during the many years of work that went into preparing this thesis. I would also like to thank Prof. Glen Deacon from Monash University for valuable advice that helped to direct my research.

I thank my fellow labmates: Elius Hossain, Mehdi Salehisaki, Areej Aldabbagh, Nazli Rad, Sophie Hamilton and Dr Guillaume Bousrez for the stimulating discussions, we were working together, and for all the fun we have had in the last three years. Also I thank my Iraqi friends in the James Cook University. In particular, I am grateful to Dr. Jun Wang for enlightening me the first glance of research, but also collection of Xray data, particularly from the Australian Synchrotron, and also for solving the structures and help in refining them.

It is with immense gratitude that I acknowledge the support and help of Iraqi families who are living in Townsville, Abo Ahmed Al Shakarji's family; Dr Mudaher's family and special thanks to Haval and Huda to host us during the first days in Townsville. My sincere thanks also goes to Dr. Reza Al Shakarji and Moayed Balasim for the linguistic support.

A very special thanks goes out to my honest friend Sam Saheb, for the support, motivation, and valuable assistance that made my moving to Australia smooth and helped me overcome the homeless feeling. Mr Sam is the one who truly made a

Chapter 1: Introduction to the general aspects of the rare earth elements

1.1.1 The rare earth elements

According to the International Union of Pure and Applied Chemistry (IUPAC), rare earth elements (REEs) comprise 17 metals. REEs include the lanthanoids (cerium to lutetium with atomic numbers 58-71) in addition to lanthanum (Z = 57), scandium (Z = 21) and yttrium (Z = 39).[1, 2] The term "rare earth elements", although widely used in literature, is a misnomer because these elements are more abundant than gold. The reason for this designation goes back to the difficulties in extracting and separating lanthanoids elements due to their chemical similarities.[3] A partially filled 4f shell means that a lanthanoid ion is shielded from external fields by $5s^2$ and $5p^6$ outer-shell electrons.[4] However, "rare earth" primarily refers to the metal oxides and not the elements themselves.[5] Although the term "lanthanides" is widely used in literature, perhaps it is more appropriate to use the term "lanthanoids" instead when referring to REEs.[1] The reason is that the "ide" suffix in chemistry is often used to describe an anion such as sulphide, oxide and bromide whereas the "oid" suffix refers to the similarity in appearance and characteristics.

The history of lanthanoids started with Karl Arrhenius, a lieutenant in the Swedish artillery forces, in 1787. Arrhenius had a strong interest in metallurgy and one day he stumbled upon a dark mineral stone. Arrhenius named the mineral ytterbite in the honour of the Swedish town of Ytterby where he found the stone.[6, 7] Johannes Gadolin (1760-1852), a Finnish chemist, examined this dark mineral and suggested that it was an oxide. In 1794 Gadolin found a new element within the dark mineral which he named ytterearth. This also represented the first attempt to identify REEs.[7] In 1797, Ekeberg, suggested the name gadolinite for the mineral and yttria for the new element.[8] The

subsequent chemical studies showed that yttria contained the oxide elements of yttrium, terbium, erbium, ytterbium, scandium, holmium, thulium, gadolinium, dysprosium, and lutetium.[9] In 1803, Klaproth, Berzelius and Hisinger discovered a different mineral near Bastnas in Sweden that was later named Ceria.[8, 10] The subsequent studies showed that Ceria contained the oxides of cerium, lanthanum, praseodymium, neodymium, samarium, and europium.[9] Table 1.1 shows the origin of designation, the date of separation, and the name of the discoverer of each lanthanoid element.

Table 1.1 Shows the origin of designation, the date of separation, and the name of the discoverer of lanthanoid element.[6, 11] (Copyright permission received, Appendix 1).

Minerals	Element	Origin of designation	Date of separation	Discoverer
	Cerium	Ceres is an asteroid	1839	Mosander
	Lanthanum	Lanthanein Greek, to escape notice	1839	Mosander
	Samarium	Its ore, samarskite	1879	De Boisbaudran
	Praseodymium	Greek, praseos = green, didymos = twin	1885	Von Welsback
	Neodymium	Greek, neos = new, didymos = twin	1885	Von Welsback
	Europium	Europe	1901	Demarcay
	Lutetium	Lutetia, Latin name of Paris	1907	Urbain, Von Welsback, James
	Dysprosium	Greek, Dysprositos = hard to get	1886	Boisbaudran
	Gadolinium	Finnish chemist, Gadolin	1880	Marignac
	Erbium	Ytterby Sweden town	1843	Mosander
	Promethium	Prometheus, Greek god	1947	Marinsky, Glendenin, Coryell
	Holmium	Holmia, Latin name of Stockholm	1879	Cleve
	Scandium	Scandinavia	1879	Nilson
	Terbium	Ytterby Sweden town	1843	Mosander
	Thulium	Thule, the Latin name of northernmost region	1879	Cleve
	Ytterbium	Ytterby Sweden town	1878	Marignac
	Yttrium	Ytterby Sweden town	1843	Mosander

Diagram (Minerals column):
- Ceria
- Klaproth, M. H.; Berzelius, J. J.; Hisinger. W. 1803
- Cerite (Cronstedt, A. F. 1751)
- Gadolinite (Arrhenius, C. A. 1787)
- (Gadolin, J. 1794)
- Ytteria

1.1.2 Abundance of the rare earth elements

More than 100 minerals contain lanthanoids but only two of them can be used commercially as a source of lanthanoid elements. Monazite is one of these two minerals containing a mix of La, Th and lanthanoid phosphate. Bastnaesite is the other mineral containing La and lanthanoid fluorocarbonate.[11] Although Monazite is found in many regions around the world, only limited deposits are commercially viable. These deposits are mostly found in India, Brazil, Australia, South Africa, USA, Sri Lanka and Malaysia. Similarly, Bastnaesite is also found in different regions in Europe and Africa but only a few deposits in USA and China are being mined on a commercial scale.[9, 10] Table 1.2 shows the distribution of lanthanoids in the Earth's crust and the percentage of each of lanthanoid elements in Monazite and Bastnaesite ores.

Table 1.2 Distribution of lanthanoids in the Earth's crust and their percentages in Monazite and Bastnaesite ores[12, 13] (Copyright permission received, Appendix 2).

Elements	Y	La	Ce	Pr	Nd	Pm	Sm	Eu	Gd	Tb	Dy	Ho	Er	Tm	Yb	Lu
Crust (ppm)	31	35	66	9.1	40	0	7	2.1	6.1	1.2	4.5	1.3	3.5	0.5	3.1	0.8
Monazite %	2.5	20	43	4.5	16	0	3	0.1	1.5	0.05	0.6	0.05	0.2	0.02	0.1	0.02
Bastnaesite %	0.1	33.2	49.1	4.3	12	0	0.8	0.12	0.17	**160**	**310**	**50**	**35**	**8**	**6**	**1**

Bold values are in ppm.

1.1.3 Extracting and separating rare earth elements

A typical process of minerals cracking often starts with chemical treatment. A variety of digestive chemicals are used depending on the nature of the ore being treated. Silicate minerals, for example, are treated with hydrochloric acid to decompose the mineral into insoluble silica and soluble chlorides. Euxenite, for example, is treated with hydrofluoric acid to produce soluble niobium, tantalum and titanium, and insoluble lanthanoid fluorides.[8]

The main ores of lanthanoids (i.e monazite and bastnaesite) are first processed via flotation to increase the concentration of lanthanoid oxides from 10 % to 60 %.[13] Both monazite and bastnaesite can be digested with either acidic or alkaline solutions. On a commercial scale, the cracking process starts by mixing sand, monazite (or bastnaesite), and 98 % sulfuric acid and heating it to 120-150 °C for several hours.[8] After this acidic treatment, bastnaesite transforms to a water-soluble sulfate and releases carbon dioxide and hydrogen fluoride. The resulting solution of monazite, however, is diluted to precipitate thorium (as a phosphate or as a fluoride) by adding hydrofluoric acid. The lanthanoids are then precipitated by using oxalic acid and converted to more reactive forms of hydrous oxides (or hydroxides) by using caustic soda.[8]

The introduction of the ion-exchange technique simplified the separation of lanthanoids. In this technique, the lanthanoid mixture is added to a cation-exchange resin and then eluted with a complexing agent such as EDTA. The first lanthanoids removed from resin are the heavier lanthanoid ions capable of forming stronger EDTA complexes. Complete separation of lanthanoids can be achieved using a long column.[9, 13] The separation of lanthanoids on a large scale (for commercial purposes) is achieved by solvent extraction. In this method, complexing agents such as tributylphosphate

(^{n}BuO)$_3$PO or di(2-ethylhexyl)phosphoric acid are used in a covalent solvent such as kerosene.[9]

1.1.4 Properties of rare earth elements

The electronic configuration of free lanthanoid atoms is mostly $[Xe]4f^{n}5d^{0}6s^{2}$ with the exception of cerium, gadolinium and lutetium.[11] The physicochemical properties of lanthanoids mainly depend on the "f" orbitals.[9] Although there is no unique method to represent "f" orbitals, they can be classified as either a cubic set or a general set depending on the way they are combined.[12] The 4f orbitals penetrate the xenon core, resulting in no overlap with the ligand's orbitals.[13] In addition, lanthanoid complexes have an inability to form covalent bonding and hence they do not tend to have fixed, but variable coordination geometries.[14] The metallic behaviour of lanthanoids is due to 5d and 6s atomic orbitals which have much higher contribution and overlap in comparison to 4f orbitals.[9]

The most common and stable oxidation state of the majority of lanthanoids is +3.[15] Some of these elements, however, have other oxidation states (+2 and +4) caused by special stability of the unfilled, partially-filled or filled shells. Examples of such elements are Ce^{+4} ($4f^{0}$), Pr^{+2} ($4f^{3}$), Eu^{+2} ($4f^{7}$), Yb^{+2} ($4f^{14}$) and Sm^{+2} ($4f^{6}$). Cerium and, to a lesser extent, praseodymium have the ability to form Ln^{+4} in the presence of a strong oxidising agent. On the other hand, europium (Eu), ytterbium (Yb) and, samarium (Sm) have the ability to form Ln^{+2}.[16] The instability of the divalent state is caused by the difference in the hydration energies of tri- and di-valent lanthanoid ions, which exceed the ionisation energies of doubly charged ions. The electronic configuration of the "f" orbital depends on a number of factors such as electrostatic interaction, spin orbital coupling, and the crystal field effect (albeit this final effect is

minimal).[15] However, the stability of divalent lanthanoids is one of the important challenges to be considered in the coordination chemistry of these elements.[14] The most common coordination numbers for lanthanoids are 8 and 9.[16] There is a gradual decrease in the radii of the Ln^{+3} ions from La^{+3} to Lu^{+3}, which is also known as the lanthanoid contraction. Similarly, metallic radii show a gradual decrease as you move across the lanthanoid series.[11, 16] Most lanthanoids have a silvery shining appearance but lose their brightness quickly when exposed to the air due to formation of oxides. These elements have slow interactions with cold water but react rapidly with dilute acids.[12]

Table 1.3 Selected properties of the rare earth elements.[8, 11-13]

Element	Atomic number	Atomic weight (u)	Outer electronic configuration		MP/°C	Density g/cm³	Metals classification	Radius M^{+3} Å	Colour of Ln^{+3}
			0	**+3**					
Sc	21	44.95	[Ar]3d^{1}4s^2	[Ar]	1539	2.99		0.74	Colourless
Y	39	88.90	[Kr]4d^{1}5s^2	[Kr]	1521	4.47	Light	0.90	Colourless
La	57	138.91	[Xe]5d^{1}6s^2	[Xe]	920	6.17		1.03	Colourless
Ce	58	140.12	[Xe]4f^{1}5d^{1}6s^2	[Xe]4f^1	795	6.77		1.01	Colourless
Pr	59	140.90	[Xe]4f^{3}6s^2	[Xe]4f^2	930	6.78		0.99	Green
Nd	60	144.24	[Xe]4f^{4}6s^2	[Xe]4f^3	1020	7.00		0.98	Lilac-red
Pm	61	145.00	[Xe]4f^{5}6s^2	[Xe]4f^4	1041	7.30		0.97	Pink
Sm	62	150.36	[Xe]4f^{6}6s^2	[Xe]4f^5	1072	7.53	Middle	0.95	Pale yellow
Eu	63	151.96	[Xe]4f^{7}6s^2	[Xe]4f^6	821	5.25		0.94	Colourless
Gd	64	157.25	[Xe]4f^{7}5d^{1}6s^2	[Xe]4f^7	1312	7.89		0.93	Colourless
Tb	65	158.92	[Xe]4f^{9}6s^2	[Xe]4f^8	1356	8.27		0.92	Pale pink
Dy	66	162.50	[Xe]4f^{10}6s^2	[Xe]4f^9	1411	8.53		0.91	Pale yellow
Ho	67	164.93	[Xe]4f^{11}6s^2	[Xe]4f^{10}	1473	8.80		0.90	Yellow
Er	68	167.26	[Xe]4f^{12}6s^2	[Xe]4f^{11}	1528	9.07	Heavy	0.89	Rose pink
Tm	69	168.93	[Xe]4f^{13}6s^2	[Xe]4f^{12}	1545	9.33		0.88	Pale green
Yb	70	173.04	[Xe]4f^{14}6s^2	[Xe]4f^{13}	818	6.97		0.86	Colourless
Lu	71	174.96	[Xe]4f^{14}5d^{1}6s^2	[Xe]4f^{14}	1662	9.84		0.86	Colourless

1.1.5 Applications of rare earth compounds

Since the nineteenth century, REEs have attracted significant interest because of their diverse characteristics, making them useful for a wide range of industrial and medical applications. Their available quantity and purity were greatly increased when separation and extraction methods became more effective as part of the Manhattan Project during World War II that created the atomic bomb.[12, 17, 18] The first commercial exploitations of REEs were the Auer light, flint stones and the use of RE fluoride as wicks in arc light carbons.[7] Organolanthanoid complexes show unique photophysical properties such as having emissions ranging from the visible to the near-infrared (NIR) and are often characterised by long lived excited state lifetime. In recent years there has been a strong focus on metal-organic lanthanoids due to important prospective applications in active dopants for laser materials as well as waveguide amplifiers.[19-21] Another field of interest is the use of REE-doped glass fibre for telecommunication and optical data storage.[22]

Some of the most important applications of REEs are in petrogenetic indicators, petroleum-cracking catalysts, luminescent solar concentrators and tracing the movement of water masses in the oceans.[17, 18, 23-28] REEs are also utilised for monitoring geological processes such as crust evolution, weathering processes and paleoclimate change.[29-31] REEs are used in industry for the production of catalysts, ceramics, alloys, and electronics.[3]

Lanthanoid complexes are used widely in the medical field as anticoagulant agents, anti-nausea agents, anticancer agents, fungicides, and in the treatment of tuberculosis. [32-33] Furthermore, rare earth complexes have important applications in biomedical analysis and are used as contrast agents in magnetic resonance imaging (MRI).[34, 35] The ability of rare earth complexes to promote the growth of animals has led recently

to considerable interest from the agricultural sector for example, addition rare earth salts to their feedstock promote the growth of the young pigs.[36] Most recently, rapid growth in the use of lanthanoids has been seen in magnets in electronic devices for example, computing, smartphones and as phosphors in lighting and displays.[37]

1.2 Rare earth organometallic compounds

Organometallic rare earth complexes first appeared in the literature as a footnote in a paper in 1902. It was an attempt to synthesise trimethyl cerium.[38] In 1954 Birmingham and Wilkinson synthesised the first π-bonded lanthanoid complex tris(cyclopentadienyl), Cp_3Ln (Ln = Sc, Y, La, Ce, Pr, Nd, Sm, Gd; Cp = $\eta5$-cyclopentadienyl).[39] In 1968, Hart and Saran synthesised the first σ–bond organometallic RE complex $[Sc(C_6H_5)_3]$.[38] Over the past two decades the bonding mode between lanthanoid metals centres and neutral O- and/or N-donor ligands has attracted great research interest due to the optimisation of steric factors, not only with the ligand set but also through selection of the best metal size from the lanthanoid series.[40] Ln ions are hard Lewis acids and prefer bonding to hard bases (or ligands) containing O and N atoms.[41, 42] Redox transmetallation and σ –bond metathesis reactions remained the dominant methods to prepare RE organometallic complexes.[38]

1.3 Rare earth amidinate complexes

In 1858 amidines ($R^2N=C(R^1)$–NHR^3) (Fig. 1.1) were prepared for the first time by Gerhardt by the reaction of aniline with *N*-phenylbenzimidyl chloride.[43] When R^1 = H, the compound is called a formamidine (Fig. 1.2).[44] Amidine group (Fig. 1.1) is the nitrogen analogue of the carboxylates. It combines the characteristics of an azomethine-like C=N double bond and an amide-like C−N single bond.[45, 46]
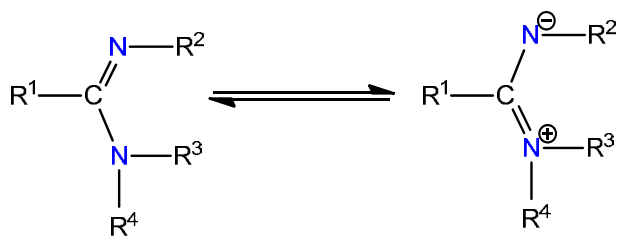
Figure 1.1 The general structure of an amidine.

R = 2,6-Me; 2,6-Et; 2,6-^{i}Pr; 2,4,6-Me; 2,6-Ph
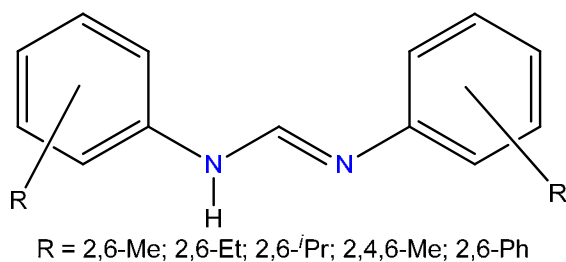
Figure 1.2 N,N′-Bis(aryl)formamidine.

Amidines are important organic compounds, which are used as starting materials and the key intermediates in synthetic chemistry.[47-56] They have gained significant interest in the last decade, due to their biochemical activities such as, some useful drugs.[45, 49-58] There are a number of natural products and medicinally active compounds that contain amidine units, for example, noformycin that has been isolated as a metabolite from actinobacteria and pentamidine contains two amidine units and is used to treat protozoan infections.[59] As well, they have very wide complexation activity with metals[60, 61] and as auxiliaries in asymmetric synthesis.[62, 63] The amidines are categorised according to the number and distribution of the substituents into five general structures (Fig. 1.3).[45]
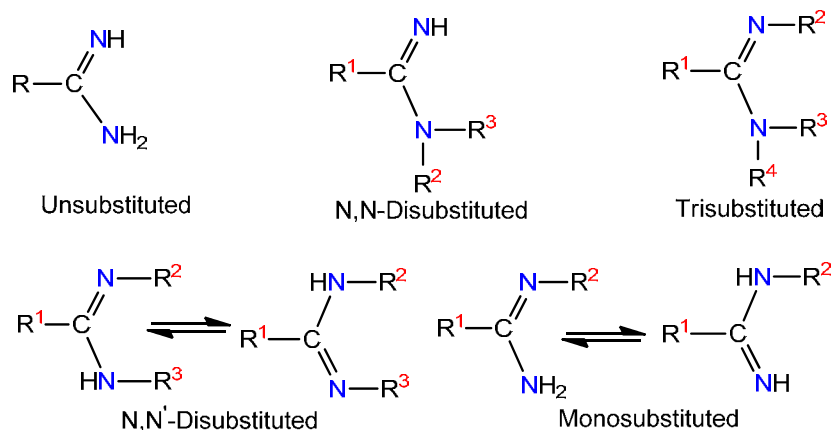
Figure 1.3 General types of the amidine.

A variety of possible binding modes of amidines to metal centres include monodentate (Fig. 1.4, I), bidentate chelating (Fig. 1.4, II), and bimetallic bridging (Fig. 1.4, III). Also, from monodentate (I) two types of four-electron donation are possible (see IV and V, Fig. 1.4). In addition to the bridging–chelating modes (Fig. 1.4, VI, VII, VIII and IX).[43, 64]
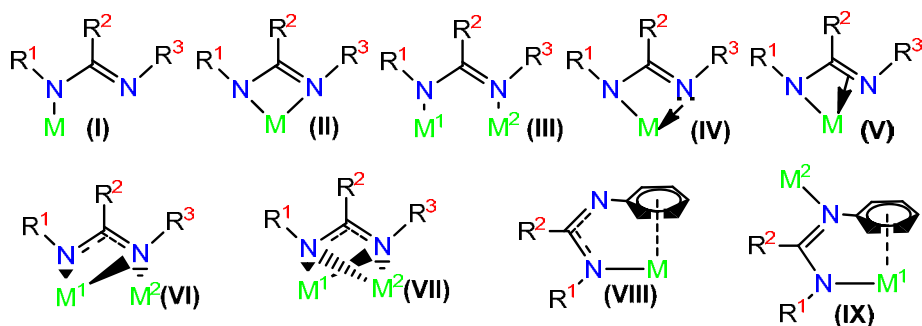
Figure 1.4 Typical binding modes of amidinate metal complexes.[43, 64]

Amidine binding modes to metal centres can be classified by the stereoisomers form of the amidinate ($R^2N=C(R^1)–NHR^3$) as E-syn, E-anti, Z-syn and Z-anti depending on the position of the substituents relative to each other with respect to the single bond (C–N) and double bond (C=N) (Fig. 1.5).[64-67]
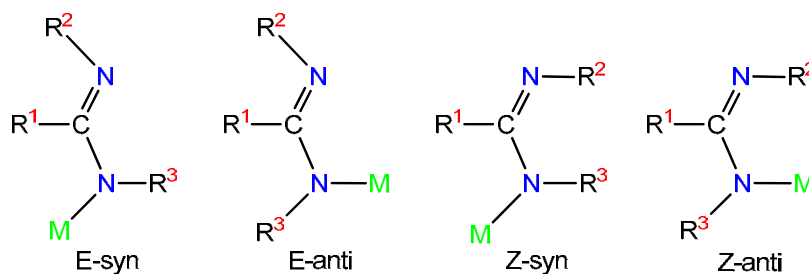
Figure 1.5 Plausible isomeric forms of the amidine in metal amidinate complexes.

The amidinate anion ligand system can stabilise lanthanoid metals in all the readily available possible oxidation states (+2, +3, and +4).[40] The amidinate ligand has a small N–M–N bite angle, typically in the range 63-65°. The steric and electronic effect of the amidinate rely on substituents on the N–C–N unit as well on the aryl rings that can be varied in order to meet requirements of the coordination geometry of the metal centre in bis(amidinato) complexes.[40, 46, 68]

N,N′-Bis(aryl)formamidines (ArN=CH–NHAr (Ar = aryl)) (Fig. 1.2), can be easily synthesised in high yields by heating to reflux one equivalent of triethyl orthoformate with two equivalents of the appropriate substituted aniline in the presence of acetic acid (eqn. 1.1).[44]
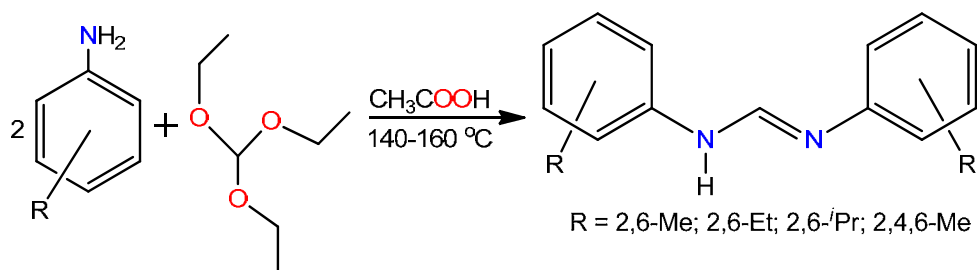
Equation 1.1

There are several accessible methods to synthesise lanthanoid formamidinates complexes. For example, redox transmetallation/protolysis reactions have been sucessfuly employed to synthesise an extensive series of

bis(formamidinato)lanthanoid(II) [Ln(Form)$_2$(thf)$_2$] (eqn. 1.2, i) and tris(formamidinato)lanthanoid(III) [Ln(Form)$_3$] (eqn. 1.2, ii) complexes involving the reaction of sterically tunable N,N′-bis(aryl)formamidines with lanthanoid metals and [Hg(C$_6$F$_5$)$_2$] in thf.[68-70]

$$Ln + Hg(C_6F_5)_2 + 2FormH \xrightarrow{\text{thf}} [Ln(Form)_2(thf)_2] + Hg + 2C_6F_5H$$

(i)

Form = ArNCHNAr, Ln = Sm; Eu, Ar = 2,6-^{i}Pr$_2$-C$_6$H$_3$, Ln = Yb,

Ar = o-MeC$_6$H$_4$; 2,6-Me$_2$-C$_6$H$_3$; o-HC$_6$F$_4$; 2,6-Et$_2$-C$_6$H$_3$;

2,6-^{i}Pr$_2$-C$_6$H$_3$; 2,4,6-Me$_3$-C$_6$H$_2$; o-PhC$_6$H$_4$; o-PhPhC$_6$H$_4$

$$2Ln + 3Hg(C_6F_5)_2 + 6FormH \xrightarrow{\text{thf}} 2[Ln(Form)_3] + 6C_6F_5H + 3Hg$$

(ii)

Ln = La; Nd; Sm; Ho; Er; Yb, Form = ArNCHNAr,

Ar = Ph; 2,6-Me$_2$-C$_6$H$_3$; 2,6-Et$_2$-C$_6$H$_3$; 2,6-^{i}Pr$_2$-C$_6$H$_3$; 2,4,6-Me$_3$-C$_6$H$_2$
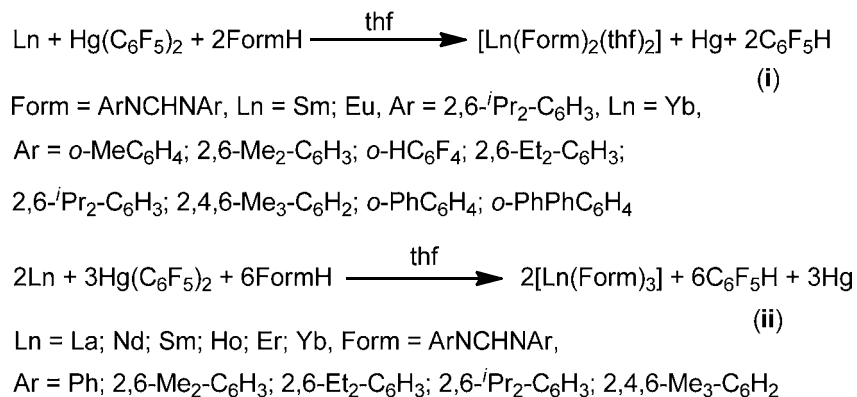
Equation 1.2

Halide metathesis represents an accessible method for introducing formamidines to lanthanoid centres to synthesise di- trivalent lanthanoid formamidinate complexes.[38] Metathesis reactions include the treatment of a rare earth halide with an alkali metal form of the ligand (eqn. 1.3).[68, 69]

$$YbCl_3 + 3[Li(o\text{-TolForm})] \xrightarrow{\text{thf}} [Yb(o\text{-TolForm})_3] + 3LiCl$$

o-TolForm = ArNCHNAr, Ar = o-MeC$_6$H$_4$

$$SmI_2 + 2[Na(DippForm)] \xrightarrow{\text{thf}} [Sm(DippForm)_2(thf)_2] + 2NaI$$

DippForm = ArNCHNAr, Ar = 2,6-^{i}Pr$_2$-C$_6$H$_3$
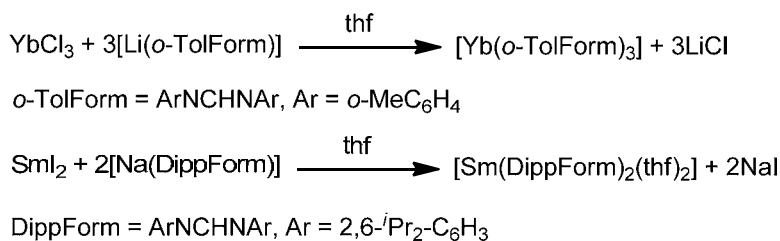
Equation 1.3

The pseudo-Grignard reaction is another synthetic route to prepare lanthanoid formamidinate complexes (eqn. 1.4).[71] This reaction involves oxidative-addition of alkyl or arylhalide to lanthanoid metal.

$$\text{Ln} + \text{PhI} \xrightarrow{\text{thf}} \text{PhLnI} + \text{LH} \xrightarrow{\text{thf}} [(L)\text{Ln(thf)}_n\text{I}] + C_6H_6$$

Ln = Eu, Yb
L = formamidinate
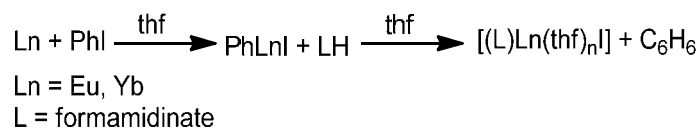
Equation 1.4

Pseudo-Grignard reagents $[\text{RLn(solv)}_n\text{X}]$ (Ln = Sm, Eu, Yb, X = I, Br, R = Me, Et, Ph) are important precursors in synthetic chemistry. They have been used as key starting materials for derivatisation of new organolanthanoid compounds, including alkyl, hydride, organoamide, and alkoxide complexes.[72-76]

Chemistry of these pseudo-Grignard reagents is still limited and a few species have been synthesised and structurally characterised such as $[\text{Yb(CH}_3\text{C}_5\text{H}_4)_2\text{Cl]}_2$ and $[\text{Er}(\eta^5\text{-C}_5\text{H}_5)\text{Cl}_2(\text{thf})_3]$[77], $[(\text{C}_5\text{Me}_5)\text{Y(Et}_2\text{O)Cl}]$[78] and [RSnLnI] (Ln = Eu, Yb).[79] Moreover, Smith and his team prepared $[\text{Yb\{C(SiMe}_3)_2(\text{SiMe}_2\text{X})\}(\text{Et}_2\text{O)I}]_2$ (X = CH=CH$_2$, OMe) as a dimeric structure [80, 81] and investigated the Schlenk equilibrium in this reaction.[82] Recently, Deacon and co-workers reported different complexes of the pseudo-Grignard reagents such as, $[\text{Ln(Ph}_2\text{pz)I(thf)}_4]$ (Ph$_2$pzH = 3,5-diphenylpyrazole; Ln = Eu, Yb)[74], $[\text{Sm(DippForm)Br}_2(\text{thf})_3]$, $[\text{Sm(DippForm)}_2\text{Cl(thf)}]$ and $[\text{Sm(DippForm)}_2\text{I(thf)}]$ (DippFormH = ArN=CH–NHAr, Ar = 2,6-^{i}Pr$_2$C$_6$H$_3$).[72] Synthesis of pseudo-Grignard formamidinato-lanthanoid(II) complexes are presented with more detail in Chapter 2 of this thesis.

1.4 Rare earth aryloxide complexes

A phenol is an aromatic ring with an hydroxyl functional group (Fig. 1.6, i). It is also called a carbolic acid and occurs naturally in coal tar. An aryloxide is the anionic form upon deprotonation of the hydroxyl group.[83] Figure 1.6 shows some common aryloxide ligands that have attracted much interest.
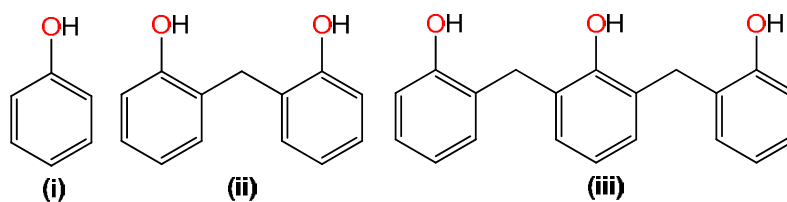
Figure 1.6 Some common aryloxide ligands.

Phenols are considered weak acids, but they are more acidic than aliphatic alcohols because the aryloxide ion is stabilised by resonance and the negative charge delocalised over the *ortho* and *para* positions (Fig. 1.7).[84] The addition of substituents can increase or decrease the acidity of the phenol protons. For example, a fluorine substituent can increase the acidity of the phenolic residue by increasing the resonance through the electron withdrawing group. On the other hand, alkyl substituents (as an electron donating group) can hamper resonance and decrease the acidity.[85]
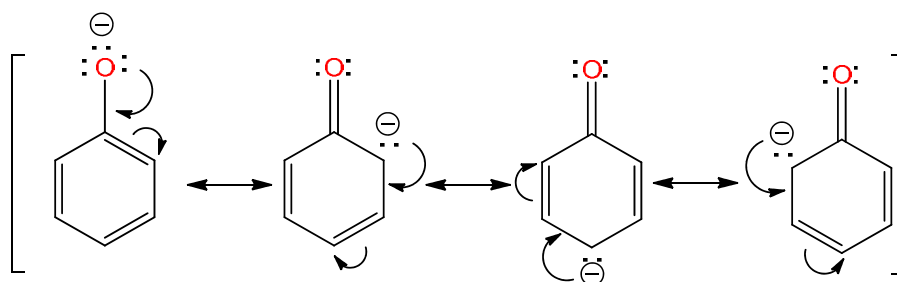
Figure 1.7 Charge delocalisation in the phenoxide ion.

The coordination mode of an aryloxide to Ln metal can be quite variable, and is dependent on the sizes, types and positions of the substituents relative to the O-atom.[86-88] Figure (1.8) shows some aryloxide coordination modes in schematic form. For example, the terminal linear coordination mode (Fig. 1.8, I) [Yb(μ−OAr)$_2$] ArO = 2,6-^{t}Bu-C$_6$H$_3$O),[89] the bridging mode [Ln(μ−OAr)Ln] (Fig. 1.8, II) in [Ln(ArO)$_3$]$_2$ (Ln = La, Yb; ArO = 2,6-dibenzylphenol).[90] η^1−η^6-intramolecular pendant arene ring

17

coordination mode (Fig. 1.8, III) [Ln(OAr)$_3$] (ArO = 2,6-Ph$_2$-C$_6$H$_3$O).[91] η^6–π-arene bridges intramolecular arene ring coordination mode (Fig. 1.8, IV) in [Ln(2,6-^{t}Bu-C$_6$H$_3$O)$_3$] (Ln = La, Nd, Sm, Er).[92] η^2-intramolecular coordination to *ipso* carbon [Er$_4$(OAr)$_{12}$] (ArO = 2,4,6-Me$_3$-C$_6$H$_2$O) (Fig. 1.8, V).[93]
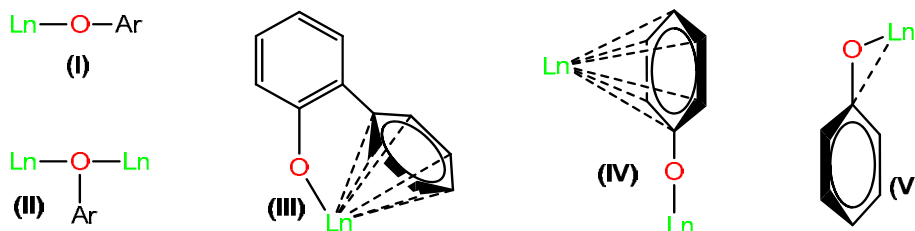
Figure 1.8 Some aryloxide coordination modes to Ln centres in schematic form.

Phenoxides containing alkyl substituents in the *para* position have little steric effect in coordination to the metal ion, though these can increase solubility and change the spectroscopic properties. Alkyl substituents in the *ortho* position can have a distinct effect on the structural properties and reactivity of the metal complex. *Meta* substituents affect the steric properties of the ligands by restricting the conformational flexibility of adjacent *ortho*-phenyl substituents.[94, 95]

The aryloxide chemistry of lanthaniod elements continues to be the subject of considerable interest, due to the applicability of these complexes as precursors to polymerisation catalysts and as catalysts for a range of organic transformations.[92] Lanthanoid phenolate complexes are accessible by a wide array of synthetic routes. For example, low-coordinate complexes for both Ln^{+2} and Ln^{+3} have been synthesised by the direct reaction between lanthanoid metal and 2,6-dibenzylphenol (eqn. 1.5).[90] The electropositive metals form a surface oxide layer with phenol that could be protecting them. At elevated temperature direct reactions of activated lanthanoid metals with a weakly protic-ligand in the presence of mercury, followed by extraction with thf

have been explored as a route to heteroleptic lanthanoid complexes.[93, 96, 97] Initially, several drops of mercury were added to the reaction mixture to form a reactive lanthanoid amalgam.[90]

$$2Ln + 2nArOH \xrightarrow{170\ ^oC} 2[Ln(OAr)_n] + nH_2$$
$$Ln = La, Yb\ n = 3,\ Eu\ n = 2$$
$$ArOH = 2,6\text{-dibenzylphenol}$$
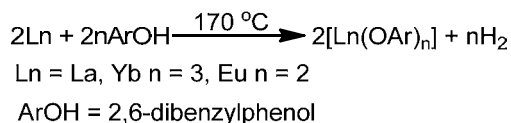
Equation 1.5

Samarium(II) phenolate was successfully synthesised by the ligand exchange reaction of $[Sm\{N(SiMe_3)_2\}_2(thf)_2]$ with $2,6\text{-}^tBu_2\text{-}4\text{-Me-}C_6H_2OH$ (eqn. 1.6).[98]

$$[Sm\{N(SiMe_3)_2\}_2(thf)_2] + 2ArOH \longrightarrow [Sm(OAr)_2] + 2NH(SiMe_3)_2$$
$$ArOH = 2,6\text{-dibenzylphenol}$$
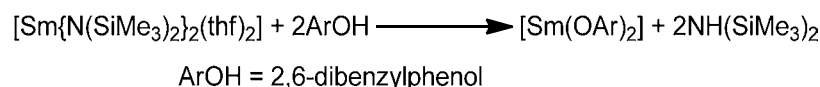
Equation 1.6

An alternative method to synthesise lanthanoid phenolate complexes is from the reaction of the elemental metals activated by iodine with a substituted phenol in thf (eqn. 1.7).[99]

Iodine can be used to activate lanthanoid metals by the addition of a catalytic amount of iodine to metals, since Ln metal powders react with iodine in tetrahydrofuran (thf) to form $[LnI_3(thf)_n]$. It is more convenient, and parallels its role in the activation of Mg in Grignard reagent synthesis. Thus, reaction of I_2-activated rare-earth metals provides an effective, environmentally friendly, metal-based route in the preparation of rare-earth phenolate, cyclooctatetraenides, thiolate and *o*-benzoquinonate complexes.[100]

$$2Ln + 6ArOH \xrightarrow{thf/I_2} 2[Ln(OAr)_3(thf)_n] + 3H_2$$
$$Ln = La, Nd\ n = 2;\ Sm, Dy, Y, Yb\ n = 3$$

$$2Eu + 4ArOH \xrightarrow{thf/I_2} [Eu(OAr)_2(thf)_2]_2 + 2H_2$$
$$ArOH = 2,6\text{-}^iPr\text{-}C_6H_3OH$$
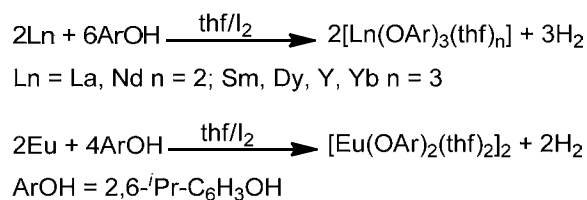
Equation 1.7

Moreover, divalent and trivalent lanthanoid phenolate complexes can be synthesised by using the one pot redox transmetallation/protolysis reaction (eqn.1.8).[89, 90] Synthesis and reactivity of lanthanoid biphenolate complexes are presented with more detail in Chapter 3 and Chapter 4 of this thesis.

$$2Ln + 3Hg(C_6F_5)_2 + 6ArOH \xrightarrow{\text{thf/Hg}} 2[Ln(OAr)_3(thf)_3] + 6C_6F_5H + 3Hg$$
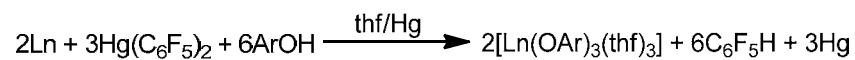
$Ln = La, Pr, Nd, Gd, Er$

$ArOH = 2,6\text{-}^tBu\text{-}C_6H_3OH$

$$Ln + Hg(C_6F_5)_2 + 2ArOH \xrightarrow{\text{thf/Hg}} [Ln(OAr)_2(thf)_n] + 2C_6F_5H + Hg$$
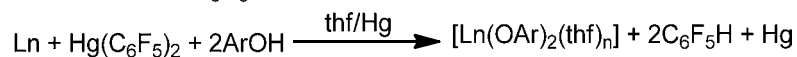
$Ln = Eu, Yb$

$ArOH = 2,4,6\text{-}^tBu\text{-}C_6H_2OH; 2,6\text{-}^tBu\text{-}4\text{-}Me\text{-}C_6H_2OH$

Equation 1.8

1.5 Current Study

This thesis further explores the non-mercury metal-based complex syntheses in lanthanoid chemistry and the redox transmetallation/protolysis reaction, and characterisation of a range of new rare earth complexes synthesised by these methods.

Chapter 2 describes the synthesis, characterisation and structural features of pseudo-Grignard reagents of formamidinatolanthanoid complexes [Yb(Form)(thf)$_n$X] {(Form (ArNCHNAr) = XylForm (Ar = 2,6-Me$_2$C$_6$H$_3$), MesForm (Ar = 2,4,6-Me$_3$C$_6$H$_2$), DippForm (Ar = 2,6-^{i}Pr$_2$C$_6$H$_3$), X = I or Br}. To increase the scope of the organolanthanoid-halide system, an investigation into the treatment of the pseudo-Grignard reagents with different kinds of ketones such as fluorenone and *p*-benzoquinone led to a deoxygenated carbonyl group in the examined ketones. The deoxygenated ketone is sitting in the lattice of the crystal structures [Yb(MesForm)$_3$].Ph$_3$ and [Yb(MesForm)$_3$].Fluorene. This result has opened the doors to much exciting new studies to investigate the deprotonation mechanism that occurred in this reaction.

Chapter 3 discusses the use of 2,2′-methylenebis(6-*tert*-butyl-4-methylphenol) in redox transmetallation/protolysis reactions. A series of mononuclear [Ln(BPO$_2$)(BP(OH)O)(thf)$_n$] (n = 1, 2, 3) and dinuclear complexes [Ln$_2$(BPO$_2$)$_3$(thf)$_n$] (n = 1, 2) of the lanthanoid(III) metals have been prepared by this method, and structural features are discussed.

Chapter 4 discusses the versatility of heterobimetallic complexes of lanthanoid biphenolate complexes demonstrated through the reactivity of [Ln(BPO$_2$)(BP(OH)O)(thf)$_n$] (n = 1, 2, 3) complexes with different metal alkyls/amides, for example, ^{n}BuLi, AlMe$_3$, KN(SiMe$_3$)$_2$ and ZnEt$_2$. Anionic

[Li(thf)$_4$][Ln(BPO$_2$)$_2$(thf)$_2$] [Ln(BPO$_2$)(thf)$_n$][AlMe$_2$(BPO$_2$)] (n = 3, 5) and non-ionic

[Li(thf)$_2$Ln(BPO$_2$)$_2$(thf)$_n$] [AlMe$_2$Ln(BPO$_2$)$_2$(thf)$_2$], [ZnEtYb(BPO$_2$)$_2$(thf)] structures

resulting from these reactions are also discussed.

1.6 References

[1]. Connelly, N. G.; Damhus, T.; Hartshorn, R. M.; Hutton, A. T. *Nomenclature of Inorganic Chemistry.* RSC: Cambridge, **2005**.

[2]. Taylor, S. R.; McLennan, S. M. Distribution of the Lanthanides in the Earth's Crust. In *Metal Ions in Biological Systems, the Lanthanides and their Interrelations with Biosystems.* Sigel, A.; Sigel, H. Eds. CRC Press: New York, **2003**, Vol. 40, 1-38.

[3]. Gupta, C. K.; Krishnamurthy, N. *Extractive Metallurgy of Rare Earths.* CRC Press: Boca Raton, FL, **2005**.

[4]. Dieke, G. H. *Spectra and Energy Levels of Rare Earth Ions.* John Wiley and Sons. Interscience Publishers: New York, **1968**.

[5]. Wheelwright, E. J. *Promethium Technology.* American Nuclear Society: Illinois, **1973**.

[6]. Evan, C. H. *Biochemistry of the Lanthanides.* Plenum Press: New York, **1990**.

[7]. Greinacher, E. History of Rare Earth Applications, Rare Earth Market Today. In *Industrial Applications of Rare Earth Elements.* Gschneider, K. A. Ed. ACS Symposium Series: **1981**, Vol. 164, 3-17.

[8]. Moeller, T. *The Chemistry of the Lanthanides.* Reinhold Publishing Corporation: New York, Chapman and Hall: London, **1963**.

[9]. Kaltsoyannis, N.; Scott, P. *The f Elements.* Oxford Science Publications: Oxford, **1999**.

[10]. Topp, N. E.; Ph. D.; F. R. I. C. *The Chemistry of the Rare-earth Elements.* Elsevier Publishing Company: Amsterdam, London, New York, **1965**.

[11]. Greenwood, N. N.; Earnshaw, A. *Chemistry of the Elements.* 2nd ed. Butterworth-Heinemann: Oxford, **1997**.

[12]. Cotton, S. *Lanthanide and Actinide Chemistry.* John Wiley and Sons Ltd: Chichester*,* **2006**.

[13]. Cotton, S. *Lanthanide and Actinide*. MacMillan Education Ltd: London, **1991**.

[14]. Spitsyn, V. I.; Martynenko, L. I. *Coordination Chemistry of Rare Earth Elements.* Izd. MGU: Moscow, **1973**.

[15]. Carnal, W. T. The Absorption and Fluorescence Spectra of Rare Earth Ions in Solution. In *Handbook on the Physics and Chemistry of Rare Earths.* Gschneidner, K. A.; Eyring, L. Eds. Elsevier, North-Holland Publishing: Amsterdam, **1979**, Vol. 3, 171-208.

[16]. Cotton, F. A.; Wilkinson, G.; Murillo, C. A.; Bochmann, M. *Advanced Inorganic Chemistry.* 6th ed. John Wiley and Sons Inc: New York, **1999**.

[17]. Nozaki. Y.; Lerche, D.; Alibi, DS.; Tsutsumi. M. *Geochim. et Cosmochim. Acta.* **2000**, *64*, 3975-3982.

[18]. Olmez, I.; Sholkovitz, E. R.; Hermann, D.; Eganhouse, R. P. *Environ. Sci Technol.* **1991**, *25*, 310-316.

[19]. Werts, M. H.; Woudenberg, R. H.; Emmerink, P. G.; Gassel, R. V.; Hofstraat, J. W.; Verhoeven, J. W. *Angew. Chem*. *Int. Ed.* **2000**, *39*, 4542-4544.

[20]. Liang, H.; Zheng, Z.; Chen, B.; Zhang, Q.; Ming, H. *Mater. Chem. Phys.* **2004**, *86*, 430-434.

[21]. Yang, J.; Diemeer, M. B.; Geskus, D.; Sengo, G.; Pollnau, M.; Dresden, A. *Opt. Lett.* **2009**, *34*, 473-475.

[22]. Coffa, S.; Franzo, G., Priolo, F. *MRS Bull.* **1998**, *23*, 25-32.

[23]. Humphris, S.; Morrison, M. A.; Thompson, R. N. *Chem. Geol*. **1978**, *23*, 125-137.

[24]. Jakes, P.; Gill, J. *Earth Planet Sci. Lett.* **1970**, *9*, 17-28.

[25]. Hanson, G. N. *Ann. Rev. Earth Planet Sci.* **1980**, *8*, 371-406.

[26]. Piepgras, D. J.; Wasserburg, G. J. *Geochim. et Cosmochim. Acta.* **1987**, *51*, 1257-1271.

[27]. McKenzie, D.; O'Nions, R. K. *J. Petrol.* **1991**, *32*, 1021-1091.

[28]. Rowan, B. C.; Wilson, L. R.; Richards, B. S. *IEEE J. Sel. Top. Quantum Electron.* **2008**, *14*, 1312-1322.

[29]. Guo, H.; Zhang, B.; Wang, G.; Shen, Z. *J. Chem. Geol.* **2010**, *270*, 117-125.

[30]. He, S.; Zhu, L.; Yang, R.; Shen, Z.; Yu, X. *J. Chinese J. Geochem.* **2011**, *30*, 114-124.

[31]. Johannesson, K. H.; Stetzenbach, K. J.; Hodge, V. F. *J. Geochim. et Cosmochim. Acta.* **1997**, *61*, 3605-3618.

[32]. Haley, J. T. *J. Pharmacol. Sci.* **1965**, *54*, 663-670.

[33]. Sharma, R. C.; Thripathi, S. P.; Kanna, K. S.; Sharma, R. S. *Curr. Sci.* **1981**, *50*, 748-750.

[34]. Picard, C.; Geum, N.; Nasso, I. *Bioorg. Med. Chem. Lett.* **2006**, *16*, 5309-5312.

[35]. Aime, S.; Crich, S. G.; Gianolio, E.; Giovenzana, G. B.; Tei, L.; Terreno, E. *Coord. Chem. Rev.* **2006**, *250*, 1562-1579.

[36]. He, M. L.; Ranz, D.; Rambeck, W. A. *J. Anim. Physiol. Anim. Nutr.* **2001**, *85*, 263-270.

[37]. Gonzalez, V.; Vignati, D. A. L.; Leyval, C.; Giamberini, L. *Environment International.* **2014**, *71*, 148-157.

[38]. Atwood, D. A. *The Rare Earth Elements, Fundamentals and Applications*. John Wiley and Sons Ltd: West Sussex, **2012**.

[39]. Wilkinson, G.; Birmingham, J. M. *J. Am. Chem. Soc.* 1954, *76*, 6210-6210.

[40]. Edelman, F. T. *Chem. Soc. Rev.* **2012**, *41*, 7657-7672.

[41]. Kiboum, B. T. *A Lanthanide Lanthology, Part II, M-Z.* Molycorp Inc: Mountain Pass, California, **1994**.

[42]. Kiboum, B. T. *A Lanthanide Lanthology, Part I, A-L.* Molycorp Inc: Mountain Pass, California, **1993**.

[43]. Barker, J.; Kilner, M. *Coord. Chem. Rev.* **1994**, *133*, 219-300.

[44]. Roberts, R. M. *J. Org. Chem.* **1949**, *14*, 277-284.

[45]. Patai, S. *The Chemistry of Amidines and Imidates*. John Wiley and Sons: London, New York, Sydney and Toronto, **1975**.

[46]. Edelman, F. T. *Chem. Soc. Rev.* **2009**, *38*, 2253-2268.

[47]. Krygowski, T. M.; Wozniak, K. Structural Chemistry of Amidines and Related Systems. In *The Chemistry of Amidines and Imidates.* Patai, S.; Rappoport, Z. Eds. John Wiley and Sons Ltd: Chichester, **1991**, Vol. 2, 101-145.

[48]. Enthaler, S.; Schröder, K.; Inoue, S.; Eckhardt, B.; Junge, K.; Beller, M.; Drieß, M. *Eur. J. Org. Chem.* **2010**, *75*, 4893-4901.

[49]. Jones, S. D.; Kennewell, P. D.; Tulley, W. R.; Westwood, R.; Sammes, P. G. *J. Chem. Soc. Perkin Trans. 1*. **1990**, 447-455.

[50]. Tsou, H. R.; Mamuya, N.; Johnson, B. D.; Reich, M. F.; Gruber, B. C.; Ye, F.; Nilakantan, R.; Shen, R.; Discafani, C.; DeBlanc, R.; Davis, R.; Koehn, F. E.; Greenberger, L. M.; Wang, Y. F.; Wissner, A. *J. Med. Chem.* **2001**, *44*, 2719-2734.

[51]. Landreau, C.; Deniaud, D.; Evain, M.; Reliquet, A.; Meslin, J. C. *J. Chem. Soc. Perkin Trans. 1*. **2002**, 741-745.

[52]. Wang, Y. D.; Boschelli, D. H.; Johnson, S.; Honores, E. *Tetrahedron.* **2004**, *60*, 2937-2942.

[53]. Yoon, D. S.; Han, Y.; Stark, T. M.; Haber, J. C.; Gregg, B. T.; Stankovich, S. B. *Org. Lett.* **2004**, *6*, 4775-4778.

[54]. Willemann, C.; Grunert, R.; Bednarski, P. J.; Troschutz, R. *Bioorg. Med. Chem.* **2009**, *17*, 4406-4419.

[55]. Foucourt, A.; DubouilhBenard, C.; Chosson, E.; Corbiere, C.; Buquet, C.; Iannelli, M.; Leblond, B.; Marsais, F.; Besson, T. *Tetrahedron.* **2010**, *66*, 4495-4502.

[56]. Kim, O.; Jeong, Y.; Lee, H.; Hong, S. S.; Hong, S. *J. Med. Chem.* **2011**, *54*, 2455-2466.

[57]. Anelli, P. L.; Brocchetta, M.; Copez, D.; Palano, D.; Visigalli, M.; Paoli, P. *Tetrahedron.* **1997**, *53*, 15827-15832.

[58]. Dineen, T. A.; Zajac, M. A.; Myers, A. G. *J. Am. Chem. Soc.* **2006**, *128*, 16406-16409.

[59]. Taylor, J. E.; Bull, S. D.; Williams, J. M. *Chem. Soc. Rev.* **2012**, *41*, 2109-2121.

[60]. Arnold, D. I.; Cotton, F. A.; Matonic, J. H.; Murillo, C. A. *Polyhedron.* **1997**, *16*, 1837-1841.

[61]. Mitzi, D. B.; Liang, K. *J. Solid State Chem.* **1997**, *134*, 376-381.

[62]. Meyers, A. I.; Hutchings, R. *Heterocycles.* **1996**, *42*, 475-478.

[63]. Matulenko, M. A.; Meyers, A. I. *J. Org. Chem.* **1996**, *61*, 573-580.

[64]. Junk, P. C.; Cole, M. L. *Chem. Commun.* **2007**, 1579-1590.

[65]. Coles, M. P. *Dalton Trans.* **2006**, 985-1001.

[66]. Boere, R. T.; Klassen, V.; Wolmershauser, G. *J. Chem. Soc. Dalton Trans.* **1998**, 4147-4154.

[67]. Oakley, S. H.; Soria, D. B.; Coles, M. P.; Hitchcock, P. B. *Dalton Trans.* **2004**. 537-546.

[68]. Cole, M. L.; Deacon, G. B.; Forsyth, C. M.; Junk, P. C.; Konstas, K.; Wang, J. *Chem. Eur. J.* **2007**, *13*, 8092-8110.

[69]. Cole, M. L.; Junk, P. C. *Chem. Commun.* **2005**, 2695-2697.

[70]. Cole, M. L.; Deacon, G. B.; Forsyth, C. M.; Junk, P. C.; Konstas, K.; Wang, J.; Bittig, H.; Werner, D. *Chem. Eur. J.* **2013**, *19*, 1410-1420.

[71]. Hamidi, S. PhD thesis, Chapter 3. Monash University, **2012**.

[72]. Cole, M. L.; Deacon, G. B.; Junk, P. C.; Wang, J. *Organometallics.* **2013**, *32*, 1370-1378.

[73]. Petrov, E. S.; Roitershtein, D. M.; Rybakova, L. F. *J. Organomet. Chem.* **2002**, *647*, 21-27.

[74]. Wiecko, M.; Deacon, G. B.; Junk, P. C. *Chem. Commun.* **2010**, *46*, 5076-5078.

[75]. Evans, D. F.; Fazakerley. G. V; Phillips, R. F. *J. Chem. Soc. A.* **1971**, 1931-1934.

[76]. Evans, D. F.; Fazakerley, G. V.; Phillips, R. F. *J. Chem. Soc. D.* **1970**, 244-244.

[77]. Day, C. S.; Day, V. W.; Ernst, R. D.; Sarah, H. V. *Organometallics.* **1982**, *1*, 998-1003.

[78]. Finke, R. G.; Keenan, S. R.; Watson, P. L. *Organometallics.* **1989**, *8*, 263-277.

[79]. Bochkarev, L. N.; Grachev, O. V.; Ziltsov, S. F.; Zakharov, L. N.; Novgorod, N.; Struchkov, Y. T. *J. Organomet. Chem.* **1992**, *436*, 299-311.

[80]. Eaborn, C.; Hitchcock, P. B.; Izod, K.; Smith, J. D. *J. Am. Chem. Soc.* **1994**, *116*, 12071-12072.

[81]. Eaborn, C.; Hitchcock, P. B.; Izod, K.; Lu, Z. R.; Smith, J. D. *Organometallics.* **1996**, *15*, 4783-4790.

[82]. Heckmann, G.; Niemeyer, M. *J. Am. Chem. Soc.* **2000**, *122*, 4227-4228.

[83]. McMurry, J. *Organic Chemistry*. 6th ed. Brooks Cole: Australia, Brazil, Canada, UK, USA, **2004**.

[84]. Kremer, T.; Schleyer, P. R. *Organometallics.* **1997**, *16*, 737-746.

[85]. Tehan, B. J.; Lloyd, E. J.; Wong, M. G.; Pitt, W. R.; Montana, J. G.; Manallack, D. T.; Gancia, E. *Quant. Struct. Act. Rel.* **2002**, *21*, 457-472.

[86]. Caulton, K. G.; Hubert-Pfalzgraf, L. G. *Chem. Rev.* **1990**, *90*, 969-995.

[87]. Mehrotra, R. C.; Singh, A.; Tripathi, U. M. *Chem. Rev.* **1991**, *91*, 1287-1303.

[88]. Marcalo, J.; Matos, A. P. *Polyhedron.* **1989**, *8*, 2431-2437.

[89]. Deacon, G. B.; Feng, T.; Mackinnon, P.; Newnham, R. H.; Nickel, S.; Skelton, B. W.; White, A. H. *Aust. J. Chem.* **1993**, *46*, 387-399.

[90]. Cole, M. L.; Deacon, G. B.; Junk, P. C.; Proctor, K. M.; Scott, J. L.; Strauss, C. R. *Eur. J. Inorg. Chem.* **2005**, 4138-4144.

[91]. Deacon, G. B.; Forsyth, C. M.; Nickel, S. *J. Organomet. Chem.* **2002**, *647*, 50-60.

[92]. Clark, D. L.; Gordon, J. C.; Watkin, J. G.; Huffman, J. C.; Zwick, B. D. *Polyhedron.* **1996**, *15*, 2279-2289.

[93]. Deacon, G. B.; Junk, P. C.; Moxey, G. J. *Chem. Asian J.* **2009**, *4*, 1717-1728.

[94]. Bradley, D. C.; Mehrotra, R. C.; Rothwell, I. P.; Singh, A. A. *Aryloxo Derivatives of Metals.* Academic Prees London: London, **2001**.

[95]. Vilardo, J. S.; Lockwood, A. M.; Hanson, L. G.; Clark, J. R.; Parkin, P. E.; Rothwell, I. J. *J. Chem. Soc. Dalton Trans.* **1997**, 3353-3362.

[96]. Boyle, T. J.; Ottley, L. A. *Chem. Rev.* **2008**, *108*, 1896-1917.

[97]. Deacon, G. B.; Forsyth, C. M. Syntheses of Rare Earth Organometallics, Organoamides, and Aryloxides. In *Inorganic Chemistry Highlights.* Meyer, G.; Naumann, D.; Weseman, L. Eds. Wiley-VCH Verlag GmbH: Germany, **2002**, Vol. 7, 139-153.

[98]. Hou, Z.; Fujita, A.; Yoshimura, T.; Jesorka, A.; Zhang, Y.; Yamazaki, H.; Wakatsuki, Y. *Inorg. Chem.* **1996**, *35*, 7190-7195.

[99]. Hamidi, S.; Deacon, G. B.; Junk, P. C.; Neumann. P. *Dalton Trans.* **2012**, *41*, 3541-3552.

[100]. Deacon, G. B.; Hamidi, S.; Junk, P. C.; Kelly, R. P.; Wang, J. *Eur. J. Inorg. Chem.* **2014**, 460-468.

Chapter 2: Syntheses and reactivity of pseudo-Grignard reagents

2.1 Introduction

2.1.1 Syntheses of pseudo-Grignard reagents

In 1900, Grignard investigated the synthesis of organomagnesium compounds. Grignard received the 1912 Nobel Prize in Chemistry for his methodology of creating organomagnesium halides $[RMg(solv)_nX]$ (R = Me, Et, Ph; X = Cl, Br, I; solv = thf, Et$_2$O, n = number) via the direct synthesis between organohalides and magnesium metal (eqn. 2.1).[1, 2]

$$Mg + RX \xrightarrow[\text{0 °C}]{\text{solv}} [RMg(solv)_nX]$$

R = Me; Et; Ph, X = Cl; Br; I
solv = thf; Et$_2$O
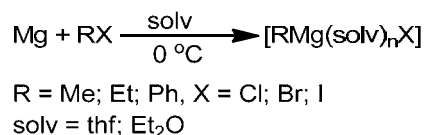
Equation 2.1

In 1971 Evans *et al*. first investigated the reaction of organoiodides with lanthanoid metals to synthesise pseudo-Grignard reagents $[RLn(thf)_nI]$ (eqn. 2.2).[3]

$$Ln + RI \xrightarrow[\text{-20 °C}]{\text{thf}} [RLn(thf)_nI]$$
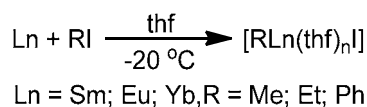
Ln = Sm; Eu; Yb,R = Me; Et; Ph

Equation 2.2

The general formula of pseudo-Grignard reagents is $[RLn(solv)_nX]$ (Ln = Sm, Eu and Yb; R = Me, Et, Ph; X = Cl, Br, I; solv = thf, Et$_2$O) which is analogous to the traditional Grignard reagents $[RMg(solv)_nX]$ (solv = thf, Et$_2$O).[4, 5]

Pseudo-Grignard reagents $[RLn(solv)_nX]$ have received moderate attention in organic and inorganic transformations and achieved some significant progress due to their analogous reactivity towards acids and electrophiles when compared to the well-known

Mg-based reagents. For these reasons, organolanthanoid halides are formulated as Grignard analogues [RLn(solv)$_n$X] and called pseudo-Grignard reagents.[6, 7]

In recent years a wide range of organolanthanoids in the +2 state with cyclopentadienyl and non-cyclopentadienyl ligands have been synthesised.[8-16] Oxidative addition of organoiodides RI to Ln^0 (Ln = Sm, Eu and Yb, R = Me, Et, Ph) (eqn. 2.2) is an accessible route to synthesise divalent lanthanoid species such as pseudo-Grignard reagents [RLn(thf)$_n$I].[3, 16]

In early studies involving these pseudo-Grignard reagents magnetic susceptibility measurements and the Ln:I (Ln = Sm, Eu, Yb) ratios revealed that the abovementioned reaction (eqn. 2.2) produces a mixture of divalent and trivalent lanthanoid complexes. The majority of the produced complexes, however, are present in the divalent state particularly for Eu^{+2} (99%) and to a lesser degree for Yb^{+2} (85%) and Sm^{+2} (50%).[3] Niemeyer *et al*. have suggested different divalent lanthanoid species may be present in a solution of pseudo-Grignard reagents (eqn. 2.2) such as, [RLn(thf)$_n$I], [RLn(thf)$_n$I]$_2$, [R$_2$Ln(thf)$_n$], [Ln(thf)$_n$I$_2$] (Ln = Sm, Eu, Yb; R = 2, 6-Ph$_2$-C$_6$H$_3$). The Schlenk equilibrium was investigated using ^{171}Yb as a probe. The main three components of the equilibrium [DppYb(thf)$_n$I], [Yb(Dpp)$_2$(thf)$_2$], [Yb(thf)$_4$I$_2$] (Dpp = 2, 6-Ph$_2$C$_6$H$_3$) present in solution were detected at three different chemical shifts in the ^{171}Yb NMR spectrum (eqn. 2.3).[17]

$$2[\text{DppYbI(thf)}_n] \rightleftharpoons [\text{Yb(Dpp)}_2(\text{thf})_2] + [\text{YbI}_2(\text{thf})_4]$$
$$\text{Dpp} = 2,6\text{-Ph}_2\text{C}_6\text{H}_3$$
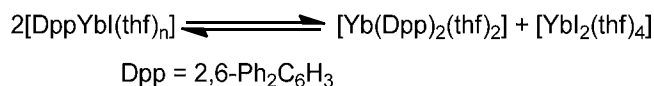
Equation 2.3

Unfortunately, little characterisation of such intermediates [DppYb(thf)$_n$I], [Yb(Dpp)$_2$(thf)$_2$] has been performed and information on the structures or the exact nature of these molecules is still limited.[18, 19]

A new pseudo-Grignard reagent [Yb{C(SiMe$_3$)$_2$(SiMe$_2$R)}I(Et$_2$O)]$_2$ (R = Me, MeO, CH=CH$_2$) has been successfully synthesised by the treatment of ytterbium metal with a very bulky silylated iodoalkyl group in thf, and exists as a dimer in the solid state (eqn. 2.4).[20, 21]

$$2Yb + 2\{C(SiMe_3)_2(SiMe_2R)I\} \xrightarrow[16\ h]{Et_2O} [Yb\{C(SiMe_3)_2(SiMe_2R)\}(Et_2O)I]_2$$
$$R = CH=CH_2, MeO, Me$$
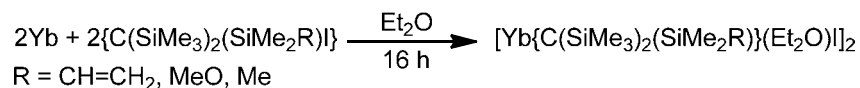
Equation 2.4

Recently, Deacon and co-workers have exploited pseudo-Grignard reagents to synthesise new species of lanthanoid pyrazolates [Ln(Ph$_2$pz)(thf)$_4$I] (Ln = Eu, Yb). This synthetic route was initiated by the sonication of the lanthanoid metal powder with aryl halide (PhI) at low temperature (-78 °C), followed by the addition of the pyrazole and stirring at room temperature overnight to prepare the final complex (eqn. 2.5).[22]
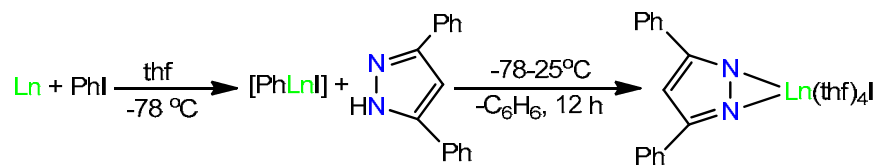
Equation 2.5

Dolgoplosk, *et. al.*[23] expanded the oxidative addition reaction and successfully employed it to synthesise pseudo-Grignard reagents of trivalent lanthanoids [(Ph$_3$C)$_2$LnCl] or [(Ph$_3$C)LnCl$_2$] (Ln = Pr^{+3}, Nd^{+3}, Gd^{+3} and Ho^{+3}) (eqn. 2.6).

$$2Ln + 3Ph_3CCl \longrightarrow [(Ph_3C)_2LnCl] + [(Ph_3C)LnCl_2]$$

Equation 2.6

The heavy alkaline-earth elements have similar ionic radii to divalent lanthanoids. For example, Ca^{+2} and Yb^{+2} (1.00 and 1.02 A, respectively) and Sr^{+2} (1.22 A) and Sm^{+2} or Eu^{+2} (1.22 and 1.21 A, respectively).[24]

Among the alkaline earth metal ions, Ca^{+2} has a striking similarity to Yb^{+2}. For example, Ca and Yb analogues have isomorphous crystal structures, similar cell constants, and their complexes display similar gas-phase behaviour.[25, 26] Calcium metal shows a higher reactivity than magnesium and forms a calcium oxide layer on the metal surface. As a result, to insert calcium into a halogen–carbon bond (direct synthesis), calcium must be activated. The most common activation technique to activate the metal surface is dissolving the metal in liquid ammonia.[27]

Pseudo-Grignard reagents of calcium are accessible by the direct reaction between arylhalides and calcium.[27] Activated calcium reacts smoothly with iodobenzene at low temperatures in thf yielding $[ArCa(thf)_4I]$ $(Ar = 2, 4, 6-Me_3-C_6H_2)$ (eqn. 2.7). There are a number of difficulties associated with this synthetic route such as the side reactions due to the nucleophilicity of the organocalcium derivatives, and the insolubility due to the highly ionic metal–carbon bonds.[27-29]
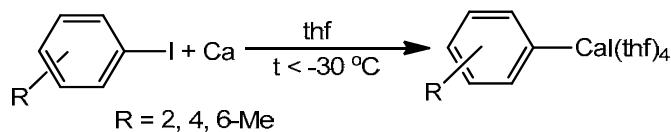
Equation 2.7

The Schlenk equilibrium for this reaction has been established by the ^{1}H-NMR spectrum of a $[ArCa(thf)_4I]$ $(Ar = 2,4,6-Me_3-C_6H_2)$ in thf which show two sets of resonances related to $[CaAr(thf)_4I]$ and $[Ca(Ar)_2(thf)_3]$. Moreover, fractional crystallisation at low temperature from this solution gave all species of the Schlenk equilibrium, $[CaI_2(thf)_4]$, $[ArCa(thf)_4I]$ and $[Ca(Ar)_2(thf)_3]$ (eqn. 2.8).[27-29]
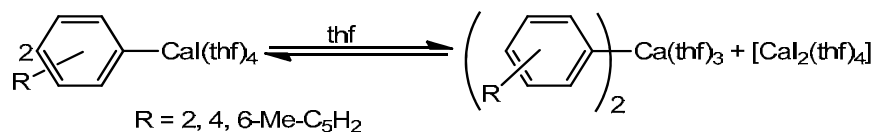
Equation 2.8

A new pseudo-Grignard reagent involving a dimethylsilyl species has been successfully synthesised by the oxidative addition of iodophenylsilyl to activated calcium metal (eqn. 2.9).[30]
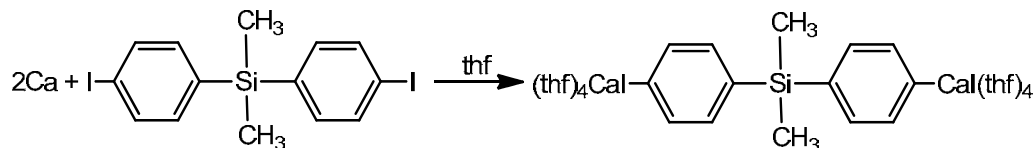
Equation 2.9

2.1.2 Reactivity of pseudo-Grignard reagents

Pseudo-Grignard reagents [RLnI] have been utilised successfully in organic transformations and compared to classical Grignard reagents[31-34] (eqn 2.10i)[3], (eqn. 2.10ii)[35, 36], (eqn 2.10iii).[6]

Evans, *et. al.*[3] have reported similar reactivities of pseudo-Grignard reagents [RYbI] to classical Grignard reagents in a range of organic transformations. For example, hydrolysis of the reaction mixture of [PhYbI] and benzophenone (eqn 2.10i) gave a good yield of triphenylmethanol which is a similar result to classical Grignard reagents.
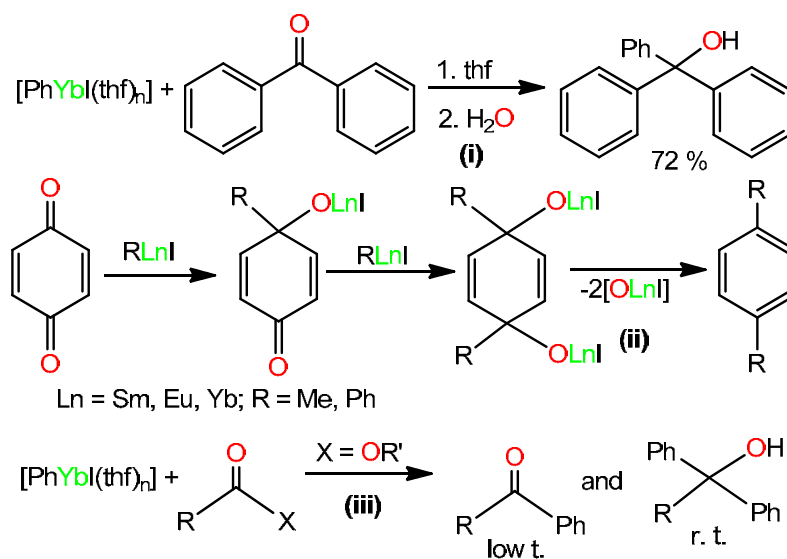
Equation 2.10

As mentioned above and in section 2.1.1 pseudo-Grignard reagents [RLnX] are similar to the classical Grignard reagents [RMgX] in reactivity and they have a similar formula, but they do have different and unique reactivities. For example, The reaction of RLnI (Ln = Yb, Eu) with esters giving ketones as predominant products instead of tertiary alcohols[7] and the reaction with aldehydes leading to Tishchenko condensation products (Ln = Sm, Pr, Nd, Dy).[6]

Moreover, 1,2-addition product ($PhCH=CHCOHPh_2$) has been prepared by treating an α,β-unsaturated carbonyl compound ($PhCH=CHCOPh$) with [RYbI] at room temperature. However, treating these carbonyl compounds with classical Grignard reagents gives a mixture of 1,2- and 1,4-addition products.[6] This reaction shows unique regioselectivity which could be explained according to the hard and soft acids and bases theory. The pseudo-Grignard reagents [RLnI] are harder than the classical Grignard reagents and in the conjugated enone system ($PhC^4H=C^3HC^2OPh$) C^2 (carbonyl carbon) is harder than C^4 in acidity. Thus the attack of [RYbI] is preferred at the harder site (C^2) leading to the l,2-addition product selectively.[6] Furthermore, the reaction of PhYbI with cinnamyl alcohol ($PhCH=CHCH_2OH$) led to 2,3-diphenyl-l-propanol (**$PhCH_2CHPhCH_2OH$**) in moderate yield. The Grignard reagents [PhMgI] did not induce this type of addition.[6]

[RLnI] are very active precursors in important processes such as alkene and alkyne reduction,[37-40] alkene polymerisation,[41-43] carbonyl[44-46] and saturated C–H activation,[47, 48] hydrosilylation[49] and olefin hydroamination.[50]

Moreover, Li and Zhang reported a direct access to a quaternary carbon centre utilising the pseudo-Grignard reagent ($CH_2=CHCH_2SmBr$). They were able to prepare 2,2-diallylated nitrogen heterocycles in good yield by addition of one mole of lactam to two moles of the pseudo-Grignard reagent under mild conditions (eqn. 2.11).[51]
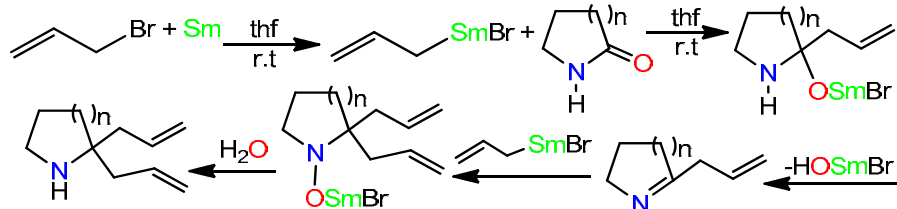
Equation 2.11

The pseudo-Grignard reagents of trivalent lanthanoids [(Ph$_3$C)$_2$LnCl] described in (eqn. 2.6) gave similar reactivity toward organic transformations (eqn. 2.12) as pseudo-Grignard species of divalent lanthanoids [RLnI] described in (eqn. 2.10) and magnesium based Grignard reagents [RMgX][52].
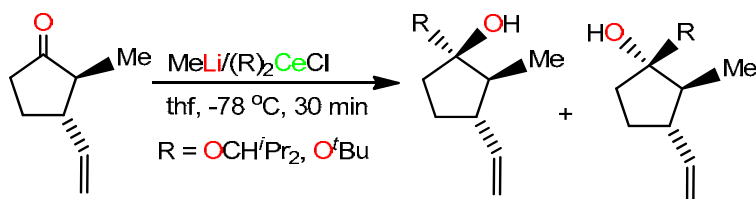
Equation 2.12

Pseudo-Grignard reagents have been investigated in a number of organic and inorganic transformations in recent years.[4, 6, 53] For example, a new pseudo-Grignard reagent involving a thiolate [(SAr)YbI(thf)$_n$] has been prepared by the protolysis reaction between HSAr and [(F$_3$CPh)YbI] (Ar = 2,6-Trip$_2$C$_6$H$_3$; Trip 2,4,6-^{i}Pr$_3$C$_6$H$_2$) (eqn. 2.13).[54]
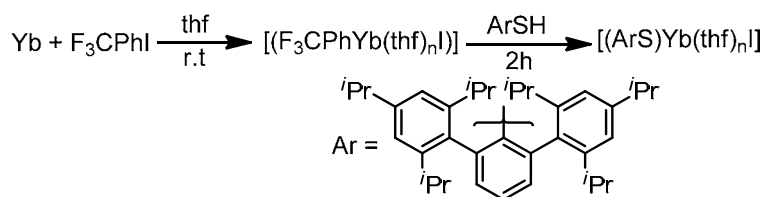
Equation 2.13

The oxidative addition of α-iodothiophene and bromo/iodo penta-fluorobenzene to lanthanoid metals has been successfully employed to synthesise a new organometallic complex of stannane [ArSnPh₃] (eqn. 2.14).[4]

$$Ln + ArX \xrightarrow[-10\,^{\circ}C]{thf} [ArLnX] \xrightarrow[20\,^{\circ}C]{Ph_3SnCl,\ thf} [ArSnPh_3] + LnClX$$

Ln = Sm; Eu; Yb, X = Br; I, ArX =
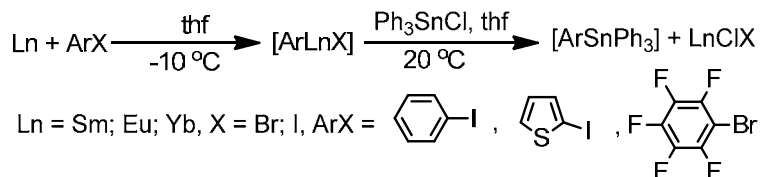
Equation 2.14

Moreover, monohydrosilanes can be prepared selectively via the reaction of excess divalent organoytterbium complexes [RYbI] with a dihydrosilane under mild conditions (eqn. 2.15).[53]

$$Yb + R\text{-}I \xrightarrow{thf,\ 0\,^{\circ}C} [RYbI] \xrightarrow[r.\,t.]{R'R''SiH_2} RR'R''SiH$$

R = aryl or alkyl
R' = Me; R" = Ph
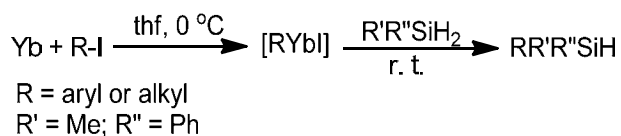
Equation 2.15

2.2 Current Study

This chapter presents uncharted divalent organoytterbium halide complexes. The reaction between the pseudo-Grignard reagents [PhYb(thf)$_n$X] (X = Br, I) and formamidines has been investigated to increase the scope of the organolanthanoid-halide system. The protolysis reaction between a formamidine (FormH) and phenylytterbium-halide produced two kinds of complexes. The usual products are dinuclear complexes bridged by bromide or iodide for example, [Yb(XylForm)(thf)$_2$Br]$_2$ **2.1a**, [Yb(DippForm)(thf)$_2$Br]$_2$.thf **2.2**, [Yb(MesForm)(thf)$_2$Br]$_2$ **2.3** and [Yb(MesForm)(thf)$_2$I]$_2$ **2.5** {Form = (ArNCHNAr), XylForm (Ar = 2,6-Me$_2$-C$_6$H$_3$), MesForm (Ar = 2,4,6-Me$_3$-C$_6$H$_2$), DippForm (Ar = 2,6-^{i}Pr$_2$-C$_6$H$_3$)}. While, the rare products are mononuclear such as [Yb(EtForm)$_2$(thf)$_2$Br] **2.4**, EtForm (Ar = 2,6-Et$_2$-C$_6$H$_3$). Reaction with europium led to the isolation of [EuI(μ–I)(dme)$_2$]$_2$ **2.7** which is one of the Schlenk equilibrium components.

This study also involved the exploration of the reactivity possibilities between pseudo-Grignard species described above and different kind of ketones such as 1,4-benzoquinone, 9-fluorenone and benzil.

Different studies have been performed to explore the nature of the solvated halide (iodide or bromide) derivatives of formamidinatolanthanoid complexes in the solid-state and in solution using techniques such as X-ray, IR, ^{1}H-NMR, microanalysis and melting point (providing thermal stability information).

2.3 Results and discussion

2.3.1 Synthesis

Scheme 2.1 shows the one pot pseudo-Grignard reaction used in this study. Freshly filed Yb metal powder was stirred at -78 °C in thf with phenyl halide (iodobenzene or bromobenzene) until a dark red or red-brown colour was observed in the solution (after 5 minutes). This was followed by addition of the protic ligand, XylFormH, DippFormH, EtFormH or MesFormH to form new pseudo-Grignard species for example, [Yb(Form)(thf)$_2$Br]$_2$ and [Yb(Form)(thf)$_2$I]$_2$ (Form = XylForm, DippForm, EtForm, MesForm). Complex [Yb$_2$(MesForm)(FusForm)(μ–I)(thf)$_2$]$_2$.2toluene (**2.6**) was isolated from recrystallisation attempts of [Yb(MesForm)(thf)$_2$I]$_2$ (**2.5**) in toluene and heating overnight to 100 °C. At these elevated temperatures the FusForm ligand (Scheme 2.1) formed presumably after a C-H activation of the *ortho* CH$_3$ occurred, followed by coupling with the backbone carbon of the formamidine which led to form a new heterocyclic ring.

The pseudo-Grignard reactions described in scheme (2.1) presumably produce +2 or +3 valent complexes of the type [PhLn(solv)$_n$X] or [Ph$_2$Ln(solv)$_n$X] (X = I, Br) followed by protolysis/ligand exchange of Ph–Ln bonds with FormH and concomitant formation of PhH. Evans and co-workers have found the divalent species is the dominant product for the oxidative addition of alkyl halide to lanthanoid metals in the zero oxidation state particularly for Eu^{+2} (99%) but less for Yb^{+2} (85%) and Sm (50%).[16, 3]

Deacon *et al.* have reported the presence of [YbPh$_3$(thf)$_3$] in the pseudo-Grignard reaction mixture.[55] Therefore, the formation of the Yb^{+3} compound such as [Yb(XylForm)$_3$] **2.1b** is plausibly from the formation of [YbPh$_3$] in the pseudo-Grignard reaction mixture according to the suggested route (eqn. 2.16) followed by protolysis by XylFormH.

$$3Yb + 4PhBr \rightleftharpoons PhYbBr + Ph_3Yb + YbBr_3 \qquad (i)$$
$$Ph_3Yb + 3XylFormH \longrightarrow [Yb(XylForm)_3] + 3PhH \qquad (ii)$$
$$2PhYbBr + 2XylFormH \longrightarrow [(XylForm)Yb(thf)_2Br]_2 + 2PhH \quad (iii)$$
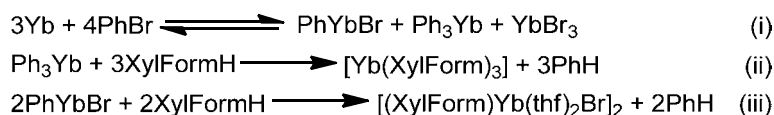
Equation 2.16

Mixed oxidation state rare earth (+2/+3) metal–organic compounds are moderately uncommon, especially charge separated complexes[56]. However, a mixture of divalent and trivalent derivatives of ytterbium present in solutions of "[PhYbI]" allows these species to become more accessible. Deacon *et al.* have isolated the mixed divalent and trivalent [{Yb(dme)$_4$}{YbPh$_4$(dme)}$_2$] compound by fractional crystallisation of [PhYbI(dme)$_n$] at -25 ^{o}C which supports the view that the oxidative reaction of Ln metals by halide alkyls produce mixed Ln (+2/+3) species.[22]

Hamidi et al[57] also reported that a mixture of divalent and trivalent ytterbium species were isolated from the ytterbium reactions, while the europium reaction gave only divalent compounds except [Eu(XylForm)I(OH)(thf)$_2$]$_2$[57] reflecting the greater stability of divalent europium species compared with ytterbium species.[16, 3]

The main difficulty associated with isolation of the pseudo-Grignard reagent is the lower solubility of solvated ytterbium diiodides [YbI$_2$] which precipitated/crystallised from the mother liquor as undesired product (being part of the Schlenk equilibrium) before isolation of the mono-halide products [Yb(Form)I(solv)$_n$]. Decomposition of the highly air sensitive pseudo-Grignard reagent was also problematic leading to the low yields of some complexes.

Following the same route described earlier to synthesise pseudo-Grignard reagents of the lanthanoids, we turned to the heavy alkaline earth metals (Ca, Sr, Ba) (eqn. 2.17) to prepare their analogues, but all attempts to isolate any components involving pseudo-Grignard reagents of these heavy metals were unsuccessful.

$$M + PhX + FormH \xrightarrow{\text{thf/-78 }^{\circ}\text{C, 3 h}} \text{Unsucessful}$$

M = Ca; Sr,;Ba, X = I; Br, FormH = XylFormH; DippFormH
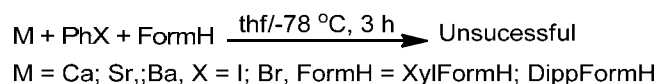
Equation 2.17

2.3.2 Reactivity

Scheme 2.1 shows the addition of a ketone, for example, 1,4-benzoquinone, 9-fluorenone or benzil to the pseudo-Grignard reaction mentioned above enabling us to explore the reactivity of the pseudo-Grignard species towards a carbonyl group. Complexes [Yb(MesForm)$_3$].Ph$_3$ (**2.8**) and [Yb(MesForm)$_3$].fluorene (**2.9**) were isolated from the pseudo-Grignard reaction mixture with common features for example, both are Yb^{+3} complexes and have a deoxygenated ketone in the lattice of the X-ray crystal structure in the solid state. The deoxygenation process of 1,4-benzoquinone of [Yb(MesForm)$_3$].Ph$_3$ and 9-fluorenone of [Yb(MesForm)$_3$].fluorene is not clear but it is possible the excess metal used may have influenced this, due to the highly oxophilic nature of the metals. Compound [(DippFormH$_2$)$-\mu-$(I)$-$]$_n$.benzil **2.10** was synthesised through the hydrolysis process of [Yb(DippForm)I)] in presence of benzil according to the suggested route (eqn. 2.18).

$$2Yb + 2PhI \xrightarrow[-78\ ^{\circ}\text{C}]{\text{thf}} 2PhYbI + 2DippFormH \xrightarrow[-78\ ^{\circ}\text{C}]{\text{thf}} 2[Yb(DippForm)I]$$

$$[DippFormH_2-\mu-I]_2.\text{benzil} + 2[Yb(OH)_3] \xleftarrow[\text{Benzil}]{6H_2O}$$
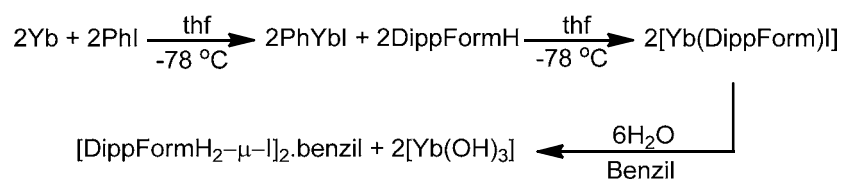
Equation 2.18
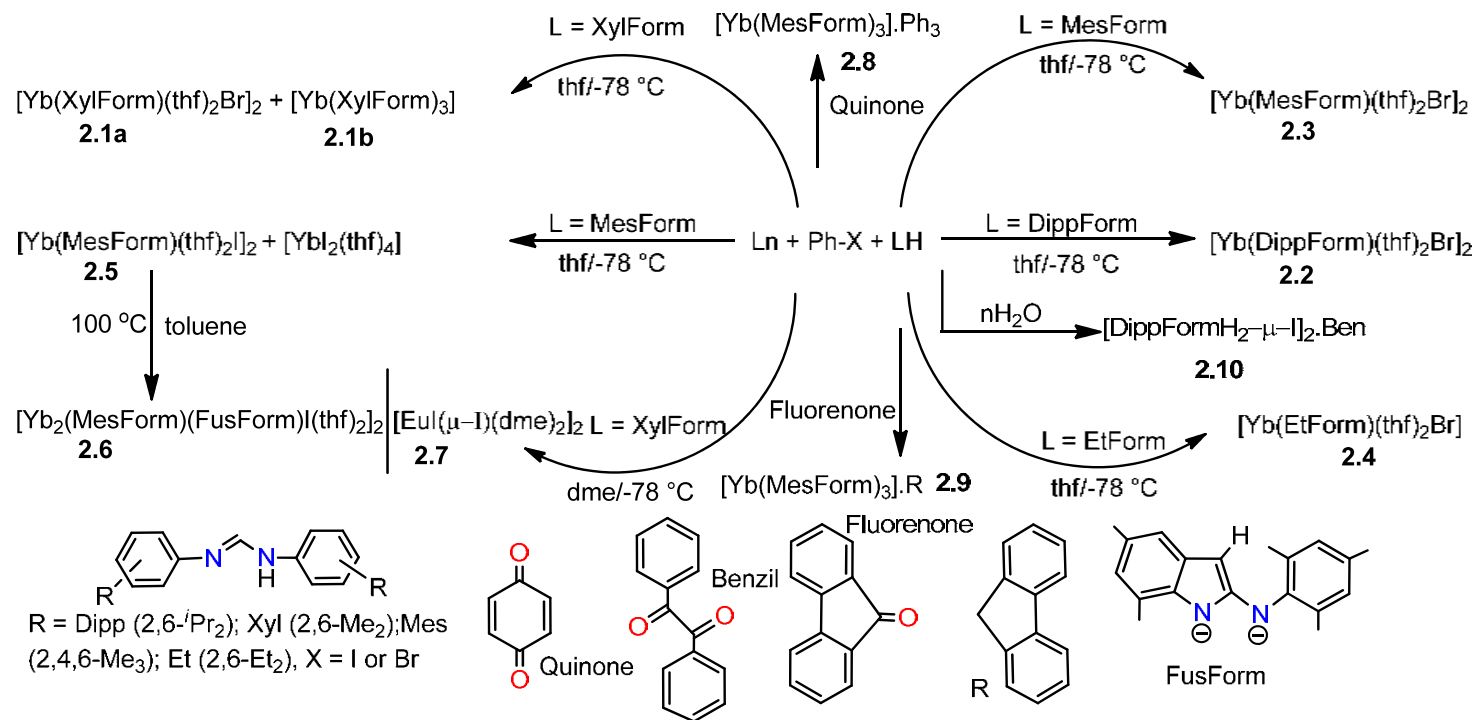
Scheme 2.1 Synthesis and reactivity of formamidinatolanthanoid halide complexes.

2.3.3 Characterisation

All products displayed in scheme 2.1 were isolated from the reaction mixture by filtration from residual metal and then fractional crystallisation from thf (**2.1a**, **2.1b 2.2**, **2.3**, **2.4, 2.5**, **2.8**, **2.9**), or the solution evaporated to dryness under vacuum and recrystallisation from toluene {[Yb$_2$(MesForm)(FusForm)I(thf)$_2$]$_2$.2toluene (**2.6**)}. Only [EuI(μ–I)(dme)$_2$]$_2$ (**2.7**) was isolated from dme. [(DippFormH$_2$)–μ–I]$_n$.benzil (**2.10**) was isolated after hydrolysis of the pseudo-Grignard reagent [Yb(DippForm)I]. The highest yield of 66 % was observed for [Yb(MesForm)I(thf)$_2$]$_2$ (**2.5**).

Pseudo-Grignard complexes [Yb(Form)(thf)$_2$X] (X = Br, I) displayed in scheme 2.1 were initially isolated as single crystals, and were identified by X-ray crystallography using the MX1 beamline at the Australian Synchrotron. These were further supported by IR spectroscopy (Table 2.1), elemental analyses, ^{1}H-NMR (Table 2.2) and melting point analysis.

The ratios of solvent to ligand for some complexes are not the same as established in the solid state X-ray crystal structure and that supported by the ^{1}H-NMR spectra which showed the loss of some thf of solvation under vacuum which were also indicated by microanalyses for some complexes such as (**2.1a**, **2.3**). For example, the ^{1}H-NMR spectrum of [Yb(XylForm)(thf)$_2$Br]$_2$ **2.1a** reveals the loss of one thf molecule as shown by the integration of two resonances at δ = 3.57 and 1.33 where a Form (24 ^{1}H; CH$_3$): thf (12 ^{1}H; O-CH$_2$) ratio of 2 to 1 was found. The methine proton resonances (NCHN) in the ^{1}H-NMR spectra of **2.1a**, **2.2**, **2.3** are shifted to higher frequencies relative to the value for the neutral ligand. For example, the methine proton resonance occurs at δ = 7.72, 7.05 and 6.88 ppm for XylFormH, DippFormH and MesFormH, respectively, and at δ = 8.08, 8.12 and 8.44 ppm in **2.1a, 2.2, 2.3** respectively.

The ^{1}H-NMR spectra of **2.4**, **2.8**, **2.9** gave a broadened spectrum, which could not be satisfactorily integrated presumably due to the presense of paramagnetic Yb^{+3} consistent with what Evans indicated in 1971[3], being a mixture of Yb^{+2}/Yb^{+3}. The paramagnetic Eu^{+2} complex $[EuI(\mu–I)(dme)_2]_2$ **2.7** gave an interpretable ^{1}H-NMR spectrum which is paramagnetically shifted $\delta = 3.12$ (s, 6H, CH$_3$), 3.35 (s, 4H, CH$_2$). The normal chemical shifts of dme are $\delta = 0.27$ (s, 12H, CH$_3$), 1.33 (s, 8H, CH$_2$).

The IR spectra of all pseudo-Grignard species showed complete deprotonation of the formamidine reagents. This was indicated by the absence of a $\nu(N–H)$ absorption usually observed at 3300-3100 cm^{-1} coupled with the lack of a NH resonance in the ^{1}H-NMR spectra of the bulk vacuum dried materials.

The N–C stretching (Table 2.1) for compounds **2.1-2.10** showed absorptions for a metal-coordinated formamidinate group observed at 1643-1723 cm^{-1}.

Table 2.1 N–C Stretching in IR spectra of 2.1-2.9 (v4000-400 cm^{-1}).

Compound	N–C stretching vibration (cm^{-1})
[Yb(XylForm)Br(thf)$_2$]$_2$ (**2.1a**)	1649
[Yb(DippForm)Br(thf)$_2$]$_2$ (**2.2**)	1667
[Yb(MesForm)Br(thf)$_2$]$_2$(**2.3**)	1643
[Yb(EtForm)$_2$Br$_2$(thf)$_2$] (**2.4**)	1686
[Yb(MesForm)I(thf)$_2$]$_2$ (**2.5**)	1646
[Yb$_2$(MesForm)(FusForm)$(\mu-I)$(thf)$_2$]$_2$ (**2.6**)	1649
[Yb(MesForm)$_3$].Ph$_3$ (**2.8**)	1723
[Yb(MesForm)$_3$].Fluorene (**2.9**)	1665

Table 2.2 Chemical shifts in ^{1}H-NMR spectra of 2.1-2.10.

^{1}H-NMR	Chemical shift (ppm)					
	2.1a	**2.2**	**2.3**	**2.5**	**2.7**	**2.10**
NC(H)N	8.08	8.12	8.44	8.03	–	–
Aromatic	7.58, 6.18	6.98, 6.23	6.77	7.05	–	7.16
CH	–	3.15	–	–	–	2.13
OCH$_2$, thf	3.57	3.85	3.19	3.29	–	–
CH$_2$, thf	1.33	1.45	1.12	0.94	–	–
CH$_3$	1.75	1.37	2.41, 1.71	1.22, 1.16	0.27, 0.90	1.09
CH$_2$	–	–	–	–	1.33, 2.10	
						3.63

2.3.4 Crystal structure determinations

[Yb(RForm)(thf)₂Br]₂ (R = Xyl 2.1a, Dipp 2.2, Mes 2.3)

Complex [Yb(XylForm)(thf)$_2$Br]$_2$ (**2.1a)** crystallises in the monoclinic space group $P2_1/c$ while complexes [Yb(DippForm)(thf)$_2$Br]$_2$.thf (**2.2**) and [Yb(MesForm)(thf)$_2$Br]$_2$ (**2.3**) crystallise in the triclinic space group P-1 (Table 2.5). Compounds **2.1a** (Fig. 2.1) adopts a centrosymmetric dimer configuration. Half of the structure is generated by symmetry through an inversion centre situated at the midpoint of the Yb(1)···Yb(1)# vector. The geometry around the six-coordinate ytterbium metal centre is best described as a distorted octahedral, with its coordination sphere consisting of two κ^2-bound Form ligands and two thf molecules in addition to two bridging bromide ions. Complex **2.1a** (Fig. 2.2) is isostructural with **2.2** and **2.3** albeit crystallising in different space groups. Complex **2.2** has one thf molecule in X-ray crystal structure lattice.

X = Br, I; R = 2,4,6-Me$_3$; 2,6-Me$_2$; 2,6-^{i}Pr$_2$
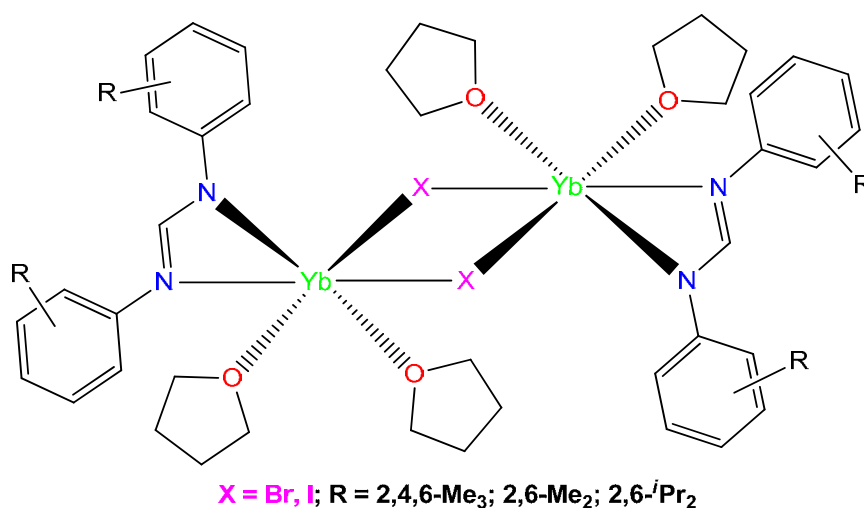
Figure 2.1 Diagram of dinuclear pseudo-Grignard compounds 2.1-2.3.
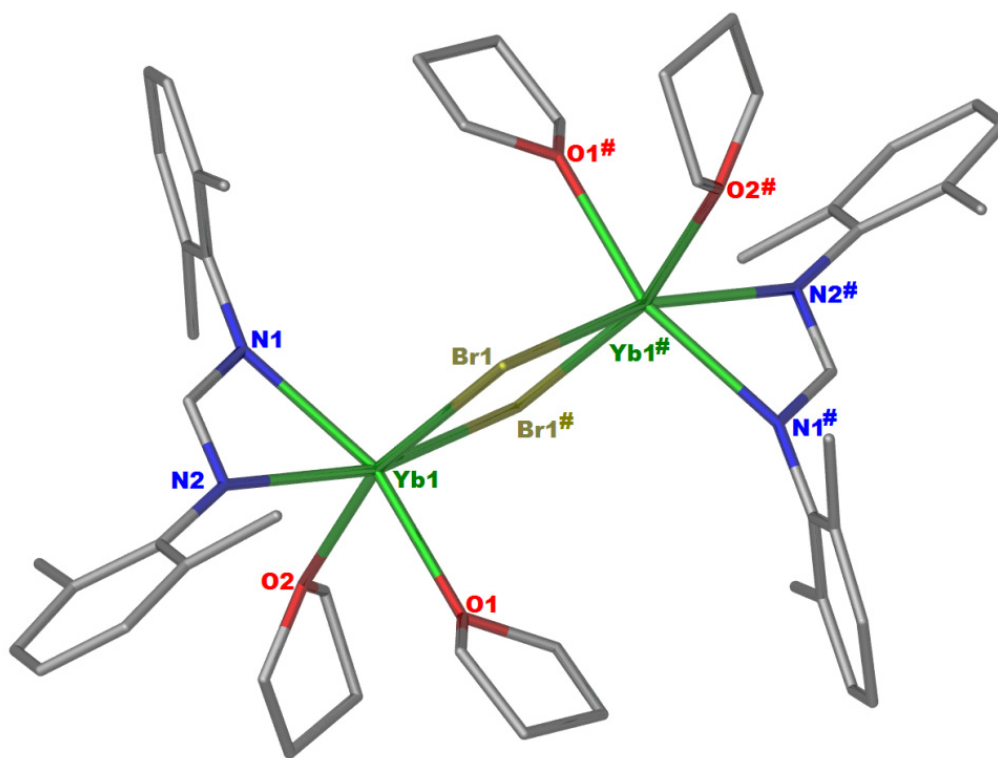
Figure 2.2 X-ray crystal structure of [Yb(XylForm)(thf)$_2$Br]$_2$ 2.1a. Hydrogen atoms are omitted for clarity. # = Atoms generated by symmetry: 1-X, 1-Y, 1-Z.

Selected bond lengths and angles of **2.1-2.3** are listed in Table 2.4. The average Yb–N bond lengths in [Yb(XylForm)(thf)$_2$Br]$_2$ **2.1a** is 2.43 Å, which is smaller than the average Yb–N bond lengths (2.46 Å) reported for [Yb(XylForm)$_2$(thf)$_2$][58] while it is close to the average Yb–N bond lengths (2.42 Å) reported for [YbL$_2$(thf)$_2$][59] (L = {N(C$_6$H$_3$-^{i}Pr$_2$-2,6)(2-C$_5$H$_3$N-6-Me)}). The average Yb–O$_{(thf)}$ bond lengths in **2.1a** is 2.42 Å which is similar to the average Yb–O bond lengths (2.42 Å) reported for [Yb(XylForm)$_2$(thf)$_2$][58]. The average Yb–N bond lengths in [Yb(DippForm)(thf)$_2$Br]$_2$ **2.2** is 2.45 Å, which is smaller than the average Yb–N bond lengths (2.47 Å) reported for [Yb(DippForm)$_2$(thf)$_2$][58] and [YbL$_2$(thf)$_2$][60] (L = Ph-C(NSiMe$_3$)$_2$). However, it is similar to the average Yb–N bond lengths (2.45 Å) reported for K[YbL$_3$][61] (L = (N(CH$_2$Bu^t)(2-C$_5$H$_3$N-6-Me). The average Yb–O$_{(thf)}$ bond lengths in **2.2** is 2.42 Å which

is smaller than the average Yb–O bond lengths (2.46 Å) reported for [Yb(DippForm)$_2$(thf)$_2$],[58] while it is comparable to the average Yb–O$_{(thf)}$ bond lengths (2.41 Å) reported for [YbL$_2$(thf)$_2$] (L = Ph-C(NSiMe$_3$)$_2$).[60]

The average Yb–N bond lengths in [Yb(MesForm)(thf)$_2$Br]$_2$ **2.3** is 2.44 Å, which is smaller than the average Yb–N bond lengths (2.46 Å) reported for [Yb(MesForm)$_2$(thf)$_2$][58]. However, it is similar to the average Yb–N bond lengths (2.44 Å) reported for [YbL$_2$(thf)$_2$][62] (L = 2,6-^{i}Pr$_2$-ph)-[6-(2,4,6-^{i}Prph)-pyridin-2-yl]-amine). The average Yb–O$_{(thf)}$ bond lengths in **2.3** is 2.41 Å which is smaller than the average Yb–O bond lengths (2.44 Å) reported to [Yb(MesForm)$_2$(thf)$_2$].[58]

The difference between the average Yb–N bond lengths of **2.1a**, **2.2** and the average Ca–N bond lengths of [LCa(thf)$_2$Cl]$_2$ (L = {(2,6-^{i}Pr$_2$C$_6$H$_3$)-NC(Me)}$_2$).[63] were found to be 0.03 Å, 0.01 Å respectively which is close to the difference between the ionic radii (0.02 Å) between Yb^{+2} and Ca^{+2} for six coordinate complexes.[64] The difference between the average Yb–N bond lengths of **2.3** and the average Ca–N bond lengths of [LCa(thf)$_2$Cl]$_2$ (L = {(2,6-^{i}Pr$_2$C$_6$H$_3$)-NC(Me)}$_2$)[63] was found to be 0.02 Å which is similar to the difference between the ionic radii between Yb^{+2} and Ca (0.02 Å) for six coordinate.[64]

The Yb–Br and the Yb–Br# bond lengths of **2.1a** and **2.3** are 2.9117(7); 2.9168(7) Å, 2.8706(10), 2.9212(10) Å respectively are comparable to the corresponding Yb–Br bond lengths (2.8995(2), 2.9233(2) Å) reported for the five-coordinate [Yb(C$_5$Ph$_4$H)(thf)$_2$Br]$_2$[65] while the Yb–Br and the Yb–Br# bond lengths (2.8927(7); 2.8987(11) Å) of **2.2** is slightly shorter than the corresponding Yb–Br bond lengths (2.8995(2), 2.9233(2) Å) reported for the five-coordinate [Yb(C$_5$Ph$_4$H)(thf)$_2$Br]$_2$[65].

The Yb–Br and Yb–Br# bond lengths 2.9117(7); 2.9168(7) Å in **2.1a** are the same as Ca–Br, Ca–Br# 2.9142(6), 2.9138(7) of [LCa(thf)$_3$Br]$_2$ L = 9-phenanthryl[66], and the

average Yb–Br and Yb–Br# bond lengths in **2.2** and **2.3** are 0.02, 0.02 Å less than the average Ca–Br bond lengths in six-coordinate [LCa(thf)$_3$Br]$_2$ L = 9-phenanthryl[66], which is same as the 0.02 Å ionic radii difference between divalent six-coordinate ytterbium and calcium.[64]

[Yb(XylForm)$_3$] (2.1b)

Yb^{+3} complex [Yb(XylForm)$_3$] (**2.1b**) was isolated by fractional crystallisation from the mother liquor of **2.1a** as another component of the Schlenk equilibrium involving trivalent species. Complex **2.1b** crystallises in the monoclinic space group *P*2$_1$/*n* (Table 2.5). Compound **2.1b** exhibits a mononuclear Yb^{+3} complex which is similar in structure to the literature complexes [Sm(XylForm)$_3$][67] and [Yb(MesForm)$_3$][67]. The six-coordinate Yb^{+3} metal centre displays distorted octahedral geometry and is coordinated by three bidentate XylForm ligands through the nitrogen donor atoms.

Selected bond lengths and angles of **2.1b** are listed in Table 2.3. The average Yb–N bond lengths of **2.1b** found to be 2.33 Å which is slightly shorter than the average Yb–N bond lengths (2.35 Å) reported for [Yb(MesForm)$_3$][67] and significantly shorter than the average Yb–N bond lengths (2.43 Å) reported for [Sm(XylForm)$_3$][67] due to the metal size differences.
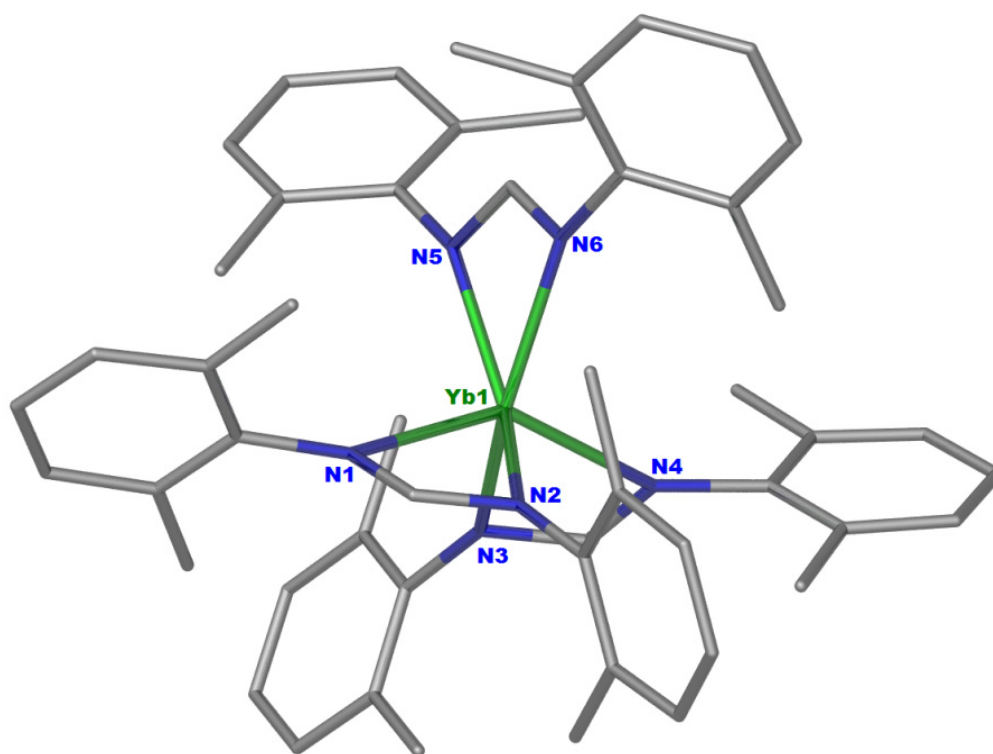
Figure 2.3 X-ray crystal structure of [Yb(XylForm)₃] 2.1b. Hydrogen atoms are omitted for clarity.

Table 2.3 Selected bond lengths and angles of [Yb(XylForm)₃], [Sm(XylForm)₃][67] and [Yb(MesForm)₃].[67]

Bond lengths (Å)	[Yb(XylForm)₃]	[Sm(XylForm)₃]	[Yb(MesForm)₃]
Ln(1)–N(1)	2.340(7)	2.447(7)	2.348(3)
Ln(1)–N(2)	2.352(8)	2.425(7)	2.375(3)
Ln(1)–N(3)	2.323(8)	2.431(7)	2.349(3)
Ln(1)–N(4)	2.337(8)	2.455(8)	2.354(3)
Ln(1)–N(5)	2.347(8)	2.421(7)	2.348(3)
Ln(1)–N(6)	2.331(8)	2.438(7)	2.329(3)
Bond angles (°)			
N(1)–Ln(1)–N(2)	57.70(3)	55.30(2)	57.55(9)
N(3)–Ln(1)–N(4)	58.30(3)	55.20(3)	58.37(10)
N(5)–Ln(1)–N(6)	57.90(3)	56.20(3)	57.92(10)

[Yb(EtForm)$_2$(thf)$_2$Br] (2.4)

The mononuclear Yb^{+3} complex [Yb(EtForm)$_2$(thf)$_2$Br] was isolated instead of an expected Yb^{+2} complex [Yb(EtForm)(thf)$_2$Br]$_2$ due to rearrangement as part of the trivalent Schlenk equilibrium. Complex (**2.4**) crystallises in the triclinic space group *P*-1 (Table 2.5). Figure (2.4) is a monomeric Yb^{+3} complex with two chelating XylForm ligands. Half of the complex is generated by a two-fold rotation axis. The coordination sphere around the seven coordinate Yb^{+3} in **2.4** is best described as a distorted pentagonal bipyramidal. [Yb(EtForm)$_2$(thf)$_2$Br] is analogous to the previously reported Yb^{+3} complex [Yb(XylForm)$_2$(dme)I][57] and supports the Ln^{+3} component present in the pseudo-Grignard system for Yb.

A notable feature of compound **2.4** is that the formation of the monomer is favoured over a dimer. The formation of halide[65, 68] bridged dimers have been more widely observed for ytterbium (Figure 2.5) organohalide complexes.
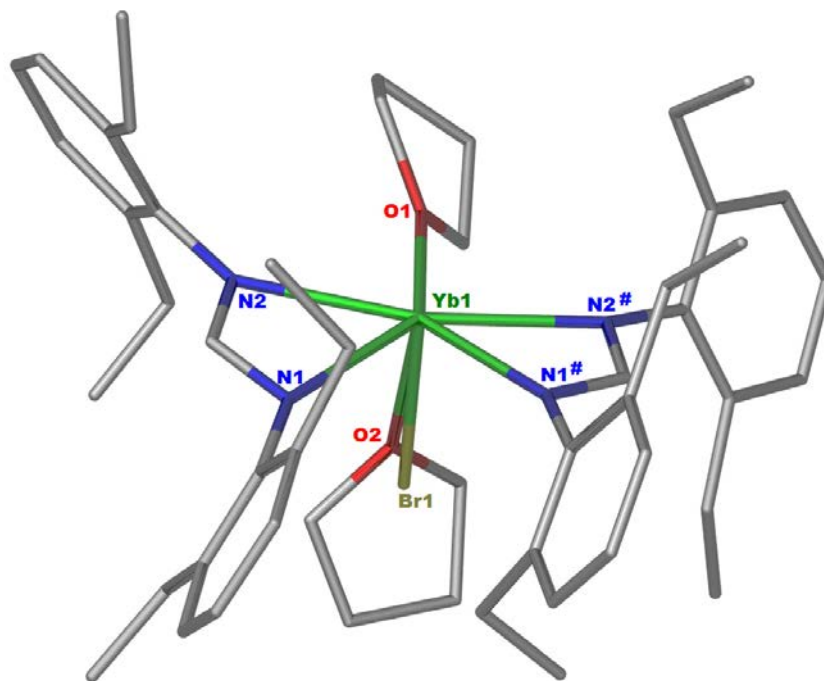
Figure 2.4 X-ray crystal structure of [Yb(EtForm)$_2$(thf)$_2$Br] 2.4. Hydrogen atoms are omitted for clarity. # = Atoms generated by symmetry: 1-X, Y, 1/2-Z.

Selected bond lengths and angles of **2.4** are listed in Table 2.4. In the literature there is no example of Yb^{+3} with seven coordination including bromide except $[Yb_2Se_3Br_2(py)_6]$ (py = pyridine).[68] The average Yb–N bond lengths of **2.4** were found to be 2.41 Å which is longer than the average Yb–N bond lengths (2.37 Å) reported for $[Yb(XylForm)_2(dme)I]$,[57] presumably due to the steric demand differences between XylForm and EtForm as well as the influence of chelating dme vs unidentate thf. Moreover, it is longer than the average Yb–N bond lengths (2.36 Å) reported for $[YbL(thf)_2Cl]_2$ {L = $(C_4H_3N\text{-}CH_2)_2\text{-}NMe$}.[69] However, it is in agreement with the average Yb–N bond lengths (2.41 Å) reported for $[YbL(ArO)(dme)]$ {L = $Me_3SiNCPhN(CH_2)_3NCPhNSiMe_3$; Ar = 2, $6\text{-}^tBu_2\text{-}C_6H_2\text{-}4\text{-}Me$}[70]. Figure 2.5 shows some known bromide-bridged dimeric and non-dimeric Yb^{+2} and Yb^{+3} complexes.[68, 71-75]
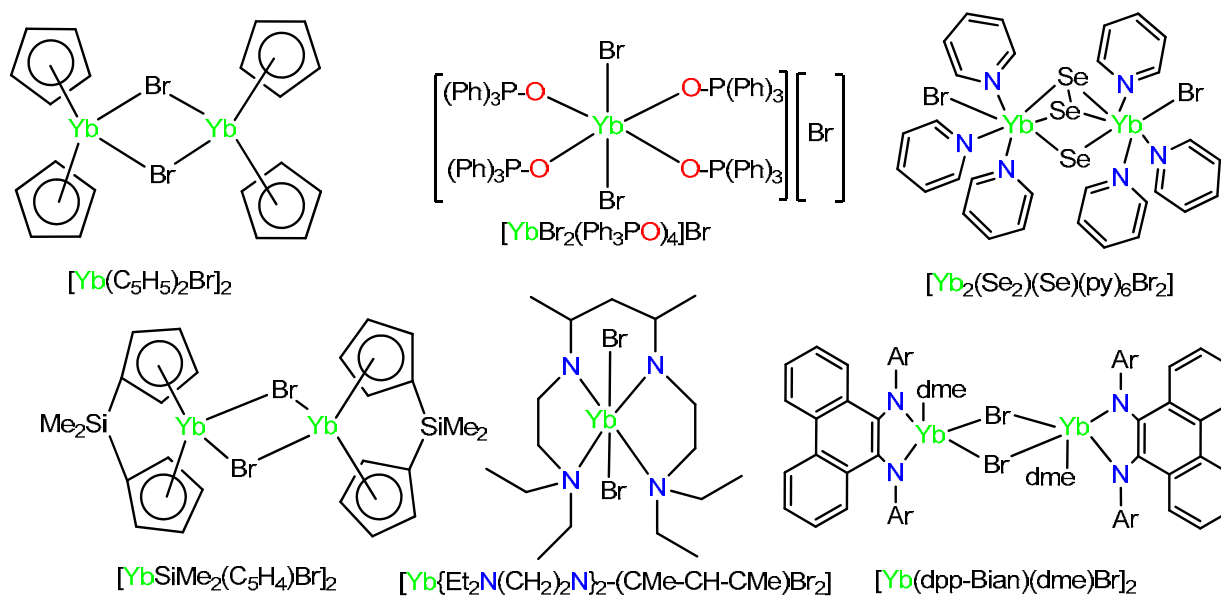
Figure 2.5 Dimeric and non-dimeric Yb^{+2} and Yb^{+3} complexes.[68, 71-75]

Table 2.4 Selected bond lengths and angles of 2.1-2.4

Bond lengths (Å)	[Yb(XylForm)Br(thf)$_2$]$_2$	[Yb(DippForm)Br(thf)$_2$]$_2$	[Yb(MesForm)Br(thf)$_2$]$_2$	[Yb(EtForm)$_2$Br(thf)$_2$]
Yb(1)–N(1)	2.408(4)	2.429(3)	2.435(3)	2.400(12)
Yb(1)–N(2)	2.468(4)	2.483(3)	2.464(3)	2.425(12)
Yb(1)–O(1)	2.414(4)	2.421(3)	2.389(3)	2.330(2)
Yb(1)–O(2)	2.433(4)	2.426(3)	2.437(3)	2.430(3)
Yb(1)–Br(1)	2.911(8)	2.892(7)	2.870(10)	2.688(4)
Bond angles (°)				
O(1)–Yb(1)–O(2)	82.76(17)	81.48(11)	78.08(11)	77.80(6)
O(1)–Yb(1)–Br(1)	97.90(10)	167.06(7)	88.57(8)	86.98(10)
N(1)–Yb(1)–Br(1)	107.16(9)	103.24(7)	106.05(8)	96.20(4)
N(2)–Yb(1)–Br(1)#	98.73(9)	101.35(7)	97.63(8)	-
Br(1)–Yb(1)–Br(1)#	86.558(18)	87.70(2)	87.26(3)	-
N(1)–Yb(1)–N(2)	56.02(13)	55.27(9)	55.90(10)	56.30(4)
N(1)–C(1)–N(2)	119.6(4)	118.7(3)	119.3(3)	118.90(13)

 # = atoms generate by symmetry: 1-X, 1-Y, 1-Z for 2.1a; 2.2; 2.3.

Table 2.5 Crystallographic data for compounds 2.1-2.4.

Compound	2.1a	2.1b	2.2	2.3	2.4
formula	$C_{50}H_{70}N_4O_4Br_2Yb_2$	$C_{52}H_{60}N_6Yb$	$C_{70}H_{110}N_4O_5Br_2Yb_2$	$C_{54}H_{78}N_4O_4Br_2Yb_2$	$C_{50}H_{70}N_4O_2BrYb$
fw	1297.03	942.13	1593.56	1353.11	1012.06
crystal system	monoclinic	monoclinic	triclinic	triclinic	monoclinic
space group	$P2_1/c$	$P2_1$	P-1	P-1	$C2/c$
a, Å	14.820(3)	19.962(4)	11.050(2)	10.744(2)	10.722(2)
b, Å	14.334(3)	10.537(2)	12.753(3)	11.766(2)	19.820(4)
c, Å	13.280(3)	20.919(4)	15.509(3)	13.059(3)	22.039(4)
α, deg	90	90	70.76(3)	95.27(3)	90
β, deg	113.64(3)	91.26(3)	78.96(3)	114.18(3)	99.23(3)
γ, deg	90	90	67.01(3)	110.39(3)	90
V, Å^3	2584(11)	4399(15)	1894(9)	1357(5)	4622(16)
Z	2	4	2	2	4
T, K	173(2)	173(2)	173(2)	173(2)	173(2)
no. of rflns collected	33191	56316	23066	22297	14677
no. of indep rflns	5764	19710	7949	6143	4069
R_{int}	0.035	0.028	0.045	0.025	0.077
Final R_1 values ($I > 2\sigma(I)$)	0.037	0.047	0.035	0.034	0.097
Final $wR(F^2)$ values ($I > 2\sigma(I)$)	0.098	0.118	0.096	0.086	0.232
Final R_1 values (all data)	0.041	0.047	0.036	0.035	0.099
Final $wR(F^2)$ values (all data)	0.106	0.118	0.097	0.087	0.233
$GooF$ (on F^2)	0.503	1.259	1.131	1.077	1.239

[Yb(MesForm)(thf)₂I]₂ (2.5)

The Yb^{+2} complex [Yb(MesForm)(thf)₂I]₂ (**2.5**) crystallises in the triclinic space group *P*-1 (Table 2.10). Compound **2.5** displays a dimeric structural motif and has two Yb metal centres bridged by two iodide ions and capped by terminal bidentate MesForm ligands. The six-coordinate Yb centre is best described as a distorted octahedron. This complex possesses an inversion centre which is situated on the midpoint of the Yb(1)···Yb(1)# vector. Complex [Yb(MesForm)(thf)₂I]₂ (**2.5**) is structurally similar to [Yb(XylForm)(thf)₂Br]₂ (**2.1a**) [Yb(DippForm)(thf)₂Br]₂ (**2.2**) and [Yb(MesForm)(thf)₂Br]₂ (**2.3**).
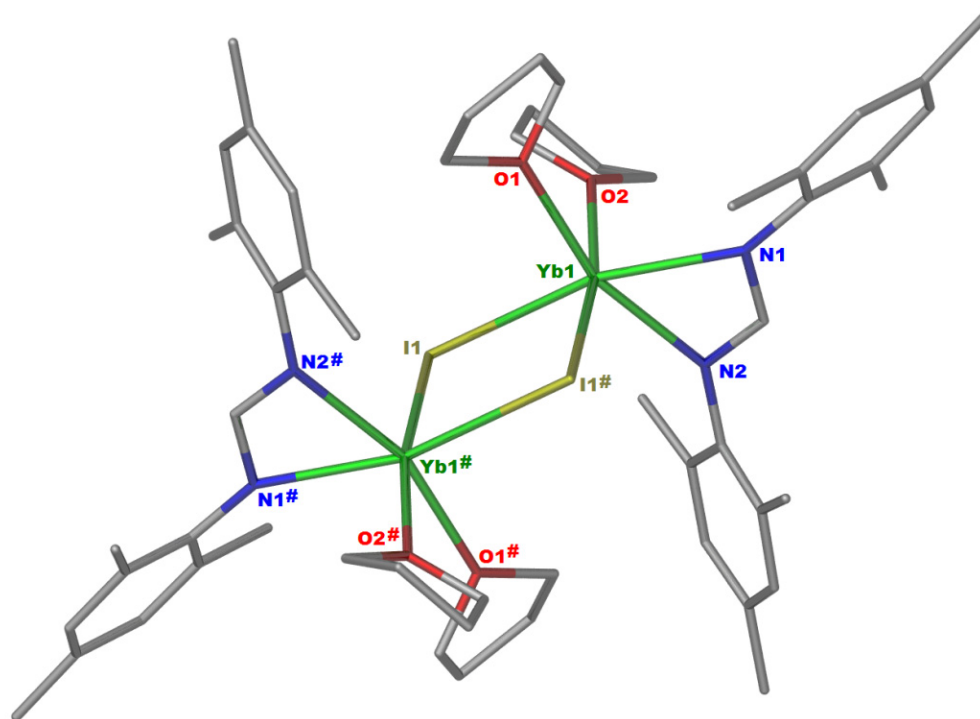
Figure 2.6 X-ray crystal structure of [Yb(MesForm)(thf)₂I]₂ 2.5. Hydrogen atoms are omitted for clarity. # = Atoms generated by symmetry: -X, 1-Y, 1-Z.

Selected bond lengths and angles of [Yb(MesForm)(thf)₂I]₂ are listed in Table 2.6. The average Yb–N bond lengths of **2.5** were found to be 2.43 Å which is shorter than the

average Yb–N bond lengths (2.46 Å) reported for [Yb(Ap)I]$_2$[76] {Ap = 2, 6-^{i}Pr$_2$-C$_6$H$_3$-N-C$_5$H$_3$N-6-(2, 4, 6- ^{i}Pr$_3$-C$_6$H$_2$)} presumably due to steric demand differences, while it is not suprisingly almost same as the average Yb–N bond lengths (2.43 Å) reported for [Yb(XylForm)I(thf)$_2$]$_2$.[57]

The Yb–N bond distances (2.446(4), 2.426(4) Å) in **2.5** are in agreement with the Ca–N bond distances 2.421(3), 2.431(2) Å in known six-coordinate Ca of [(Ar$_2$N$_3$)Ca(thf)$_2$I]$_2$ Ar = 2,6-diisopropylphenyl.[77]

The Yb–I and the Yb–I# bond lengths of [Yb(MesForm)(thf)$_2$I]$_2$ were found to be 3.0962(13); 3.1788(8) Å respectively which is comparable to the Yb–I and the Yb–I# bond lengths of [Yb(XylForm)(thf)$_2$I]$_2$[57] (3.1690(7); 3.1344(7) Å respectively) and [Yb(Ap)I]$_2$[76] (3.1225(10); 3.1241(8) Å respectively). Table 2.7 Shows the Yb–I bond lengths in the known ytterbium complexes containing a terminal iodide. Figure 2.9 shows some known iodide-bridged dimeric ytterbium(II) complexes (I[41], II[78], III[79], IV[80], V[81]).

The Yb–I and Yb–I# bond lengths 3.0962(13); 3.1788(8) Å respectively in **2.5** are approximately in agreement with the Ca–I, Ca–I# 3.1316(6), 3.0962(6) Å of [(Ar$_2$N$_3$)Ca(thf)$_2$I]$_2$ Ar = 2,6-diisopropylphenyl.[77] The average Yb–I bond lengths in **2.5** 0.02 Å are less than the average Ca–I bond lengths in six-coordinate [(Ar$_2$N$_3$)Ca(thf)$_2$I]$_2$ Ar = 2,6-diisopropylphenyl[77], which is same as the 0.02 Å ionic radii difference between divalent six-coordinate ytterbium and calcium.[64]
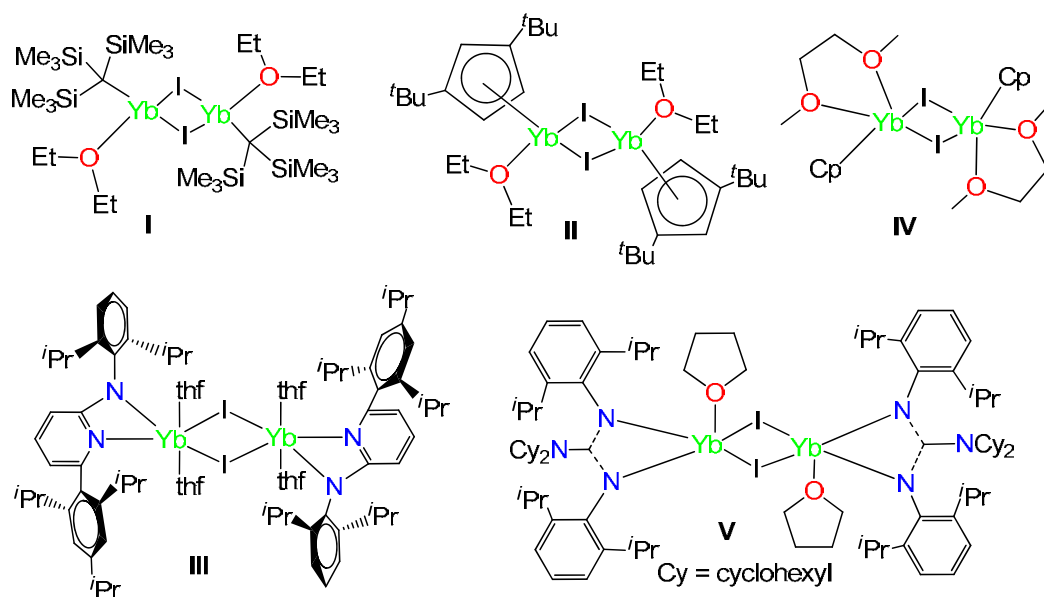
Figure 2.7 Iodide-bridged dimeric Yb^{+2} complexes (I[41], II[78], III[79], IV[80], V[81]).

[Yb$_2$(MesForm)(FusForm)(μ–I)(thf)$_2$]$_2$.2Toluene (2.6)

The unexpected Yb^{+2} [Yb$_2$(MesForm)(FusForm)(μ–I)(thf)$_2$]$_2$.2toluene (**2.6**) complex was isolated from the pseudo-Grignard reaction involving PhI, Yb and MesFormH. This complex was isolated from recrystallisation attempts of [Yb(MesForm)(thf)$_2$I]$_2$ (**2.5**) in toluene and heating overnight to 100 ^{o}C. Compound **2.6** crystallises in the triclinic space group *P*-1 (Table 2.10). Compound **2.6** displays a tetranuclear structure of a pseudo-Grignard reagent. The terminal ytterbium metal centres Yb(1) and Yb(4) bridge with the interior centres Yb(2) and Yb(3) by two iodide atoms and two FusForm ligands (Fig. 2.9). The seven coordinate terminal Yb centres {Yb(1) and Yb(4)} are best described as having distorted pentagonal bipyramidal geometry. The six coordinate internal centres {Yb(2) and Yb(3)} are best described as having distorted octahedral geometry.

This structure [Yb$_2$(MesForm)(FusForm)(μ–I)(thf)$_2$]$_2$ has interesting features. For example, there is an interesting η^6-intramolecular interaction between Yb and the phenyl group of the FusForm ligand to satisfy the electronic requirements of the metal. This

is an interesting phenomenon given there was thf bound but lost in boiling toluene. Moreover, the terminal metal centre Yb(1) and the interior metal centre Yb(2) are bridged by two different ligands, the FusForm and iodide.

In complex **2.6** the two nitrogen atoms N(1) and N(2) of the MesForm ligand and iodide ligand I(1) are approximately located in the same plane with the ytterbium metal Yb(1). However, O(1) of the thf molecule is located above the plane N(1)–Yb(1)–I(1). The phenyl group of the FusForm is approximately in the same plane as the ytterbium metal Yb(1). The N(3) atom of FusForm and iodide ligand I(1) are approximately in the same plane with the ytterbium metal Yb(2) while, the O(1) of the thf molecule and the N(4) atom of FusForm are on opposite sides of the plane I(I)–Yb(2)–N(5).

Selected bond lengths and angles of (**2.6**) are listed in Table 2.6. The average Yb–N bond lengths of the seven coordinate centres Yb(1) and Yb(4) were found to be 2.44 Å which is similar to the average Yb–N bond lengths 2.43 Å, 2.44 Å reported for $[Yb(Ph_2pz)(thf)_4I]^{[22]}$ and $[\{YbI(dme)_2\}_2(\mu_2–L)]$ (L = $(Me_3SiN(Ph)CN)_2(CH_2)_3)^{[82]}$ respectively. The average Yb–N bond lengths of the six coordinate centres Yb(2) and Yb(3) were found to be 2.54 Å which is longer than the average Yb–N bond lengths 2.43 Å determined for $[Yb(MesForm)(thf)_2I]_2$. Also, it is longer than the average Yb–N bond lengths 2.46 Å reported for $[Yb(Ap)I]_2^{[76]}$ {Ap = 2, 6-^{i}Pr$_2$-C$_6$H$_3$-N-C$_5$H$_3$N-6-(2, 4, 6-^{i}Pr$_3$-C$_6$H$_2$)}.

The Yb–I bond lengths of the seven coordinate centres Yb(1) and Yb(4) found to be 3.0807(12), 3.0777(12) Å respectively which are slightly shorter than Yb–I bond lengths 3.0966(6) Å reported for $[Yb(Ph_2pz)(thf)_4I]^{[22]}$. The Yb–I bond lengths of the six coordinate centres Yb(2) and Yb(3) found to be 3.1469(12), 3.1280(12) Å respectively which are longer than the Yb–I bond lengths 3.0962(13) Å calculated for

[Yb(MesForm)(thf)$_2$I]$_2$ but it is close to the Yb–I bond lengths 3.1225(10) Å reported for

[Yb(Ap)I]$_2$[76] {Ap = 2,6-^{i}Pr$_2$-C$_6$H$_3$-N-C$_5$H$_3$N-6-(2,4,6-^{i}Pr$_3$-C$_6$H$_2$)}. Table 2.7 Shows the

Yb–I bond lengths in the known ytterbium complexes containing a terminal iodide.
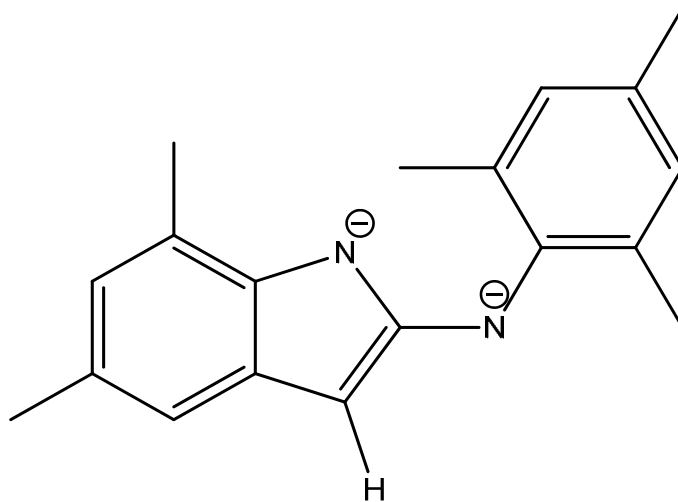
Figure 2.8 Diagram of FusForm ligand.
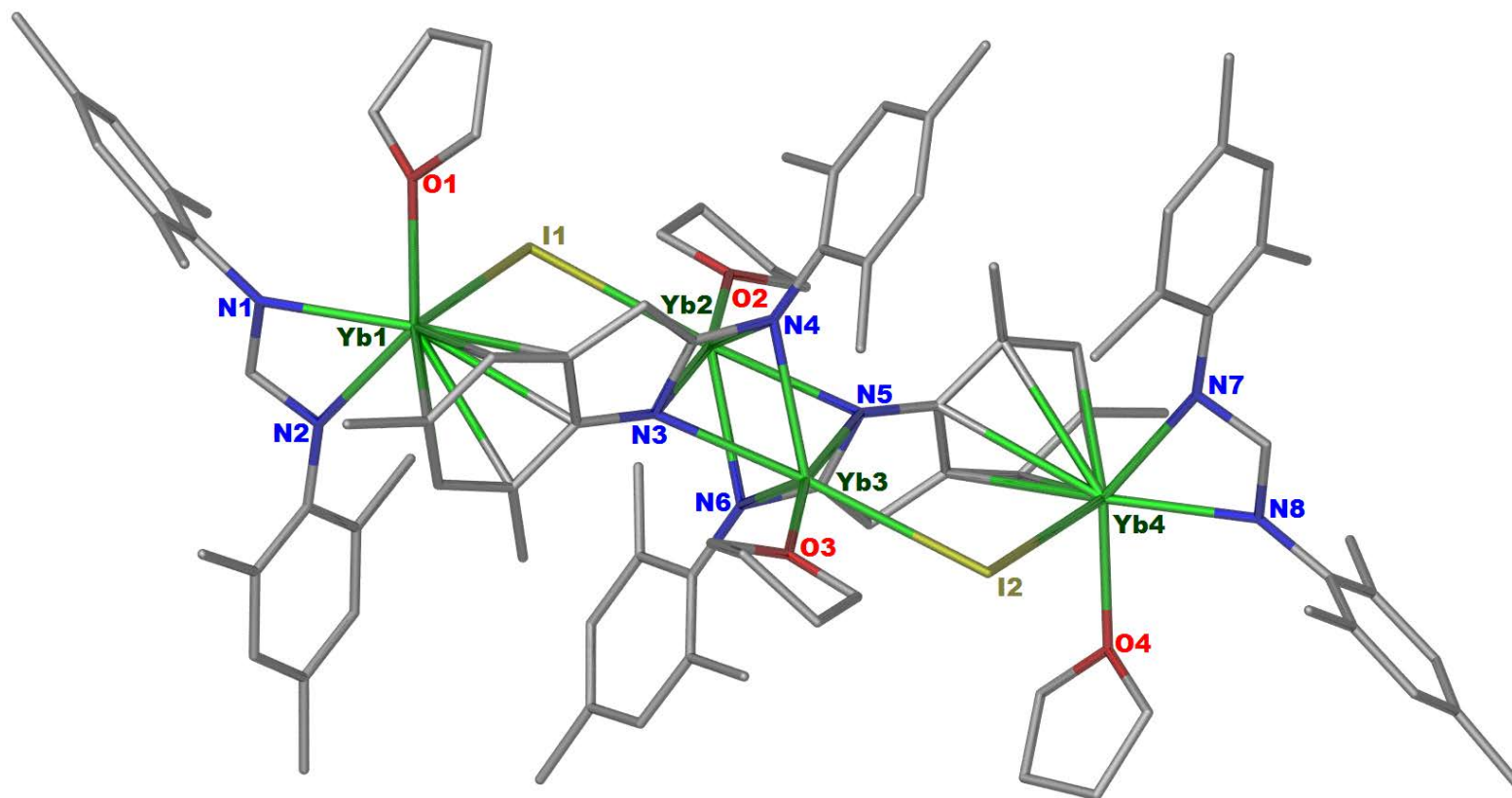
Figure 2.9 X-ray crystal structure of [Yb₂(MesForm)(FusForm)(μ−I)(thf)₂]₂ 2.6. Hydrogen atoms are omitted for clarity.

Table 2.6 Selected bond lengths (Å) **and angles** (°) **of [Yb(MesForm)(thf)₂I]₂ (2.5) and [Yb₂(MesForm)(FusForm)(μ−I)(thf)₂]₂ (2.6).**

Bond lengths (Å)	[Yb(MesForm)(thf)₂I]₂	Bond lengths (Å)		[Yb₂(MesForm)(FusForm)(μ−I)(thf)₂]₂	
Yb(1)–N(1)	2.446(4)	Yb(1)–N(1)	2.424(8)	Yb(2)–O(2)	2.464(6)
Yb(1)–N(2)	2.426(4)	Yb(1)–N(2)	2.467(8)	Yb(3)–O(3)	2.473(6)
Yb(1)–O(1)	2.387(4)	Yb(2)–N(3)	2.633(7)	Yb(4)–O(4)	2.448(6)
Yb(1)–O(2)	2.443(4)	Yb(2)–N(4)	2.493(8)	Yb(1)–I(1)	3.077(8)
Yb(1)–I(1)	3.096(13)	Yb(2)–N(5)	2.543(7)	Yb(2)–I(1)	3.145(8)
-	-	Yb(2)–N(6)	2.509(7)	Yb(3)–I(2)	3.130(8)
-	-	Yb(3)–N(5)	2.632(7)	Yb(4)–I(2)	3.077(8)
-	-	Yb(3)–N(6)	2.468(7)	Yb(1)–C(25)(Ph)	2.746(9)
-	-	Yb(3)–N(3)	2.537(7)	Yb(1)–C(26)(Ph)	2.770(9)
-	-	Yb(3)–N(4)	2.518(7)	Yb(1)–C(27)(Ph)	2.822(9)
-	-	Yb(4)–N(7)	2.453(8)	Yb(1)–C(29)(Ph)	2.915(8)
-	-	Yb(4)–N(8)	2.427(7)	Yb(1)–C(30)(Ph)	2.933(9)
-	-	Yb(1)–O(1)	2.453(7)	Yb(1)–C(31)(Ph)	2.957(8)
Bond angles (°)	**[Yb(MesForm)(thf)₂I]₂**	**Bond angles** (°)	**[Yb₄(MesForm)₂(FusForm)₂(μ−I)₂(thf)₄]**		
O(1)–Yb(1)–N(1)	107.03(13)	N(1)–Yb(1)–N(2)	55.60(4)	I(2)–Yb(4)–N(7)	102.60(3)
O(2)–Yb(1)–N(2)	94.51(13)	O(1)–Yb(1)–N(1)	83.50(4)	N(7)–Yb(4)–N(8)	55.90(4)
O(1)–Yb(1)–O(2)	79.53(13)	I(1)–Yb(1)–N(1)	112.00(3)	Yb(2)–N(3)–Yb(3)	75.70(3)
O(1)–Yb(1)–I(1)	92.10(9)	I(1)–Yb(1)–O(1)	85.00(3)	Yb(2)–N(5)–Yb(3)	80.00(4)
N(1)-Yb(1)-N(2)	55.77(13)	Yb(1)–I(1)–Yb(2)	108.74(3)	Yb(2)–N(4)–Yb(3)	79.50(4)
N(1)–Yb(1)–I(1)	160.14(9)	N(3)–Yb(2)–N(4)	54.00(4)	Yb(2)–N(6)–Yb(3)	76.20(3)
I(1)–Yb(1)–I(1)#	88.92(2)	N(3)–Yb(2)–I(1)	83.60(3)	N(3)–Yb(3)–N(5)	79.30(4)
Yb(1)–I(1)–Yb(1)#	91.08(3)	N(5)–Yb(2)–I(1)	129.60(3)	N(3)–Yb(2)–N(5)	76.20(4)
-	-	O(2)–Yb(2)–N(5)	108.90(4)	N(3)–Yb(3)–N(4)	55.00(4)
-	-	N(3)–Yb(3)–O(3)	88.70(4)	O(3)–Yb(3)–N(6)	167.00(4)
-	-	N(5)–Yb(3)–N(6)	54.00(4)	N(3)–Yb(3)–I(2)	172.50(3)

Ph = Phenyl group; # = Atoms generated by symmetry: -X, 1-Y, 1-Z.

Table 2.7 The Yb–I bond lengths in the known ytterbium complexes containing a terminal iodide.

Compound	Coordination number	Oxidation state	Ln–I (Å)
[YbI$_2$(thf)$_4$][83]	6	+2	3.103(1)
[Yb(μ–OCPh$_3$)(dme)I]$_2$[79]	5	+2	3.090(2)
[Yb{(Me$_3$SiNPPh$_2$)$_2$CH}(thf)$_2$I][84]	4	+2	3.058(6)
[Yb$_2$(Appy)$_3$I$_2$][85]	7	+2/+3	3.033(8), 2.942(7)

Appy = (6-Me-pyridine-2-yl)-[6-(2,4,6-^{i}Pr$_3$-C$_6$H$_2$)-pyridin-2-yl]-aminate.

[EuI(μ–I)(dme)$_2$]$_2$ (2.7)

The europium complex [EuI(μ–I)(dme)$_2$]$_2$ (**2.7**) crystallises in the monoclinic space group $P2_1/n$ (Table 2.10). Compound **2.7** exhibits a dinuclear form composed of two [EuI(μ–I)(dme)$_2$] units which are bridged via iodide atoms. This complex possesses an inversion centre which is situated on the midpoint of the Eu(1)···Eu(1)# vector. The geometry of the seven-coordinate Eu metal centre is best described as distorted pentagonal bipyramidal.

Selected bond lengths and angles of [EuI(μ–I)(dme)$_2$]$_2$ (**2.7**) are listed in Table 2.8. The average Eu–O bond lengths of [EuI(μ–I)(dme)$_2$]$_2$ found to be 2.60 Å which is almost similar to the average Eu–O bond lengths 2.59 Å reported for [EuI$_2$(thf)$_5$][17] and slightly longer than the average Eu–O bond lengths 2.58 Å reported for [Eu(Ph$_2$pz)(thf)$_4$I][22].
The Eu–I$_{(terminal)}$ bond length of [EuI(μ–I)(dme)$_2$]$_2$ found to be 3.194(9) Å which is similar to the Eu–I bond lengths 3.198(2) Å reported for [Eu(Ph$_2$pz)(thf)$_4$I][22] but, it is shorter than the Eu–I bond lengths 3.228(2), 3.239(2) Å reported for [EuI$_2$(thf)$_5$][17] due to steric demand differences. The Eu–I$_{(bridge)}$ bond lengths of [EuI(μ–I)(dme)$_2$]$_2$ found to be 3.302(9) Å which is larger than the Eu–I$_{(terminal)}$ bond lengths 3.194(9) Å.
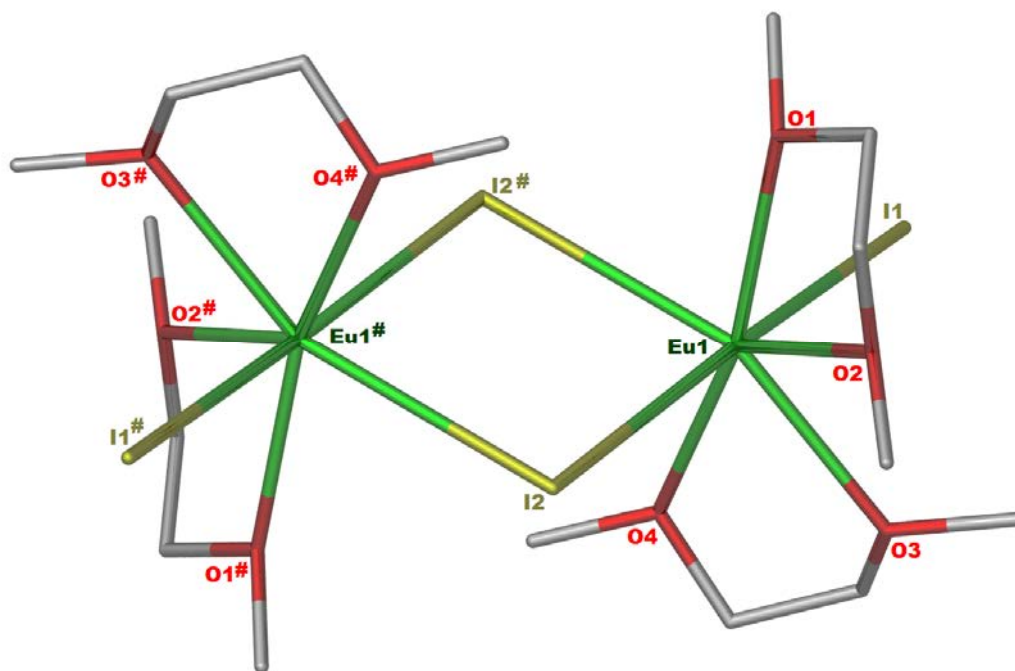
Figure 2.10 X-ray crystal structure of [EuI(μ–I)(dme)₂]₂ 2.7. Hydrogen atoms are omitted for clarity. # = Atoms generated by symmetry: 1-X, 1-Y, 1-Z.

Table 2.8 Selected bond lengths (Å) and angles (°) of [EuI(μ–I)(dme)₂]₂ (2.7).

Bond lengths (Å)			
Eu(1)–O(1)	2.604(5)	Eu(1)–I(1)	3.194(9)
Eu(1)–O(2)	2.586(4)	Eu(1)–I(2)	3.302(9)
Eu(1)–O(3)	2.634(5)	Eu(1)–I(2)#	3.300(9)
Eu(1)–O(4)	2.587(6)	I(2)–Eu(1)#	3.300(9)
Bond angles (°)			
I(1)–Eu(1)–I(2)	97.55(14)	Eu(1)–I(2)–Eu(1)#	98.09(14)
I(1)–Eu(1)–I(2)#	174.25(18)	I(2)#–Eu(1)–O(1)	103.9(10)
I(1)–Eu(1)–O(1)	81.53(10)	I(2)#–Eu(1)–O(2)	79.06(10)
I(1)–Eu(1)–O(2)	105.22(10)	O(1)–Eu(1)–O(2)	64.43(14)
I(2)–Eu(1)–O(1)	78.89(10)	O(3)–Eu(1)–O(4)	64.69(16)
I(2)–Eu(1)–O(2)	132.55(10)		

 # = Atoms generated by symmetry: 1-X, 1-Y, 1-Z.

[Yb(MesForm)$_3$].Ph$_3$ (2.8) and [Yb(MesForm)$_3$].Fluorene (2.9)

Yb^{+3} Complexes [Yb(MesForm)$_3$].Ph$_3$ (Fig. 2.11) and [Yb(MesForm)$_3$].Fluorene (Fig. 2.12) crystallise in the monoclinic space group *P*2$_1$/*c* (Table 2.10). Compounds **2.8** and **2.9** are mononuclear Yb^{+3} complexes. The six-coordinate Yb^{+3} metal centres of [Yb(MesForm)$_3$].Ph$_3$ and [Yb(MesForm)$_3$].Fluorene display a distorted octahedral geometry which is coordinated by three bidentate MesForm ligands through the nitrogen donor atoms. The metal containing moieties in [Yb(MesForm)$_3$].Ph$_3$ and [Yb(MesForm)$_3$].Fluorene are similar in structure to the literature complexes [Yb(MesForm)$_3$][67] and [Yb(EtForm)$_3$][67]. In the lattice of **2.8** there is a 1,4-diphenylbenzene molecule filling the lattice space while in the lattice of **2.9** there is a fluorene molecule.

Selected bond lengths and angles of [Yb(MesForm)$_3$].Ph$_3$ and [Yb(MesForm)$_3$].Fluorene are listed in Table 2.9. The average Yb–N bond lengths of **2.8** and **2.9** found to be 2.34 Å, 2.33 Å respectively which are in agreement with the average Yb–N bond lengths 2.35 Å, 2.34 Å reported for [Yb(MesForm)$_3$][67] and [Yb(EtForm)$_3$][67] respectively.

The average N–Yb–N bond angles of [Yb(MesForm)$_3$].Ph$_3$ and [Yb(MesForm)$_3$].Fluorene found to be 57.96°, 58.26° respectively which are in agreement with the average N–Yb–N bond angles 57.94°, 57.96° reported for [Yb(MesForm)$_3$][67] and [Yb(EtForm)$_3$][67].
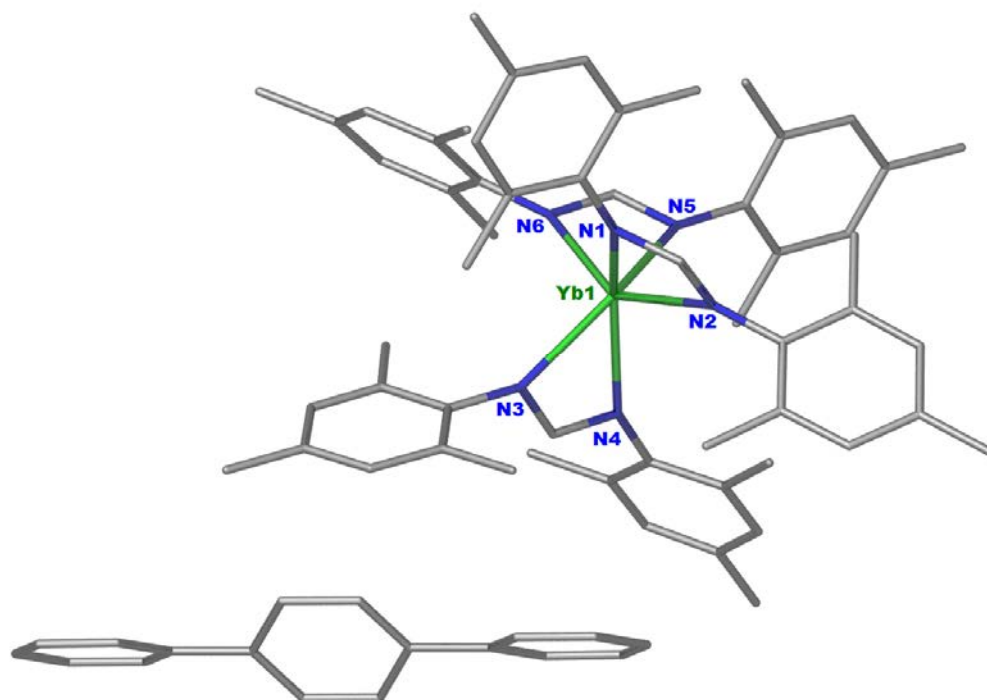
Figure 2.11 X-ray crystal structure of [Yb(MesForm)₃].Ph₃ 2.8. Hydrogen atoms are omitted for clarity.
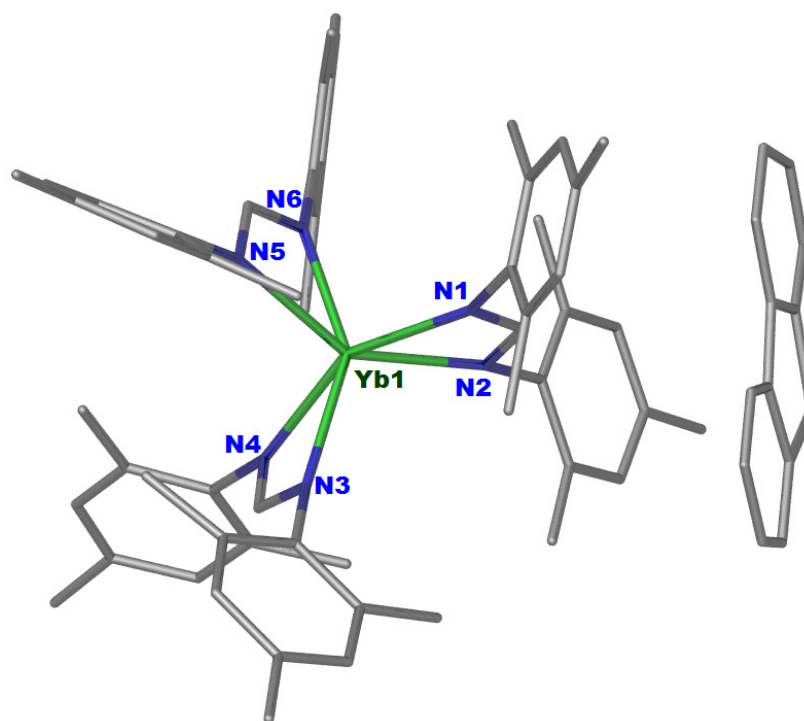
Figure 2.12 X-ray crystal structure of [Yb(MesForm)₃].Fluorene 2.9. Hydrogen atoms are omitted for clarity.

[(DippFormH$_2$)−μ−I]$_2$.Benzil (2.10)

A yellow crystalline complex of [(DippFormH$_2$)−μ−I]$_2$.Benzil was isolated after the hydrolysis of [Yb(DippForm)I)] in presence the benzil (eqn. 2.16). Compound **2.10** crystallises in the monoclinic space group *P*2$_1$/*c* (Table 2.10). The molecular structure of compound **2.10** is displayed in Figure 2.13 as a polymeric structure. Compound **2.10** exhibits two [DippFormH$_2$]$^+$ ions with a single iodide atom bridging the two [DippFormH$_2$]$^+$ ions molecules through H−I−H interactions. In the lattice of **2.10** in addition to [(DippFormH$_2$)−μ−I]$_2$ there is a benzil molecule filling the lattice space. Selected bond lengths of **2.10** are listed in Table 2.9.
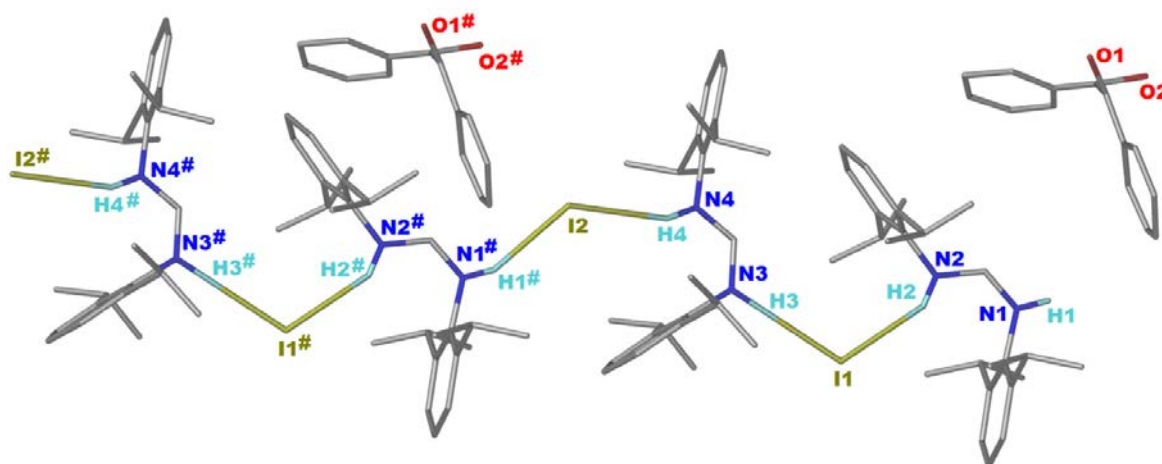
Figure 2.13 X-ray crystal structure of [(DippFormH$_2$)−μ−I]$_2$.Benzil 2.10. Hydrogen atoms are omitted for clarity. # = Atoms generated by symmetry: X-1, Y, Z.

Table 2.9 Selected bond lengths and angles of [Yb(MesForm)₃].Ph₃, [Yb(MesForm)₃].Fluorene and [(DippFormH₂)−μ−I]₂.Benzil.

Bond lengths (Å)	[Yb(MesForm)₃].Ph₃	[Yb(MesForm)₃].Fluorene	[(DippFormH₂)−μ−I]₂.Benzil
Yb(1)–N(1)	2.373(3)	2.330(11)	-
Yb(1)–N(2)	2.329(3)	2.319(11)	-
Yb(1)–N(3)	2.355(3)	2.340(11)	-
Yb(1)–N(4)	2.327(3)	2.345(11)	-
Yb(1)–N(5)	2.351(3)	2.349(11)	-
Yb(1)–N(6)	2.346(3)	2.331(12)	-
H(2)–I(1)	-	-	2.694
H(3)–I(1)	-	-	2.605
H(4)–I(2)	-	-	2.739
Bond angles (°)			
N(1)–Yb(1)–N(2)	57.84(10)	58.70(4)	-
N(3)–Yb(1)–N(4)	58.25(11)	58.20(4)	-
N(5)–Yb(1)–N(6)	57.81(10)	57.90(4)	-

Table 2.10 Crystallographic data for compounds 2.5-2.10.

Compound	2.5	2.6	2.7	2.8	2.9	2.10
formula	$C_{54}H_{78}N_4O_4I_2Yb_2$	$C_{106}H_{134}N_8O_4I_2Yb_4$	$C_{16}H_{40}Eu_2O_8I_4$	$C_{75}H_{83}N_6Yb$	$C_{70}H_{79}N_6Yb$	$C_{64}H_{86}N_4O_2I_2$
fw	1447.11	2530.22	1172.03	1241.54	1177.46	1197.20
crystal system	triclinic	orthorhombic	monoclinic	monoclinic	monoclinic	monoclinic
space group	*P*-1	*Pna*2$_1$	*P*2$_1$/*n*	*P*2$_1$/*c*	*P*2$_1$/*c*	*P*2$_1$/*c*
a, Å	10.923(2)	33.008(7)	8.5150(17)	11.828(2)	12.699(6)	14.986(14)
b, Å	11.924(2)	11.822(2)	16.055(3)	22.058(4)	64.203(3)	10.871(11)
c, Å	13.169(3)	25.321(5)	12.265(3)	22.128(4)	14.673(7)	39.277(3)
α, deg	66.31(3)	90	90	90	90	90
β, deg	65.54(3)	90	105.31(3)	101.82(3)	108.75(2)	91.72(5)
γ, deg	69.06(3)	90	90	90	90	90
V, Å^3	1391(7)	9881(3)	1617(6)	5651(2)	11328(10)	6396(10)
Z	2	4	2	4	4	4
T, K	173(2)	173(2)	173(2)	173(2)	173(2)	173(2)
no. of rflns collected	16017	132400	9529	49053	138197	81645
no. of indep rflns	4330	23733	2720	12994	24511	14669
R_{int}	0.068	0.051	0.095	0.060	0.096	0.102
Final R_1 values ($I > 2\sigma(I)$)	0.035	0.064	0.046	0.041	0.123	0.068
Final $wR(F^2)$ values ($I > 2\sigma(I)$)	0.090	0.174	0.123	0.101	0.246	0.184
Final R_1 values (all data)	0.035	0.068	0.048	0.050	0.161	0.186
Final $wR(F^2)$ values (all data)	0.090	0.177	0.125	0.105	0.258	0.241
GooF (on *F*^{2})	1.058	1.507	0.991	1.065	1.250	1.019

2.4 Conclusions

This chapter explores the synthesis and reactivity of pseudo-Grignard reagents of divalent lanthanoids. Pseudo-Grignard reactions produced dimeric structures such as, [Yb(Form)(thf)$_2$X]$_2$ (Form = MesForm, XylForm, DippForm, X = Br or I) and mononuclear structures such as [Yb(EtForm)$_2$(thf)$_2$Br]. These [Yb(Form)(thf)$_2$X]$_2$ (**2.1a**, **2.2**, **2.3** and **2.5**) and [Yb(EtForm)$_2$(thf)$_2$Br] reagents were prepared by the addition of various formamidines to Yb metal pre-treated with iodobenzene or bromobenzene. [Yb(XylForm)$_3$] (**2.1b**) was isolated by fractional crystallisation, the presence of the main product [Yb(XylForm)(thf)$_2$Br]$_2$ (**2.1a**) contributed to the low yield of **2.**1b which is consistent with the previous findings reported by Evans, *et. al.*[3] Isolation of a Yb^{+3} monomeric structure of [Yb(EtForm)$_2$(thf)$_2$Br] occurred instead of an expected Yb^{+2} dimeric structure. The polymeric complex [Yb$_2$(MesForm)(FusForm)(μ−I)(thf)$_2$]$_2$ (**2.6**) was prepared in an attempt to recrystallise [Yb(MesForm)(thf)$_2$I]$_2$ (**2.5**) from toluene after heating the solution at 100 °C overnight. The only dme solvated dimeric compound [EuI(μ−I)(dme)$_2$]$_2$ (**2.7**) was prepared by performing the reaction in dme and isolated as a main product instead of isolation of the expected product [Eu(MesForm)(thf)$_n$I] due to a shift in the Schlenk equilibrium. Shifts in the Schlenk equilibrium could easily contribute to low isolated yields for most complexes. Subsequently, "real yields" from solution are difficult to determine as herein we depended on isolated crystal yields.

Reactivity process involves addition the ketone to pseudo-Grignard mixture led to a similar result with two different ketones which deoxygenate the ketones. For example, adding 1,4-benzoquinone to the pseudo-Grignard reaction mixture led to deoxygenation the carbonyl groups and formation of a C–C bond between three phenyl groups [Yb(MesForm)$_3$].Ph$_3$ (**2.8**). While adding 9-fluorenone to the pseudo-Grignard reaction mixture led to deoxygenation of the 9-fluorenone producing the corresponding fluorene

[Yb(MesForm)$_3$].Fluorene (**2.9**). [(DippFormH$_2$)–μ–(I)–]$_n$.Benzil **2.10** was synthesised

by the hydrolysis of [Yb(DippForm)I)] in presence the benzil (eqn. 2.16).

2.5 Experimental

General considerations

All the products of pseudo-Grignard reagents are highly air- and moisture-sensitive, requiring the use of Schlenk flask and interfaced to a high vacuum (10^{-2} Torr) line techniques. Hence all manipulations were carried out with rigorous exclusion of oxygen and moisture in vacuum Schlenk-type glassware under a dinitrogen atmosphere.

All solvents (thf, dme, Et$_2$O and hexane) were dried and deoxygenated by distillation from sodium benzophenone ketyl under nitrogen, while toluene was dried by LC solvent purification system. After distillation they were stored in vacuum Schlenk flasks. Iodobenzene, bromobenzene (all ≥ 99 %), and *perdeutero*-benzene (C$_6$D$_6$) (all ≥ 99 atom % D) were obtained from Sigma-Aldrich and were degassed, dried, and stored in Schlenk flasks prior to use. Formamidine compounds (XylFormH, DippFormH, MesFormH, and EthylFormH) were prepared by literature methods.[86, 87] Lanthanoid metals were obtained from Rhone Poulenc or Santoku, stored under nitrogen and freshly filed before use.

^{1}H-NMR spectra were recorded on a Bruker 400 MHz spectrometer. The chemical shifts are expressed in parts per million (ppm). Infrared spectra (4000-400 cm^{-1}) were obtained as Nujol mulls between NaCl plates with a Nicolet-Nexus FT-IR spectrometer. Samples were sent in sealed glass pipettes under nitrogen for elemental analyses (C, H, N) to the Microanalytical Laboratory, Science Centre, London Metropolitan University, England. Melting points were measured in sealed capillaries.

[Yb(Form)(thf)₂Br]₂ (Form = XylForm 2.1a, DippForm 2.2, MesForm 2.3),

[Yb(XylForm)₃] (2.1b)

A Schlenk flask was charged with ytterbium metal filings (0.27 g, 1.6 mmol) and dry thf
(~20 ml). PhBr (0.20 g, 1.3 mmol) was added at -78 °C. The mixture was stirred and
within 5 minutes developing a dark red-brown colour. 1.3 mmol solid FormH (XylFormH
0.32 g, DippFormH 0.48 g, MesFormH 0.36 g) was added and the mixture was stirred at
-78 °C for another 3 h and then at room temperature overnight giving a red-brown solution
that was filtered through a filter cannula to remove the residual metal and concentrated
under vacuum to ca. 5 ml. Small yellow crystals of **2.1a** (0.19 g, 59 %), **2.2** (0.25 g, 52
%), **2.3** (0.18 g, 50 %) were grew upon standing overnight. Fractional crystallisation from
the mother liquor of **2.1a** yielded small orange crystals of [Yb(XylForm)₃] **2.1b** (0.03 g, 9
%).

2.1a: m. p. 208-210 °C. Elemental analysis calcd for $C_{50}H_{70}N_4O_4Br_2Yb_2$ (1297.03 g.mol^{-1}): C 46.30, H 5.44, N 4.32. Calcd for $C_{46}H_{62}N_4O_3Br_2Yb_2$ (1224.93 g.mol^{-1} after lost of
one thf of solvation) C 45.10, H 5.10, N 4.57. Found: C 44.92, H 4.80, N 4.04. ^{1}H-NMR
(400 MHz, C_6D_6, 25°C): δ = 8.08 (s, 2H, NC(H)N), 7.58 (d, ^3J-(H, H) = 6.52 Hz, 8H, *m*-
H−Ar), 6.18 (t, ^3J-(H, H) = 6.50 Hz, 4H, *p*-H−Ar), 3.57 (s, br, 12H; OCH₂, thf), 1.75 (s,
24H, CH₃), 1.33 (s, br, 12H; CH₂, thf) ppm. IR (Nujol, cm^{-1}): 2293 w, 2190 m, 2142 m,
2031 s, 1920 s, 1908 s, 1852 s, 1784 s, 1649 s, 1593 m, 1526 s, 1251 w, 1204 s, 1164 m,
1092 s, 1037 s, 933 w, 878 w, 762 s, 671 s.

2.1b: no characterisation could be obtained owing to the low yield limitation.

2.2: m. p. 176-178 °C; Elemental analysis calcd for [Yb(DippForm)(thf)₂Br]₂.thf
$C_{70}H_{110}N_4O_5Br_2Yb_2$ (1593.56 g.mol^{-1}): C 52.76, H 6.96, N 3.52. Calcd for
[Yb(DippForm)(thf)₂Br]₂ $C_{66}H_{102}N_4O_4Br_2Yb_2$ (1521.46 g.mol^{-1} after loss of one lattice

thf): C 52.10, H 6.76, N 3.68. Found: C 51.96, H 6.23, N 3.37. ^{1}H-NMR (400 MHz, C_6D_6,

25°C): δ = 8.12 (s, 2H, NC(H)N), 6.98 (m, 8H, *m*-H−Ar), 6.23 (m, 4H, *p*-H−Ar), 3.85 (br,

m, 12H; OCH$_2$, thf), 3.15 (m, 8H; C*H*(CH$_3$)), 1.37 (d, ^3J (H, H) = 7.21 Hz, 48H,

CH(C*H$_3$*)$_2$), 1.45 (br, m, 12H; CH$_2$, thf), ppm. IR (Nujol, cm^{-1}): 1667 w, 1591 w, 1519 s,

1295 s, 1260 m, 1190 w, 1096 w, 1034 m, 936 w, 918 m, 883 w, 800 m, 767 m, 756 w,

722 m, 666 w.

2.3: m. p. 168-170 °C; Elemental analysis calcd for $C_{54}H_{78}N_4O_4Br_2Yb_2$ (1353.11 g.mol^{-1}): C 47.93, H 5.81, N 4.14. Calcd for $C_{46}H_{62}N_4O_2Br_2Yb_2$ (1208.90 g.mol^{-1} after lost two

thf of solvation) C 45.70, H 5.17, N 4.63. Found: C 45.36, H 4.73, N 4.31. ^{1}H-NMR (400

MHz, C_6D_6, 25°C): δ = 8.44 (s, 2H, NC(H)N), 6.77 (s, br, 8H, *m*-H−Ar), 3.19 (s, br, 8H;

OCH$_2$, thf), 2.41 (s, 24H; *o*-CH$_3$), 1.71 (s, 12H; *p*-CH$_3$), 1.12 (s, br, 8H; CH$_2$, thf) ppm.

IR (Nujol, cm^{-1}): 1717 s, 1643 m, 1608 m, 1524 m, 1262 m, 1208 m, 1149 m, 1033 m,

963 s, 877 s, 851 m, 606 s.

[Yb(EtForm)$_2$(thf)$_2$Br] (2.4)

Following same method that described to synthesise **2.1**-**2.3** with equivalent amount of

solid EtFormH (0.40 g, 1.3 mmol) led to isolated Yb^{+3} mononuclear structure

[Yb(EtForm)$_2$Br(thf)$_2$] rather than Yb^{+2} dinuclear structure as it occurred with **2.1a**, **2.2**,

2.3. Big pink crystals of **2.4** (0.22 g, 55 %) were grown upon standing for one week.

2.4: m. p. 246-248 °C. Elemental analysis calcd for $C_{50}H_{70}N_4O_2BrYb$ (1012.06 g.mol^{-1}):

C 59.34, H 6.97, N 5.54. Found: C 58.94, H 5.95, N 5.13. IR (Nujol, cm^{-1}): 1686 w, 1591

w, 1519 s, 1295 s, 1260 m, 1190 w, 1096 w, 1034 m, 936 w, 918 m, 883 w, 800 m, 767

m, 756 w, 722 m, 666 w.

[Yb(MesForm)(thf)$_2$I]$_2$ (2.5)

Following same method to that employed to synthesise **2.1a-2.3** except using PhI (0.27 g, 1.3 mmol) instead of PhBr. Small yellow crystals of **2.5** (0.24 g, 66 %) separated from yellow crystals of [YbI$_2$(thf)$_4$] through fractional crystallisation and grew upon standing after two days (full structural determination of [YbI$_2$(thf)$_4$], unit cell: triclinic, $a = 8.4268(17)$, $b = 9.805(2)$, $c = 13.646(3)$ Å, $\alpha = 80.18(3)°$, $\beta = 87.58(3)°$, $\gamma = 86.97(3)°$, $V = 1108.8(4)$ Å^3).[83]

2.5: m. p. 168-170 °C. Elemental analysis calcd for C$_{54}$H$_{78}$N$_4$O$_4$I$_2$Yb$_2$ (1447.11 g.mol^{-1}): C 44.82, H 5.43, N 3.87. Found: C 44.51, H 4.94, N 3.60. ^{1}H-NMR (400 MHz, C$_6$D$_6$, 25°C): δ = 8.03 (s, 2H, NC(H)N), 7.05 (m, br, 8H, *m*-H−Ar), 3.29 (s, br, 8H; OCH$_2$, thf), 1.22 (s, 24H; *o*-CH$_3$), 1.16 (s, 12H; *p*-CH$_3$), 0.94 (s, br, 16H; CH$_2$, thf) ppm. IR (Nujol, cm^{-1}): 2025 s, 1907 s, 1835 s, 1768 s, 1646 m, 1280 m, 1195 m, 1086 s, 880 s, 728 s.

[Yb$_2$(MesForm)(FusForm)$_{(μ−I)}$(thf)$_2$]$_2$.2Toluene (2.6)

Complex (**2.6**) was prepared through attempting to separate **2.6** from the yellow crystals of [YbI$_2$(thf)$_4$] through recrystalisation with toluene. This attempted started by drying the red-brown filtrate of **2.5** and dissolved in dry toluene (~25 ml) and heated overnight at 100°C. This mixture was filtered through a filter cannula to separate the yellow precipitate of [YbI$_2$(thf)$_4$] which undissolved in toluene and the filtrate concentrated under vacuum to ca. 5 ml. Big red crystals of **2.6** (0.09 g, 25 %) were grown upon standing for one week.

2.6: m. p. 196-198 °C. IR (Nujol, cm^{-1}): 2405 m, 2293 w, 2142 s, 2031 s, 1908 m, 1748 m, 1649 m, 1526 m, 1204 m, 1092 m, 1037 m, 878 w, 762 w, 671 s.

[EuI(μ−I)(dme)$_2$]$_2$ (2.7)

Following same method to that employed to synthesise **2.5** except using europium metal filings (0.25 g, 1.6 mmol), in dme (~20 ml) instead of ytterbium metal in thf. Instead of

isolated the desired compound of pseudo-Grignard [Eu(MesForm)I(dme)$_n$], small colourless crystals of **2.7** (0.08 g, 22 %) grew upon standing for one week.

2.7: m. p. 105-107 °C; Elemental analysis calcd for C$_{16}$H$_{40}$O$_8$I$_4$Eu$_2$ (1172.03 g.mol^{-1}): C 16.40, H 3.44. Calcd for C$_8$H$_{20}$O$_4$I$_4$Eu$_2$ (991.79 g.mol^{-1} after lost of two dme of solvation) C 9.69, H 2.03. Found C 9.24, H 2.01. ^{1}H-NMR (400 MHz, C$_6$D$_6$, 25°C): Spectrum has shown chemicals shifts from δ = 3.12 (s, 6H, CH$_3$), 3.35 (s, 4H, CH$_2$) the normal chemicals shifts of dme to δ = 0.27 (s, br, 12H, CH$_3$), 1.33 (s, br, 8H, CH$_2$) due to paramagnetism of europium in addition to two peaks for dme residual at solution δ = 0.90 (s, br, 6H, CH$_3$), 2.10 (s, br, 4H, CH$_2$). IR (Nujol, cm^{-1}): 1743 m, 1466 s, 1330 m, 1215 w, 1110 w, 934 w, 865 m, 818 s, 768 m, 694 m.

[Yb(MesForm)$_3$].R (R = Ph$_3$ 2.8, Fluorene 2.9)

Following same method to that described to synthesise (**2.5**). After 12 h of stirring the pseudo-Grignard mixture, (0.10 g) of ketone (0.92 mmol) 1, 4-benzoquinone (**2.8**) or (0.05 mmol) 9-fluorenone (**2.9**) was added and the mixture stirred overnight at room temperature gave a red-brown solution that was filtered through a filter cannula to remove the residual metal and concentrated under vacuum to ca. 5 ml. Big red crystals of **2.8** (0.07 g, 19 %), **2.9** (0.05 g, 13 %), were grew up standing for two days.

2.8: m. p. 216-218 °C. Elemental analysis calcd for C$_{75}$H$_{83}$N$_6$Yb (1241.54 g.mol^{-1}): C 72.56, H 6.74, N 6.77. Found: C 72.17, H 6.35, N 6.43. IR (Nujol, cm^{-1}): 2050 w, 1940 m, 1875 m, 1723 s, 1213 s, 750 m, 849 s, 804 s, 739 s, 698 m, 571 s.

2.9: m. p. 228-230 °C. Elemental analysis calcd for C$_{70}$H$_{79}$N$_6$Yb (1177.46 g.mol^{-1}): C 71.40, H 6.76, N 7.14. Found: C 70.93, H 6.42, N 6.88. IR (Nujol, cm^{-1}): 2630 w, 2010 w, 1665 m, 1406 s, 1252 s, 1200 w, 1015 s, 904 m, 841 m, 812 s, 737 s.

[(DippFormH$_2$)−μ−I]$_2$.Benzil (2.10)

Following same method that described to synthesise (**2.8**, **2.9**). After (0.10 g, 0.47 mmol) the ketone (benzil) was added and the mixture stirred overnight at room temperature gave a red-brown solution that was filtered through a filter cannula to remove the residual metal. After that the filtrate hydrolysed and concentrated under vacuum to ca. 5 ml. Small yellow crystals of [(DippFormH$_2$)−μ−(I)]$_n$.Benzil **2.10** (0.07 g, 14 %) grew up standing for two days.

2.10: m. p. 114-116 °C. Elemental analysis calcd for C$_{64}$H$_{86}$N$_4$O$_2$I$_2$ (1197.20 g.mol^{-1}): C 64.32, H 7.08, N 4.69. Found: C 63.97, H 6.90, N 4.29. ^{1}H-NMR (400 MHz, C$_6$D$_6$, 25°C): δ = 7.16 (m, 10H, Ar), 7.05 (m, 12H, Ar), 6.73 (br, 2H, NH(CH)NH), 3.13 (sep, $^3J_{HH}$ = 6.9 Hz, 8H, CH(CH$_3$)$_2$), 1.09 (d, 48H, CH(CH_3)$_2$). IR (Nujol, cm^{-1}): 3285 m, 2350 w, 2179 m, 1995 m, 1928 s, 1860 m, 1802 s, 1456 s, 1258 m, 1096 s, 997 m, 800 s, 755 m, 517 m.

2.6 Crystal and refinement data

Suitable crystals were immersed in viscous hydrocarbon oil (Paratone-N) and mounted on a glass fibre that was mounted on the diffractometer under a stream of liquid nitrogen. Intensity data of crystalline samples of compounds **2.1**-**2.10** were collected using the MX1 beamline at the Australian Synchrotron at 173 K using a single wavelength ($\lambda = 0.712$ Å). Structure solutions and refinements were performed using SHELXS-97 and SHELXL-97[88] program through the graphical interface X-Seed[89] which was also used to generate the figures. Absorption corrections using MULTISCAN were applied. All CIF files were checked at www.iucr.org.

[Yb(XylForm)(thf)$_2$Br]$_2$ (2.1a)

$C_{50}H_{70}N_4O_4Br_2Yb_2$, $M = 1297.03$, $0.10 \times 0.07 \times 0.05$ mm^3, monoclinic, space group $P2_1/c$, $a = 14.820(3)$, $b = 14.334(3)$, $c = 13.280(3)$ Å, $\alpha = \gamma = 90°$, $\beta = 113.64(3)°$, $V = 2584(11)$ Å^3, $Z = 2$, ρ_c 1.667 g/cm^3, $T = 173$ K, $\mu = 5.187$ mm^{-1}, $2\theta_{max} = 55°$, 33191 reflections collected, 5764 independent reflections ($R_{int} = 0.035$), Final $GooF = 0.503$, $R_1 = 0.037$, $wR_2 = 0.098$, R indices based on 5207 reflections with I $>= 2\sigma$(I) (refinement on F^2), 284 parameters, 0 restraint. Lp and absorption corrections applied.

[Yb(XylForm)$_3$] (2.1b)

$C_{52}H_{60}N_6Yb$, $M = 942.13$, $0.11 \times 0.04 \times 0.06$ mm^3, monoclinic, space group $P2_1$, $a = 19.962(4)$, $b = 10.537(2)$, $c = 20.919(4)$ Å, $\alpha = \gamma = 90°$, $\beta = 91.26(3)°$, $V = 4399(15)$ Å^3, $Z = 4$, ρ_c 1.400 g/cm^3, $\mu = 2.168$ mm^{-1}, $T = 173$ K, $2\theta_{max} = 55°$, 56316 reflections collected, 19710 independent reflections ($R_{int} = 0.028$), Final $GooF = 1.259$, $R_1 = 0.047$, $wR_2 = 0.118$, R indices based on 19628 reflections with I $>= 2\sigma$(I) (refinement on F^2), 1060 parameters, 1 restraint. Lp and absorption corrections applied.

[Yb(DippForm)(thf)$_2$Br]$_2$.thf (2.2)

C$_{70}$H$_{110}$N$_4$O$_5$Br$_2$Yb$_2$, M = 1593.56, 0.12 × 0.08 × 0.07 mm^3, triclinic, space group P-1, a = 11.050(2), b = 12.753(3), c = 15.509(3) Å, α = 70.76(3)°, β = 78.96(3)°, γ = 67.01(3)°, V = 1894(9) Å^3, Z = 2, ρ_c 2.667 g/cm^3, μ = 7.097 mm^{-1}, T = 173 K, 2θ_{max} = 55°, 23066 reflections collected, 7949 independent reflections (R_{int} = 0.045), Final $GooF$ = 1.130, R_1 = 0.035, wR_2 = 0.096, R indices based on 7630 reflections with I > = 2σ(I) (refinement on F^2), 405 parameters, 0 restraint. Lp and absorption corrections applied.

[Yb(MesForm)(thf)$_2$Br]$_2$ (2.3)

C$_{54}$H$_{78}$N$_4$O$_4$Br$_2$Yb$_2$, M = 1353.11, 0.10 × 0.06 × 0.05 mm^3, triclinic, space group P-1, a = 10.744(2), b = 11.766(2), c = 13.059(3) Å, α = 95.27(3)°, β = 114.18(3)°, γ = 110.39(3)°, V = 1357(5) Å^3, Z = 2, ρ_c 1.655 g/cm^3, μ = 4.942 mm^{-1}, T = 173 K, 2θ_{max} = 55°, 6143 reflections collected, 6143 independent reflections (R_{int} = 0.025), Final $GooF$ = 1.076, R_1 = 0.0343, wR_2 = 0.0866, R indices based on 5868 reflections with I > = 2σ(I) (refinement on F^2), 305 parameters, 0 restraint. Lp and absorption corrections applied.

[Yb(EtForm)$_2$(thf)$_2$Br] (2.4)

C$_{50}$H$_{70}$N$_4$O$_2$BrYb, M = 1012.06, 0.10 × 0.09 × 0.08 mm^3, monoclinic, space group C2/c, a = 10.722(2), b = 19.820(4), c = 22.039(4) Å, α = γ = 90°, β = 99.23(3)°, V = 4622(16) Å^3, Z = 4, ρ_c 1.454 g/cm^3, μ = 2.930 mm^{-1}, T = 173 K, 2θ_{max} = 55°, 14677 reflections collected, 4069 independent reflections (R_{int} = 0.077), Final $GooF$ = 1.239, R_1 = 0.097, wR_2 = 0.232, R indices based on 3901 reflections with I > = 2σ(I) (refinement on F^2), 295 parameters, 6 restraints. Lp and absorption corrections applied.

[Yb(MesForm)(thf)$_2$I]$_2$ (2.5)

C$_{54}$H$_{78}$N$_4$O$_4$I$_2$Yb$_2$, M = 1447.11, 0.12 × 0.06 × 0.09 mm^3, triclinic, space group P-1, a = 10.923(2), b = 11.924(2), c = 13.169(3) Å, α = 66.31(3)°, β = 65.54(3)°, γ = 69.06(3)°, V = 1391(7) Å^3, Z = 2, ρ_c 1.727 g/cm^3, μ = 4.494 mm^{-1}, T = 173 K, 2θ_{max} = 55°, 16017

reflections collected, 4330 independent reflections (R_{int} = 0.068), Final *GooF* = 1.058, R_1 = 0.035, wR_2 = 0.090, *R* indices based on 4248 reflections with I $> = 2\sigma$(I) (refinement on F^2), 304 parameters, 0 restraint. Lp and absorption corrections applied.

[Yb₂(MesForm)(FusForm)(μ−I)(thf)₂]₂.2Toluene (2.6)

$C_{106}H_{134}N_8O_4I_2Yb_4$, *M* = 2530.22, 0.12 × 0.08 × 0.04 mm³, orthorhombic, space group *Pna2₁*, *a* = 33.008(7), *b* = 11.822(2), *c* = 25.321(5) Å, $\alpha = \beta = \gamma = 90°$, *V* = 9881(3) Å³, *Z* = 4, ρ_c 7.710 g/cm³, μ = 22.104 mm⁻¹, *T* = 173 K, $2\theta_{max}$ = 55 °, 132400 reflections collected, 23733 independent reflections (R_{int} = 0.051), Final *GooF* = 1.507, R_1 = 0.064, wR_2 = 0.174, *R* indices based on 22313 reflections with I $> = 2\sigma$(I) (refinement on F^2), 497 parameters, 1 restraint. Lp and absorption corrections applied.

[EuI(μ−I)(dme)₂]₂ (2.7)

$C_{16}H_{40}O_8I_4Eu_2$, *M* = 1172.03, 0.10 × 0.07 × 0.06 mm³, monoclinic, space group *P2₁/n*, *a* = 8.515(17), *b* = 16.055(3), *c* = 12.265(3) Å, $\alpha = \gamma = 90°$, β= 105.72(3)°, *V* = 1617(6) Å³, *Z* = 2, ρ_c = 2.407 g/cm³, μ = 7.691 mm⁻¹, *T* = 173 K, $2\theta_{max}$ = 55º, 9529 reflections collected, 2720 independent reflections (R_{int} = 0.095). Final *GooF* = 0.991, R_1 = 0.046, wR_2 = 0.123, *R* indices based on 2494 reflections with I $> = 2\sigma$(I) (refinement on F^2), 141 parameters, 0 restraint. Lp and absorption corrections applied.

[Yb(MesForm)₃].Ph₃ (2.8)

$C_{75}H_{83}N_6Yb$, *M* = 1241.54, 0.10 × 0.04 × 0.08 mm³, monoclinic, space group *P2₁/c*, *a* = 11.828(2), *b* = 22.058(4), *c* = 22.128(4) Å, $\alpha = \gamma = 90°$, β= 101.82(3)°, *V* = 5651(2) Å³, *Z* = 4, ρ_c = 1.320 g/cm³, μ = 1.700 mm⁻¹, *T* = 173 K, $2\theta_{max}$ = 55º, 49053 reflections collected, 12994 independent reflections (R_{int} = 0.060). Final *GooF* = 1.065, R_1 = 0.041, wR_2 = 0.101, *R* indices based on 11062 reflections with I $> = 2\sigma$(I) (refinement on F^2), 676 parameters, 0 restraints. Lp and absorption corrections applied.

[Yb(MesForm)$_3$].Fluorene (2.9)

C$_{70}$H$_{79}$N$_6$Yb, M = 1177.46, 0.10 × 0.05 × 0.10 mm^3, monoclinic, space group $P2_1/c$, a = 12.699(6), b = 64.203(3), c = 14.673(7) Å, $\alpha = \gamma = 90°$, β = 108.756(2)°, V = 11328(10) Å^3, Z = 4, ρ_c = 1.284 g/cm^3, , μ = 1.695 mm^{-1}, T = 173 K, $2\theta_{max}$ = 55º, 138197 reflections collected, 24511 independent reflections (R_{int} = 0.096). Final *GooF* = 1.250, R_1 = 0.123, wR_2 = 0.246, *R* indices based on 17201 reflections with I $> = 2\sigma$(I) (refinement on F^2), 1297 parameters, 0 restraint. Lp and absorption corrections applied.

[(DippFormH$_2$)−μ−I]$_2$.Benzil (2.10)

C$_{64}$H$_{86}$N$_4$O$_2$I$_2$, M = 1197.20, 0.10 × 0.04 × 0.03 mm^3, monoclinic, space group $P2_1/c$, a = 14.9867(14), b = 10.8715(11), c = 39.277(3) Å, $\alpha = \gamma = 90°$, β = 91.726(5)°, V = 6396(10) Å^3, Z = 4, ρ_c = 1.241 g/cm^3, , μ = 1.025 mm^{-1}, T = 173 K, $2\theta_{max}$ = 55º, 81645 reflections collected, 14669 independent reflections (R_{int} = 0.102). Final *GooF* = 1.019, R_1 = 0.068, wR_2 = 0.184, *R* indices based on 5657 reflections with I $> = 2\sigma$(I) (refinement on F^2), 665 parameters, 13 restraints. Lp and absorption corrections applied.

2.7 References

[1]. Bickelhaupt, F. *J. Organomet. Chem.* **1994**, *475*, 1-14.

[2]. Carey, F. A.; Sundberg. R. J. *Advanced Organic Chemistry, Reactions and Synthesis, Part B.* 4th ed. Plenum Publishers: New York, **2001**.

[3]. Evans, D. F.; Fazakerley, G. V.; Phillips, R. F. *J. Chem. Soc. A.* **1971**, 1931-1934.

[4]. Syutkina, O. P.; Rybakova, L. F.; Petrov, E. S.; Beletskaya, I. P. *J. Organomet. Chem.* **1985**, *280*, C67-C69.

[5]. Petrov, E. S.; Roitershtein, D. M.; Rybakova, L. F. *J. Organomet. Chem.* **2002**, *647*, 21-27.

[6]. Hou, Z.; Fujiwara, Y.; Jintoku, T.; Mine, N.; Yokoo, K.; Taniguchi, H. *J. Org. Chem.* **1987**, *52*, 3524-3528.

[7]. Fukagawa, T.; Fujiwara, Y.; Yokoo, K.; Taniguchi, H. *Chem. Lett.* **1981**, 1771-1774.

[8]. Deng, M.; Yao, Y.; Shen, Q.; Zhang, Y.; Lang, J.; Zhou, Y. *J. Organomet. Chem.* **2003**, *681*, 174-179.

[9]. Evans, W. J. *J. Organomet. Chem.* **2002**, *647*, 2-11.

[10]. Hou, Z.; Wakatsuki, Y. *J. Organomet. Chem.* **2002**, *647*, 61-70.

[11]. Edelmann, F. T.; Freckmann, D. M.; Schumann, H. *Chem. Rev.* **2002**, *102*, 1851-1896.

[12]. Evans, W. J.; Zucchi, G.; Ziller, J. W. *J. Am. Chem. Soc.* **2003**, *125*, 10-11.

[13]. Hazin, P. N.; Lakshminarayan, C.; Brinen, L. S.; Knee, J. L.; Bruno, J. W.; Streib, W. E.; Folting, K. *Inorg. Chem.* **1988**, *27*, 1393-1400.

[14]. Evans, W. J.; Allen, N. T.; Ziller, J. W. *Angew. Chem. Int. Ed.* **2002**, *41*, 359-361.

[15]. Heeres, H. J.; Renkema, J.; Booij, M.; Meetsma, A.; Teuben, J. H. *Organometallics.* **1988**, *7*, 2495-2502.

[16]. Watson, P. L. *J. Chem. Soc. Chem. Commun.* **1980**, 652-653.

[17]. Heckmann, G.; Niemeyer, M. *J. Am. Chem. Soc.* **2000**, *122*, 4227-4228.

[18]. Bochkarev, M. N.; Zakharov, L. N.; Kalinina, G. S. *Organoderivatives of Rare Earth Elements*. Kluwer Academic: Dordrecht, **1995**.

[19]. Cotton, S. A. *Coord. Chem. Rev.* **1997**, *160*, 93-127.

[20]. Eaborn, C.; Hitchcock, P. C.; Izod, K.; Smith, J. D. *J. Am. Chem. Soc.* **1994**, *116*, 12071-12072.

[21]. Eaborn, C.; Hitchcock, P. C.; Izod, K.; Lu, Z.; Smith, J. D. *Organometallics.* **1996**, *15*, 4783-4790.

[22]. Wiecko, M.; Deacon, G. B.; Junk, P. C. *Chem. Commun.* **2010**, *46*, 5076-5078.

[23]. Dolgoplosk, B. A.; Tinyakova, E. I.; Markevich, I. N.; Soboleva, T. V.; Chernenko, G. M.; Sharaev, O. K.; Yakovlev, V. A. *J. Organomet. Chem.* **1983**, *255*, 71-79.

[24]. Timothy, P. H. *Polyhedron.* **1990**, *9*, 1345-1362.

[25]. Harder, S. *Angew. Chem. Int. Ed.* **2004**, *43*, 2714-2718.

[26]. Shannon, R. D. *Acta. Crystallogr. A.* **1976**, *A32*, 751-767.

[27]. Westerhausen, M.; Gartner, M.; Fischer, R.; Langer, J.; Yu, L.; Reiher, M. *Chem. Eur. J.* **2007**, *13*, 6292-6306.

[28]. Fischer, R.; Gartner, M.; Gorls, H.; Westerhausen, M. *Angew. Chem. Int. Ed.* **2006**, *45*, 609-612.

[29]. Westerhausen, M. *Coord. Chem. Rev.* **2008**, *252*, 1516-1531.

[30]. Langer, J.; Gorls, H.; Westerhausen, M. *Inorg. Chem. Commun.* **2007**, *10*, 853-855.

[31]. Schuman, H.; Meese-Marktscheffel, J. A.; Esser, L. *Chem. Rev.* **1995**, *95*, 865-986.

[32]. Edelman, F. T. Scandium, Yttrium, and the Lanthanide and Actinide Elements, Excluding their Zero Oxidation State Complexes. In *Comprehensive Organometallic Chemistry II*. Wilkinson, G.; Stone, F. A.; Abel, E. W. Eds. Pergamon: Oxford, **1995**, Vol. 4, 11-212.

[33]. Anwander, R.; Herrmann, W. A. *Top Curr. Chem.* **1996**, *179*, 1-32.

[34]. Kobayashi, S. *Lanthanides Chemistry and Use in Organic Synthesis*. Springer: Berlin, **1999**.

[35]. Negishi, E. *Acc. Chem. Res.* **1982**, *15*, 340-348.

[36]. Beletskaya, I. P. *J. Organomet. Chem.* **1983**, *250*, 551-564.

[37]. Evans, W. J.; Meadows, J. H.; Hunter, W. E.; Atwood, J. L. *J. Am. Chem. Soc.* **1984**, *106*, 1291-1300.

[38]. Jeske, G.; Lauke, H.; Mauermann, H.; Schumann, H.; Marks, T. J. *J. Am. Chem. Soc.* **1985**, *107*, 8111-8118.

[39]. Watson, P. *J. Am. Chem. Soc.* **1982**, *104*, 337-339.

[40]. Molander, G. A.; Hoberg, J. O. *J. Am. Chem. Soc.* **1992**, *114*, 3123-3125.

[41]. Jeske, G.; Lauke, H.; Mauermann, H.; Swepston, P.; Schumann, H.; Marks, T. *J. Am. Chem. Soc.* **1985**, *107*, 8091-8103.

[42]. Burger, B. J; Thompson, M. E; Cotter, W. D.; Bercaw, J. E. *J. Am. Chem. Soc.* **1990**, *112*, 1566-1577.

[43]. Clair, M. S.; Schaefer, W. P.; Bercaw, J. E. *Organometallics.* **1991**, *10*, 525-527.

[44]. Evans, W. J.; Wayda, A. L. *J. Chem. Soc. Chem. Commun.* **1981**, 706-708.

[45]. Evans, W. J.; Grate, J. W.; Doedens, R. J. *J. Am. Chem. Soc.* **1985**, *107*, 1671-1679.

[46]. Evans, W. J.; Grate, J. W.; Hughes, L. A.; Zhang, H.; Atwood, J. L. *J. Am Chem. Soc.* **1985**, *107*, 3728-3730.

[47]. Watson, P. L. *J. Am. Chem. Soc.* **1983**, *105*, 6491-6493.

[48]. Thompson, M. E.; Baxter, S. M.; Bulls, A. R.; Burger, B. J.; Nolan, M. C.; Santarsiero, B. D.; Schaefer, W. P.; Bercaw, J. E. *J. Am. Chem. Soc.* **1987**, *109*, 203-219.

[49]. Forsyth, C. M.; Nolan, S. P.; Marks, T. J. *Organometallics.* **1991**, *10*, 2543-2545.

[50]. Gagne, M. R.; Stern, C. L.; Marks, T. J. *J. Am. Chem. Soc.* **1992**, *114*, 275-294.

[51]. Li, Z.; Zhang, Y. *Tetrahedron Lett.* **2001**, *42*, 8507-8510.

[52]. Hyeon, J.; Edelman, F. T. *Coord. Chem. Rev.* **2003**, *241*, 249-272.

[53]. Jin, W.; Makioka, Y.; Kitamura, T.; Fujiwara, Y. *Chem. Commun.* **1999**, 955-956.

[54]. Niemeyer, M. *Eur. J. Inorg. Chem.* **2001**, 1969-1981.

[55]. Forsyth, C. M.; Deacon, G. B. *Organometallics.* **2003**, *22*, 1349-1352.

[56]. Deacon, G. B.; Junk, P. C.; Moxey, G. J. *Chem. Asian J.* **2009**, *4*, 1309-1317.

[57]. Hamidi, S. PhD thesis, Chapter 3. Monash University, **2012**.

[58]. Junk, P. C.; Cole, M. L.; Deacon, G. B.; Forsyth, C. M.; Konstas, K.; Wang, J.; Bittig, H.; Werner, D. *Chem. Eur. J.* **2013**, *19*, 1410-1420.

[59]. Ku, K. W.; Au, C. W.; Chan, H.; Lee, H. K. *Dalton Trans.* **2013**, *42*, 2841-2852.

[60]. Michael, W.; Noltemeyer, M.; Pieper, U.; Schmidt, H.; Stalke, D.; Edelmann, F. T. *Angew. Chem. Int. Ed.* **1990**, *29*, 894-896.

[61]. Pan, C.; Hou, C.; Zhang, L.; Fan, Y.; Sheng, S. *Mendeleev Commun.* **2012**, *22*, 109-110.

[62]. Qayyum, S.; Noor, A.; Glatz, G.; Kempe, R. *Z. Anorg. Allg. Chem.* **2009**, *635*, 2455-2458.

[63]. Liu, Y.; Zhao, Y.; Yang, XJ.; Li, S.; Gao, J.; Yang, P.; Xia, Y.; Wu, B. *Organometallics.* **2011**, *30*, 1599-1606.

[64]. Shsnnon, R. D.; Prewitt, C. T. *Acta. Crystallogr. B.* **1969**, *B25*, 925-946.

[65]. Deacon, G. B.; Jaroschik, F.; Junk, P. C.; Kelly, R. P. *Organometallics.* **2015**, *34*, 2369-2377.

[66]. Köhler, M.; Langer, J.; Fischer, R.; Görls, H.; Westerhausen, M. *Chem. Eur. J.* **2013**, *19*, 10497-10500.

[67]. Cole, M. L.; Deacon, G. B.; Forsyth, C. M.; Junk, P. C.; Konstas, K.; Wang, J. *Chem. Eur. J.* **2007**, *13*, 8092-8110.

[68]. Huebner, L.; Kornienko, A.; Emge, T. J.; Brennan, J. G. *Inorg. Chem.* **2005**, *44*, 5118-5122.

[69]. Zhou, F.; Zhang, S.; Zhao, Y.; Zhang, C.; Cheng, X.; Zheng, L.; Zhang, Y.; Li, Y. *Z. Anorg. Allg. Chem.* **2009**, *635*, 2636-2641.

[70]. Tu, J.; Li, W.; Xue, M.; Zhang, Y.; Shen, Q. *Dalton Trans.* **2013**, *42*, 5890-5901.

[71]. Lueken, H.; Schmitz, J.; Lamberts, W.; Hannibal, P.; Handrick, K. *Inorg. Chim. Acta.* **1989**, *156*, 119-124.

[72]. Fischer, R. D.; Qiao, K.; Li, X.; Akhnoukh, T.; Muller, J. *J. Organomet. Chem.* **1991**, *408*, 47-60.

[73]. Andrew, W. G.; Bowden, A.; Singh, K.; Townsend, R. *Inorg. Chim. Acta.* **2010**, *363*, 243-249.

[74]. Roesky, H. W.; Neculai, A. M.; Neculai, D.; Magull, J. *Polyhedron.* **2004**, *23*, 183-187.

[75]. Fedushkin, I. L.; Maslova, O. V.; Baranov, E. V.; Shavyrin, A. S. *Inorg. Chem.* **2009**, *48*, 2355-2357.

[76]. Scott, N. M.; Kempe, R. *Eur. J. Inorg. Chem.* **2005**, 1319-1324.

[77]. Barrett, A. G. M.; Crimmin, M. R.; Hill, M. S.; Hitchcock, P. B.; Kociok-Kohn, G.; Procopiou. P. A. *Inorg. Chem.* **2008**, *47*, 7366-7376.

[78]. Schultz, M. *Acta Crystallogr. E.* **2008**, *E64*, m232.

[79]. Duncalf, D. J.; Hitchcock, P. B.; Lawless, G. A. *Chem. Commun.* **1996**, 269-271.

[80]. Constantine, S. P.; De Lima, G. M.; Hitchcock, P. B.; Keates, J. M.; Lawless, G. A. *Chem. Commun.* **1996**, 2421-2422.

[81]. Heitmann, D.; Jones, C.; Junk, P. C.; Lippert, K.; Stasch, A. *Dalton Trans.* **2007**, 187-189.

[82]. Yan, L.; Liu, H.; Wang, J.; Zhang, Y.; Shen, Q. *Inorg. Chem.* **2012**, *51*, 4151-4160.

[83]. Van den Hende, J. R.; Hitchcock, P. B.; Holmes, S. A.; Lappert, M. F.; Leung, W.; Mak, T. C.; Prashar, S. *J. Chem. Soc. Dalton Trans.* **1995**, 1427-1433.

[84]. Panda, T. K.; Zulys, A.; Gamer, M. T.; Roesky, P. W. *J. Organomet. Chem.* **2005**, *690*, 5078-5089.

[85]. Dietel, A. M.; Doering, C.; Glatz, G.; Butovskii, M.; Tok, O.; Schappacher, F. M.; Pottgen, R.; Kempe, R. *Eur. J. Inorg. Chem.* **2009**, 1051-1059.

[86]. Roberts, R. M. *J. Org. Chem.* **1949**, *14*, 277-284.

[87]. Kuhn, K. M.; Grubbs, R. H. *Org. Lett.* **2008**, *10*, 2075-2077.

[88]. Sheldrick, G. M. *SHELXL-97*. University of Gottingen, Gottingen, **1997**.

[89]. Barbour, L. J. *J. Supramol. Chem.* **2001**, *1*, 189-191.

Chapter 3: Synthesis of biphenolate lanthanoid complexes

3.1 Introduction

The redox transmetallation (RT) reaction was introduced in Chapter one as an increasingly common synthetic pathway to lanthanoid complexes.[1-5] RT involves treating oxidising agents, such as mercury, thallium, tin and bismuth reagents, with more electropositive lanthanoid metals in a donor solvent.[6-10, 22, 24]

3.1.1 Redox transmetallation by mercury reagents

The first exploitation of RT was carried out in 1976 by Deacon and Vince to synthesise a σ-bonded fluorocarbon-ytterbium complex, $[Yb(C_6F_5)_2(thf)_4]$ (Fig. 3.1) using $[Hg(C_6F_5)_2]$ as the oxidant (eqn. 3.1). The compound (deep orange-red crystals) was a highly air- and moisture-sensitive organolanthanoid complex. This complex decomposed if heated to 75 °C, and exploded at 78 °C.[12, 13]

$$Ln + Hg(C_6F_5)_2 \xrightarrow{\text{thf}} [Ln(C_6F_5)_2] + Hg$$
$$Ln = Yb, Eu, Sm$$
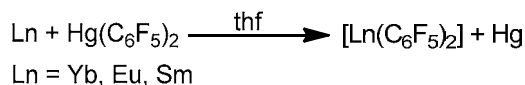
Equation 3.1
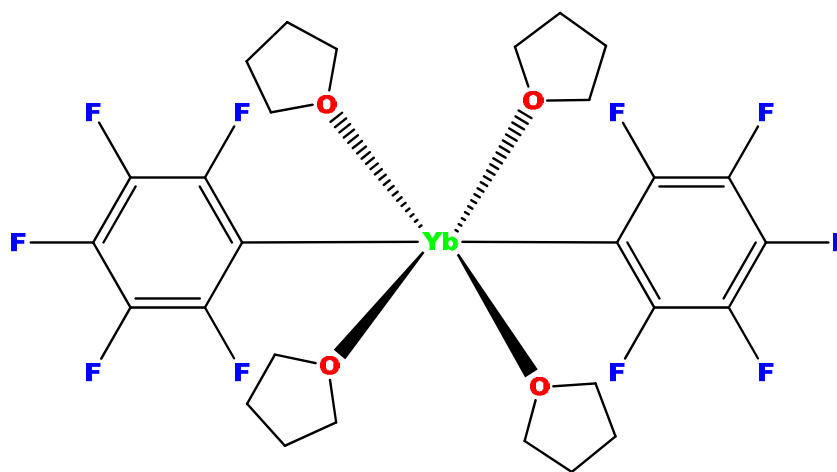
Figure 3.1 Molecular structure of $[Yb(C_6F_5)_2(thf)_4]$.

90

The solid state structure of $[Yb(C_6F_5)_2(thf)_4]$ (Fig. 3.1) comprises a six-coordinated ytterbium metal centre that is coordinated by four oxygen atoms of thf molecules, and two *transoid* pentafluorophenyl groups in an octahedral geometry.[10] The europium analogue has been reported by Deacon and co-workers in 2000 by a similar route (eqn. 3.1). This analogue has an additional coordinated thf molecule, to give a seven coordinate pentagonal bipyramidal complex and is a good example of the lanthanoid contraction.[13] Bochkarev, et. al.[24] have expanded the redox transmetallation reaction to synthesise trivalent lanthanoid complexes $[LnPh_3]$ (Er, Tm) by the direct reaction between lanthanoid metal and mercury reagent $HgPh_2$ (eqn. 3.2).

$$2Ln_{(metal)} + 3HgPh_2 \xrightarrow{thf, \ LnI_3} 2[LnPh_3] + 3Hg$$
$$Ln = Er, Tm$$
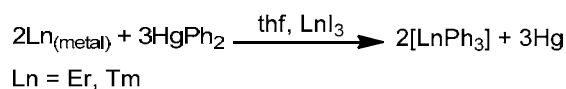
Equation 3.2

Transmetallation reactions between lanthanoid elements and diphenylmercury $[Hg(Ph)_2]$ are generally harder to induce than those with $[Hg(C_6F_5)_2]$, without an activation source such as elemental Hg, $HgCl_2$ or I_2 and heating.[14]

Mercuric amides have been used as oxidants in RT to synthesise different organoamido lanthanoid(II) complexes (eqn. 3.3). This has been shown with a number of amides, e.g. for NR_2; R = $SiMe_3$, Ln = Sm, Eu, Yb[15], NR_2 = $N(SiMe_3)(2,6-^iPr_2-C_6H_3)$,[16] Ln = Sm, Yb; NR_2; R = $3,5-Ph_2pz$ (pz = pyrazole), Ln = Yb.[6]

$$Ln_{(metal)} + Hg(NR_2)_2 \xrightarrow{thf} [Ln(NR_2)_2] + Hg$$
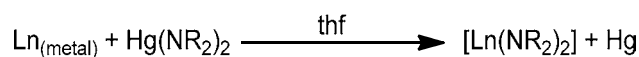
Equation 3.3

Redox transmetallation reaction has a distinct advantage compared with other methods. The process is a simple one-pot procedure with easy separation of the products.[14] Moreover, it provides a cheaper and more convenient alternative to the lanthanoid(II)

halides. Furthermore, the starting materials, for example mercurial organometallics or organoamidometallics used in this process are easily prepared and air stable. The elemental mercury resulting from reduction of the mercury compound can simply be removed by filtration of the mother liquor by a filter cannula.

Mercurial species $[Hg(C_6F_5)_2]$, $[Hg(C_6H_5)_2]$, $[Hg(NR_2)_2]$ play a substantial role in RT reactions (eqn. 3.1; eqn. 3.2 eqn. 3.3), but they are not the only oxidants in the chemistry of lanthanoids.

3.1.2 Redox transmetallation by thallium reagents

Thallium(I) organoamides and aryloxides derivatives have been exploited as oxidants in redox transmetallation for the synthesis of the corresponding lanthanoid complexes (eqn. 3.4). Its origins go back to the synthesis of lanthanoid cyclopentadienyls since 1980.[4, 6, 7, 16-20]

$$Ln + nTlR \xrightarrow{\text{solv}} [LnR_n(solv)_x] + nTl$$

Ln = Eu; Yb, R = Ph_2pz, solv = dme, n = 2; x = 2
Ln = Yb, R = $2,6\text{-}Bu^t_2\text{-}C_6H_3O$, solv = thf, n = 2; x = 3
Ln = Yb, R = $2, 4, 6\text{-}Bu^t_3\text{-}C_6H_2O$, solv = thf, n = 3; x = 1
Ln = Sm, Nd n = 3, Yb n = 2, R = C_5H_5, solv = thf; x = 1
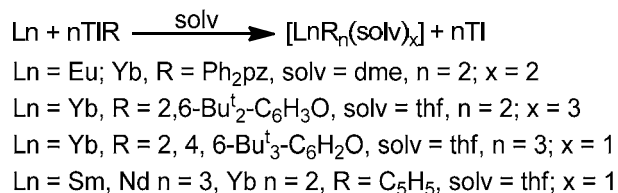
Equation 3.4

This method has attractive features, such as its simplicity and the fact that key reagents are commercially available. In addition, this route is one of the most accessible synthetic pathways to lanthanoid complexes. However, the most significant drawbacks associated with this method are the toxicity and air and light sensitivity of thallium reagents.

3.1.3 Redox transmetallation by tin reagents

Using tin precursors as oxidants in RT represents one of the recent expansions in the evolution of the RT reaction. The first example of the investigation of tin reagents as potential redox transmetallation oxidants was undertaken by Lappert *et. al.* in 1992. They

reported the use of the tin(II) reagent [Sn{N(SiMe$_3$)$_2$}$_2$] as an oxidant in RT involving a reduction of Sn^{+2} to Sn^0 (eqn 3.5).[21]

$$Yb + [Sn\{N(SiMe_3)_2\}_2] \xrightarrow{\text{dme}} [Yb\{N(SiMe_3)_2\}_2] + Sn$$
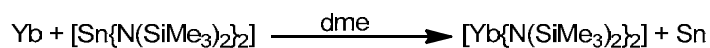
Equation 3.5

This reaction was recently modified to synthesise a variety of species of organolanthanoid complexes, such as [Ln(Ph$_2$pz)$_2$(dme)$_2$] (Ln = Sm, Eu, Yb)[22], [Ln(Ph$_2$pz)$_3$(solv)$_2$] (Ln = La; solv = dme, Yb; solv = thf)[31], (Ln = Y, Nd, Eu) and [Sm(OAr)$_3$(thf)], by using tin(IV) pyrazolates or aryloxides as oxidants. During the reaction Sn^{IV} is reduced to Sn^{+3} as hexamethylditin (eqn 3.6).[22, 23]

$$Ln + 2[SnMe_3(Ph_2Pz)] \xrightarrow{\text{dme}} [Ln(Ph_2Pz)_2(dme)_2] + Sn_2Me_6 \quad \textbf{(i)}$$
$$Ln = Sm, Eu, Yb$$
$$Sm + n/2[SnMe_2(Ph_2Pz)_2] \xrightarrow{\text{dme}} [Sm(Ph_2Pz)_3(dme)_2] + n/2SnMe_2 \quad \textbf{(ii)}$$

$$2Ln + 6SnMe_3L \xrightarrow{\text{solv}} 2[LnL_3(solv)_n] + 3Sn_2Me_6 \quad \textbf{(iii)}$$
Ln = Y, La, Nd, Eu; L = Ph$_2$pz; solv = dme; n = 2
Ln = Nd, Sm n = 3, Yb n = 2; solv = thf; n = 3; L = Ph$_2$pz;
Ln = Sm; L = 2,6-Bu$^t_2$-4-MeC$_6$H$_2$O; solv = thf; n = 1
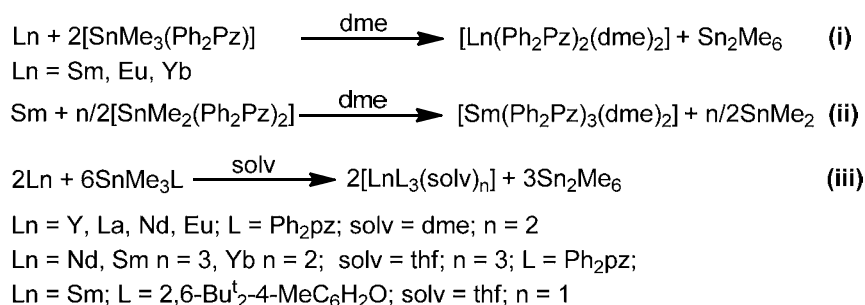
Equation 3.6

3.1.4 Redox transmetallation by bismuth reagents

Equation 3.7 shows an alternative RT synthetic route that has been reported by Bochkarev *et al* for preparing an organolanthanoid complex [ErPh$_3$(thf)$_3$] by direct oxidation of Er by BiPh$_3$ in the presence of ErI$_3$.[24] This reaction (eqn. 3.7) is a much greener reaction as Bi is essentially non-toxic. However, the oxidising agent [BiPh$_3$] is less reactive than mercurial species [Hg(C$_6$F$_5$)$_2$] and [Hg(C$_6$H$_5$)$_2$].

$$Er + BiPh_3 \xrightarrow{\text{ErI}_3, \text{thf}} [ErPh_3(thf)_3] + Bi$$
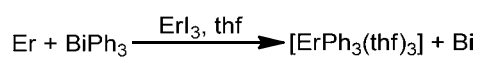
Equation 3.7

3.1.5 Redox transmetallation/protolysis (RTP)

RTP is an extension of the RT route. RT has been modified to synthesise different species of divalent and trivalent complexes, by merging the redox transmetallation and ligand exchange reactions (eqn. 3.8).[14, 17, 25-30]

$$M + Hg(C_6F_5)_2 + 2LH \xrightarrow{thf} [ML_2(thf)_n] + 2C_6F_5H + Hg \qquad \textbf{(i)}$$

M = Ca; Sr; Ba, L = Pyrazolate; formamidinate
M = Yb; L = 2, 4, 6-Bu^t_3-C_6H_2O
M = Eu; L = 2,6-Bu^t_2-4-MeC_6H_2O, n = 2, 3

$$2M + 3Hg(C_6F_5)_2 + 6LH \xrightarrow{thf} 2[ML_3(thf)_n] + 6C_6F_5H + 3Hg \qquad \textbf{(ii)}$$

M = Ce, Nd, Sm, Gd; L = C_6H_5; n = 1
M = Sm, Tb, Er, Yb; L = 2, 4, 6-Me-C_6H_2O; n = 3
M = Ho; L = 2,6-Bu^t_2-4-MeO-C_6H_2O; n = 1

Equation 3.8

RTP (eqn. 3.8) has two steps. Firstly, the reaction between the organomercurial and freshly filed Ln metal or group 2 forms the organometallic intermediate which is $[M(C_6F_5)_n]$ (M = Ln or group 2; n = 2, 3). This step involves redox transmetallation, which involves the oxidation of M metal to M^{+2} and the reduction of Hg^{+2} to Hg^0 metal. Secondly, the organometallic intermediate $[M(C_6F_5)_2]$ or $[M(C_6F_5)_3]$ reacts further with the a protic ligand through ligand exchange (eqn. 3.9)[10, 13, 30] this step depends on the thermodynamic acidities (pKa values) of LH vs C_6F_5H, if LH has a lower pKa than C_6F_5H then the reaction occurs. The protic ligand should be more acidic than pentafluorobenzene (pKa 26) in order to form the desired metal-organic complex.[31]

$$M + Hg(C_6F_5)_2 \xrightarrow{thf} M(C_6F_5)_2 + 2LH \xrightarrow{thf} [ML_2(thf)_n] + 2C_6F_5H + Hg$$

M = Ln or group2

$$2M + 3Hg(C_6F_5)_2 \xrightarrow{thf} 2M(C_6F_5)_3 + 6LH \xrightarrow{thf} 2[LnL_3(thf)_n] + 6C_6F_5H + 3Hg$$
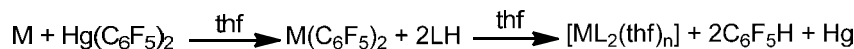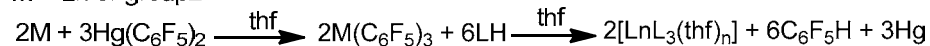
M = Ln

Equation 3.9

3.1.6 Lanthanoid biphenolate complexes

Biphenol {2,2′-methylenebis(6-*tert*-butyl-4-methylphenol)} has been employed as a proligand to synthesise a number of rare earth complexes through different synthetic routes. For example, ionic and non-ionic heterobimetallic lanthanoid complexes can be synthesised in good yield via the halide metathesis of lanthanoids with biphenolate alkali metal salt complexes (eqn. 3.10, 3.11).[11, 32, 33]
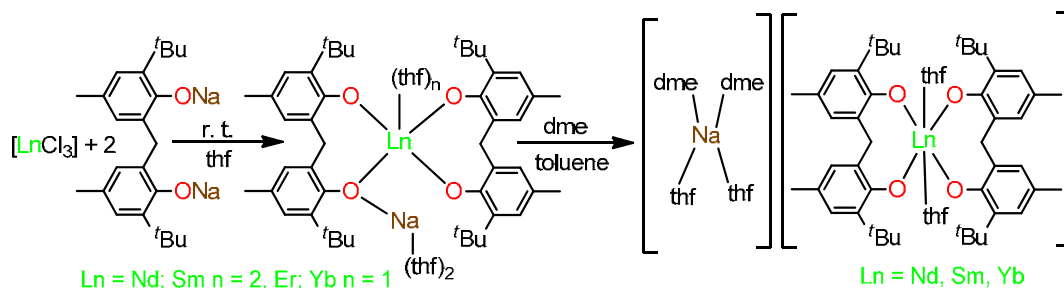
Equation 3.10
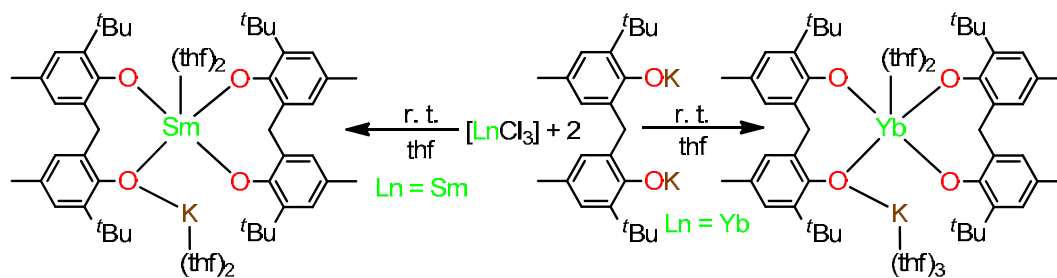
Equation 3.11

Moreover, the protolysis/ligand exchange reaction has been reported as a synthetic route to prepare neutral trivalent lanthanoid alkoxides by using [Ln(C$_5$H$_5$)$_3$] as starting material (eqn. 3.12).[34, 35]
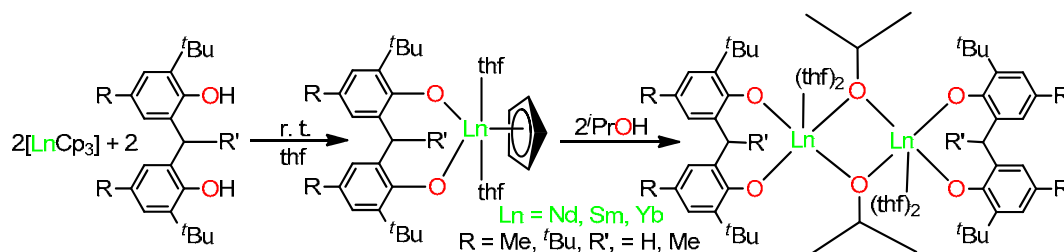
Equation 3.12

Furthermore, Yao, *et. al* have synthesised dinuclear heteroleptic lanthanoid complexes through ligand exchange by using [Ln(C₅H₅)₃(thf)] as precursors (eqn. 3.13).[36, 37]
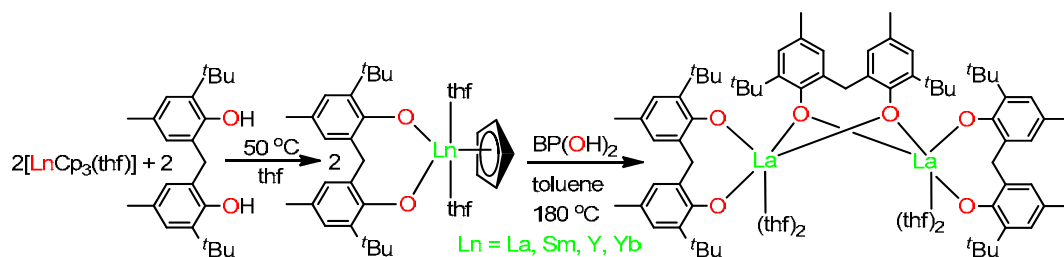
Equation 3.13

In addition, the partial hydrolysis of the neutral biphenolate neodymium amide [Ln(BPO$_2$){N(SiMe$_3$)$_2$}(thf)$_2$] gives neodymium hydroxide first, followed by insertion of phenyl isocyanate to the O–H bond to form dinuclear biphenolate neodymium complex (eqn. 3.14).[38]
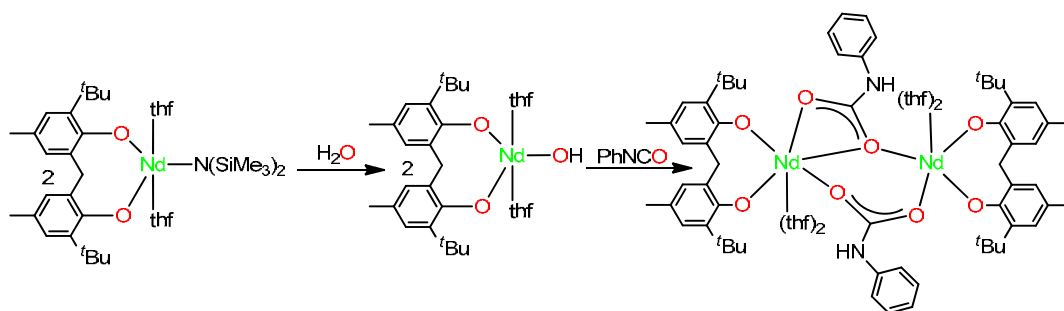
Equation 3.14

This work was recently further developed by treating [Ln{N(SiMe$_3$)$_2$}$_2$Cl(thf)$_2$] with a biphenol proligand to prepare bridged biphenolate lanthanoid chloride complexes. These lanthanoid chlorides were found to be useful precursors for the synthesis of the corresponding lanthanoid amido derivatives (eqn. 3.15).[39]

Equation 3.15

96
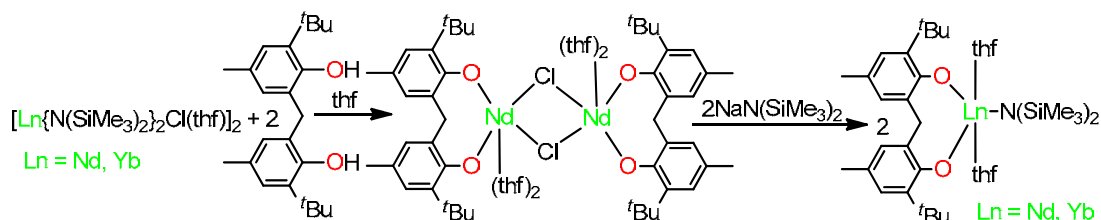
In 2004 Deng *et al.*[40] synthesised heteroleptic dimeric lanthanoid(II) derivatives with a biphenol ligand via a protolysis reaction (eqn. 3.16), followed by Bao *et al.* who prepared the first europium(II) biphenolate as a dinuclear complex by the halide metathesis reaction which involves reduction of Eu^{+3} to Eu^{+2} by Na–K alloy (eqn. 3.17).[41]
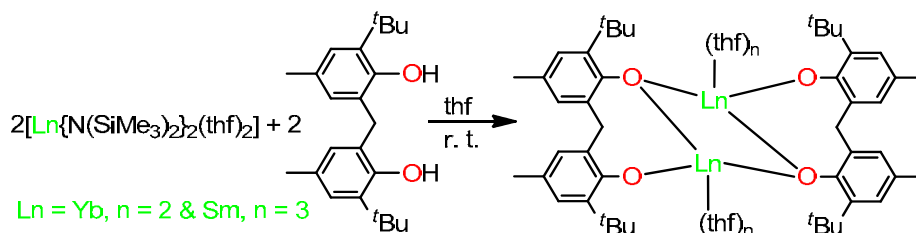
Equation 3.16
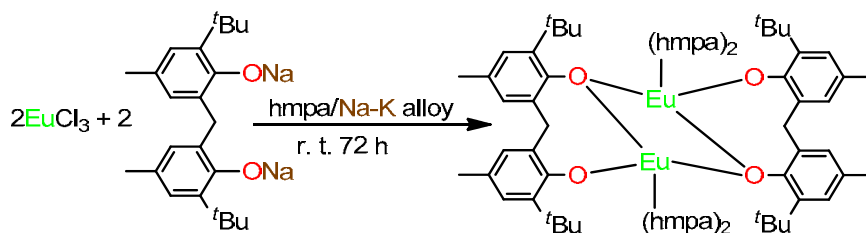
Equation 3.17

Fang *et al.* have synthesised and characterised an ionic heterobimetallic complex using a salt metathesis reaction. However, they used a lanthanoid borohydride as the precursor instead of lanthanoid chloride, because of the better solubility of the former in dme (eqn 3.18).[42]

Equation 3.18

97
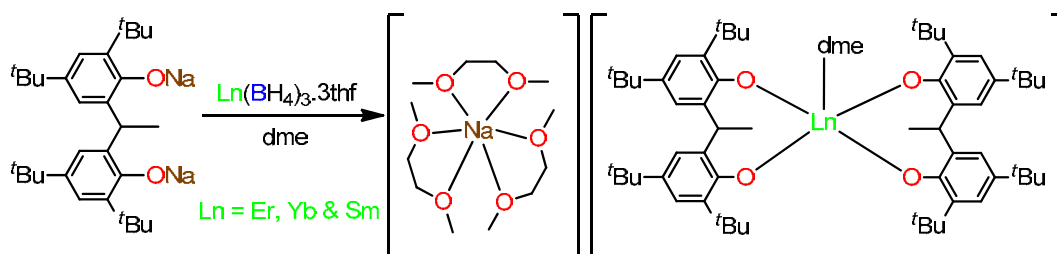
3.2 Current study

Biphenolate lanthanoid chemistry is still limited in contrast to the rich lanthanoid chemistry of the calixarene and other polyphenol ligands. Also, due to the lack of research into biphenolate alkaline earth complexes, the original aims were to synthesise mononuclear and dinuclear lanthanoid and alkaline earth biphenolate complexes. In addition, the current study is a prelude to Chaper four within this thesis, demonstrating a synthesis protocol which has been employed to synthesise mononuclear complexes which can be further used to synthesise heterobimetallic complexes.

Redox transmetallation/protolysis has been used to explore possibilities between lanthanoid metals and the biphenol proligand (Fig. 3.2). These reactions produced mononuclear and dinuclear complexes depending on the metal used. When the biphenol ligand was partially deprotonated it gave mononuclear complexes. For example, $[Ln(BPO_2)(BP(OH)O)(thf)_3]$ (Ln = Gd, Er, Y). $[Ce(BPO_2)_2(thf)_2]$ has a fully deprotonated set of ligands but it gave mononuclear complex due to the high oxidation number (+4) owned by cerium. Meanwhile, when the biphenol ligand was fully deprotonated it gave dinuclear complexes such as, $[Ln_2(BPO_2)_3(thf)_n]$ (Ln = Ho, Yb, n = 2; Sm, Tb, n = 3). Various structural comparisons can be made to each obtained complex with analogous species. Complex $[Eu(BPO_2)(thf)_2]_2$ (**3.9**) is the divalent lanthanoid biphenolate isolated from redox transmetallation in this study. In addition, a single example of a dinuclear strontium-biphenolate cluster $[Sr_2(BPO_2)_2(thf)_5]$ has been synthesised and structurally characterised. It is interesting to compare divalent europium biphenolate with strontium biphenolate as Eu^{+2} and Sr^{+2} have approxymately similar sizes and expected chemistry (ionic radius 1.17 Å and 1.18 Å respectively for six coodinate)[56]. However, no reaction occurred with other alkaline earth metals such calcium or barium. The partially

deprotonated complexes were then utilised in Chapter 4 to synthesise heterobimetallic complexes by treating $[Ln(BPO_2)(BP(OH)O)(thf)_n]$ with different metal alkyls.

The redox transmetallation/protolysis reaction was carried out in a donor solvent (thf). Structures of all the complexes have been confirmed by X-ray crystallography and further support by ^{1}H-NMR and IR spectroscopies as well as elemental analysis and melting point.

3.3 Results and discussion

3.3.1 Synthesis

The proligand used in the redox transmetallation synthesis was 2,2′-methylenebis(6-*tert*-butyl-4-methylphenol) (BP(OH)$_2$) (Fig. 3.2). Syntheses of complexes containing this ligand have been reported previously, allowing for comparisons in this work. The BP(OH)$_2$ proligand has attractive features including many proton environments providing easily interpretable ^{1}H-NMR spectra. Moreover, the bridging methylene group Ar-*CH$_2$*-Ar provides a flexibility that can allow the metal centre to reside in a range of different geometries. Furthermore, either mono- or double-deprotonation at the OH groups can occur. This ligand is also rather sterically demanding and has ^{t}Bu and Me groups to help provide solubility in organic solvents, while the O atoms allow a range of structural variation.
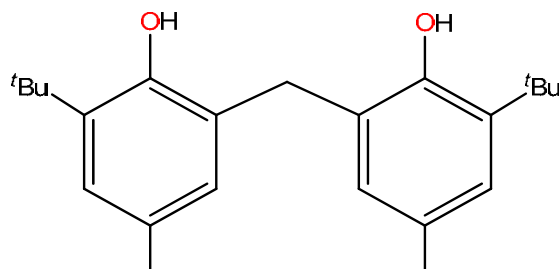
Figure 3.2 Ligand system used in redox transmetallation/protolysis syntheses (BP(OH)$_2$).

All the Ln^{+3} biphenolate complexes [Ln(BPO$_2$)(BP(OH)O)(thf)$_3$] (Ln = Y **3.1a**, Gd **3.2**, Er **3.3**) and [Ln$_2$(BPO$_2$)$_3$(thf)$_n$] (Ln = Ho **3.5**, Yb **3.6**, n = 2; Sm **3.7**, Tb **3.8**, n = 3) were synthesised by the redox transmetallation route (eqn. 3.19) between lanthanoid metals and the stoichiometric amount of the corresponding Hg(C$_6$F$_5$)$_2$ and BP(OH)$_2$.

$$2Ln + 3Hg(C_6F_5)_2 + 4BP(OH)_2 \xrightarrow[\text{r. t.}]{\text{thf}} 2[Ln(BPO_2)(BP(OH)O)(thf)_3] + 3Hg + 6C_6F_5H \quad (i)$$
$$Ln = Y, Gd, Er; n = 2, 3$$

$$2Ln + 3Hg(C_6F_5)_2 + 3BP(OH)_2 \xrightarrow[\text{r. t}]{\text{thf}} [Ln_2(BPO_2)_3(thf)_n] + 3Hg + 6C_6F_5H \quad (ii)$$
$$Ln = Ho, Yb; n = 2, Sm, Tb; n = 3$$

$$BP(OH)_2 =$$

Equation 3.19

Complexes [Ln(BPO₂)(BP(OH)O)(thf)₃] (Ln = Y **3.1a, Gd 3.2, Er 3.3**) were isolated directly from the reaction mixture (thf) while complex [Y(BPO₂)(BP(OH)O)(thf)₂] (**3.1b**) was recrystallised (**3.1a**) from deuterated benzene after the reaction had been performed in thf (eqn. 20).

$$2Y + 3Hg(C_6F_5)_2 + 4BP(OH)_2 \xrightarrow[\text{r. t.}]{\text{thf}} 2[Y(BPO_2)(BP(OH)O)(thf)_3] \xrightarrow{C_6D_6} 2[Y(BPO_2)(BP(OH)O)(thf)_2]$$

Equation 3.20

Previously, this structure [Y(BPO₂)(BP(OH)O)(thf)₂] had been reported by Yao *et. al* (2008) for the yttrium analogue.[37] They used a ligand exchange reaction to synthesise it.

The oxidative chemistry of cerium still rather limited[51, 52] particularly oxidation reactions that could lead to synthesise cerium(IV) species[54] compared with the reductive chemistry of the lanthanoids (trivalent to divalent) which has advanced considerably in recent years.[53, 54]

Oxygen-donor ligands such as BP(OH)₂ (Fig. 3.2) used in this study can effectively stabilise cerium(IV) complexes because of the large electronegativity of oxygen.[55] In addition, the presence of both *t*Bu and Me substituents on the BP(OH)₂ could support the electon deficient Ce(IV) ion.[43]

The tetravalent cerium biphenolate complex [Ce(BPO₂)₂(thf)₂] (**3.4**) was synthesised by redox transmetallation reaction (eqn. 21 i) between freshly filed cerium metal, two equivalents Hg(C₆F₅)₂ and two equivalents of the bulky proligand BP(OH)₂ in thf. This

reaction represents the first successful attempt to access the Ce(IV) valency through the one pot redox transmetallation protolysis reaction. [Ce(BPO$_2$)$_2$(thf)$_2$] was reported by Schelter *et. al* (2013)[43] through a ligand exchange reaction involving three steps to obtain the Ce(IV) complex by oxidation of the corresponding cerium(III) species by CuCl$_2$. By contrast, a one pot redox transmetallation protolysis reaction was used here to synthesise [Ce(BPO$_2$)$_2$(thf)$_2$] (**3.4**). [Ce(BPO$_2$)$_2$(thf)$_2$] was isolated from a thf solution under partial vacuum as a dark-purple crystals and rapidly decomposes to a dark solid when exposed to air.

[Eu(BPO$_2$)(thf)$_2$]$_2$ (**3.9**) is the only divalent lanthanoid complex isolated from RTP in this chemistry (eqn. 21 ii). Attempts to synthesise a divalent ytterbium complex failed and the reaction led to the isolation of the trivalent ytterbium compound. With the successful formation of [Sr$_2$(BPO$_2$)$_2$(thf)$_5$] (**3.10**) (eqn. 21 ii) by the one pot redox transmetallation reaction in thf, an attempt to synthesise a calcium or barium analogue were attempted but no reaction occurred after several days of stirring. Even after activation of the metal (I$_2$ or Hg) no reaction occurred.

$$Ce + 2Hg(C_6F_5)_2 + 2BP(OH)_2 \xrightarrow[\text{r. t.}]{\text{thf}} [Ce(BPO_2)_2(thf)_2] + 2Hg + 4C_6F_5H \quad (i)$$

$$2M + 2Hg(C_6F_5)_2 + 2BP(OH)_2 \xrightarrow[\text{r. t}]{\text{thf}} [Sr_2(BPO_2)_2(thf)_5] + 2Hg + 4C_6F_5H \quad (ii)$$

M = Sr or Eu

BP(OH)$_2$ = ... or [Eu(BPO$_2$)(thf)$_2$]$_2$

Equation 3.21

3.3.2 Characterisation

Complexes **3.1-3.10** (described above in section 3.3.1) were initially isolated as single crystals, and were identified by X-ray crystallography using the MX1 beamline of the Australian Synchrotron. These results were further supported by ^{1}H-NMR data (Table

3.1), elemental analyses, melting point and IR spectroscopic (Table 3.2). Due to the paramagnetic nature of [Gd(BPO$_2$)(BP(OH)O)(thf)$_3$] **3.2**, [Ln$_2$(BPO$_2$)$_3$(thf)$_2$] (Ln = Ho **3.5**, Yb **3.6**), [Sm$_2$(BPO$_2$)$_3$(thf)$_2$] **3.7** and [Eu(BPO$_2$)(thf)$_2$]$_2$ **3.9**, no useful information could be obtained from their ^{1}H-NMR spectra. They gave a broadened spectrum, which could not be satisfactorily interpreted. The paramagnetic Er^{+3} complex [Er(BPO$_2$)(BP(OH)O)(thf)$_3$] **3.3** gave an interpretable ^{1}H-NMR spectrum but the resonance for CH$_2$ moves upfield (0.54 ppm) due to this paramagnetism. The ^{1}H-NMR spectrum of **3.3** showed that the complex had lost two co-ligands of thf and three thf molecules from the lattice (compared with the composition obtained by X-ray crystallography) upon drying the material *in vacuo*. The IR spectra of biphenolate lanthanoid complexes showed complete deprotonation of the biphenol ligand indicated by the absence of a ν(O-H) absorption at 3610-3640 cm^{-1} {except [Y(BPO$_2$)(BP(OH)O)(thf)$_3$] **(3.1a)**, [Y(BPO$_2$)(BP(OH)O)(thf)$_2$] **(3.1b)**, [Gd(BPO$_2$)(BP(OH)O)(thf)$_3$] **(3.2)** and [Er(BPO$_2$)(BP(OH)O)(thf)$_3$] **(3.3)** as they were partially deprotonated}. In addition, there were no OH resonances in the ^{1}H-NMR spectra of the bulk vacuum dried materials. These results indicated successful synthesis of the biphenolate lanthanoid complexes.

The O–C stretching frequencies (Table 3.2) for compounds **3.1-3.11** showed the vibration of a metal-coordinated phenolate group, observed at 1212–1270 cm^{-1}. The absorption band related to O–C stretching previously reported for biphenolatolanthanoid complexes approximately same as that observed for the present complexes.[11, 34, 36]

Table 3.1 Chemical shifts in ^{1}H-NMR spectra of [Er(BPO$_2$)(BP(OH)O)(thf)$_3$] 3.3 and [Tb$_2$(BPO$_2$)$_3$(thf)$_3$] 3.8.

	Chemical shift (ppm)			
^{1}H-NMR	**3.1a**	**3.3**	**3.8**	**3.10**
Aromatic	6.91	7.41	7.78	7.15
CH$_2$	1.87, 1.50	6.20	2.55	2.17
OCH$_2$, thf	3.33	4.00	2.28	3.45
CH$_2$, thf	1.05	0.54	-0.83	1.51
CH$_3$	2.03	2.39	1.19	1.39
C(CH$_3$)$_3$	1.32	1.72	0.32	0.28

Table 3.2 O–C Stretching absorption bands in IR spectra (ν4000–400 cm^{-1}).

Compound	O–C stretching vibration (cm^{-1})
[Y(BPO$_2$)(BP(OH)O)(thf)$_3$] (**3.1a**)	1254
[Y(BPO$_2$)(BP(OH)O)(thf)$_2$] (**3.1b**)	1212
[Gd(BPO$_2$)(BP(OH)O)(thf)$_3$] (**3.2**)	1262
[Er(BPO$_2$)(BP(OH)O)(thf)$_3$] (**3.3**)	1270
[Ho$_2$(BPO$_2$)$_3$(thf)$_2$] (**3.5**)	1260
[Yb$_2$(BPO$_2$)$_3$(thf)$_2$] (**3.6**)	1259
[Sm$_2$(BPO$_2$)$_3$(thf)$_3$] (**3.7**)	1249
[Tb$_2$(BPO$_2$)$_3$(thf)$_3$] (**3.8**)	1266
[Sr$_2$(BPO$_2$)$_2$(thf)$_5$] (**4.10**)	1260

3.3.3 Crystal structure determinations

[Ln(BPO$_2$)(BP(OH)O)(thf)$_3$].3thf (Ln = Y 3.1a, Gd 3.2, Er 3.3) [Y(BPO$_2$)(BP(OH)O)(thf)$_2$].2C$_6$D$_6$ (3.1b)

Compounds **3.1a**, **3.2** and **3.3** (Fig. 3.3) crystallise in the monoclinic space group *P*2$_1$/*c* while complex [Y(BPO$_2$)(BP(OH)O)(thf)$_2$] **3.1b** crystallises in the monoclinic space group *P*2$_1$/*n* (Table 3.4). Figure 3.3 displays mononuclear complexes for **3.1a**, **3.2**, **3.3**. The Ln (Ln = Y **3.1a**, Gd **3.2**, Er **3.3**) metal centre is six-coordinate, being bound by three oxygen atoms of the two (BPO$_2$) ligands, and three oxygen atoms of thf molecules. Complex [Y(BPO$_2$)(BP(OH)O)(thf)$_2$] **3.1b**, is depicted in (Fig. 3.5), and the metal centre has the same coordination number as [Ln(BPO$_2$)(BP(OH)O)(thf)$_3$] **3.1a** (Fig. 3.4) but it coordinates to two thf molecules in a *trans* form instead of three thf molecules in a facial form in **3.1a**. To complete the six coordination in **3.1b** the Y metal centre was coordinated to both biphenolate ligands as bidentates. However, the Y metal centre of **3.1a** was coordinated as a monodentate with one ligand of biphenolate, and as a bidentate with the other biphenolate molecule. The overall molecular geometry around the six-coordinate Y metal centre is best described as a distorted octahedral for **3.1a** and **3.1b** as well for **3.2**, **3.3**. The X-ray crystal structure of [Y(BPO$_2$)(BP(OH)O)(thf)$_3$] (Fig. 3.4) is isotypic with [Gd(BPO$_2$)(BP(OH)O)(thf)$_3$], [Er(BPO$_2$)(BP(OH)O)(thf)$_3$] and therefore only one compound is depicted.

The most interesting feature in the structures of **3.1-3.3** is the unbound OH of the mono-deprotonated biphenol, which provides an opportunity for preparing heterobimetallic complexes by treatment with Li, K, Zn, Al alkyls or amides. This unbound OH group was successfully deprotonated by using these reactive metal alkyls or amides to prepare the heterobimetallic complexes in Chapter four.

The methylene group bridges the two arms of phenolate groups, giving the ligand more flexibility about the metal centre. For example, in **3.1a** (Fig. 3.4) the pendant phenol group is rotated away from the metal core while the other three phenolate groups are rotated towards the metal centre.

Selected bond lengths and angles of $[Ln(BPO_2)(BP(OH)O)(thf)_3]$ (Ln = Y **3.1a**, **3.1b**, Gd **3.2**, Er **3.3**) are listed in Table 3.3. The average $Y-O_{(phenolate)}$ bond length of $[Y(BPO_2)(BP(OH)O)(thf)_3]$ (2.12 Å) are in agreement with those determined for $[Y(BPO_2)(BP(OH)O)(thf)_2]$ (2.13 Å). Also, it is comparable to those reported for $[Y(BPO_2)(PhO)(L)_2]$ (average 2.14 Å; L = N-^{i}Pr-imidazole; Ph = 4,6-di-^{t}Bu-C_6H_2O-CH_2-^{i}Pr-imidazole)[44] and $[Na(dme)_3][Y(BPO_2)_2(dme)]$ (average 2.13 Å).[45]

The average $Gd-O_{(phenolate)}$ bond length of $[Gd(BPO_2)(BP(OH)O)(thf)_3]$ (2.16 Å) are shorter than the Gd–O bond lengths reported for $[Gd(L)_2(thf)_3]$ (average 2.24 Å; L = 2, 2', 2"-methanetriyl-*tris*(4,6-bis(2-methyl-2-propanyl)phenol) due to steric demand differences.[46]

The average $Er-O_{(phenolate)}$ bond length of $[Er(BPO_2)(BP(OH)O)(thf)_3]$ was found to be 2.11 Å which is shorter than the average $Er-O_{(phenolate)}$ bond length of the known structure $[Na(dme)_3][Er(BPO_2)_2(dme)]$ (2.14 Å).[42]
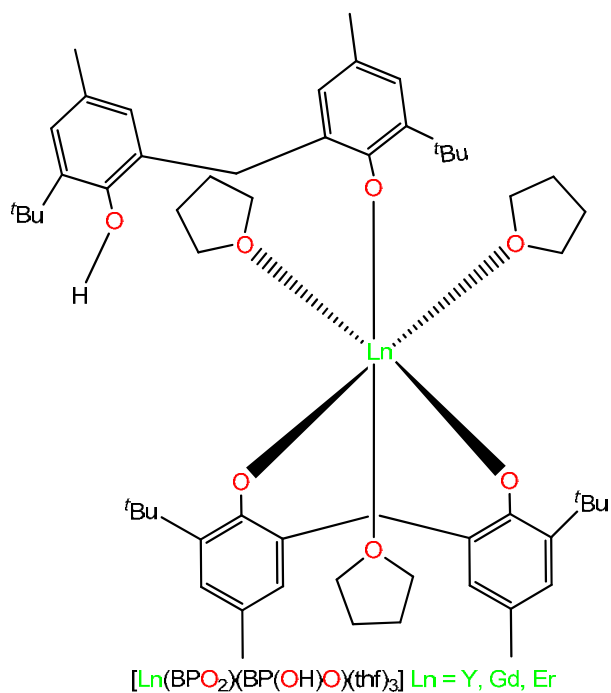
Figure 3.3 Lanthanoid biphenolate diagram of 3.1a, 3.2 and 3.3.
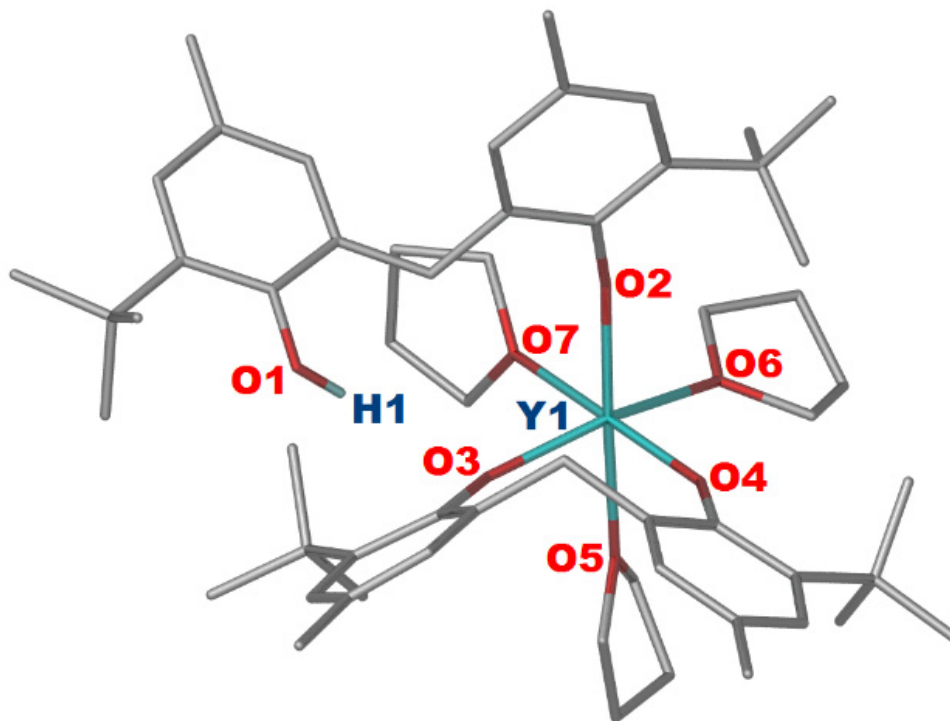
Figure 3.3 X-ray crystal structure of [Y(BPO$_2$)(BP(OH)O)(thf)$_3$] 3.1a which is isostructural with 3.2 and 3.3 (thf ligands are arranged a in facial form). Hydrogen atoms are omitted for clarity.
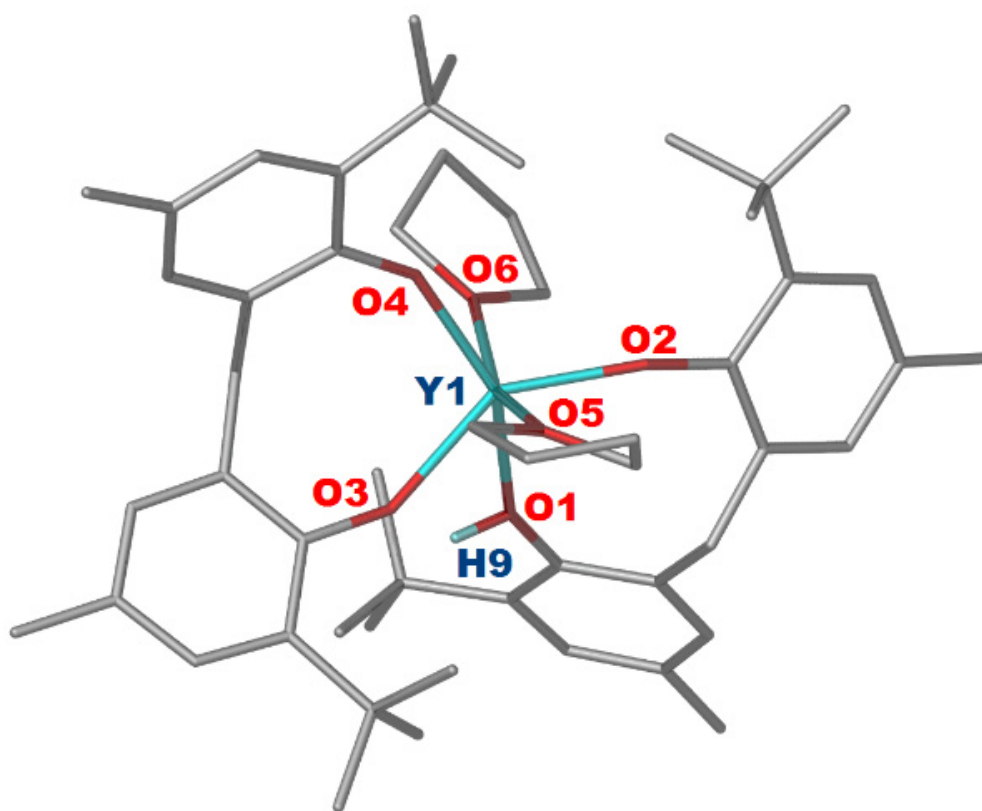
Figure 3.5 X-ray crystal structure of [Y(BPO$_2$)(BP(OH)O)(thf)$_2$] 3.1b (thf ligands are arranged in a *trans* form). Hydrogen atoms are omitted for clarity.

Table 3.1 Selected bond lengths and angles of [Ln(BPO₂)(BP(OH)O)(thf)₃] (Ln = Y, Gd, Er) and [Y(BPO₂)(BP(OH)O)(thf)₂].

Bond lengths (Å)	[Y(BPO₂)(BP(OH)O)(thf)₃]	[Y(BPO₂)(BP(OH)O)(thf)₂]	[Gd(BPO₂)(BP(OH)O)(thf)₃]	[Er(BPO₂)(BP(OH)O)(thf)₃]
Ln(1)–OH(1)	-	2.443(14)	-	-
Ln(1)–O(2)	2.132(2)	2.113(16)	2.160(2)	2.113(3)
Ln(1)–O(3)	2.123(2)	2.190(14)	2.171(3)	2.122(4)
Ln(1)–O(4)	2.118(2)	2.106(15)	2.161(3)	2.118(4)
Ln(1)–O(5)	2.435(2)	2.355(15)	2.463(3)	2.408(4)
Ln(1)–O(6)	2.448(2)	2.378(16)	2.487(3)	2.433(4)
Ln(1)–O(7)	2.415(2)	-	2.475(3)	2.425(4)
Bond angles (°)				
O(1)–Ln(1)–O(2)	97.02(8)	88.04(6)	95.67(10)	97.64(14)
O(3)–Ln(1)–O(1)	-		101.86(10)	102.95(14)
O(1)–Ln(1)–O(5)	99.80(8)	119.08(5)	82.83(10)	83.09(14)
O(2)–Ln(1)–O(3)	103.22(8)	141.90(6)	99.21(11)	99.63(15)
O(5)–Ln(1)–O(3)	85.28(8)	85.25(5)	173.25(11)	171.39(15)

[Ce(BPO$_2$)$_2$(thf)$_2$].thf (3.4)

The dark-purple crystals of [Ce(BPO$_2$)$_2$(thf)$_2$] were obtained from a thf solution at room temperature. Complex **3.4** is the first successful attempt to access Ce(IV) by the one pot redox transmetallation with a mercury reagent. [Ce(BPO$_2$)$_2$(thf)$_2$] crystallises in the monoclinic space group *P*2$_1$ (Table 3.4) and the molecular structure of **3.4** is monomeric (Fig. 3.6). This Xray structure was previously published after synthesis by another route.[43] The cerium atom is six coordinate with two bidentate biphenolate ligands two monodentate thf ligands. The geometry around the six coordinate cerium metal centre is best described as a distorted octahedral. The metal core in compounds **3.4** and **3.1b** has the same coordination number while they have a different oxidation state. The metal centre in **3.4** is coordinated by two thf molecules in the *cis* form as they are mutually adjacent and the O(5)−Ce−O(6) angle is 86.31(12)° while in **3.1b** the two thf molecules are coordinated to the metal centre in the *trans* form and the O(5)−Y−O(6) angle is 160.19(6)°.
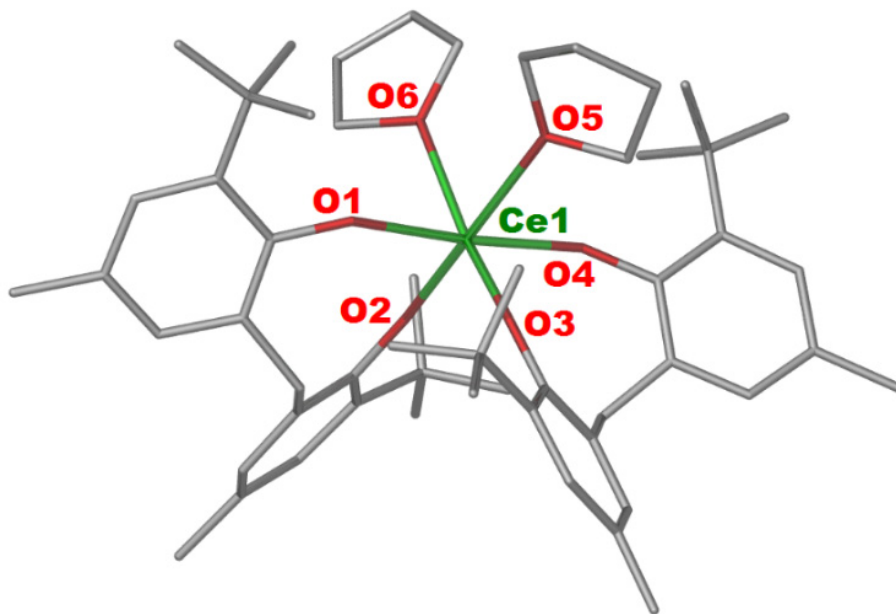
Figure 3.6 X-ray crystal structure of [Ce(BPO$_2$)$_2$(thf)$_2$] 3.4. Hydrogen atoms are omitted for clarity.

The oxygen atoms O(5), O(2) and O(6), O(3) occupy equatorial positions, whilst the axial positions are accommodated by O(1) and O(4) with the O(1)–Ce–O(4) angle close to ideal (175.32(12)°). The phenolate groups of the biphenolate ligands are collapsed toward -CH_2- to accommodate the Ce(IV) metal centre and angles are C(14)–C(12)–C(6) 114.9(4)°, C(29)–C(35)–C(37) 118.1(4)° respectively. The four oxygen atoms O(1), O(2), O(3), O(4) of the biphenolate ligands coordinate to cerium at a short distance of 2.155(3) Å, 2.129(3) Å, 2.113(3) Å and 2.146(3) Å respectively, indicating that all oxygen atoms of biphenolate ligand are anionic. Also, the Ce–O$_{(phenolate)}$ bond lengths abovementioned are in a similar range to Ce–O$_{(phenolate)}$ reported for [Ce(BPO$_2$)$_2$(thf)$_2$] (range 2.113(2)-2.152(2) Å).[43]

Table 3.2 Crystallographic data for compounds 3.1-3.4.

Compound	3.1a	3.1b	3.2	3.3	3.4
formula	$C_{70}H_{109}O_{10}Y$	$C_{66}H_{89}O_6Y$	$C_{70}H_{109}O_{10}Gd$	$C_{70}H_{109}O_{10}Er$	$C_{58}H_{84}O_7Ce$
fw	1199.51	1067.32	1267.86	1277.87	1033.40
crystal system	monoclinic	monoclinic	monoclinic	monoclinic	monoclinic
space group	$P2_1/c$	$P2_1/n$	$P2_1/c$	$P2_1/c$	$P2_1$
a, Å	13.254(3)	19.936(4)	13.228(3)	13.221(3)	11.277
b, Å	17.600(4)	25.372(5)	17.675(4)	17.566(4)	18.087
c, Å	28.387(6)	23.753(5)	28.481(6)	28.410(6)	14.159
α, deg	90	90	90	90	90
β, deg	93.72(3)	103.50(3)	94.11(3)	93.79(3)	113.40
γ, deg	90	90	90	90	90
V, Å^3	6608(2)	11683(4)	6642(2)	6583(2)	2650
Z	4	8	4	4	2
T, K	100(2)	100(2)	173(2)	100(2)	173(2)
no. of rflns collected	62698	72099	88396	79410	44232
no. of indep rflns	11451	19484	15714	14969	12145
R_{int}	0.053	0.097	0.034	0.048	0.094
Final R_1 values ($I > 2\sigma(I)$)	0.058	0.052	0.057	0.061	0.039
Final $wR(F^2)$ values ($I > 2\sigma(I)$)	0.150	0.138	0.201	0.137	0.098
Final R_1 values (all data)	0.068	0.060	0.062	0.073	0.040
Final $wR(F^2)$ values (all data)	0.157	0.147	0.205	0.143	0.099
$GooF$ (on F^2)	1.091	1.056	1.774	1.147	1.052

[Ln$_2$(BPO$_2$)$_3$(thf)$_2$].sol (Ln = Ho 3.5 sol = 3C$_6$D$_6$, Yb 3.6 sol = 2thf)

[Ho$_2$(BPO$_2$)$_3$(thf)$_2$] crystallises in the monoclinic space group *P*2$_1$/c after recrystallisation from benzene while crystals of [Yb$_2$(BPO$_2$)$_3$(thf)$_2$] were isolated from thf and crystallise in the triclinic space group *P*-1 (Table 3.6). The crystal structure of [Ho$_2$(BPO$_2$)$_3$(thf)$_2$] (Fig. 3.8) is isostructural with complex [Yb$_2$(BPO$_2$)$_3$(thf)$_2$]. [Ln$_2$(BPO$_2$)$_3$(thf)$_2$] (Ln = Ho, Yb) (Fig. 3.7) displays a dinuclear form with the two metals being bridged by two oxygen atoms of the fully deprotonated biphenolate. The overall molecular geometry around the five-coordinate Ln(1) and Ln(2) metal centres is a distorted trigonal-bipyramid. Three phenolate oxygen atoms are arranged in the equatorial positions around the Ln(1) centre with two other oxygen atoms O$_{(thf)}$ and O$_{(phenolate)}$ in the axial positions. For Ln(2) two phenolate oxygen atoms and one oxygen atom of a thf ligand occupy the equatorial positions around Ln(2) with two other phenolate oxygen atoms in the axial positions (Fig. 3.7). For example, in [Ho$_2$(BPO$_2$)$_3$(thf)$_2$] **3.5** (Fig. 3.8) the oxygen atoms O(7), O(3) occupy the axial positions and the angle is close to ideal angle O(7)−Ho(1)−O(3) (170.43(13)°) whilst other oxygen atoms O(1), O(2), O(5) are approximately arranged in equatorial poistions. For Ho(2) the oxygen atoms O(5), O(8) occupy the axial positions with O(5)−Ho(2)−O(8) (156.20(15)°) whilst other oxygen atoms O(3), O(4), O(6) occupy equatorial positions.

The bond lengths and bond angles of [Ln$_2$(BPO$_2$)$_3$(thf)$_2$] (Ln = Ho, Yb) are listed in Table 3.5. In the literature there are no reported examples of a holmium phenolate complex with five-coordinate holmium. The average Ho−O$_{(terminal\ phenolate)}$ bond lengths were found to be 0.18 Å less than the average Ho−O$_{(bridging\ phenolate)}$ bond lengths.

The average Yb−O$_{(terminal\ phenolate)}$ bond lengths of [Yb$_2$(BPO$_2$)$_3$(thf)$_2$] were found to be 2.08 Å, which are approximately in agreement with the average Yb−O$_{(terminal\ phenolate)}$ 2.07 Å

reported for [Li(thf)$_2$Yb(BPO$_2$)$_2$(thf)][37], but it is shorter than the average Yb−O$_{(bridge}$ $_{phenolate)}$ 2.22 Å bond length of [Yb$_2$(BPO$_2$)$_3$(thf)$_2$].

The average Ho−O$_{(terminal\ phenolate)}$ and Ho−O$_{(bridge\ phenolate)}$ bond lengths 2.08 Å, 2.26 Å respectively of **3.5** are in concordance with the average Yb−O$_{(terminal\ phenolate)}$ and Yb−O$_{(bridge\ phenolate)}$ bond lengths 2.08 Å, 2.22 Å respectively of **3.6** since they have approximately similar size, the difference between ionic radii is 0.03 Å for the six coordinate Ho and Yb.

The notable feature of [Ln$_2$(BPO$_2$)$_3$(thf)$_2$] (Ln = Ho, Yb) (Fig. 3.7) is the uncommon low coordination number of five for the Ho and Yb metal centres in **3.5** and **3.6** compared with the more common six coordination displayed by complexes **3.1-3.6**.

[Ln₂(BPO₂)₃(thf)₂] Ln = Ho, Yb
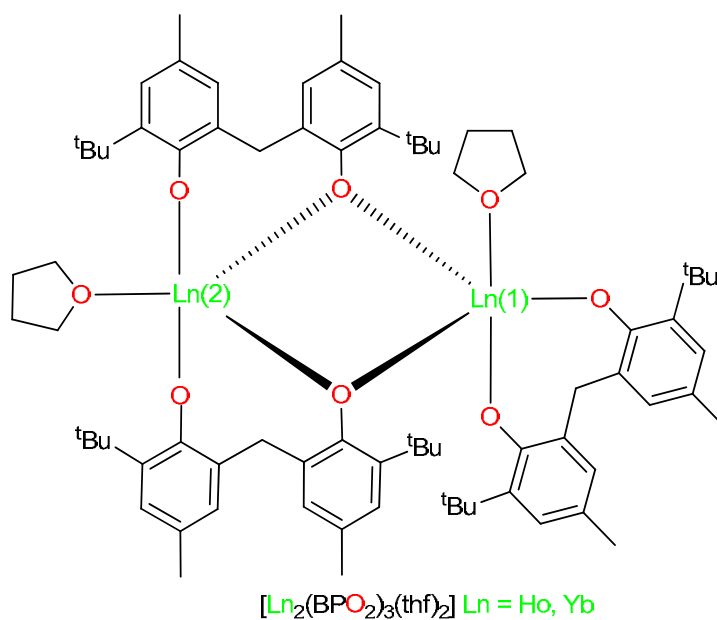
Figure 3.7 Dinuclear lanthanoid biphenolate diagram of 3.5 and 3.6.
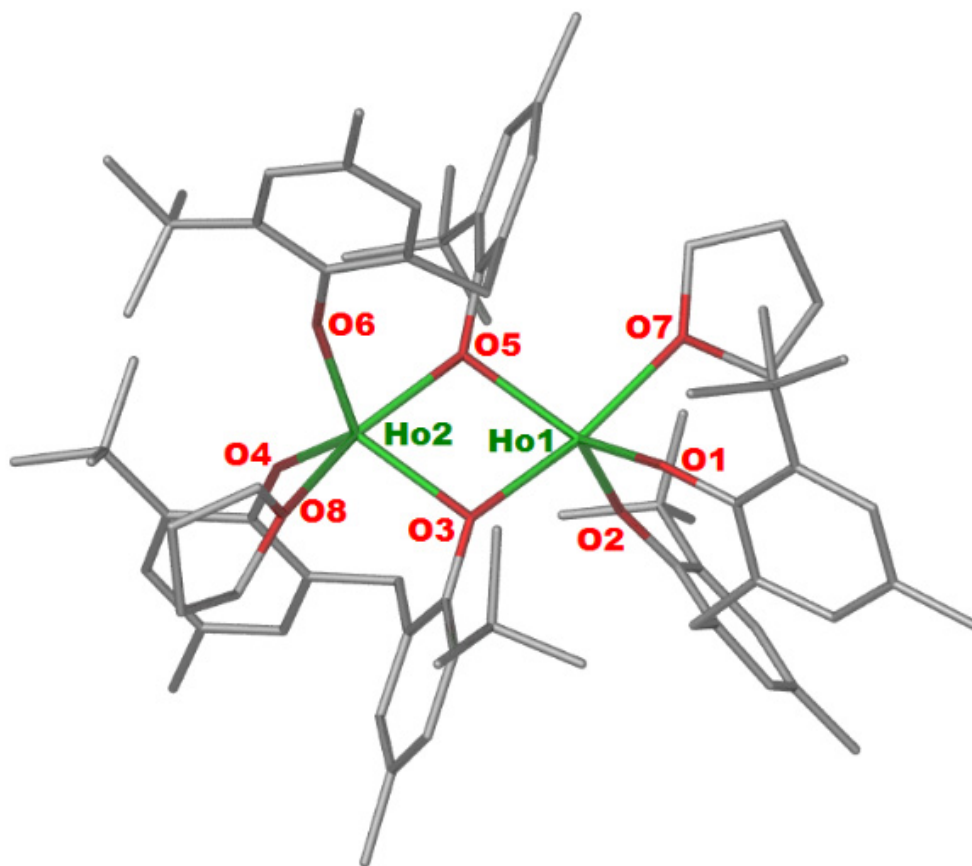
Figure 3.8 X-ray crystal structure of [Ho₂(BPO₂)₃(thf)₂] 3.5 and it is isostructural to [Yb₂(BPO₂)₃(thf)₂] 3.6. Hydrogen atoms are omitted for clarity.

Table 3.3 Selected bond lengths and angles of [Ln₂(BPO₂)₃(thf)₂] (Ln = Ho, Yb).

Bond lengths (Å)	[Ho₂(BPO₂)₃(thf)₂]	[Yb₂(BPO₂)₃(thf)₂]
Ln(1)–O(1)	2.080(4)	2.051(5)
Ln(1)–O(2)	2.081(4)	2.066(6)
Ln(1)–O(3)	2.269(4)	2.246(5)
Ln(1)–O(5)	2.288(4)	2.217(5)
Ln(1)–O(7)	2.385(4)	2.365(5)
Ln(2)–O(3)	2.258(4)	2.201(6)
Ln(2)–O(4)	2.084(4)	2.037(5)
Ln(2)–O(5)	2.248(4)	2.241(5)
Ln(2)–O(6)	2.103(4)	2.061(5)
Bond angles (°)		
O(1)–Ln(1)–O(2)	106.31(16)	107.20(2)
O(3)–Ln(1)–O(5)	71.21(16)	71.61(19)
O(5)–Ln(1)–O(7)	100.67(17)	93.44(18)
O(1)–Ln(1)–O(3)	95.36(18)	105.28(19)
O(2)–Ln(1)–O(5)	129.82(17)	126.90(2)
O(3)–Ln(2)–O(4)	105.46(17)	91.19(19)
O(3)–Ln(2)–O(8)	97.46(16)	94.80(2)
O(5)–Ln(2)–O(4)	108.50(16)	110.10(2)
O(6)–Ln(2)–O(4)	114.51(19)	118.40(2)
Ln(1)–O(3)–Ln(2)	108.31(18)	108.00(2)
Ln(2)–O(5)–Ln(1)	108.26(19)	108.40(2)

Table 3.4 Crystallographic data for compounds 3.5 and 3.6.

Compound	**3.5**	**3.6**
formula	C₉₅H₁₂₄O₈Ho₂	C₈₅H₁₂₂O₁₀Yb₂
fw	1723.86	1649.98
crystal system	monoclinic	triclinic
space group	*P*2₁	*P*-1
a, Å	17.241(3)	12.725(3)
b, Å	18.156(4)	13.175(3)
c, Å	26.717(5)	23.950(5)
α, deg	90	93.97(3)
β, deg	89.92(3)	91.56(3)
γ, deg	90	92.70(3)
V, Å³	8363(3)	3999(14)
Z	4	2
T, K	100(2)	100(2)
no. of rflns collected	42737	25185
no. of indep rflns	20866	12690
*R*ᵢₙₜ	0.036	0.030
Final *R₁* values (*I* > 2σ(*I*))	0.026	0.056
Final *wR*(*F*²) values (*I* > 2σ(*I*))	0.069	0.133
Final *R₁* values (all data)	0.026	0.058
Final *wR*(*F*²) values (all data)	0.069	0.134
GooF (on *F*²)	1.082	1.159

[Ln$_2$(BPO$_2$)$_3$(thf)$_3$].sol (Ln = Sm 3.7 sol = 6thf, Tb 3.8 sol = 2C$_6$D$_6$)

The isostruturcal complexes [Ln$_2$(BPO$_2$)$_3$(thf)$_3$] (Ln = Sm **3.7**, Tb **3.8**) (Fig. 3.9) crystallise in the triclinic space group *P*-1 (Table 3.8). Compounds **3.7** and **3.8** are structurally similar to previously reported complex [La$_2$(BPO$_2$)$_3$(thf)$_3$].[37] Figure 3.9 displays dinuclear complex bridged by two oxygen atoms of the two biphenolates with two different environments around metal centres. The overall molecular geometry around the five-coordinate Ln(1) (Ln = Sm, Tb) metal centre is a distorted trigonal-bipyramid (Fig. 3.9). One oxygen atom of thf and one oxygen atom of phenolate occupy axial positions and other three oxygen atom of phenolate are located in equatorial positions. For example, in **3.7** O(3) and O(7) occupy axial positions O(3)−Sm(1)−O(7) 165.93(15)° with other three oxygen atoms O(1), O(2), O(5) are located in equatorial positions (Fig. 3.10). However, the six-coordinate Ln(2) is exhibiting distorted octahedral stereochemistry. Two phenolate oxygen atoms are arranged in the axial positions around the Ln(2) centre with two other thf oxygen atoms and two phenolate oxygen atoms in the equatorial positions (Fig. 3.9). For example, in **3.7** two phenolate oxygen atoms O(4), O(6) occupy axial positions O(4)−Sm(1)−O(6) 167.07(16)° with other four oxygen atoms O(3), O(5), O(8), O(9) are arranged in equatorial positions (Fig. 3.10).

The bond lengths and bond angles of [Ln$_2$(BPO$_2$)$_3$(thf)$_3$] (Ln = Sm, Tb) are listed in Table 3.7. The average Sm−O$_{(terminal\ phenolate)}$ bond length of **3.7** was found to be 2.17 Å, which is comparable to the average Sm−O$_{(terminal\ phenolate)}$ bond length reported for [AlMe$_2$Sm(BPO$_2$)$_2$(thf)$_2$][47] (2.15 Å) and [Na(solv)Sm(BPO$_2$)$_2$(thf)][11] (solv = tetramethylethylenediamine) (2.16 Å). The average Sm−O$_{(bridge\ phenolate)}$ bond length of **3.7** (2.36 Å) is larger than the average Sm−O$_{(bridge\ phenolate)}$ bond length reported for [Na(solv)Sm(BPO$_2$)$_2$(thf)][11] (2.25 Å), but it is shorter than that reported for [AlMe$_2$Sm(BPO$_2$)$_2$(thf)$_2$] (2.45 Å).[47]

In the literature there is no example for terbium phenolate complexes where the terbium metal centre has five coordination. The average Tb–O$_{(phenolate)}$ of the six coordinate Tb centre is 2.26 Å which is similar to the average Tb–O$_{(phenolate)}$ 2.26 Å previously reported for a six coordinate Tb^{+3}.[57]

The difference between the average Sm–O$_{(phenolate)}$ **3.7** and the average Tb–O$_{(phenolate)}$ bond length **(3.8)** (0.02 Å) is very close to the difference between the ionic radii (0.03 Å) of the six-coordinate Sm^{+3} and the six-coordinate Tb^{+3}.[56]

The notable feature for [Sm$_2$(BPO$_2$)$_3$(thf)$_3$] **(3.7)** and [Tb$_2$(BPO$_2$)$_3$(thf)$_3$] **(3.8)** is the two different environments around metal centres which led to a wide range of O–Sm–O bond angles 70.04(18)°-165.74(19)° and O–Tb–O bond angles of 71.55(8)°-158.81(8)° (Table 3.7).
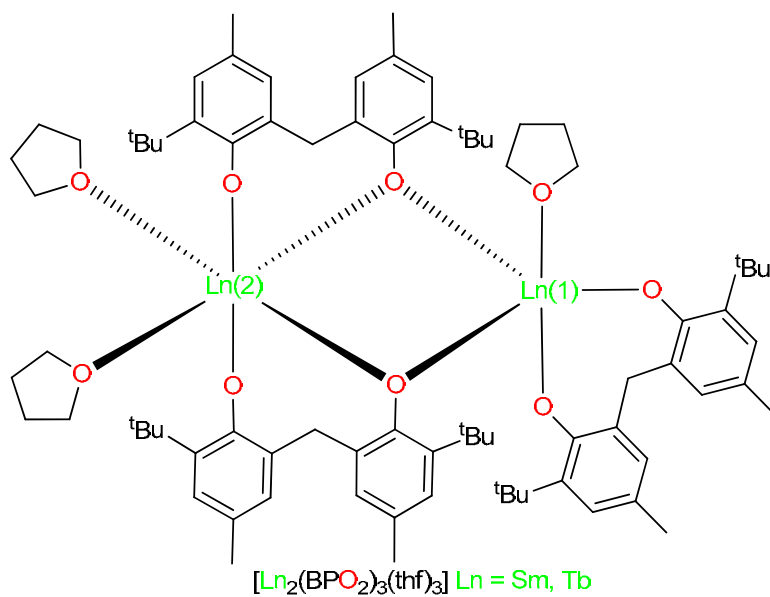
Figure 3.9 Dinuclear lanthanoid biphenolate diagram of compounds 3.7 and 3.8.
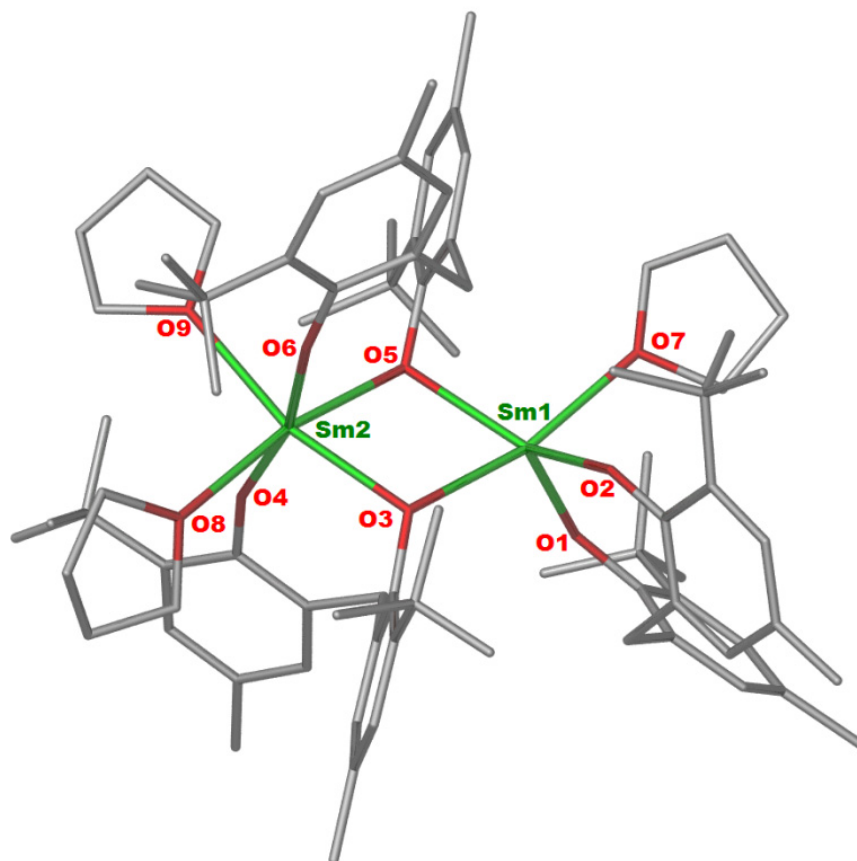
Figure 3.10 X-ray crystal structure of [Sm$_2$(BPO$_2$)$_3$(thf)$_3$] 3.7 which is isostructural

with [Tb$_2$(BPO$_2$)$_3$(thf)$_3$] (3.8). Hydrogen atoms are omitted for clarity.

Table 3.5 Selected bond lengths and angles of [Ln$_2$(BPO$_2$)$_3$(thf)$_3$] (Ln = Sm, Tb).

Bond lengths (Å)	[Sm$_2$(BPO$_2$)$_3$(thf)$_3$]	[Tb$_2$(BPO$_2$)$_3$(thf)$_3$]
Ln(1)–O(1)	2.143(4)	2.107(2)
Ln(1)–O(2)	2.142(5)	2.119(2)
Ln(1)–O(3)	2.354(4)	2.351(2)
Ln(1)–O(5)	2.377(4)	2.331(2)
Ln(2)–O(3)	2.353(4)	2.292(2)
Ln(2)–O(4)	2.215(4)	2.192(2)
Ln(2)–O(5)	2.357(4)	2.362(2)
Ln(2)–O(8)	2.505(4)	2.422(3)
Bond angles (°)		
O(1)–Ln(1)–O(2)	100.32(17)	99.95(9)
O(3)–Ln(1)–O(5)	70.06(15)	71.55(8)
O(5)–Ln(1)–O(7)	100.95(18)	91.73(8)
O(3)–Ln(1)–O(7)	165.74(19)	158.81(8)
O(1)–Ln(1)–O(5)	120.99(19)	136.92(8)
O(2)–Ln(1)–O(3)	95.71(18)	115.39(8)
O(3)–Ln(2)–O(4)	97.24(18)	94.96(8)
O(5)–Ln(2)–O(6)	92.78(17)	94.81(9)
O(3)–Ln(2)–O(8)	99.71(17)	98.96(8)
O(5)–Ln(2)–O(4)	95.51(17)	95.49(8)
O(6)–Ln(2)–O(8)	93.54(17)	91.62(9)
Ln(1)–O(3)–Ln(2)	115.4(5)	108.98(9)

Table 3.6 Crystallographic data for compounds 3.7 and 3.8.

Compound	**3.7**	**3.8**
formula	C$_{105}$H$_{162}$O$_{15}$Sm$_2$	C$_{93}$H$_{126}$O$_9$Tb$_2$
fw	1965.12	1705.84
crystal system	triclinic	triclinic
space group	*P*-1	*P*-1
a, Å	13.264(3)	13.124(3)
b, Å	16.128(3)	16.719(3)
c, Å	24.350(5)	21.865(4)
α, deg	84.36(3)	71.03(3)
β, deg	79.31(3)	75.37(3)
γ, deg	73.90(3)	68.52(3)
V, Å^3	4911(19)	4173(19)
Z	2	2
T, K	100(2)	100(2)
no. of rflns collected	59148	38462
no. of indep rflns	20536	13407
R$_{int}$	0.020	0.028
Final *R$_1$* values (*I* > 2σ(*I*))	0.064	0.029
Final *wR*(*F*^{2}) values (*I* > 2σ(*I*))	0.181	0.074
Final *R$_1$* values (all data)	0.069	0.030
Final *wR*(*F*^{2}) values (all data)	0.185	0.074
GooF (on *F*^{2})	1.066	1.083

[Eu(BPO$_2$)(thf)$_2$]$_2$.thf (3.9)

For this compound small colourless crystals were of poor quality were obtained, but an X-ray crystal structure was possible establishing only connectivity. [Eu(BPO$_2$)(thf)$_2$]$_2$ (Fig. 3.10) crystallises in the triclinic space group *P*-1 (Table 3.10). The compound is a dinuclear complex and resides on an inversion centre midway between the two Eu centres with the five coordinate europium centre bridging two phenolate oxygen centres and thf terminally bound to europium. The coordination molecular geometry at the five coordinate Eu(1) is best described as a distorted trigonal-bipyramid. Two oxygen atoms O(3) and O(1) occupy axial positions O(3)–Eu(1)–O(1) 156.3(3) with three other oxygen atoms O(2), O(1)# and O(4) in equatorial positions. A characteristic feature of **3.9** is the oxidation state of Eu metal. It is the only divalent lanthanoid biphenolate isolated from redox transmetallation in this study. The bond lengths and bond angles of **3.9** are listed in Table 3.9.

Compound **3.9** is structurally analogous with the previously reported complex [Eu(BPO$_2$)(hmpa)$_2$]$_2$ (hmpa = hexamethylphosphoric triamide) by Qi, *et. al* (2006).[41] The europium(II) complex was synthesised using a metathesis reaction (eqn. 3.16 see Introduction section 3.1.5). This route included two steps, by contrast to the one pot redox transmetallation that was used in this study to synthesise [Eu(BPO$_2$)(thf)$_2$]$_2$.
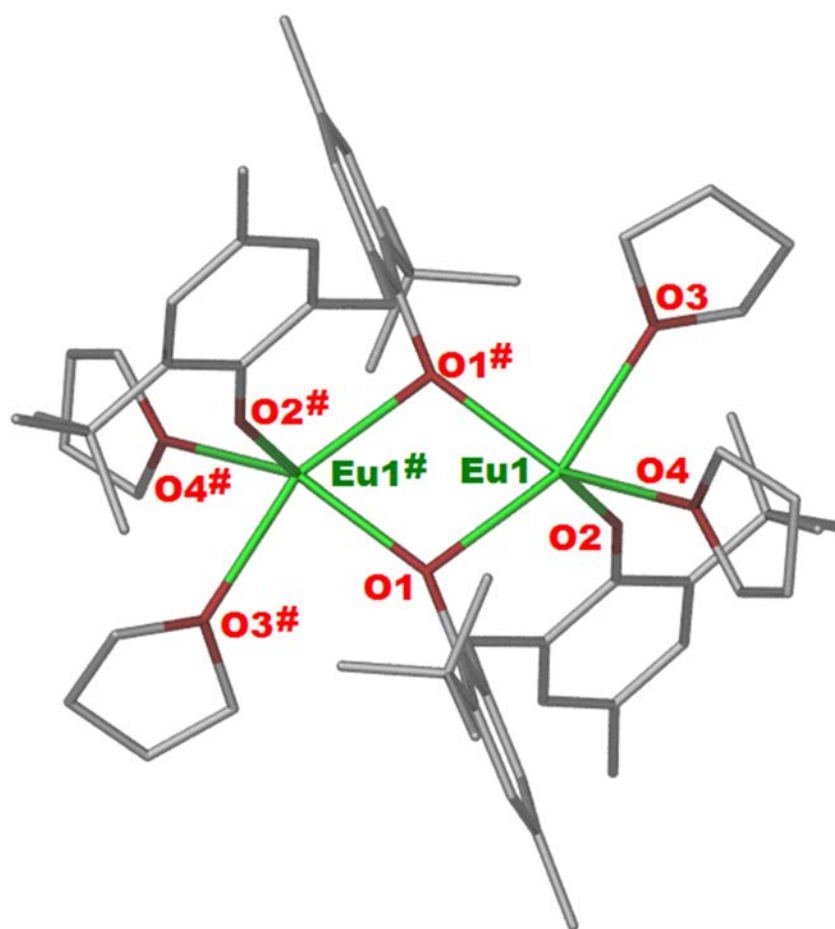
Figure 3.11 X-ray crystal structure of [Eu(BPO$_2$)(thf)$_2$]$_2$ 3.9. Hydrogen atoms are

omitted for clarity.

[Sr$_2$(BPO$_2$)$_2$(thf)$_5$] (3.10)

Complex 3.10 crystallises as colourless blocks from thf were of poor quality leading to poor quality data. Complex [Sr$_2$(BPO$_2$)$_2$(thf)$_5$] (Fig. 3.11) crystallises in the triclinic space group *P*-1 Table 3.8. This structure comprises two Sr metal centres bridged by two oxygen atoms. Interestingly, each Sr metal centre in this structure has a different coordination number. The coordination geometry of Sr(1) with six oxygen donor atoms around strontium is best described as a distorted octahedron. Two oxygen atoms O(2), O(7) are located in the axial positions O(2)–Sr(1)–O(7) 155.89(3)° with other four oxygen atoms O(1), O(5) O(6), O(7) occupy equatorial positions (Fig. 3.12). However, Sr(2) has five coordination. It is coordinated to three oxygen atoms from two phenolate ligands and two oxygen atoms from two thf molecules. Sr(2) is in a distorted pentagonal-bipyramidal environment. Two oxygen atoms O(3), O(9) are located in the axial positions O(3)–Sr(2)–O(9) 154.40(3)° with other three oxygen atoms O(1), O(4) O(8) arrange in equatorial positions (Fig. 3.12).

The Sr–O$_{(phenolate)}$ bond lengths are in the expected range for strontium compounds (2.284(10)-2.485(7) Å, Table 3.7) that are approximately consistent with those Sr–O$_{(phenolate)}$ bond lengths ranges (2.30-2.32) and (2.34-2.53 Å) previously reported for [Sr(OAr)$_2$(thf)$_3$] (ArO = 2,4,6-^{t}Bu$_3$-C$_6$H$_2$)[48] and [Sr$_2$(OAr)(μ–OAr)$_3$(dme)$_3$] (ArO = 2,6-Me$_2$-C$_6$H$_3$)[49] respectively. As expected the Sr–O$_{(thf)}$ lengths are larger than Sr–O$_{(phenolate)}$ and range from (2.534(10) to 2.865(10) Å, Table 3.7).

The Sr–O$_{(phenolate)}$ bond lengths related to the five-coordinate Sr(2) in [Sr$_2$(BPO$_2$)$_2$(thf)$_5$] were found to be 2.284(10) Å, 2.485(7) Å which are similar to the Eu–O$_{(phenolate)}$ bond lengths 2.283(9) Å, 2.484(9) Å in [Eu(BPO$_2$)(thf)$_2$]$_2$. Eu^{+2} and Sr^{+2} have approximately similar sizes and have similar expected chemistry (ionic radius 1.17 Å and 1.18 Å

respectively for six coodinate)[56]. However, as Sr^{+2} is ever so slightly larger than Eu^{+2} one

extra thf binds to Sr.
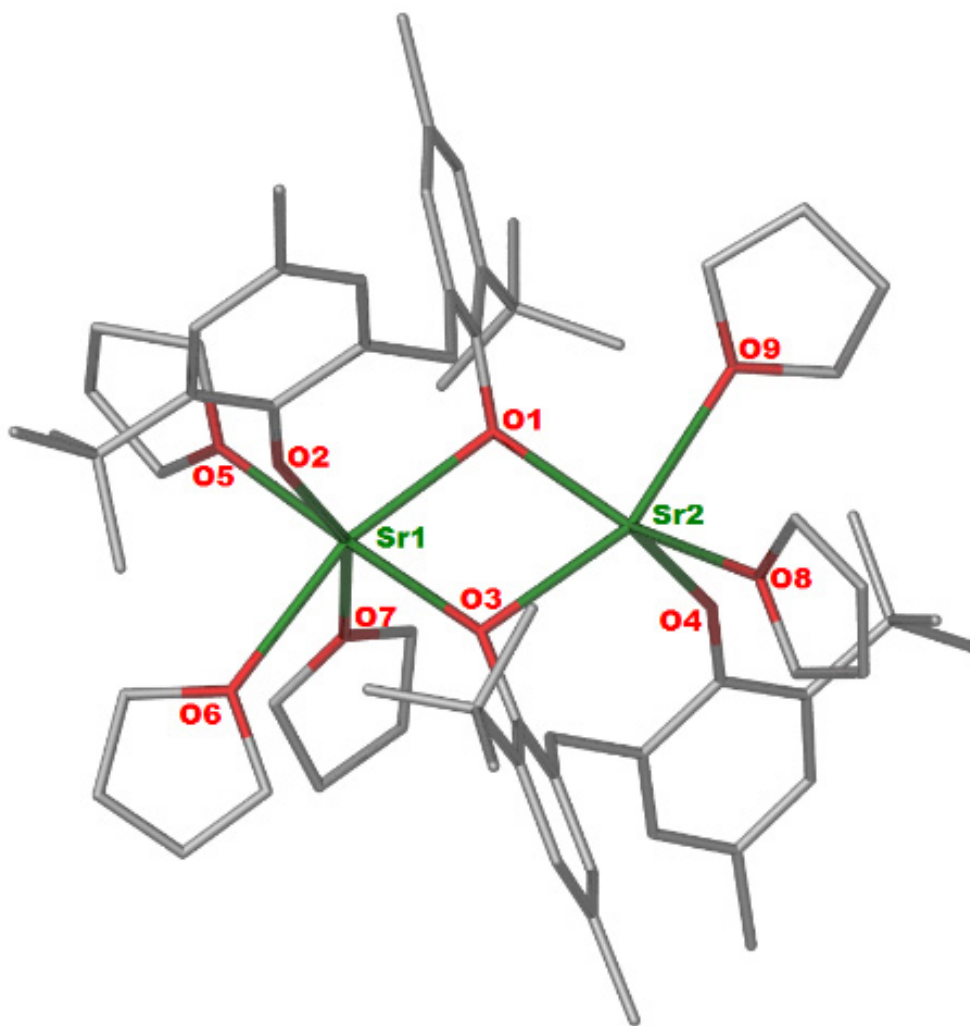
Figure 3.12 X-ray crystal structure of [Sr₂(BPO₂)₂(thf)₅] 3.10. Hydrogen atoms are

omitted for clarity.

Table 3.7 Selected bond lengths and angles of 3.9 and 3.10.

[Eu(BPO$_2$)(thf)$_2$]$_2$	Bond lengths (Å)	[Sr$_2$(BPO$_2$)$_2$(thf)$_5$]	Bond lengths (Å)
Eu(1)–O(1)	2.484(9)	Sr(1)–O(1)	2.468(8)
Eu(1)–O(2)	2.283(9)	Sr(1)–O(2)	2.339(9)
Eu(1)–O(3)	2.554(11)	Sr(1)–O(3)	2.429(7)
Eu(1)–O(4)	2.600(2)	Sr(1)–O(5)	2.553(8)
-	-	Sr(2)–O(3)	2.485(7)
-	-	Sr(2)–O(4)	2.284(10)
-	-	Sr(2)–O(1)	2.428(8)
-	-	Sr(2)–O(8)	2.534(10)
	Bond angles (°)		Bond angles (°)
O(1)–Eu(1)–O(2)	102.70(3)	O(1)–Sr(1)–O(2)	98.2(3)
O(3)–Eu(1)–O(4)	72.90(6)	O(3)–Sr(1)–O(1)	75.8(2)
O(1)–Eu(1)–O(1#)	75.00(4)	O(3)–Sr(1)–O(5)	172.9(3)
O(2)–Eu(1)–O(1#)	113.90(3)	O(6)–Sr(1)–O(1)	164.4(3)
O(4)–Eu(1)–O(1)	113.30(5)	O(3)–Sr(2)–O(4)	103.9(3)
-	-	O(1)–Sr(2)–O(3)	75.6(2)
-	-	O(3)–Sr(2)–O(8)	106.7(3)
-	-	O(1)–Sr(2)–O(9)	89.9(3)

Table 3.8 Crystallographic data for compounds 3.9 and 3.10.

Compound	3.9	3.10
formula	C$_{66}$H$_{100}$O$_9$Eu$_2$	C$_{66}$H$_{100}$O$_9$Sr$_2$
fw	1341.42	1212.73
crystal system	triclinic	triclinic
space group	*P*-1	*P*-1
a, Å	12.128(2)	12.571(3)
b, Å	12.353(3)	16.608(3)
c, Å	12.910(3)	17.227(3)
α, deg	61.99(3)	79.92(3)
β, deg	79.51(3)	75.35(3)
γ, deg	81.41(3)	74.22(3)
V, Å^3	1674(7)	3326(13)
Z	4	2
T, K	173(2)	173(2)
no. of rflns collected	11113	27356
no. of indep rflns	5483	7291
R_{int}	0.090	0.199
Final R_1 values ($I > 2\sigma(I)$)	0.148	0.112
Final $wR(F^2)$ values ($I > 2\sigma(I)$)	0.401	0.284
Final R_1 values (all data)	0.178	0.155
Final $wR(F^2)$ values (all data)	0.420	0.310
GooF (on F^2)	1.625	1.036

3.4 Conclusions

Redox transmetallation has been used in this study to synthesise biphenolate lanthanoid complexes. It led to isolated biphenolate lanthanoid complexes with different valency such as divalent $[Eu(BPO_2)(thf)_2]_2$, trivalent $[Ln(BPO_2)(BP(OH)O)(thf)_3]$ (Ln = Gd, Er, Y) and tetravalent $[Ce(BPO_2)_2(thf)_2]$. This one pot reaction acts as an excellent method to synthesise mononuclear and dinuclear lanthanoid biphenolate complexes depending on the stoichiometry of reagents in the reaction. Moreover, it is a one-step reaction that allows the synthesis of extremely air sensitive biphenolate lanthanoid complexes. This reaction leads to the isolation of two forms of lanthanoid biphenolate complexes, depending on the extent of deprotonation. When the biphenol ligand was mono-deprotonated it gave mononuclear complexes such as $[Ln(BPO_2)(BP(OH)O)(thf)_3]$ (Ln = Gd, Er, Y) except $[Ce(BPO_2)_2(thf)_2]$ which was fully deprotonated but it gave mononuclear complex due to cerium being able to have an accessible oxidation state of four. These complexes $[Ln(BPO_2)(BP(OH)O)(thf)_3]$ (Ln = Gd, Er, Y) with mono-deprotonated biphenolate ligand represent compounds that can now be used to synthesise heterobimetallic complexes explored in Chapter four of this thesis. When the biphenolate ligand was fully deprotonated for trivalent species it gave dinuclear complexes for example, $[Ln_2(BPO_2)_3(thf)_n]$ (Ln = Ho, Yb, n = 2; Sm, Tb, n = 3), or $[Eu(BPO_2)(thf)_2]_2$ for divalent Eu. In addition, phenolate alkaline earth complexes, in this case for strontium, was accessed by redox transmetalation and showed that the biphenol ligand was fully deprotonated to give a dinuclear complex $[Sr_2(BPO_2)_2(thf)_5]$. Comparisons between the divalent Eu complex and the strontium complex showed compounds of differing extents of solvation at the metal centre occurred.

This study illustrates that redox transmetallation can be used as a convenient method to synthesise biphenolate lanthanoid complexes, and provides a basis for future developments in a range of polyphenolic ligands.

3.5 Experimental

2,2′-Methylenebis(6-*tert*-butyl-4-methylphenol) was purchased from Sigma Aldrich. [$Hg(C_6F_5)_2$] was prepared by the literature method.[50] [$Hg(C_6F_5)_2$] and the biphenol ligand were dried under vacuum prior to use.

Lanthanoid metal analyses were determined by titration of the digested sample against a standardised Na_2H_2EDTA solution using xylenol orange as the indicator and hexamethylenetetramine as a buffer. Further details regarding general considerations were described in Chapter two (experiment section 2.5).

[Ln(BPO₂)(BP(OH)O)(thf)₃].3thf (Ln = Y 3.1a, Gd 3.2, Er 3.3), [Y(BPO₂)(BP(OH)O)(thf)₂].2C₆D₆ (3.1b)

A Schlenk flask was charged with $BP(OH)_2$ (1.36 g; 4.00 mmol), $Hg(C_6F_5)_2$ (1.60 g; 3 mmol), one drop of Hg (to activate the lanthanoid metal by forming highly reactive amalgam) and freshly filed lanthanoid metal powder (Ln 2.00 mmol = Y 0.17 g, Gd 0.31 g, Er 0.33 g). Dry thf (~20 ml) was added via cannula and the reaction mixture was stirred at ambient temperature for two days to give appropriate coloured solution for (Y, Er yellow; Gd dusty grey). The reaction mixture was allowed to stand at room temperature until the excess rare earth metal and mercury had settled to the bottom of the Schlenk. The supernatant solution was isolated by filtration through filter cannula to remove the residual metal. The filtrate was concentrated under vacuum to ca. 5 ml to induce crystallisation. Small colourless crystals of **3.1a, 3.2, 3.3** (0.65 g, 47 %, 0.60 g, 44 %, 0.70 g, 51 %) grew upon standing for two days, while large colourless crystals of **3.1b** (0.35 g, 53 %) grew overnight after **3.1a** was recrystallised from deuterated benzene.

3.1a: m. p. 158-160 °C. Elemental analysis calcd for $C_{70}H_{109}O_{10}Y$ (1199.51 g.mol⁻¹): C 70.09, H 9.16, Y 7.41. Calcd for $C_{58}H_{85}O_7Y$ (983.20 g.mol⁻¹ after loss of three lattice thf): C 70.85, H 8.71, Y 9.04. Found: C 70.43, H 8.20, Y 8.76. ¹H-NMR (400 MHz, C₆D₆,

25°C): δ = 6.91 (m, 8 H, Ar), 3.33 (s, br, 24H, OCH$_2$, thf), 2.03 (s, 12 H, CH$_3$), 1.87 (d, 2H, CH$_2$), 1.50 (d, 2H, CH$_2$), 1.32 (s, 36 H, C(CH_3)$_3$), 1.05 (s, br, 24H, CH$_2$, thf). IR (Nujol, cm^{-1}): 3501 s, 1960 w, 1887 w, 1740 s, 1568 s, 1254 w, 1070 m, 1012 m, 914 s, 861 m, 792 w, 726 m, 669 s.

3.1b: m. p. 152-154 °C; Elemental analysis calcd for C$_{66}$H$_{89}$O$_6$Y (1067.32 g.mol^{-1}): C 74.27, H 8.40, Y 8.33. Calcd for C$_{54}$H$_{77}$O$_6$Y (911.09 g.mol^{-1} after loss of two lattice C$_6$D$_6$ molecules): C 71.19, H 8.52, Y 9.76. Found: C 70.83, H 8.13, Y 9.37. IR (Nujol, cm^{-1}): 3451 s, 2060 w, 1977 m, 1690 s, 1488 m, 1212 m, 1125 w, 997 s, 920 w, 855 m, 781 m, 712 m, 664 s.

3.2: m. p. 168-170 °C. Elemental analysis calcd for C$_{70}$H$_{109}$O$_{10}$Gd (1267.86 g.mol^{-1}): C 66.31, H 8.67, Gd 12.40. Calcd for C$_{58}$H$_{85}$O$_7$Gd (1051.54 g.mol^{-1} after loss of three lattice thf): C 66.25, H 8.15, Gd 14.95. Found: C 65.87, H 7.95, Gd 14.80. IR (Nujol, cm^{-1}): 3626 m, 3486 m, 2366 w, 1959 w, 1885 w, 1738 m, 1639 w, 1598 s, 1569 s, 1532 s, 1262 s, 1204 w, 1167 w, 1069 m, 1011 s, 917 s, 863 s, 814 w, 794 w, 720 w, 666 s.

3.3: m. p. 178-180 °C; Elemental analysis calcd for C$_{70}$H$_{109}$O$_{10}$Er (1277.87 g.mol^{-1}): C 65.79, H 8.60, Er 13.09. Calcd for C$_{50}$H$_{69}$O$_5$Er (917.34 g.mol^{-1} after lost of five thf of solvation): C 65.46, H 7.58, Er 18.23. Found: C 65.11, H 7.19, Er 18.02. ^{1}H-NMR (400 MHz, C$_6$D$_6$, 25°C): δ = 7.41 (m, 8 H, Ar), 6.20 (s, 4H, CH$_2$), 4.00 (s, br, 4H, OCH$_2$, thf), 2.39 (s, 12 H, CH$_3$), 1.72 (s, 36 H, C(CH_3)$_3$), 0.54 (s, br, 4H, CH$_2$, thf). IR (Nujol, cm^{-1}): 3628 m, 3509 s, 2365 m, 2271 w, 1960 m, 1887 w, 1740 s, 1593 m, 1560 m, 1270 s, 1204 w, 1160 m, 1066 m, 1017 m, 959 m, 914 m, 861 w, 762 w, 669 s.

[Ce(BPO$_2$)$_2$(thf)$_2$].thf (3.4)

Compound **3.4** was synthesised following same procedure described to synthesise **3.1-3.3** with equivalent stoichiometry. A dark purple filtrate was concentrated under vacuum to

ca. 5 ml to induce crystallisation. Small colourless crystals of **3.4** (0.05 g, 7 %) grew upon standing after one week from the mother liquor.

3.4: no characterisation could be obtained owing to the low yield limitation.

[Ln₂(BPO₂)₃(thf)₂].sol (Ln = Ho 3.5 sol = 3C₆D₆, Yb 3.6 sol = 2thf), [Ln₂(BPO₂)₃(thf)₃].sol (Ln = Sm 3.7 sol = 6thf, Tb 3.8 sol = 2C₆D₆)

These compounds were synthesised following same procedure described to synthesise **3.1-3.3** with equivalent stoichiometries. In each case a yellow filtrate was concentrated under vacuum to ca. 5 ml to induce crystallisation. Small colourless crystals of **3.6**, **3.7** (0.40 g, 39 %, 0.52 g, 50 %) grew upon standing after two days from the mother liquor. Large colourless crystals of **3.5**, **3.8** (0.35 g, 34 %, 0.32 g, 31 %) grew overnight after recrystallisation from benzene.

3.5: m. p. 243-245 $^{\circ}$C; Elemental analysis calcd for $C_{95}H_{124}O_8Ho_2$ (1723.86 g.mol^{-1}): C 66.19, H 7.25, Ho 19.14. Calcd for $C_{77}H_{106}O_8Ho_2$ (1489.52 g.mol^{-1} after loss of three lattice C_6D_6): C 62.09, H 7.17, Ho 22.15. Found: C 61.85, H 7.08, Ho 22.06. IR (Nujol, cm^{-1}): 2284 w, 1936 m, 1854 m, 1795 m, 1747 s, 1600 s, 1570 s, 1260 w, 1208 w, 1003 m, 914 s, 861 s, 819 m, 861 s, 819 m, 777 w, 725 s, 689 m.

3.6: m. p. 210-212 $^{\circ}$C; Elemental analysis calcd for $C_{85}H_{122}O_{10}Yb_2$ (1649.98 g.mol^{-1}): C 61.87, H 7.45, Yb 20.98. Calcd for $C_{77}H_{106}O_8Yb_2$ (1505.77 g.mol^{-1} after loss of two lattice thf): C 61.42, H 7.10, Yb 22.98. Found: C 61.05, H 6.50, Yb 22.45. IR (Nujol, cm^{-1}): 1943 w, 1738 m, 1569 m, 1259 s, 1120 m, 1093 w, 1023 s, 917 m, 859 s, 798 s, 662 w.

3.7: m. p. 218-220 $^{\circ}$C; Elemental analysis calcd for $C_{105}H_{162}O_{15}Sm_2$ (1965.12 g.mol^{-1}): C 64.18, H 8.31, Sm 15.30. Calcd for $C_{81}H_{114}O_9Sm_2$ (1532.49 g.mol^{-1} after loss of six lattice thf): C 63.48, H 7.50, Sm 19.62. Found: C 63.19, H 7.11, Sm 19.14. IR (Nujol, cm^{-1}):

2058 w, 1750 m, 1249 s, 1138 s, 1060 m, 1011 m, 917 s, 863 s, 814 s, 794 s, 724 m, 670 s.

3.8: m. p. 243-245 °C; Elemental analysis calcd for $C_{93}H_{126}O_9Tb_2$ (1705.84 g.mol^{-1}): C 65.48, H 7.45, Tb 18.63. Calcd for $C_{81}H_{114}O_9Tb_2$ (1549.62 g.mol^{-1} after loss of two lattice C_6D_6): C 62.78, H 7.42, Tb 20.51. Found: C 62.25, H 7.19, Tb 20.12. ^{1}H-NMR (400 MHz, C_6D_6, 25°C): δ = 7.78 (m, 12 H, Ar), 2.55 (s, br, 6H, CH_2), 2.28 (s, br 12H, OCH_2, thf), 1.19 (s, 18 H, CH_3), 0.32 (s, 54 H, C(CH_3)$_3$), -0.83 (s, br, 12H, CH_2, thf). IR (Nujol, cm^{-1}): 1738 w, 1565 m, 1528 w, 1463 s, 1376 s, 1266 s, 1204 m, 1171 w, 1138 m, 1073 m, 1007 s, 913 s, 859 s, 818 s, 789 m, 724 w.

[Eu(BPO$_2$)(thf)$_2$]$_2$.thf (3.9)

Following the same procedure described to synthesise **3.1-3.3**, compound **3.9** was prepared using a stoichiometry of 2:2 for BP(OH)$_2$ to Eu. The reaction mixture was stirred for two days and dried under vacuum then dissolved in dry toluene (~20 ml) followed by stirring at ambient temperature for two days then allowed to stand at room temperature until the excess rare earth metal and mercury had settled to the bottom of the Schlenk. The supernatant solution was isolated by filtration through a filter cannula to remove the residual metal. The filtrate was concentrated under vacuum to ca. 5 ml to induce crystallisation. Small colourless crystals of **3.9** (0.09 g, 26 %) grew upon standing after one week.

3.9: m. p. 248-250 °C. IR (Nujol, cm^{-1}): 2362 w, 2055 m, 1936 m, 1830 m, 725 w.

[Sr$_2$(BPO$_2$)$_2$(thf)$_5$] (3.10)

Following same procedure that described to synthesise **3.1-3.3**, compound **3.10** was prepared using a stoichiometry of 2:2 for BP(OH)$_2$ to Sr. The reaction mixture was stirred for two days at ambient temperature then allowed to stand at room temperature until the excess strontium metal and mercury had settled to the bottom of the Schlenk. The

supernatant solution was isolated by filtration through a filter cannula to remove the residual metal. A yellow filtrate was concentrated under vacuum to ca. 5 ml to induce crystallisation. Small colourless crystals of **3.10** (0.09 g, 26 %) grew upon standing after two days.

3.10: m. p. 168-170 °C. ^{1}H-NMR (400 MHz, C$_6$D$_6$, 25°C): The ^{1}H-NMR spectrum showed the lost of four thf molecules under vacuum. $\delta = 7.15$ (m, 8 H, Ar), 3.45 (s, br, 8H, OCH$_2$, thf), 2.17 (s, 4H, CH$_2$), 1.51 (s, br, 8 H, CH$_2$, thf), 1.39 (s, 12H, CH$_3$), 0.28 (s, 36 H, C(CH_3)$_3$). IR (Nujol, cm^{-1}): 2358 w, 2052 w, 1943 m, 1745 w, 1647 m, 1596 m, 1529 m, 1505 w, 1455 s, 1382 s, 1260 s, 1100 w, 1023 m, 865 w, 800 s, 710 m, 665 w.

3.6 Crystal and refinement data

Intensity data of crystalline samples of compounds **3.1-3.10** were collected using the MX1 beamline at the Australian Synchrotron at 100 or 173 K using a single wavelength (λ = 0.71073 Å. Further details regarding structure solutions and refinements were described in Chapter two (crystal and refinement data section 2.6).

[Y(BPO$_2$)(BP(OH)O)(thf)$_3$].3thf (3.1a)

$C_{70}H_{109}O_{10}Y$, M = 1199.51, $0.110 \times 0.040 \times 0.030$ mm^3, monoclinic, space group $P2_1/c$ (No. 4), a = 13.254(3), b = 17.600(4), c = 28.387(6), $\alpha = \gamma = 90$, β = 93.72(3), V = 6608(2) Å^3, Z = 4, ρ_c = 1.203 g/cm^3, μ = 0.938 mm^{-1}, F_{000} = 2580, λ = 0.71073 Å, T = 173(2) K, $2\theta_{max}$ = 50º, 62698 reflections collected, 11451 unique (R_{int} = 0.053). Final $GooF$ = 1.091, R_1 = 0.058, wR_2 = 0.150, R indices based on 18140 reflections with I > 2σ(I) (refinement on F^2), 842 parameters, 43 restraints. Lp and absorption corrections applied.

[Y(BPO$_2$)(BP(OH)O)(thf)$_2$].2C$_6$D$_6$ (3.1b)

$C_{66}H_{89}O_6Y$, M = 1067.32, $0.110 \times 0.050 \times 0.045$ mm^3, monoclinic, space group $P2_1/n$ (No. 14), a = 19.936(4), b = 25.372(5), c = 23.753(5), $\alpha = \gamma = 90$, β = 103.50(3), V = 11683(4) Å^3, Z = 8, ρ_c = 1.212 g/cm^3, μ = 1.048 mm^{-1}, F_{000} = 4568, λ = 0.71073 Å, T = 100(2) K, $2\theta_{max}$ = 50º, 72099 reflections collected, 19484 unique (R_{int} = 0.097). Final $GooF$ = 1.056, R_1 = 0.052, wR_2 = 0.138, R indices based on 16605 reflections with I > 2σ(I) (refinement on F^2), 1347 parameters, 0 restraint. Lp and absorption corrections applied.

[Gd(BPO$_2$)(BP(OH)O)(thf)$_3$].3thf (3.2)

$C_{70}H_{109}O_{10}Gd$, M = 1267.86, $0.100 \times 0.075 \times 0.050$ mm^3, monoclinic, space group $P2_1/c$ (No. 14), a = 13.228(3), b = 17.675(4), c = 28.481(6), $\alpha = \gamma = 90.00$, β = 94.11(3), V = 6642(2) Å^3, Z = 4, ρ_c = 2.060 g/cm^3, μ = 6.208 mm^{-1}, F_{000} = 4000, MoKα radiation, λ =

0.71073 Å, T = 173(2) K, $2\theta_{max}$ = 55.8°, 88396 reflections collected, 15714 unique (R_{int} = 0.0341). Final *GooF* = 1.768, R_1 = 0.0578, *wR₂* = 0.2011, *R* indices based on 14038 reflections with I > 2σ(I) (refinement on F^2), 664 parameters, 0 restraints. Lp and absorption corrections applied.

[Er(BPO₂)(BP(OH)O)(thf)₃].3thf (3.3)

C₇₀H₁₀₉O₁₀Er, M = 1277.87, 0.120 × 0.055 × 0.030 mm³, monoclinic, space group $P2_1/c$ (No. 14), a = 13.221(3), b = 17.566(4), c = 28.410(6), $\alpha = \gamma = 90$, β = 93.79(3), V = 6583(2) Å³, Z = 4, ρ_c = 1.289 g/cm³, μ = 1.330 mm⁻¹, F_{000} = 2708, λ = 0.71073 Å, T = 100(2) K, $2\theta_{max}$ = 55°, 79410 reflections collected, 14969 unique (R_{int} = 0.048). Final *GooF* = 1.147, R_1 = 0.061, *wR₂* = 0.137, *R* indices based on 12571 reflections with I > 2σ(I) (refinement on F^2), 826 parameters, 20 restraints. Lp and absorption corrections applied.

[Ce(BPO₂)₂(thf)₂].thf (3.4)

C₅₈H₈₄O₇Ce, M = 1033.40, 0.100 × 0.070 × 0.030 mm³, monoclinic, space group $P2_1$ (No. 4), a = 11.277, b = 18.087, c = 14.159, $\alpha = \gamma = 90$, β = 113.40, V = 2650 Å³, Z = 2, ρ_c = 1.295 g/cm³, μ = 0.909 mm⁻¹, F_{000} = 1092, λ = 0.71073 Å, T = 173(2) K, $2\theta_{max}$ = 55°, 44232 reflections collected, 12145 unique (R_{int} = 0.094). Final *GooF* = 1.052, R_1 = 0.039, *wR₂* = 0.098, *R* indices based on 11750 reflections with I > 2σ(I) (refinement on F^2), 612 parameters, 1 restraint. Lp and absorption corrections applied.

[Ho₂(BPO₂)₃(thf)₂].3C₆D₆ (3.5)

C₉₅H₁₂₄O₈Ho₂, M = 1723.86, 0.100 × 0.055 × 0.030 mm³, monoclinic, space group $P2_1$ (No. 4), a = 17.241(3), b = 18.156(4), c = 26.717(5), $\alpha = \gamma = 90$, β = 89.92(3), V = 8363(3) Å³, Z = 4, ρ_c = 1.369 g/cm³, μ = 1.934 mm⁻¹, F_{000} = 3568, λ = 0.71073 Å, T = 100(2) K, $2\theta_{max}$ = 55°, 42737 reflections collected, 20866 unique (R_{int} = 0.036). Final *GooF* = 1.082,

$R_1 = 0.026$, $wR_2 = 0.069$, R indices based on 20738 reflections with I > 2σ(I) (refinement on F^2), 1939 parameters, 1 restraint. Lp and absorption corrections applied.

[Yb$_2$(BPO$_2$)$_3$(thf)$_2$].2thf (3.6)

C$_{85}$H$_{122}$O$_{10}$Yb$_2$, $M = 1649.98$, $0.120 \times 0.085 \times 0.050$ mm, triclinic, space group P-1 (No. 2), $a = 12.725(3)$, $b = 13.175(3)$, $c = 23.950(5)$, $\alpha = 93.97(3)$, $\beta = 91.56(3)$, $\gamma = 92.70(3)$, $V = 3999(14)$ Å^3, $Z = 2$, $\rho_c = 1.340$ g/cm^3, $\mu = 2.377$ mm^{-1}, $F_{000} = 1664$, $\lambda = 0.71073$ Å, $T = 100(2)$ K, $2\theta_{max} = 50°$, 25185 reflections collected, 12690 unique ($R_{int} = 0.030$). Final $GooF = 1.159$, $R_1 = 0.056$, $wR_2 = 0.133$, R indices based on 11992 reflections with I > 2σ(I) (refinement on F^2), 901 parameters, 30 restraints. Lp and absorption corrections applied.

[Sm$_2$(BPO$_2$)$_3$(thf)$_3$].6thf (3.7)

C$_{105}$H$_{162}$O$_{15}$Sm$_2$, $M = 1965.12$, $0.120 \times 0.045 \times 0.030$ mm^3, triclinic, space group P-1 (No. 2), $a = 13.264(3)$, $b = 16.128(3)$, $c = 24.350(5)$, $\alpha = 84.36(3)$, $\beta = 79.31(3)$, $\gamma = 73.90(3)$, $V = 4911(19)$ Å^3, $Z = 2$, $\rho_c = 1.329$ g/cm^3, $\mu = 1.246$ mm^{-1}, $F_{000} = 2072$, $\lambda = 0.71073$ Å, $T = 100(2)$ K, $2\theta_{max} = 55$, 59148 reflections collected, 20536 unique ($R_{int} = 0.020$). Final $GooF = 1.066$, $R_1 = 0.064$, $wR_2 = 0.181$, R indices based on 18675 reflections with I > 2σ(I) (refinement on F^2), 1123 parameters, 0 restraints. Lp and absorption corrections applied.

[Tb$_2$(BPO$_2$)$_3$(thf)$_3$].2C$_6$D$_6$ (3.8)

C$_{93}$H$_{126}$O$_9$Tb$_2$, $M = 1705.84$, $0.100 \times 0.065 \times 0.030$ mm^3, triclinic, space group P-1 (No. 2), $a = 13.124(3)$, $b = 16.719(3)$, $c = 21.865(4)$, $\alpha = 71.03(3)$, $\beta = 75.37(3)$, $\gamma = 68.52(3)$, $V = 4173(19)$ Å^3, $Z = 2$, $\rho_c = 8.824$ g/cm^3, $\mu = 12.101$ mm^{-1}, $F_{000} = 11928$, $\lambda = 0.71073$ Å, $T = 100(2)$ K, $2\theta_{max} = 50°$, 38462 reflections collected, 13407 unique ($R_{int} = 0.028$). Final $GooF = 1.083$, $R_1 = 0.029$, $wR_2 = 0.074$, R indices based on 12899 reflections with I >

$2\sigma(I)$ (refinement on F^2), 986 parameters, 0 restraints. Lp and absorption corrections applied.

[Eu(BPO₂)(thf)₂]₂.thf (3.9)

$C_{66}H_{100}O_9Eu_2$, $M = 1341.42$, $0.120 \times 0.050 \times 0.030$ mm³, triclinic, space group P-1 (No. 2), $a = 12.128(2)$, $b = 12.353(3)$, $c = 12.910(3)$, $\alpha = 61.99(3)$, $\beta = 79.51(3)$, $\gamma = 81.41(3)$, $V = 1674(7)$ Å³, $Z = 4$, $\rho_c = 1.406$ g/cm³, $\mu = 1.911$ mm⁻¹, $F_{000} = 732$, $\lambda = 0.71073$ Å, $T = 173(2)$ K, $2\theta_{max} = 50°$, 11113 reflections collected, 5483 unique ($R_{int} = 0.090$). Final *GooF* $= 1.625$, $R_1 = 0.148$, $wR_2 = 0.401$, R indices based on 3980 reflections with $I > 2\sigma(I)$ (refinement on F^2), 423 parameters, 0 restraints. Lp and absorption corrections applied.

[Sr₂(BPO₂)₂(thf)₅] (3.10)

$C_{66}H_{100}O_9Sr_2$, $M = 1212.73$, $0.100 \times 0.080 \times 0.055$ mm³, triclinic, space group P-1 (No. 2), $a = 12.571(3)$, $b = 16.608(3)$, $c = 17.227(3)$, $\alpha = 79.92(3)$, $\beta = 75.35(3)$, $\gamma = 74.22(3)$, $V = 3326(13)$ Å³, $Z = 2$, $\rho_c = 1.283$ g/cm³, $\mu = 1.659$ mm⁻¹, $F_{000} = 1368$, $\lambda = 0.71073$ Å, $T = 173(2)$ K, $2\theta_{max} = 50°$, 27356 reflections collected, 7291 unique ($R_{int} = 0.199$). Final *GooF* $= 1.036$, $R_1 = 0.112$, $wR_2 = 0.284$, R indices based on 4309 reflections with $I > 2\sigma(I)$ (refinement on F^2), 755 parameters, 0 restraints. Lp and absorption corrections applied.

3.7 References

[1]. Cotton, S. Scandium, Yttrium, and the Lanthanides. In *Comprehensive Coordination Chemistry II*. McCleverty, J. A.; Meyer, T. J. Eds. Elsevier Ltd: Oxford, **2004**, Vol. 3, 93-188.

[2]. Bradley, D.; Mehrotra, R.; Rothwell, I.; Singh, A. *Alkoxo and Aryloxo Derivatives of Metals*. Academic Press: London, **2001**.

[3]. Boyle, T. J.; Ottley, L. A. *Chem. Rev*. **2008**, *108*, 1896-1917.

[4]. Bochkarev, M. N.; Zakharov, L. N.; Kalinina, G. S. *Organoderivatives of the Rare Earth Elements*. Kluwer Academic Publishers: Dordrecht, **1995**.

[5]. Lappert, M.; Protchenko, A.; Power, P.; Seeber, A. *Metal Amide Chemistry*. John Wiley and Sons Ltd: West Sussex, **2009**.

[6]. Deacon, G. B., Delbridge, E. E.; Skelton, B. W.; White, A. H. *Eur. J. Inorg. Chem*. **1999**, 751-761.

[7]. Deacon, G. B.; Delbridge, E. E.; Skelton, B. W.; White, A. H. *Eur. J. Inorg. Chem*. **1998**, 543-545.

[8]. Deacon, G. B.; Raverty, W. D.; Vince, D. G. *J. Organomet. Chem*. **1977**, *135*, 103-114.

[9]. Deacon, G. B.; Koplick, A. J.; Raverty, W. D.; Vince, D. G. *J. Organomet. Chem*. **1979**, *182*, 121-141.

[10]. Forsyth, C. M.; Deacon, G. B. *Organometallics*. **2003**, *22*, 1349-1352.

[11]. Xu, X.; Ma, M.; Yao, Y.; Zhang, Y.; Shen, Q. *J. Mol. Struct*. **2005**, *743*, 163-168.

[12]. Deacon, G. B.; Vince, W. D. *J. Organomet. Chem*. **1976**, *112*, C1-C2.

[13]. Forsyth, C. M.; Deacon, G. B. *Organometallics*. **2000**, *19*, 1205-1207.

[14]. Deacon, G. B.; Forsyth, C. M.; Nickel, S. *J. Organomet. Chem*. **2002**, *647*, 50-60.

[15]. Radkov, Y.; Fedorova, E.; Khorshev, S.; Kalinina, G.; Bochkarev, M.; Razuvaev, G. *J. Gen. Chem. U.S.S.R.* **1985**, *55*, 1911-2550.

[16]. Deacon, G. B.; Koplick, A. J.; Tuong, T. D. *Aust. J. Chem.* **1984**, *37*, 517-525.

[17]. Deacon, G. B.; Feng, T.; MacKinnon, P.; Newnham, R.; H.; Nickel, S.; Skelton, B. W.; White, A. H. *Aust. J. Chem.* **1993**, *46*, 387-399.

[18]. Edelmann, F. T. Lanthanides and Actinides. In *Synthesis Methods of Organometallic and Inorganic Chemistry*. Herrmann, W. A. Ed. Theime: Stuttgar, **1997**, Vol. 6, 48-51.

[19]. Deacon, G. B.; Feng, T.; Nickel, S.; Ogden, M. I. *Aust. J. Chem.* **1992**, *45*, 671-683.

[20]. Deacon, G. B.; Koplick, A. J.; Tuong, T. D. *Polyhedron*. **1982**, *1*, 423-424.

[21]. Cetinkaya, B.; Hitchcock, P. B.; Lappert, M. F.; Smith, R. G. *J. Chem. Soc. Chem. Commun.* **1992**, 932-934.

[22]. Beaini, S.; Deacon, G. B.; Delbridge, E. E.; Junk, P. C.; Skelton, B. W.; White, A. H. *Eur. J. Inorg. Chem.* **2008**, 4586-4596.

[23]. Beaini, S.; Deacon, G. B.; Hilder, M.; Junk, P. C.; Turner, D. R. *Eur. J. Inorg. Chem.* **2006**, 3434-3441.

[24]. Bochkarev, L. N.; Stepantseva, T. A.; Zakharov, L. N.; Fukin, G. K.; Yanovsky, A. I.; Struchkov, Y. T. *Organometallics*. **1995**, *14*, 2127-2129.

[25]. Cole, M. L.; Junk, P. C. *New J. Chem.* **2005**, *29*, 135-140.

[26]. Hitzbleck, J.; O'Brien, A. Y.; Forsyth, C. M.; Deacon, G. B.; Ruhlandt-Senge, K. *Chem. Eur. J.* **2004**, *10*, 3315-3323.

[27]. Clark, L.; Deacon, G. B.; Forsyth, C. M.; Junk, P. C.; Mountford, P.; Townley, J. P. *Dalton Trans*. **2010**, *39*, 6693-6704.

[28]. Deacon, G. B.; Forsyth, C. M.; Newnham, R. H. *Polyhedron*. **1987**, *6*, 1143-1145.

[29]. Deacon, G. B.; Junk, P. C.; Moxey, G. J. *Chem. Asian. J.* **2009**, *4*, 1717-1728.

[30]. Deacon, G. B.; Fallon, G. D.; Forsyth, C. M.; Harris, S. C.; Junk, P. C.; Skelton, B. W.; White, A. H. *Dalton Trans*. **2006**, 802-812.

[31]. Streitwieser, A.; Scannon, P. J.; Niemeyer, H. M. *J. Am. Chem. Soc*. **1972**, *94*, 7936-7937.

[32]. Xu, X.; Ma, M.; Yao, Y.; Zhang, Y.; Shen, Q. *Eur. J. Inorg. Chem.* **2005**, 676-684.

[33]. Xu, B.; Huang, L.; Yang, Z.; Yao, Y.; Zhang, Y.; Shen, Q. *Organometallics*. **2011**, *30*, 3588-3595.

[34]. Xu, X.; Hu, M.; Yao, Y.; Qi, R.; Zhang, Y.; Shen, Q. *J. Mol. Struct*. **2007**, *829*, 189-194.

[35]. Yao, Y.; Xu, X.; Liu, B.; Zhang, Y.; Shen, Q.; Wong, W. *Inorg. Chem*. **2005**, *44*, 5133-5140.

[36]. Tan, Y.; Xu, X.; Guo, K.; Yao, Y.; Zhang, Y.; Shen, Q. *Polyhedron*. **2013**, *61*, 218-224.

[37]. Qi, R.; Liu, B.; Xu, X.; Yang, Z.; Yao, Y.; Zhang, Y.; Shen, Q. *Dalton Trans*. **2008**, 5016-5024.

[38]. Xu, X.; Qi, R.; Xu, B.; Yao, Y.; Nie, K.; Zhang, Y.; Shen, Q. *Polyhedron*. **2009**, *28*, 574-578.

[39]. Xu, X.; Zhang, Z.; Yao, Y.; Zhang, Y.; Shen, Q. *Inorg. Chem*. **2007**, *46*, 9379-9388.

[40]. Deng, M.; Yao, Y.; Shen, Q.; Zhanga, Y.; Jin, S. *Dalton Trans*. **2004**, 944-950.

[41]. Liu, B.; Yao, Y.; Deng, M.; Zhang, Y.; Qi, S. *J. Rare Earths*. **2006**, *24*, 264-267.

[42]. Fang, Y.; Ming, W.; Jing, H.; Lin, S.; Quan, S. *Sci. China Ser. B-Chem*. **2009**, *52*, 1711-1714.

[43]. Mahoney, B. D.; Piro, N. A.; Carroll, P. J.; Schelter, E. J. *Inorg. Chem*. **2013**, *52*, 5970-5977.

[44]. Wang, Z.; Sun, H.; Yao, H.; Shen, Q.; Zhang, Y. *Organometallics*. **2006**, *25*, 4436-4438.

[45]. Wu, G.; Liu, J.; Sun, W.; Shen, Z.; Ni, X. *Polym. Int.* **2010**, *59*, 431-436.

[46]. Zhang, M.; Liang, Z.; Ling, J.; Ni, X.; Shen, Z. *Dalton Trans.* **2015**, *44*, 11182-11190.

[47]. Korobkov, I.; Gambarotta, S. *Organometallics.* **2009**, *28*, 4009-4019.

[48]. Drake, S. R.; Otway, D. J.; Hursthouse, M. B.; Malik, K. M. A. *Polyhedron.* **1992**, *11*, 1995-2007.

[49]. Clark, L.; Deacon, G. B.; Forsyth, C. M.; Junk, P. C.; Mountford, P.; Townley, J. P.; Wang, J. *Dalton Trans.* **2013**, *42*, 9294-9312.

[50]. Edelmann, F. T. Lanthanides and Actinides. In *Synthesis Methods of Organometallic and Inorganic Chemistry.* Herrmann, W. A. Ed. Theime: Stuttgar, **1997**, Vol. 6, 48-51.

[51]. Dröse, P.; Crozier, A. R.; Lashkari, S.; Gottfriedsen, J.; Blaurock, S.; Hrib, C. G.; Maichle-Mössmer, C. C.; Schädle, C.; Anwander, R.; Edelmann, F. T. *J. Am. Chem. Soc.* **2010**, *132*, 14046-14047.

[52]. Hitchcock, P. B.; Hulkes, A. G.; Lappert, M. F. *Inorg. Chem.* **2004**, *43*, 1031-1038.

[53]. Nief, F. *Dalton Trans.* **2010**, *39*, 6589-6598.

[54]. Hitchcock, P. B.; Lappert, M. F.; Maron, L.; Protchenko, A. V. *Angew. Chem. Int. Ed.* **2008**, *47*, 1488-1491.

[55]. Eller, P. G.; Penneman, R. A. *J. Less-Common Met.* **1987**, *127*, 19-33.

[56]. Shsnnon, R. D.; Prewitt, C. T. *Acta. Crystallogr. B.* **1969**, *B25*, 925-946.

[57]. Masuya, A.; Igarashi, C.; Kanesato, M.; Hoshino, H.; Iki, N. *Polyhedron.* **2015**, *85*, 76-82.

Chapter 4: Further reactivity of lanthanoid biphenolate complexes

4.1 Introduction

Lanthanoid biphenolate complexes with the Ln–O bond continue to attract much academic attention because of their outstanding performance as catalysts.[1, 2] Moreover, due to its ability to act as a dianionic chelating ligand 2,2′-methylene-bis(6-*tert*-butyl-4-methylphenol) $BP(O_2)^{2-}$ (see previous chapter) has been employed to stabilise the metal centre in a range of oxidation states.[3-6] Furthermore, the biphenol $BP(OH)_2$ proligand 2,2′-methylene-bis(6-*tert*-butyl-4-methylphenol) (Fig. 4.1) has a flexible coordination geometry, which allows the coordination of a wide range of metals, and thus could be useful for many kinds of reactions. For example, lanthanoid binolate derivatives have been applied as homoleptic, symmetric and asymmetric Lewis acidic catalysts for organic transformations.[7] In addition, the biphenolate ligand system (2,2′-methylene-bis(6-*tert*-butyl-4-methylphenol) has been exploited in coordination chemistry to stabilise complexes either by thermodynamic or kinetic means.[8] As a result, this ligand system has been used to synthesise different species of transition and main group metal coordination complexes, and some of these complexes have shown significant and selective catalytic activity. For example, biphenolate titanium, and aluminium complexes can catalyse the polymerisation of some polar monomers, and organic transformations such as, α-olefins, propylene oxide[9-20] and the ring-opening of cyclic esters.[21-24] In addition, a number of studies have been conducted on the catalytic activity of lanthanoid complexes stabilised by the biphenolate ligand in organic transformations. For example, amine biphenolate lanthanoid complexes such as $[(BPO_2)La\{N(SiHMe_2)_2\}]$ ($BPO_2 = (2,4$-^tBu-C_6H_2O-$CH_2)_2$-NCH_2CH_2OMe) are efficient initiators for the polymerisation of L-lactide and the highly heteroselective polymerisation of rac-lactide.[18-20] Also, Xiaoping Xu *et al.*[3] have reported the synthesis and characterisation of trivalent lanthanoid

complexes supported by $BP(O_2)$ ligand, and their catalytic activity for the Diels-Alder reaction of cyclopentadiene with methyl methacrylate.
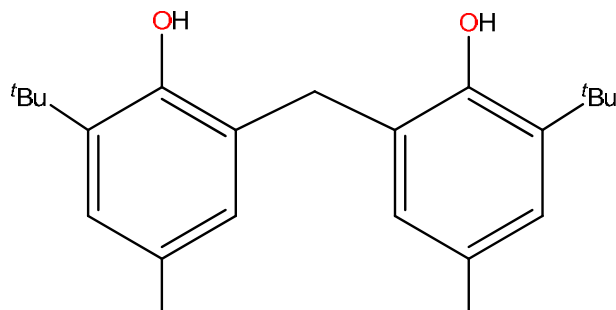
Figure 4.1 Ligand system used in RT/P synthesis and reactivity (RT/P = redox transmetallation/protolysis).

Xu *et al*. (2007) have employed general metathesis reactions by using the corresponding lanthanoid chloride as a precursor to synthesise an anionic heterobimetallic biphenolate complex (eqn. 4.1).[25]
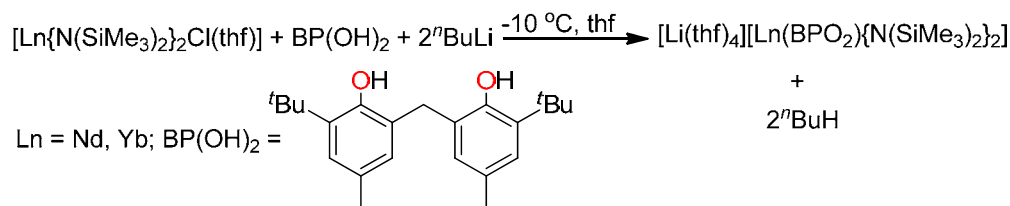
Equation 4.1

An alternate method for synthesising heterobimetallic biphenolate complexes makes use of the ligand exchange reaction between a cerium triflate complex and an alkali metal biphenolate compound (eqn. 4.2).[26]
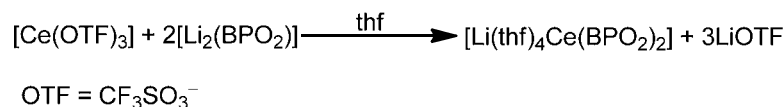
Equation 4.2

The reactivity of complex $[Yb(BPO_2)(BP(OH)O)(thf)_2]$ with a metal alkyl (butyllithium) was explored to prepare a heterobimetallic biphenolate complex (eqn. 4.3).[27]

$$[Yb(BPO_2)(BP(OH)O)(thf)_2] + {}^nBuLi \longrightarrow [Li(thf)_2Yb(BPO_2)_2(thf)] + {}^nBuH$$

Equation 4.3

A one pot reaction of $NdCl_3$ and $LiCH_2SiMe_3$ with biphenol was exploited to synthesise a heterobimetallic biphenolate complex (eqn. 4.4).[28]

$$NdCl_3 + 4LiCH_2SiMe_3 + 2BPO(OH)_2 \longrightarrow [Li(thf)_2Nd(BPO_2)_2(thf)] + 3LiCl + 4SiMe_4$$
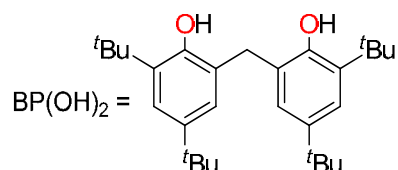
Equation 4.4

A redox transmetallation reaction was utilised to synthesise lanthanoid biphenolate complexes $[Ln(BPO_2)(BP(OH)O)(thf)_n]$ (n = 1, 2, 3) (eqn. 4.5)[14, 15] in Chapter Three of this thesis including the reaction between the organomercury with freshly filed Ln metal and $BP(OH)_2$ ligand. Lanthanoid biphenolate complexes $[Ln(BPO_2)(BP(OH)O)(thf)_n]$ (n = 1, 2, 3) can be transformned into heterobimetallic complexes for example, $[Li(thf)_4][Y(BPO_2)_2(thf)_2]$, $[Li(thf)_2Pr(BPO_2)_2(thf)_2]$, $[AlMe_2Tb(BPO_2)_2(thf)_2]$ and $[ZnEtYb(BPO_2)_2(thf)]$ by treatment with different metal alkyls such as (^nBuLi, $AlMe_3$ and $ZnEt_2$) scheme 4.1.

$$Ln_{(excess)} + 3Hg(C_6F_5)_2 + 4BP(OH)_2 \xrightarrow{thf} 2[Ln(BPO_2)(BP(OH)O)(thf)_n] + 3Hg + 6C_6F_5H$$

n = 2, 3
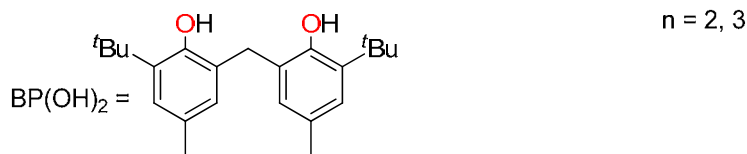
Equation 4.5

4.2 Current study

There has been a lot of interest in synthesising heterobimetallic complexes using a biphenol ligand such as 2,2′-methylene-bis(6-*tert*-butyl-4-methylphenolate), especially in transition metal chemistry. Heterobimetallic chemistry of the lanthanoid metals is still limited and few complexes have been reported. This study aimed to synthesise heterobimetallic complexes with the biphenolate ligand by exploring some reactivity possibilities of $[Ln(BPO_2)(BP(OH)O)(thf)_n]$ (n = 1, 2, 3) complexes prepared in Chapter Three of this thesis with different metal alkyls/amides, for example ^nBuLi, $AlMe_3$, $KN(SiMe_3)_2$ and $ZnEt_2$. In addition, the aim was to investigate their properties, and characteristics, and compare the synthesised complexes with those reported in the literature. $[Ln(BPO_2)(BP(OH)O)(thf)_n]$ (n = 1, 2, 3) complexes were prepared by the redox transmetallation reaction between lanthanoid metals and biphenolate ligand (Chapter three). The redox transmetallation reaction and reactivity processes were carried out in a donor solvent (thf). Structures have been characterised by X-ray crystallography, ^{1}H-NMR, IR, elemental analyses and melting point.

4.3 Results and discussion

4.3.1 Synthesis

Scheme 4.1 shows that the heterobimetallic complexes can be obtained by metallating [Ln(BPO$_2$)(BP(OH)O)(thf)$_n$] with a different metal alkyl. For example, using the smallest alkali ion as ^{n}BuLi (n-butyllithium) as metallating reagent to form wide range of ionic and non-ionic heterobimetallic complexes [Li(thf)$_4$][Ln(BPO$_2$)$_2$(thf)$_2$] (Ln = Y **4.1**, Sm **4.2**, Dy **4.3** and Ho **4.4**); [Li(thf)$_2$Ln(BPO$_2$)$_2$(thf)$_n$] (Ln = La **4.5**, Pr **4.6**, n = 2; Er **4.7**, Yb **4.8**, Lu **4.9**, n = 1) (Scheme 4.1). Using a large alkali ion such as potassium KN(SiMe$_3$)$_2$ gives a non-ionic heterobimetallic complex [K(thf)$_3$Gd(BPO$_2$)$_2$(thf)$_2$] **4.10** (Scheme 4.1). Adding aluminium (AlMe$_3$) as metallating agent gives a variety of ionic and non-ionic heterobimetallic complexes such as [La(BPO$_2$)(thf)$_5$][AlMe$_2$(BPO$_2$)] **4.11** and [AlMe$_2$Ln(BPO$_2$)$_2$(thf)$_2$] (Ln = Y **4.14**, Pr **4.15**, Sm **4.16**, Tb **4.17**) (Scheme 4.1) in addition to biphenolate aluminium complexes, for example, [AlMe(BPO$_2$)(thf)] **4.19** and [Al$_2$(BPO$_2$)$_3$(thf)$_2$] **4.18** (Scheme 4.1). [(BPO$_2$) Ln(thf)$_5$(μ−F)AlMe(BPO$_2$)] (Ln = Sm **4.12**, Tb **4.13**) were isolated as unexpected products from attempts to synthesise [AlMe$_2$Ln(BPO$_2$)$_2$(thf)$_2$] (Ln = Sm, Tb) (Scheme 4.1). Complexes **4.12** and **4.13** were halogenated by C$_6$F$_5$H after redox transmetallation reaction between Ln (Ln = Sm, Tb), Hg(C$_6$F$_5$)$_2$ and BP(OH)$_2$ was run and filterated then AlMe$_3$ was added to the filterated mother liquor with the generated C$_6$F$_5$H still present. The AlMe$_3$ deprotonated the biphenol, but also obviously reacts with the residing C$_6$F$_5$H to give the bridging F ligand. Using a transition metal such as zinc (ZnEt$_2$) gives a non-ionic heterobimetallic complex [ZnEtYb(BPO$_2$)$_2$(thf)] **4.21** (Scheme 4.1). Yields ranged from moderate such as **4.20** (0.25 g, 18 %) to good such as **4.1** (0.70 g, 51 %).

^{n}BuLi
thf, r. t.

$[Li_4(BPO_2)_2(thf)_4]$ **4.20**

^{n}BuLi
thf, r. t.

$[Li(thf)_2Ln(BPO_2)_2(thf)_n]$

Ln = La **4.5**, Pr **4.6**, n = 2;
Er **4.7**, Yb **4.8**, Lu **4.9**, n = 1

^{n}BuLi thf, r. t.

$[Li(thf)_4][Ln(BPO_2)_2(thf)_2]$
Ln = Y **4.1**, Sm **4.2**, Dy **4.3**, Ho **4.4**

$Ln_{(excess)}$ + $3Hg(C_6F_5)_2$ + $4BP(OH)_2$ $\xrightarrow{\text{thf, r. t.}}$ $[Ln(BPO_2)(BP(OH)O)(thf)_n]$

$[La(BPO_2)(thf)_5][AlMe_2(BPO_2)]$ **4.11**

$[(BPO_2)Ln(thf)_3(\mu{-}F)AlMe(BPO_2)]$
(Ln = Sm **4.12**, Tb **4.13**)

$[AlMe_2Ln(BPO_2)_2(thf)_2]$
(Ln = Y **4.14**, Pr **4.15**, Tb **4.16**, Sm **4.17**)

$[AlMe(BPO_2)(thf)]$; $[Al_2(BPO_2)_3(thf)_2]$
4.19 **4.18**

BP(OH)$_2$ =

$[ZnEtYb(BPO_2)_2(thf)]$
4.21

thf, r. t.
ZnEt$_2$

thf, r.t.
$KN(SiMe_3)_2$

$[K(thf)_3Gd(BPO_2)_2(thf)_2]$
4.10

AlMe$_3$, thf, r. t.

Scheme 4.1 Synthesis of heterobimetallic biphenolate complexes.

4.3.2 Characterisation

Biphenolate heterobimetallic complexes **4.1-4.21** were initially isolated as single crystals, and were identified by X-ray crystallography using the MX1 beamline of the Australian Synchrotron or a Bruker APEX II diffractometer. This characterisation was further supported by IR spectroscopy (Table 4.1), elemental analyses, melting point and ^{1}H-NMR spectroscopy (Table 4.2).

IR spectra of biphenolate heterobimetallic complexes that were isolated from the mother liquor of the redox transmetallation reaction showed complete deprotonation of the biphenolate ligand. This outcome was indicated by the absence of a ν(O−H) absorption in infrared spectrum, which is often observed at 3610-3640 cm^{-1}, in addition to the lack of an OH resonance in the ^{1}H-NMR spectra of the bulk vacuum dried materials. These results indicated successful synthesis of the biphenolate heterobimetallic complexes. The O–C stretching for compounds **4.1-4.21** showed vibration of a metal-coordinated phenolate group observed at 1204-1278 cm^{-1} Table 4.1.

Due to the paramagnetic nature of (**4.3**, **4.6**, **4.10**, **4.12**, **4.15**, **4.16, 4.21)** no reasonable structural information could be obtained from their H-NMR spectra. They gave a broadened spectrum, which could not be satisfactorily integrated. However, the paramagnetic Ln^{+3} complexes (**4.2**, **4.4**, **4.7**, **4.13**, **4.17)** gave an interpretable ^{1}H-NMR spectrum, some peaks are paramagnetically shifted down field. For example, in complex **4.17** the ^{1}H-NMR spectrum showed that the peak related to Al-Me appears at -0.38 ppm and the peak related to CH$_2$ appear at 0.19 ppm compared with the BP(OH)$_2$ ^{1}H-NMR. Same behaviour on the ^{1}H-NMR spectrum of Al-Me has been reported by Gambarotta *et. al*.[29] for [AlMe$_4$Sm(BPO$_2$)]$_2$.

The two protons of the bridging Ar−*CH$_2$*−Ar unit in complexes **4.2**, **4.4**, **4.5**, **4.7** display considerably two different chemical shifts. Their X-ray crystal structures show that the

two protons of CH_2 are non-equivalent with one diverted towards the metal and one away providing magnetically inequivalent environments and shows the solid state structures are maintained in the solution state. The free ligand shows only a singlet for the CH_2 resonances.

The ^{1}H-NMR spectra of some complexes show they lose some thf molecules of solvation. This result is further supported by microanalysis. For example, ^{1}H-NMR spectra of $[Tb(BPO_2)(thf)_3][AlMe_2(BPO_2)]$ **4.13** show two thf molecules have been lost upon isolation compared with that established by X-ray crystallography and supported by the elemental analysis calcd for **4.13** $C_{63}H_{95}O_7FTbAl$ (1185.33 g.mol^{-1}): C, 63.84, H, 8.08, Tb, 13.41. Calcd for $C_{55}H_{79}O_6FTbAl$ (1041.12 g.mol^{-1} after lost one thf): C, 63.45, H, 7.65, Tb, 15.26. Found: C, 63.11, H, 7.48, Tb, 15.08.

$[Li(thf)_4][Y(BPO_2)_2(thf)_2]$ **4.1** and $[Li(thf)_2Er(BPO_2)_2(thf)]$ **4.7** have lost two thf molecules. The ^{1}H-NMR spectrum of $[Li(thf)_4][Ho(BPO_2)_2(thf)_2]$ **4.4** shows it has lost four thf molecules upon isolation compared with the composition shown in the X-ray crystal structure.

Table 4.1 O–C stretching absorption bands in IR spectra (ν4000–400 cm^{-1}).

Compound	O–C stretching vibration (cm^{-1})
[Li(thf)$_4$][Y(BPO$_2$)$_2$(thf)$_2$] (**4.1**)	1254
[Li(thf)$_4$][Sm(BPO$_2$)$_2$(thf)$_2$] (**4.2**)	1258
[Li(thf)$_4$][Dy(BPO$_2$)$_2$(thf)$_2$] (**4.3**)	1262
[Li(thf)$_4$][Ho(BPO$_2$)$_2$(thf)$_2$] (**4.4**)	1204
[Li(thf)$_2$La(BPO$_2$)$_2$(thf)$_2$] (**4.5**)	1258
[Li(thf)$_2$Pr(BPO$_2$)$_2$(thf)$_2$] (**4.6**)	1225
[Li(thf)$_2$Er(BPO$_2$)$_2$(thf)] (**4.7**)	1204
[Li(thf)$_2$Lu(BPO$_2$)$_2$(thf)] (**4.9**)	1258
[K(thf)$_3$Gd(BPO$_2$)$_2$(thf)$_2$] (**4.10**)	1233
[La(BPO$_2$)(thf)$_5$][AlMe$_2$(BPO$_2$)] (**4.11**)	1239
[Sm(BPO$_2$)(thf)$_3$][AlMe$_2$(BPO$_2$)] (**4.12**)	1262
[Tb(BPO$_2$)(thf)$_3$][AlMe$_2$(BPO$_2$)] (**4.13**)	1258
[AlMe$_2$Y(BPO$_2$)$_2$(thf)$_2$] (**4.14**)	1258
[AlMe$_2$Pr(BPO$_2$)$_2$(thf)$_2$] (**4.15**)	1250
[AlMe$_2$Tb(BPO$_2$)$_2$(thf)$_2$] (**4.17**)	1278
[Al$_2$(BPO$_2$)$_3$(thf)$_2$] (**4.18**)	1204
[AlMe(BPO$_2$)(thf)] (**4.19**)	1255
[Li$_4$(BPO$_2$)$_2$(thf)$_4$] (**4.20**)	1230
[ZnEtYb(BPO$_2$)$_2$(thf)] (**4.21**)	1208

Table 4.2 Chemical shifts in ^{1}H-NMR spectra of 4.1, 4.2, 4.4, 4.5, 4.7, 4.9, 4.11, 4.13, 4.17-4.20.

	Chemical shift (ppm)											
^{1}H-NMR	**4.1**	**4.2**	**4.4**	**4.5**	**4.7**	**4.9**	**4.11**	**4.13**	**4.17**	**4.18**	**4.19**	**4.20**
Aromatic	7.03	5.42	7.00	6.82	6.99	6.98	6.78	7.08	7.04	7.08	6.98	6.88
CH$_2$	4.02	4.68	5.74	4.70	5.06	4.49	5.32	5.70	0.19	3.90	3.15	3.96
CH$_2$	-	4.13	3.76	3.32	4.31	3.59	-	-	-	-	-	-
thf	3.38	1.42	1.85	2.97	2.11	2.96	3.34	3.70	3.44	2.71	3.86	2.95
thf	1.27	-0.73	0.29	0.78	0.97	0.87	0.12	0.27	0.85	0.86	0.75	0.95
CH$_3$	2.18	0.82	2.09	1.99	1.34	2.08	2.25	2.13	2.17	1.96	2.28	2.06
Al-CH$_3$	-	-	-	-	-	-	0.26	-0.37	-0.38	-	2.12	-
C(CH$_3$)$_3$	1.50	-1.43	1.40	1.26	0.28	0.42	1.36	1.48	1.49	1.33	1.60	1.33

4.3.3 Crystal structure determinations

[Li(thf)₄][Ln(BPO₂)₂(thf)₂].thf (Ln = Y 4.1, Sm 4.2, Dy 4.3 and Ho 4.4)

Compound **4.1** crystallises in the triclinic space group *P*-1, while compounds **4.2-4.4** crystallise in the monoclinic space group $P2_1$ (Table 4.4). X-ray crystal structure of [Li(thf)₄][Ho(BPO₂)₂(thf)₂] **4.4** (Fig. 4.3) is isostructure to other structures [Li(thf)₄][Y(BPO₂)₂(thf)₂] **4.1**, [Li(thf)₄][Sm(BPO₂)₂(thf)₂] **4.2**, [Li(thf)₄][Dy(BPO₂)₂(thf)₂] **4.3**. The unit cells of **4.1-4.4** are comprised of four molecules of [Li(thf)₄][Ln(BPO₂)₂(thf)₂] (Ln = Y, Sm, Dy and Ho). The molecular structure of [Li(thf)₄][Ln(BPO₂)₂(thf)₂] (Fig. 4.2) is an ionic heterobimetallic with two biphenolate ligands and six thf molecules. The overall molecular geometry around the six-coordinate Ln (Ln = Y, Sm, Dy and Ho) metal centre is best described as a distorted octahedron coordinated by four oxygen atoms of the two (BPO₂) ligands as bidentates, and two oxygen atoms of thf molecules in a *cisoid* form. For example, in **4.4** O(1), O(4) occupy axial positions O(1)−Ho−O(4) 170.5(2) with other four oxygen atoms O(2), O(3), O(5), O(6) arranged in equatorial positions around Ho centre. Li has four coordination with four oxygen atoms of thf molecules and the geometry around the Li metal centre is distorted tetrahedral.

Selected bond lengths and angles of [Li(thf)₄][Y(BPO₂)₂(thf)₂], [Li(thf)₄][Sm(BPO₂)₂(thf)₂], [Li(thf)₄][Dy(BPO₂)₂(thf)₂] and [Li(thf)₄][Ho(BPO₂)₂(thf)₂] are in Table 4.3 while X-ray data are in Table 4.4.

The average Y−O₍phenolate₎ bond length of [Li(thf)₄][Y(BPO₂)₂(thf)₂] is 2.16 Å, which is comparable to that of [Na(dme)₃][Y(BPO₂)₂(dme)][30] (average 2.14 Å). The average Ln−O₍phenolate₎ bond lengths of [Li(thf)₄][Ln(BPO₂)₂(thf)₂] (Ln = Sm, Dy and Ho) were found to be 2.22, 2.18, 2.17 Å respectively, which are comparable to the average Ln−O₍phenolate₎ bond length reported for [Na(thf)₂(dme)₂][Yb(BPO₂)₂(thf)₂][31],

[Na(dme)$_3$][Er(BPO$_2$)$_2$(dme)$_2$][32] and [Na(dme)$_3$][Y(BPO$_2$)$_2$(dme)][30] (averages 2.14, 2.14, 2.15 Å respectively) with consideration the metal size differences.

The average Sm−O$_{(thf)}$ bond lengths in **4.2** were found to be 2.51 Å which is longer than that Ln−O$_{(thf)}$ in complexes **4.1**, **4.3** and **4.4** (averages 2.43, 2.46 and 2.43 respectively) due to the metal size differences as Sm^{+3} (ionic radius 0.95 Å for six coordinate)[48] larger than Y, Dy, Ho (ionic radii 0.90 Å, 0.91 Å, 0.90 Å respectively for six coordinate).[48]

The bond lengths Ln−O$_{(phenolate)}$ and the bond angles O−Ln−O$_{(phenolate)}$ in [Li(thf)$_4$][Y(BPO$_2$)$_2$(thf)$_2$], [Li(thf)$_4$][Sm(BPO$_2$)$_2$(thf)$_2$], [Li(thf)$_4$][Dy(BPO$_2$)$_2$(thf)$_2$] and [Li(thf)$_4$][Ho(BPO$_2$)$_2$(thf)$_2$] are comparable to others with consideration of the metal size differences.
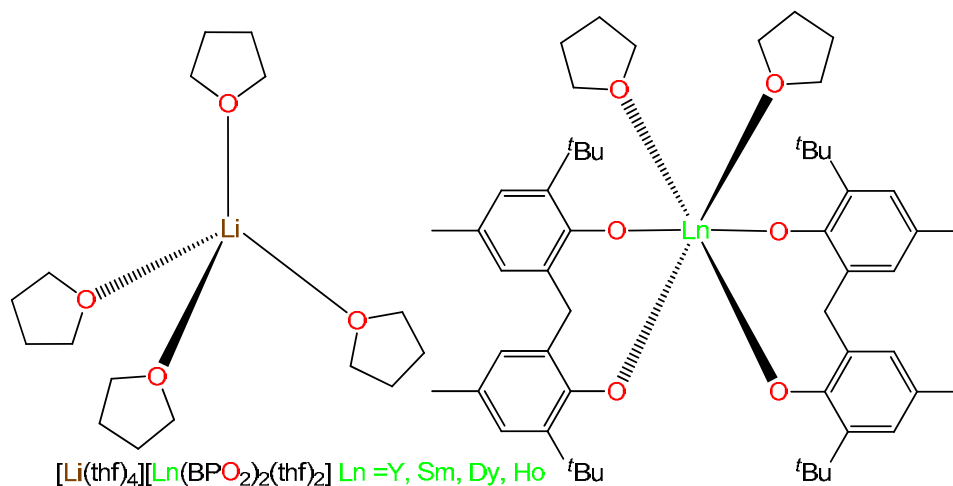
Figure 4.2 Ionic heterobimetallic diagram of compounds 4.1-4.4.
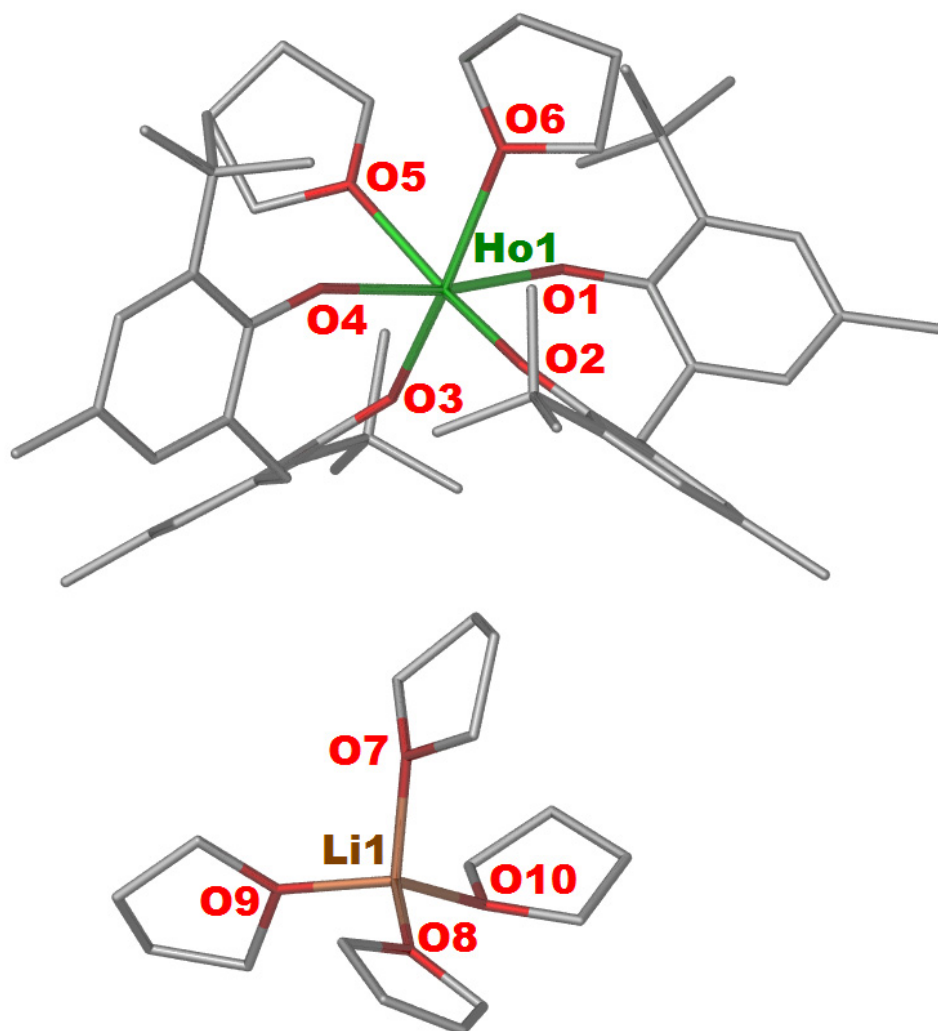
Figure 4.3 X-ray crystal structure of 4.4. Hydrogen atoms are omitted for clarity.

Table 4.3 Selected bond lengths and angles of [Li(thf)₄][Y(BPO₂)₂(thf)₂], [Li(thf)₄][Sm(BPO₂)₂(thf)₂], [Li(thf)₄][Dy(BPO₂)₂(thf)₂] and [Li(thf)₄][Ho(BPO₂)₂(thf)₂].

Bond lengths (Å)	[Li(thf)₄][Y(BPO₂)₂(thf)₂]	[Li(thf)₄][Sm(BPO₂)₂(thf)₂]	[Li(thf)₄][Dy(BPO₂)₂(thf)₂]	[Li(thf)₄][Ho(BPO₂)₂(thf)₂]
Ln(1)–O(1)	2.125(4)	2.214(4)	2.165(4)	2.130(4)
Ln(1)–O(2)	2.180(4)	2.274(4)	2.205(4)	2.206(4)
Ln(1)–O(3)	2.131(4)	2.161(4)	2.173(4)	2.167(4)
Ln(1)–O(4)	2.204(4)	2.256(4)	2.215(4)	2.200(4)
Ln(1)–O(5)	2.434(4)	2.526(4)	2.454(4)	2.443(4)
Ln(1)–O(6)	2.441(4)	2.508(4)	2.468(4)	2.429(4)
Li(1)–O(13)	1.918(14)	1.912(19)	1.855(17)	1.821(17)
Li(1)–O(14)	1.939(14)	1.979(16)	1.915(13)	1.972(19)
Bond angles (°)				
O(1)–Ln(1)–O(2)	94.02(15)	92.02(16)	93.84(18)	93.53(19)
O(3)–Ln(1)–O(4)	93.98(16)	91.82(16)	93.51(19)	93.90(2)
O(5)–Ln(1)–O(6)	86.09(14)	82.41(16)	83.00(17)	82.90(2)
O(1)–Ln(1)–O(3)	105.15(16)	103.30(19)	102.70(2)	91.00(2)

Table 4.4 Crystallographic data for compounds 4.1-4.4.

Compound	4.1	4.2	4.3	4.4
formula	$C_{74}H_{116}O_{11}YLi$	$C_{74}H_{116}O_{11}SmLi$	$C_{74}H_{116}O_{11}DyLi$	$C_{74}H_{116}O_{11}HoLi$
fw	1277.55	1339.01	1351.15	1353.58
crystal system	triclinic	monoclinic	monoclinic	monoclinic
space group	P-1	$P2_1$	$P2_1$	$P2_1$
a, Å	14.141(3)	12.984(3)	12.993(3)	12.997(3)
b, Å	17.116(3)	37.320(8)	37.364(8)	37.232(7)
c, Å	30.903(6)	15.010(3)	14.907(3)	14.912(3)
α, deg	105.04(3)	90	90	90
β, deg	92.37(3)	106.79(3)	106.44(3)	106.40(3)
γ, deg	90.60(3)	90	90	90
V, Å^3	7216(3)	6963(3)	6941(3)	6922(3)
Z	4	4	4	4
T, K	173(2)	173(2)	173(2)	173(2)
no. of rflns collected	46574	92998	110447	86174
no. of indep rflns	23591	32648	31072	32278
R_{int}	0.035	0.046	0.030	0.053
Final R_1 values ($I > 2\sigma(I)$)	0.093	0.034	0.036	0.037
Final $wR_2(F^2)$ values ($I > 2\sigma(I)$)	0.250	0.094	0.128	0.093
Final R_1 values (all data)	0.108	0.036	0.040	0.040
Final $wR_2(F^2)$ values (all data)	0.260	0.097	0.134	0.096
$GooF$ (on F^2)	1.082	0.998	1.181	1.037

[Li(thf)₂Ln(BPO₂)₂(thf)₂] (Ln = La 4.5, Pr 4.6)

The isotypical complexes $[Li(thf)_2Ln(BPO_2)_2(thf)_2]$ (Ln = La **4.5**, Pr **4.6**) (Fig. 4.4) crystallise in the monoclinic space group *C*c (Table 4.6). Compounds **4.5** and **4.6** display a dinuclear form bridged by two oxygen atoms from two different biphenolate ligands as a heterobimetallic structure. The overall molecular geometry around the six-coordinate Ln (Ln = La, Pr) metal centres is a distorted octahedron, coordinated by four oxygen atoms of the two (BPO_2) ligands, and two oxygen atoms of thf molecules. Two oxygen atoms O(1), O(3) in **4.5** are located in axial positions O(1)–La–O(3) 161.02(6)° while other four oxygen atoms O(2), O(4), O(5), O(6) arranged in equatorial positions around La (Fig. 4.5). Li has four coordination with two oxygen atoms of thf molecules and two oxygen atoms of biphenolate ligand and the geometry around Li metal centre is distorted square planar.

The average bond lengths of La−O$_{(phenolate)}$ were found to be 2.36 Å in $[Li(thf)_2La(BPO_2)_2(thf)_2]$, which is close to the average bond lengths Pr−O$_{(phenolate)}$ 2.32 Å of $[Li(thf)_2Pr(BPO_2)_2(thf)_2]$. The difference between the average La–O and Pr–O bond lengths is 0.04 Å, which is similar to the difference between the ionic radii of La^{+3} (CN = 6) and Pr^{+3} (CN = 6) (0.04 Å).[48] The average bond angles O–La–O of **4.5** were found to be 94.46° which is close to the average bond angles O–Pr–O 93.93° of **4.6** Table 4.5.

The average bond lengths La−O$_{(phenolate)}$ 2.36 Å of $[Li(thf)_2La(BPO_2)_2(thf)_2]$ are in agreement with the average bond lengths La−O$_{(phenolate)}$ (2.35 Å) reported in the literature for $[Li(thf)_2La(BPO_2)_2(bpy)]$.[26] The average Ln−O$_{(phenolate)}$ (Ln = La, Pr) bond lengths of **4.5** and **4.6** (averages 2.36 Å, 2.32 Å; ionic radii 1.032 Å, 0.99 Å[48] for six coordinate La, Pr respectiviely) are larger than the average Ln−O$_{(phenolate)}$ bond lengths reported for $[Na(thf)_2(dme)_2][Yb(BPO_2)_2(thf)_2]$[31] (2.11 Å) and $[Na(dme)_3][Er(BPO_2)_2(dme)_2]$ (2.13 Å).[32] Also they are larger than the average Ln–O$_{(phenolate)}$ bond lengths determined for **4.1**, **4.2**, **4.3** and **4.4** (averages 2.16 Å, 2.22 Å, 2.18 Å, 2.17 Å respectively) due to metals

size difference (ionic radii 0.90 Å, 0.95 Å, 0.91 Å, 0.90 Å for six coordinate Y, Sm, Dy, Ho respectively).[48]

[Li(thf)$_2$Ln(BPO$_2$)$_2$(thf)$_2$] Ln = La, Pr
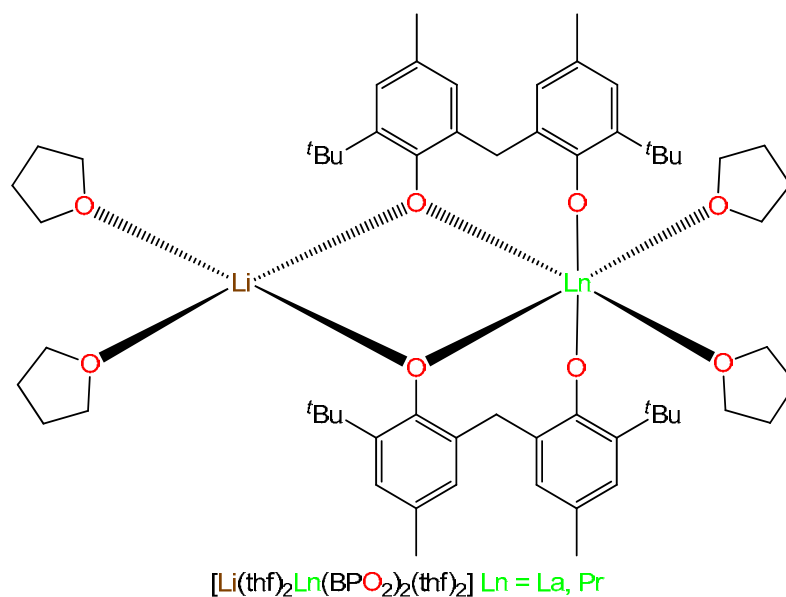
Figure 4.2 Non-ionic heterobimetallic diagram of compounds 4.5 and 4.6.
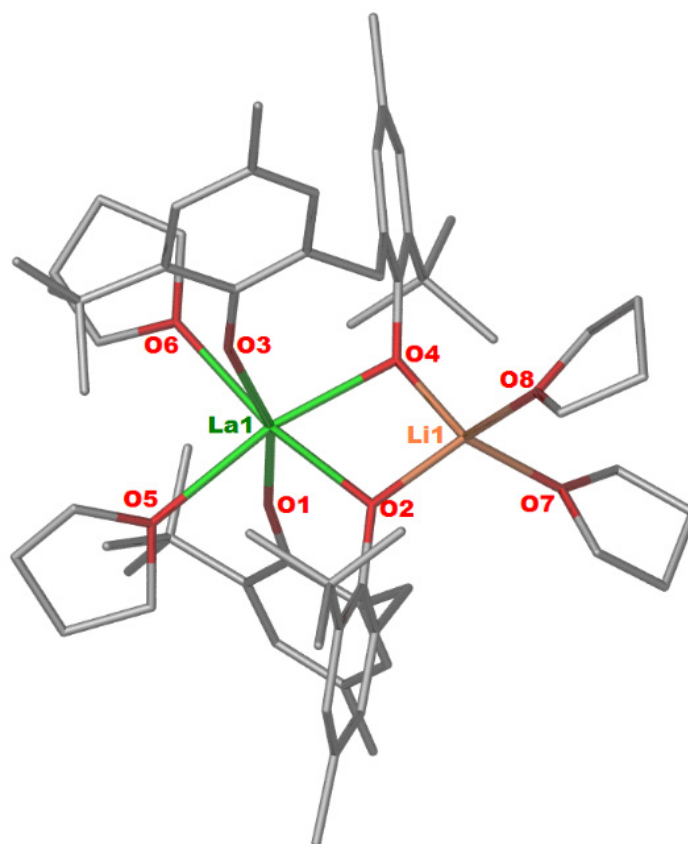
Figure 4.5 X-ray crystal structure of 4.5. Hydrogen atoms are omitted for clarity.

Table 4.5 Selected bond lengths and angles of [Li(thf)₂La(BPO₂)₂(thf)₂], [Li(thf)₂Pr(BPO₂)₂(thf)₂].

Bond lengths (Å)	[Li(thf)$_2$La(BPO$_2$)$_2$(thf)$_2$]	[Li(thf)$_2$Pr(BPO$_2$)$_2$(thf)$_2$]
Ln(1)–O(1)	2.351(4)	2.255(9)
Ln(1)–O(2)	2.402(4)	2.344(9)
Ln(1)–O(3)	2.326(4)	2.332(9)
Ln(1)–O(4)	2.389(4)	2.381(9)
Ln(1)–O(5)	2.590(5)	2.502(9)
Ln(1)–O(6)	2.611(5)	2.609(9)
Li (1)–O(2)	1.957(11)	2.101(15)
Li (1)–O(4)	1.975(10)	1.891(16)
Li (1)–O(7)	2.012(10)	2.020(2)
Li (1)–O(8)	2.041(11)	2.020(2)
Bond angles (°)		
O(1)–Ln(1)–O(2)	95.96(16)	94.00(4)
O(3)–Ln(1)–O(4)	96.12(15)	98.10(3)
O(5)–Ln(1)–O(6)	91.31(9)	89.70(2)
O(2)–Li(1)–O(4)	91.86(19)	90.70(5)
O(7)–Li(1)–O(8)	89.74(18)	88.90(5)
O(7)–Li(1)–O(2)	117.00(6)	113.00(9)
O(4)–Li(1)–O(8)	119.00(6)	125.40(10)

Table 4.6 Crystallographic data for compounds 4.1-4.4.

Compound	**4.5**	**4.6**
formula	C$_{62}$H$_{92}$O$_8$LaLi	C$_{62}$H$_{92}$O$_8$PrLi
fw	1111.24	1113.24
crystal system	monoclinic	monoclinic
space group	*Cc*	*Cc*
a, Å	18.153(4)	18.145(4)
b, Å	17.589(4)	17.484(4)
c, Å	18.005(4)	18.003(4)
α, deg	90	90
β, deg	98.04(3)	97.45(3)
γ, deg	90	90
V, Å^3	5693(2)	5663(2)
Z	4	4
T, K	173(2)	173(2)
no. of rflns collected	31367	38831
no. of indep rflns	12776	13383
R$_{int}$	0.029	0.044
Final R_1 values ($I > 2\sigma(I)$)	0.026	0.054
Final $wR_2(F^2)$ values ($I > 2\sigma(I)$)	0.073	0.134
Final R_1 values (all data)	0.027	0.057
Final $wR_2(F^2)$ values (all data)	0.074	0.136
GooF (on F^2)	0.932	1.114

[Li(thf)$_2$Ln(BPO$_2$)$_2$(thf)].sol (Ln = Er 4.7 sol = 2C$_6$D$_6$, Yb 4.8 sol = hexane, Lu 4.9 sol = 3C$_6$D$_6$) [K(thf)$_3$Gd(BPO$_2$)$_2$(thf)$_2$].2thf (4.10)

The X-ray crystal structure of [Li(thf)$_2$Ln(BPO$_2$)$_2$(thf)] **4.7** (Fig. 4.7) is isostructural with **4.8**, **4.9**. Compounds **4.7** and **4.9** crystallise in the triclinic space group *P*-1, while **4.8** and **4.10** crystallise in the monoclinic space groups *Pn*, *P*2$_1$ respectively (Table 4.8). Compounds **4.7-4.9** (Fig. 4.6, 4.7) and **4.10** (Fig. 4.8) display a dinuclear form involving two different metals bridged by two oxygen atoms from two different biphenolate ligands. The trivalent Ln (Ln = Er, Yb, Lu) metal centre in **4.7-4.9** is five-coordinate with a distorted trigonal bipyramidal geometry, which is coordinated by four oxygen atoms of the two (BPO$_2$) ligands, and one oxygen atom of a thf molecule. In the case of [Li(thf)$_2$Ln(BPO$_2$)$_2$(thf)] **4.7** O(2) and O(5) are arranged in axial positions O(2)–Er–O(5) 150.28(6)° with other three oxygen atoms O(1), O(3), O(4) occupying equatorial positions (Fig. 4.7). Li has four coordination with two oxygen atoms of thf molecules and two oxygen atoms of the biphenolate ligands and the geometry around the Li metal centre is distorted square planar. The trivalent Gd metal centre is six-coordinate with a distorted octahedral geometry, which is coordinated by two oxygen atoms O(2), O(5) in axial positions O(2)–Gd–O(5) 173.16(14)° with other four oxygen atoms O(1), O(3), O(4), O(6) arranged in equatorial positions around the Gd centre (Fig. 4.8). K has five coordination with three oxygen atoms of thf molecules and two oxygen atoms of the biphenolate ligands. The geometry around the K metal centre is distorted trigonal bipyramidal. Two oxygen atoms O(4) and O(8) are arranged in axial positions O(4)–K–O(8) 150.8(3)° with three other oxygen atoms O(2), O(7), O(9) in equatorial positions (Fig. 4.8).

The distinguishing aspect of the trivalent metal Ln (Ln = Er, Yb, Lu) in **4.7-4.9** is the coordination number, which has five coordinate, while complexes **4.1-4.6** have six coordinate might be due to the size of the metal centre.

Compound [Li(thf)$_2$Yb(BPO$_2$)$_2$(thf)] **4.8** described here was synthesised via a one pot redox transmetallation reaction followed by metalation using ^{n}BuLi (Scheme 4.1) instead of the ligand exchange reaction that Yao *et. al*[27] employed.

Selected bond lengths and angles of **4.7-4.10** are listed in Table 4.7. The average bond lengths Er–O$_{(phenolate)}$ of [Li(thf)$_2$Er(BPO$_2$)$_2$(thf)] were found to be 2.15 Å, which is comparable to the Er–O$_{(phenolate)}$ bond length average 2.13 Å reported for [Na(thf)$_2$Er(BPO$_2$)$_2$(thf)][3]. The average bond lengths Lu–O$_{(phenolate)}$ of [Li(thf)$_2$Lu(BPO$_2$)$_2$(thf)] were found to be 2.10 Å, which is comparable to the Yb–O$_{(phenolate)}$ bond lengths reported for [Li(thf)$_2$Yb(BPO$_2$)$_2$(thf)][27] and [Na(thf)$_2$Yb(BPO$_2$)$_2$(thf)][31] (averages 2.11 and 2.11 Å respectively) as Yb^{+3} and Lu^{+3} have similar size (ionic radii 0.86 Å for six coordinate Yb^{+3} and Lu^{+3}).[48]

The average bond lengths Gd–O$_{(phenolate)}$ of [K(thf)$_3$Gd(BPO$_2$)$_2$(thf)$_2$] were found to be 2.20 Å, which is shorter than the Sm–O$_{(phenolate)}$ bond lengths reported for [K(thf)$_2$Sm(BPO$_2$)$_2$(thf)$_2$][33] and larger than the Yb–O$_{(phenolate)}$ bond lengths reported for [K(thf)$_3$Yb(BPO$_2$)$_2$(thf)$_2$][33] (averages 2.23, 2.14 Å respectively) due to metal size differences. The Gd–O$_{(thf)}$ bond lengths (average = 2.52 Å) are longer than the average bond lengths Gd–O$_{(phenolate)}$ of [K(thf)$_3$Gd(BPO$_2$)$_2$(thf)$_2$] but they are almost similar to the Gd–O$_{(thf)}$ of [K(thf)$_2$Sm(BPO$_2$)$_2$(thf)$_2$][33] and [K(thf)$_3$Yb(BPO$_2$)$_2$(thf)$_2$][33]. The Ln–O bond lengths and the O–Ln–O bond angles of [Li(thf)$_2$Ln(BPO$_2$)$_2$(thf)] (Ln = Er, Lu) are different to each other due to metal size differences (ionic radii of Er^{+3} 0.89 Å and Lu^{+3} 0.86 Å)[48] Table 4.7.

[Li(thf)$_2$Ln(BPO$_2$)$_2$(thf)] Ln = Er, Yb, Lu
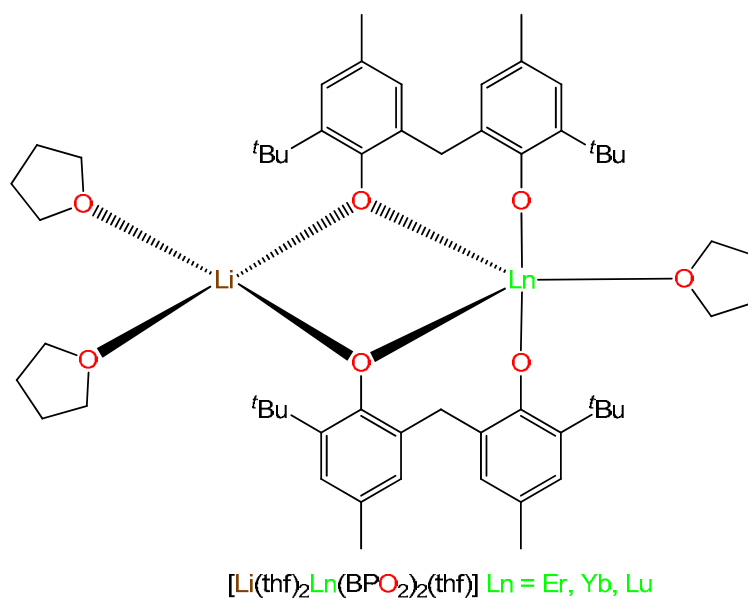
Figure 4.3 Non-ionic heterobimetallic diagram of compounds 4.7-4.9.
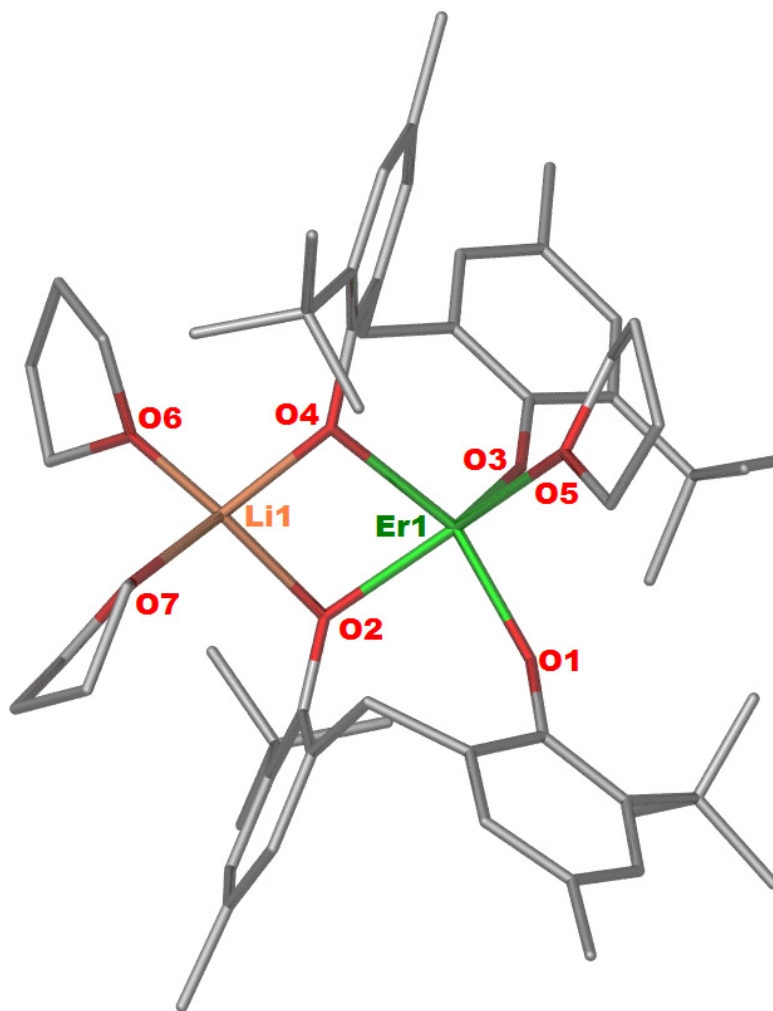
Figure 4.4 X-ray crystal structure of 4.7. Hydrogen atoms are omitted for clarity.
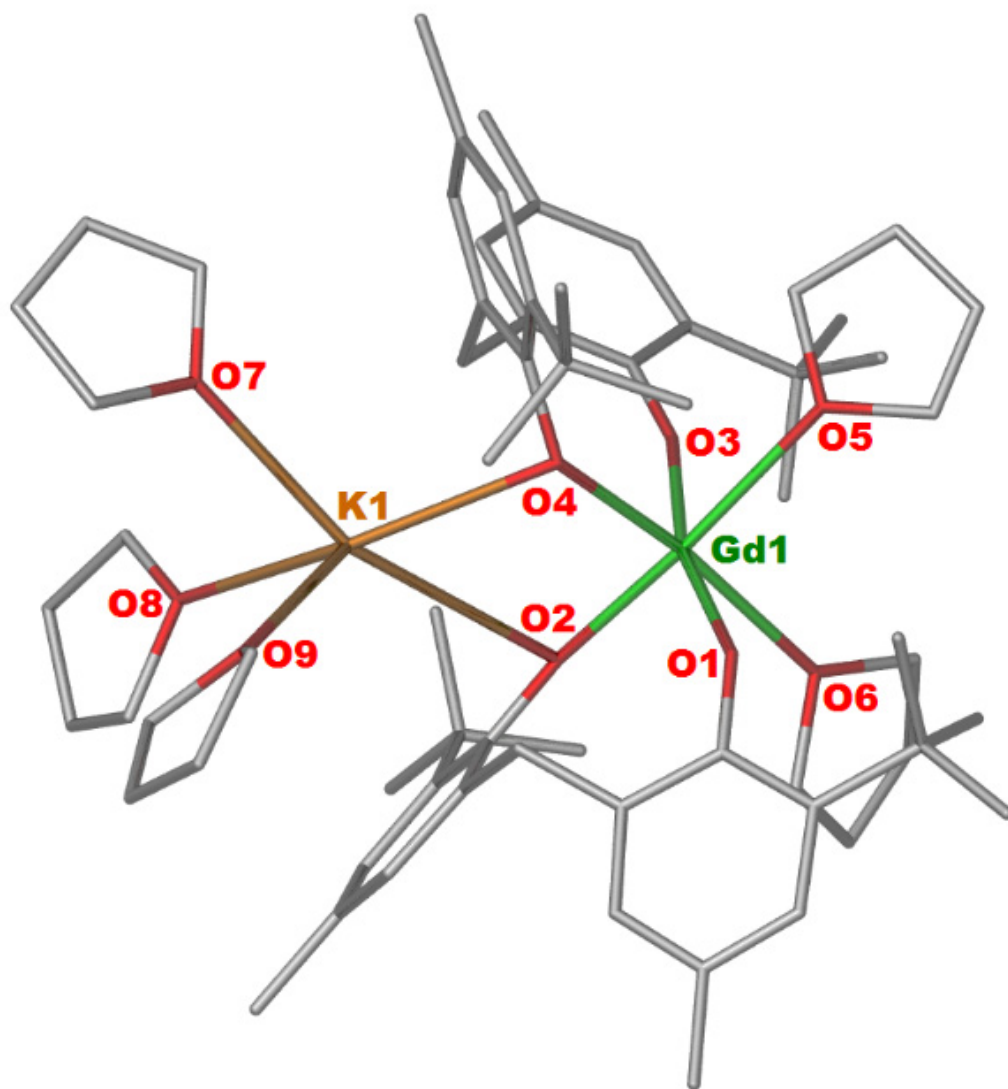
Figure 4.5 X-ray crystal structure of 4.10. Hydrogen atoms are omitted for clarity.

Table 4.7 Selected bond lengths and angles of [Li(thf)$_2$Er(BPO$_2$)$_2$(thf)], [Li(thf)$_2$Lu(BPO$_2$)$_2$(thf)] and [K(thf)$_3$Gd(BPO$_2$)$_2$(thf)$_2$].

Bond lengths (Å)	[Li(thf)$_2$Er(BPO$_2$)$_2$(thf)]	[Li(thf)$_2$Lu(BPO$_2$)$_2$(thf)]	[K(thf)$_3$Gd(BPO$_2$)$_2$(thf)$_2$]
Ln(1)–O(1)	2.109(16)	2.147(18)	2.227(4)
Ln(1)–O(2)	2.172(16)	2.077(2)	2.168(4)
Ln(1)–O(3)	2.085(19)	2.160(18)	2.211(4)
Ln(1)–O(4)	2.240(16)	2.051(18)	2.226(4)
Ln(1)–O(5)	2.358(17)	2.312(19)	2.530(4)
Li(1)–O(2)	2.005(4)	1.985(5)	-
Li(1)–O(4)	1.953(4)	1.978(5)	-
Li(1)–O(6)	1.953(4)	2.015(5)	-
Li(1)–O(7)	1.969(5)	1.973(5)	-
K(1)–O(2)	-	-	3.363(4)
K(1)–O(4)	-	-	2.789(4)
K(1)–O(7)	-	-	2.807(7)
K(1)–O(8)	-	-	2.678(8)
Bond angles (°)			
O(1)–Ln(1)–O(2)	88.20(6)	93.37(8)	95.34(14)
O(3)–Ln(1)–O(4)	109.26(7)	108.67(7)	95.93(14)
O(2)–Ln(1)–O(4)	77.33(6)	79.13(7)	90.03(14)
O(2)–Ln(1)–O(5)	150.28(6)	161.09(7)	173.16(14)
O(2)–Li(1)–O(4)	88.31(17)	87.60(2)	-
O(6)–Li(1)–O(7)	103.80(2)	96.60(2)	-
O(4)–Li(1)–O(6)	108.60(2)	105.90(2)	-
O(2)−K(1)–O(4)	-	-	59.83(10)
O(7)−K(1)–O(9)	-	-	82.70(3)

Table 4.8 Crystallographic data for compounds 4.7-4.10.

Compound	**4.7**	**4.8**	**4.9**	**4.10**
formula	$C_{70}H_{96}O_7ErLi$	$C_{63}H_{96}O_7YbLi$	$C_{76}H_{102}O_7LuLi$	$C_{74}H_{116}O_{11}GdK$
fw	1223.71	1145.67	1309.53	1378.05
crystal system	triclinic	monoclinic	triclinic	monoclinic
space group	P-1	Pn	P-1	$P2_1/c$
a, Å	13.704(3)	13.951(3)	12.698(3)	15.065(5)
b, Å	15.874(3)	30.577(6)	14.857(3)	17.317(6)
c, Å	16.614(3)	14.784(3)	19.178(4)	28.544(9)
α, deg	71.89(3)	90	79.95(3)	90
β, deg	76.93(3)	101.09(3)	81.34(3)	95.08(2)
γ, deg	69.80(3)	90	80.65(3)	90
V, Å^3	3195(14)	6189(2)	3487(13)	7417(4)
Z	2	4	2	4
T, K	173(2)	173(2)	173(2)	298(2)
no. of rflns collected	43476	103588	56817	123821
no. of indep rflns	13552	29272	14861	17026
R_{int}	0.032	0.043	0.025	0.109
Final R_1 values ($I > 2\sigma(I)$)	0.029	0.033	0.032	0.065
Final $wR_2(F^2)$ values ($I > 2\sigma(I)$)	0.081	0.087	0.086	0.183
Final R_1 values (all data)	0.029	0.042	0.033	0.124
Final $wR_2(F^2)$ values (all data)	0.082	0.092	0.088	0.235
$GooF$ (on F^2)	1.035	1.059	0.929	1.103

[La(BPO$_2$)(thf)$_5$][AlMe$_2$(BPO$_2$)].thf (4.11)

Compound **4.11** crystallises in the monoclinic space group *C*2/*c* (Table 4.10). Figure 4.9 displays the ionic heterobimetallic form of the complex. The overall molecular geometry around the seven-coordinate La centre is best described as a distorted pentagonal bipyramid coordinated by two oxygen atoms of the (BPO$_2$) ligand as a bidentate, and five oxygen atoms of thf molecules. Two oxygen atoms O(2) and O(7) are arranged in axial positions O(2)–La–O(7) 166.49(9)° with other five oxygen atoms O(1), O(5), O(7), O(8), O(9) in equatorial positions (Fig. 4.9). The Al is four-coordinate with two oxygen atoms of the (BPO$_2$) ligand and two methyl groups coordinated and the geometry around Al metal centre is distorted tetrahedral.

In the literature there are no reported examples of ionic biphenolate heterobimetallics containing lanthanum and aluminium. There is an example of a biphenolate lanthanum complex [La(BPO$_2$)(PO)(dme)$_2$] (PO = 4-^{t}Bu-C$_6$H$_4$O; 2,6-diMe-C$_6$H$_4$O)[34] that contains La and has the same coordination number as La in [La(BPO$_2$)(thf)$_5$][AlMe$_2$(BPO$_2$)]. Selected bond lengths and angles of **4.11** are listed in Table 4.9. The average La–O$_{(phenolate)}$ bond lengths of [La(BPO$_2$)(thf)$_5$][AlMe$_2$(BPO$_2$)] were found to be 2.23 Å, which is same to the average La–O$_{(phenolate)}$ 2.23 Å reported for [La(BPO$_2$)(PO)(dme)$_2$] (PO = 4-^{t}Bu-C$_6$H$_4$O).[34]

The average Al–O$_{(phenolate)}$ bond lengths of **4.11** were found to be 1.77 Å, which is shorter than the Al–O$_{(phenolate)}$ of the known structure [AlMe$_2$Sm(BPO$_2$)$_2$(thf)$_2$][29] (average 1.83 Å). Also, it is shorter than the average Al–O$_{(phenolate)}$ determined for other structures [AlMe$_2$Ln(BPO$_2$)(thf)$_2$] (Ln = Y, Pr, Sm, Tb) 1.83, 1.82, 1.83 and 1.83 Å respectively.
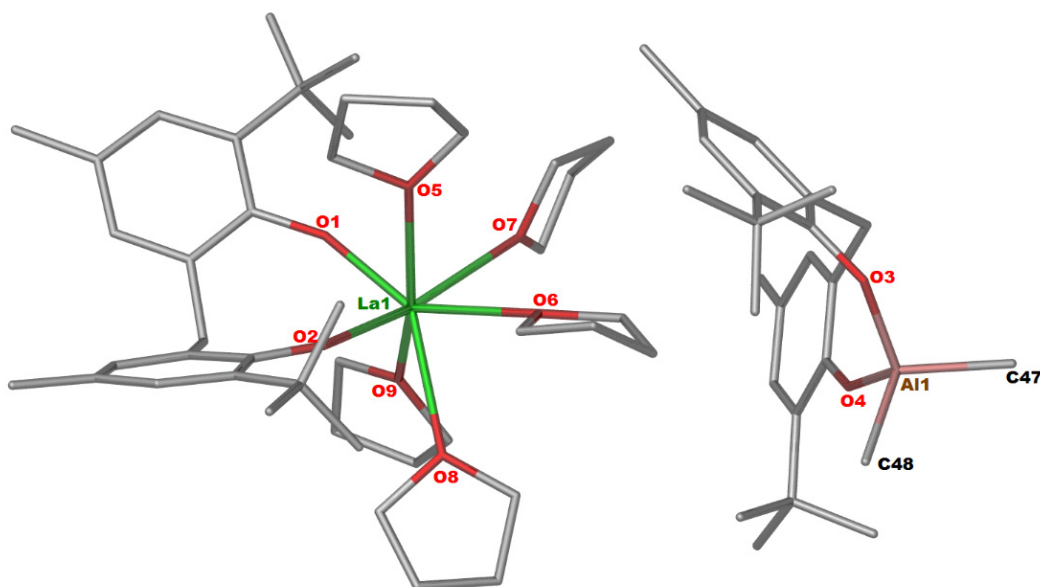
Figure 4.6 X-ray crystal structure of 4.11. Hydrogen atoms are omitted for clarity.

[(BPO$_2$)Ln(thf)$_3$(μ–F)AlMe(BPO$_2$)].thf (Ln = Sm 4.12, Tb 4.13)

X-ray crystal structure of [(BPO$_2$)Sm(thf)$_3$(μ–F)AlMe(BPO$_2$)] **4.12** is isotypic with [(BPO$_2$)Tb(thf)$_3$(μ–F)AlMe(BPO$_2$)] **4.13** (Fig. 4.11). Compounds **4.12** and **4.13** crystallise in the monoclinic space group $P2_1/c$ (Table 4.10). Figure 4.10 displays the heterobimetallic form complex bridged by a fluorine atom. The overall molecular geometry around the Ln (Ln = Sm, Tb) centres is best described as a distorted octahedral. The Ln metal centre is a six coordinate with a bidentate BPO$_2$ and three monodentate thf molecules and one bridging fluorine atom. The Al is four-coordinate with two oxygen atoms of the (BPO$_2$) ligand, one methyl group and one bridging fluorine atom coordinated and the geometry around Al metal centre is distorted tetrahedral.

Selected bond lengths and angles of **4.12** and **4.13** are listed in Table 4.9. The average Ln–O$_{(phenolate)}$ (Ln = Sm, Tb) bond lengths of [(BPO$_2$)(thf)$_3$Ln(μ–F)AlMe(BPO$_2$)] were found to be 2.13, 2.11 Å respectively, which is comparable to the average Sm–O$_{(phenolate)}$ reported for [Na(tmeda)Sm(BPO$_2$)(thf)] (tmeda = tetramethylethylenediamine)[3] and [Sm(BPO$_2$)(PO)(thf)$_2$][5](PO = 4-Me, 2,6-^{t}Bu-C$_6$H$_2$O) 2.19, 2.14 Å respectively.

165

The average Al–O$_{(phenolate)}$ bond lengths of **4.12** and **4.13** were found to be 1.72, 1.72 Å, which is slightly shorter than the Al–O$_{(phenolate)}$ of the known structure [AlMe$_2$Sm(BPO$_2$)$_2$(thf)$_2$][29] (average 1.83 Å). Also, the bond lengths Al–O$_{(phenolate)}$ of **4.12** and **4.13** are shorter than the Al–O$_{(phenolate)}$ determined for other structures [AlMe$_2$Ln(BPO$_2$)(thf)$_2$] (Ln = Y, Pr, Sm, Tb) 1.83, 1.82, 1.83 and 1.83 Å respectively. The Sm–F bond length of **4.12** was found to be 2.331(4) Å, which is larger than the Sm–F bond length 2.093(2) Å reported for [Sm(DippForm)$_2$(thf)F][49] presumably due to it being in a bridging mode rather than a terminal mode. In the literature, there is no example of fluorinated six coordinate terbium. The difference between Sm–F bond length and Tb–F bond length is 0.05 Å which is close to the difference between ionic radii 0.03 Å for six coordinate Sm^{+3} and Tb^{+3}.[48]

The Al–F bond length of **4.12** and **4.13** 1.747(4), Å 1.749(3) Å respectively is comparable to the Al–F bond length (1.7858(17) Å) reported for {Me$_2$C(Cp)(Flu)ZrMe$^+$FAl(2-C$_6$F$_5$C$_6$F$_4$)$_3$$^-$} (Flu = fluorenyl).[50]
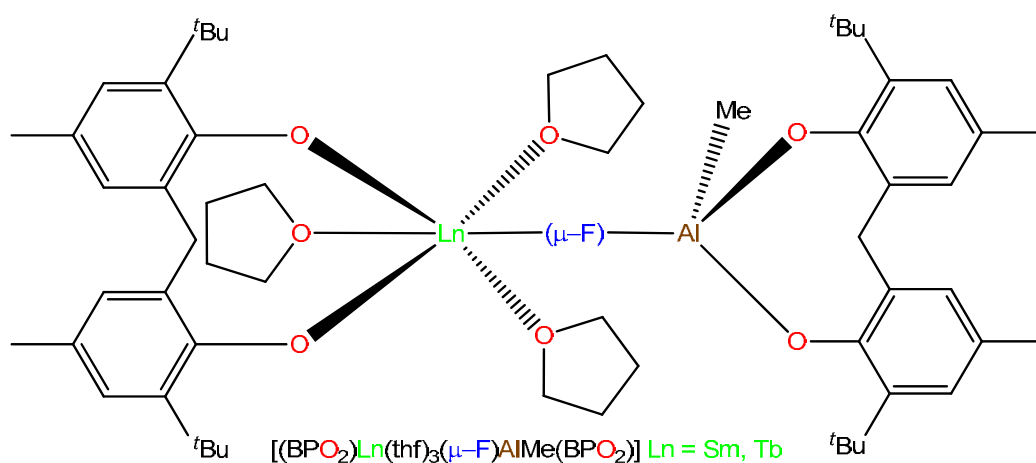
Figure 4.10 Heterobimetallic diagram of compounds 4.12 and 4.13.
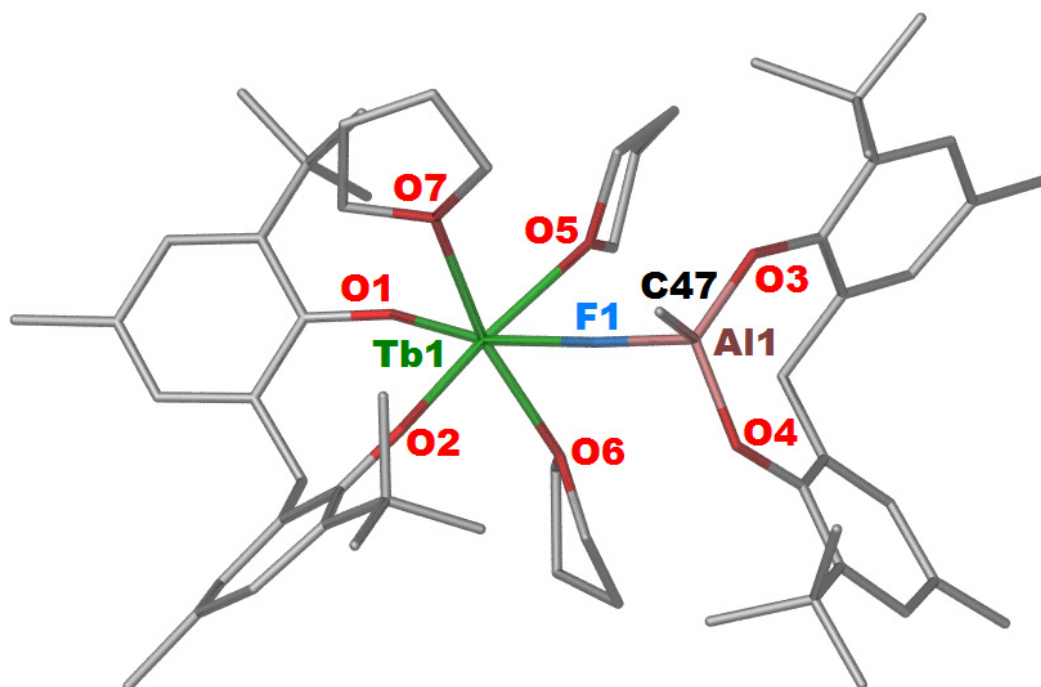
Figure 4.7 X-ray crystal structure of [(BPO₂)Tb(thf)₃(μ−F)AlMe(BPO₂)] 4.13. Hydrogen atoms are omitted for clarity.

Table 4.9 Selected bond lengths and angles of [La(BPO₂)(thf)₅][AlMe₂(BPO₂)], [(BPO₂)(thf)₃Ln(μ−F)AlMe(BPO₂)] (Ln = Sm, Tb).

Bond lengths (Å)	[La(BPO₂)(thf)₅][AlMe₂(BPO₂)]	[(BPO₂)(thf)₃Sm(μ−F)AlMe(BPO₂)]	[(BPO₂)(thf)₃Tb(μ−F)AlMe(BPO₂)]
Ln(1)–O(1)	2.228(2)	2.161(5)	2.133(3)
Ln(1)–O(2)	2.246(2)	2.113(5)	2.096(3)
Ln(1)–O(3)	2.571(2)	2.424(5)	2.338(4)
Ln(1)–O(5)	2.597(3)	2.480(4)	2.366(4)
Ln(1)–F(1)	-	2.331(4)	2.278(3)
F(1)–Al(1)	-	1.747(4)	1.749(3)
Al(1)–O(6)	1.785(3)	1.729(6)	1.728(4)
Al(1)–O(7)	1.766(3)	1.721(6)	1.725(4)
Al(1)–C(Me)	1.979(4)	-	-
Al(1)–C(Me)	1.992(4)	1.948(9)	1.938(5)
Bond angles (°)			
O(1)–Ln(1)–O(2)	92.90(8)	96.16(17)	97.26(13)
O(3)–Ln(1)–O(4)	74.68(9)	87.70(2)	88.02(13)
O(6)–Al(1)–O(7)	109.00(12)	114.40(3)	114.23(18)
F(1)–Al(1)–C(48)	-	107.90(4)	108.10(2)

Me = Methyl group

Table 4.10 Crystallographic data for compounds 4.11 and 4.13.

Compound	**4.11**	**4.12**	**4.13**
formula	$C_{72}H_{114}O_{10}LaAl$	$C_{63}H_{95}O_8FSmAl$	$C_{63}H_{95}O_8FTbAl$
fw	1305.56	1176.76	1185.33
crystal system	monoclinic	monoclinic	monoclinic
space group	*C*2/*c*	*P*2$_1$/*c*	*P*2$_1$/*c*
a, Å	17.306(4)	30.493(6)	14.585(3)
b, Å	20.132(4)	14.633(3)	27.725(6)
c, Å	39.877(8)	27.807(6)	30.613(6)
α, deg	90	90	90
β, deg	94.87(3)	90.30(3)	90.002(3)
γ, deg	90	90	90
V, Å^3	13843(5)	12407(4)	12379(4)
Z	8	8	8
T, K	173(2)	173(2)	173(2)
no. of rflns collected	88149	122736	104760
no. of indep rflns	16560	21604	27387
R_{int}	0.035	0.045	0.068
Final R_1 values ($I > 2\sigma(I)$)	0.042	0.082	0.056
Final $wR_2(F^2)$ values ($I > 2\sigma(I)$)	0.159	0.181	0.153
Final R_1 values (all data)	0.051	0.086	0.096
Final $wR_2(F^2)$ values (all data)	0.167	0.183	0.180
GooF (on F^2)	1.388	1.206	1.110

[AlMe$_2$Ln(BPO$_2$)$_2$(thf)$_2$].2C$_6$D$_6$ (Ln = Y 4.14, Pr 4.15, Sm 4.16, Tb 4.17)

Compounds **4.14-4.17** are isostructural and crystallise in the monoclinic space group *P*2$_1$/n (Table 4.12). Figure 4.12 displays the heterobimetallic complex with Al and Ln bridged by two oxygen atoms from two different biphenolate ligands. The overall molecular geometry around the six-coordinate Ln (Ln = Y, Pr, Sm, Tb) centre is distorted octahedral, which is coordinated by four oxygen atoms of the two (BPO$_2$) ligands, and two oxygen atoms of thf molecules in a *cisoid* form. Al has four coordination with two oxygen atoms of biphenolate ligand and two carbon atoms of methyl groups. The geometry around the Al metal centre is distorted tetrahedral. X-ray crystal structure of **4.16** shows it has thf molecule sitting in the lattice in addition to the two C$_6$D$_6$.

Selected Ln–O bond lengths and the O–Ln–O bond angles of **4.14-4.17** are listed in Table 4.11. The average Ln–O$_{(Phenolate)}$ (Ln = Y, Pr, Sm, Tb) bond lengths of **4.14-4.17** were found to be 2.24, 2.34 2.30, 2.34 Å respectively. The average Sm–O$_{(Phenolate)}$ bond lengths of **4.16** found to be 2.30 Å which is same as the average Sm–O$_{(Phenolate)}$ bond lengths reported for [AlMe$_2$Sm(BPO$_2$)$_2$(thf)$_2$][29] (average 2.30 Å). The difference between the average Ln–O$_{(Phenolate)}$ (Ln = Y, Tb) and reported Sm–O$_{(Phenolate)}$ bond lengths (average 2.30 Å) of [AlMe$_2$Sm(BPO$_2$)$_2$(thf)$_2$][29] is (0.06, 0.04 Å respectively) which is close to the difference between the ionic radii of Y^{+3}, Tb^{+3} (CN = 6) and Sm^{+3} (CN = 6) (0.05, 0.03 Å respectively).[48] The difference between the average Pr–O$_{(Phenolate)}$ and reported Sm–O$_{(Phenolate)}$ bond lengths (average 2.30 Å) of [AlMe$_2$Sm(BPO$_2$)$_2$(thf)$_2$][29] is (0.04 Å) which is same as the difference between the ionic radii of Pr^{+3}, (CN = 6) and Sm^{+3} (CN = 6) (0.04 Å).[48]

The average Al–O$_{(Phenolate)}$ bond lengths of **4.14-4.17** were found to be 1.83, 1.82, 1.83 and 1.83 Å respectively, which are similar to the Al−O$_{(Phenolate)}$ of the known structure [AlMe$_2$Sm(BPO$_2$)$_2$(thf)$_2$][29] (average 1.83 Å).

[AlMe₂Ln(BPO₂)₂(thf)₂] Ln = Y, Pr, Sm, Tb
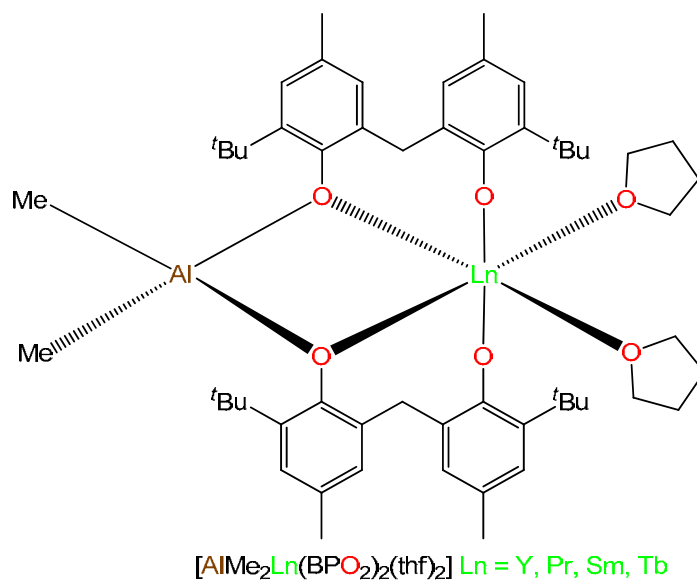
Figure 4.8 Heterobimetallic diagram of compounds 4.14-4.17.
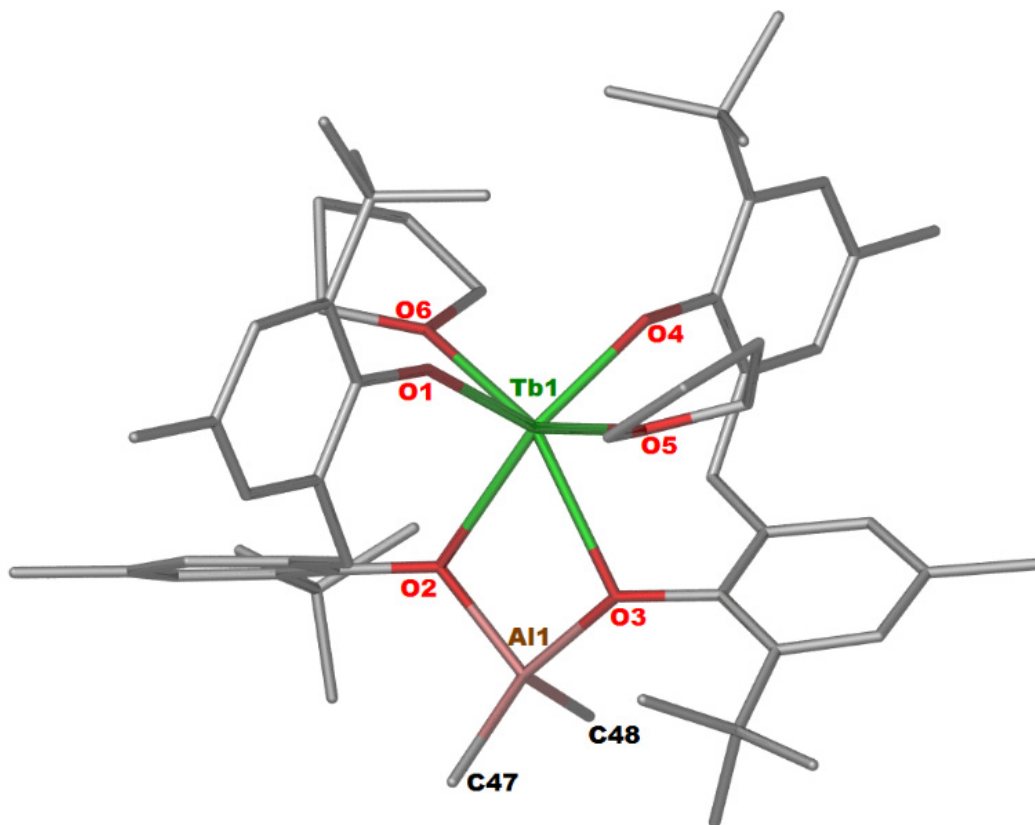
Figure 4.9 X-ray crystal structure of 4.17. Hydrogen atoms are omitted for clarity.

Table 4.11 Selected bond lengths and angles of 4.14-4.17.

Bond lengths (Å)	[AlMe$_2$Y(BPO$_2$)$_2$(thf)$_2$]	[AlMe$_2$Pr(BPO$_2$)$_2$(thf)$_2$]	[AlMe$_2$Sm(BPO$_2$)$_2$(thf)$_2$]	[AlMe$_2$Tb(BPO$_2$)$_2$(thf)$_2$]
Ln(1)–O(1)	2.093(3)	2.170(3)	2.163(3)	2.159(5)
Ln(1)–O(2)	2.375(3)	2.497(3)	2.448(3)	2.493(5)
Ln(1)–O(3)	2.388(3)	2.509(3)	2.145(3)	2.517(5)
Ln(1)–O(4)	2.110(3)	2.201(4)	2.447(3)	2.195(5)
Ln(1)–O(5)	2.399(4)	2.540(4)	2.476(3)	2.519(6)
Ln(1)–O(6)	2.409(4)	2.526(4)	-	2.539(6)
Al(1)–O(2)	1.834(4)	1.831(4)	1.828(3)	1.841(6)
Al(1)–O(3)	1.828(4)	1.818(4)	1.834(3)	1.835(6)
Al(1)–C(Me)	1.970(6)	1.974(7)	1.969(5)	1.977(9)
Al(1)–C(Me)	1.979(6)	1.984(7)	1.971(5)	1.984(9)
Bond angles (°)				
O(1)–Ln(1)–O(2)	101.76(13)	101.73(13)	105.95(9)	101.91(18)
O(3)–Ln(1)–O(4)	104.15(13)	105.33(12)	102.49(10)	105.74(17)
O(2)–Ln(1)–O(3)	63.67(12)	61.04(12)	62.44(10)	60.98(16)
O(6)–Ln(1)–O(5)	148.71(14)	148.36(16)	-	148.60(2)
O(3)–Al(1)–O(2)	86.66(17)	88.32(18)	87.70(14)	87.50(3)

Me = Methyl group

Table 4.12 Crystallographic data for compounds 4.14-4.17.

Compound	**4.14**	**4.15**	**4.16**	**4.17**
formula	$C_{68}H_{94}O_6YAl$	$C_{68}H_{94}O_6PrAl$	$C_{72}H_{102}O_7SmAl$	$C_{68}H_{94}O_6TbAl$
fw	1123.36	1175.36	1256.92	1193.38
crystal system	monoclinic	monoclinic	monoclinic	monoclinic
space group	$P2_1/n$	$P2_1/n$	$P2_1/n$	$P2_1/n$
a, Å	9.845(2)	10.009(10)	9.860(2)	10.004(10)
b, Å	19.536(4)	19.875(2)	19.597(4)	19.930(2)
c, Å	32.429(7)	32.781(3)	32.532(7)	32.763(3)
α, deg	90	90	90	90
β, deg	94.32(3)	94.66(4)	94.70(3)	94.62(6)
γ, deg	90	90	90	90
V, Å^3	6219(2)	6500(11)	6265(2)	6511(11)
Z	4	4	4	4
T, K	173(2)	298(2)	173(2)	298(2)
no. of rflns collected	76823	54481	47064	81485
no. of indep rflns	10557	11384	10455	14924
R_{int}	0.074	0.084	0.046	0.281
Final R_1 values ($I > 2\sigma(I)$)	0.098	0.066	0.052	0.080
Final $wR_2(F^2)$ values ($I > 2\sigma(I)$)	0.259	0.169	0.145	0.185
Final R_1 values (all data)	0.111	0.087	0.053	0.248
Final $wR_2(F^2)$ values (all data)	0.275	0.189	0.146	0.258
$GooF$ (on F^2)	1.065	1.108	1.085	0.941

[Al$_2$(BPO$_2$)$_3$(thf)$_2$].thf (4.18)

[Al$_2$(BPO$_2$)$_3$(thf)$_2$] crystallises in the triclinic space group *P*-1 (Table 4.16). Figure 4.14 exhibits a dinuclear structure bridged by a biphenolate ligand. The overall molecular geometry around the four-coordinate Al(1) and Al(2) metal centres is best described as a distorted tetrahedral. Each metal centre of Al(1) and Al(2) is coordinated by two oxygen atoms of the (BPO$_2$) ligand as bidentate, and one oxygen atom of thf molecule in addition to one oxygen atom of the bridging (BPO$_2$) ligand. Complex **4.18** incorporates several unusual features. In particular, the bridging (BPO$_2$) ligand which clearly showed the flexibility of Ar−*CH$_2$*−Ar unit by twisting the (BPO$_2$) ligand to accommodate two Al centres in a K^1, K^1 mode.

Selected Al–O bond lengths and O−Al–O bond angles of [Al$_2$(BPO$_2$)$_3$(thf)$_2$] are listed in Table 4.13. The average Al–O$_{(phenolate)}$ bond lengths of **4.18** were found to be 1.70 Å, which is slightly shorter than the average Al–O$_{(phenolate)}$ bond lengths (average 1.73 Å) reported for [AlMe(BPO$_2$)(thf)][15] and [AlMe(BPO$_2$)]$_2$[35] Table 4.13. Also, it is slightly shorter than the average Al–O$_{(phenolate)}$ bond lengths calculated for [AlMe(BPO$_2$)(thf)] (average 1.72 Å). As expected, the average Al–O$_{(thf)}$ bond lengths of [Al$_2$(BPO$_2$)$_3$(thf)$_2$] is 0.14 Å longer than the average Al–O$_{(phenolate)}$ bond lengths. The bond angle Ar−*CH$_2$*−Ar of the twisted (BPO$_2$) ligand 114.8(5)° which is close to the bond angles Ar−*CH$_2$*−Ar of the terminal ligands 113.1(5)°, 114.8(6)°.
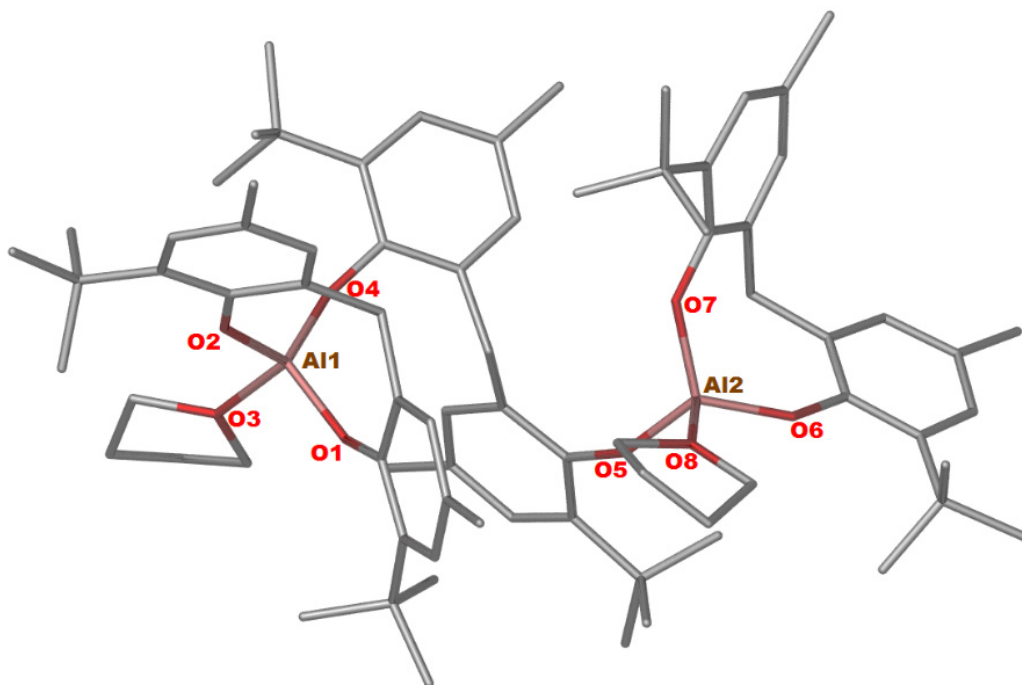
Figure 4.10 X-ray crystal structure of 4.18. Hydrogen atoms are omitted for clarity.

[AlMe(BPO$_2$)(thf)].C$_6$D$_6$ (4.19)

Compound [AlMe(BPO$_2$)(thf)] crystallises in the monoclinic space group *P*2$_1$/c (Table 4.16). Figure 4.15 shows this compound crystallises as a mononuclear structure. The Al metal centre has four-coordination, which is coordinated by two oxygen atoms of the (BPO$_2$) ligand as a bidentate, and one oxygen atom of thf molecule in addition to one carbon atom of the methyl group. The overall molecular geometry around the Al metal centre is best described as a distorted tetrahedral. Complex **4.19** is isotypic with [Al(BPO$_2$)Br(Et$_2$O)][36], [AlMe(BPO$_2$)(thf)][15] (BP(OH)$_2$ = 2, 2′-methylene-bis(4-chloro-6-isopropyl-3-methylphenol) (Fig. 4.16).

Selected bond lengths Al–O of [AlMe(BPO$_2$)(thf)] are listed in Table 4.13. The average Al–O bond lengths of **4.19** were found to be 1.72 Å, which is in agreement with the average Al–O bond lengths reported for [AlMe(BPO$_2$)(thf)][15] (BP(OH)$_2$ = 2, 2′-

methylene-bis(4-chloro-6-isopropyl-3-methylphenol) and [AlMe(BPO$_2$)]$_2$[36] (Fig. 4.18)

(average 1.73 Å) (Table 4.13) and they are slightly longer than the Al–O bond lengths for

[Al$_2$(BPO$_2$)$_3$(thf)$_2$]. Figure 4.18 shows some known aluminium biphenolate structures.
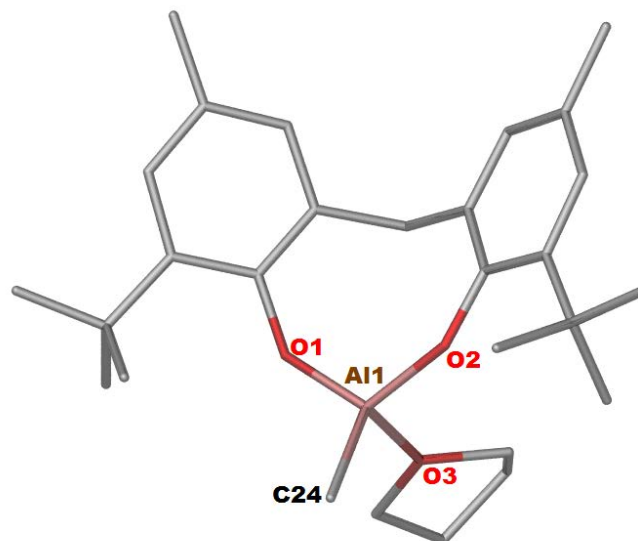
Figure 4.11 X-ray crystal structure of 4.19. Hydrogen atoms are omitted for clarity.
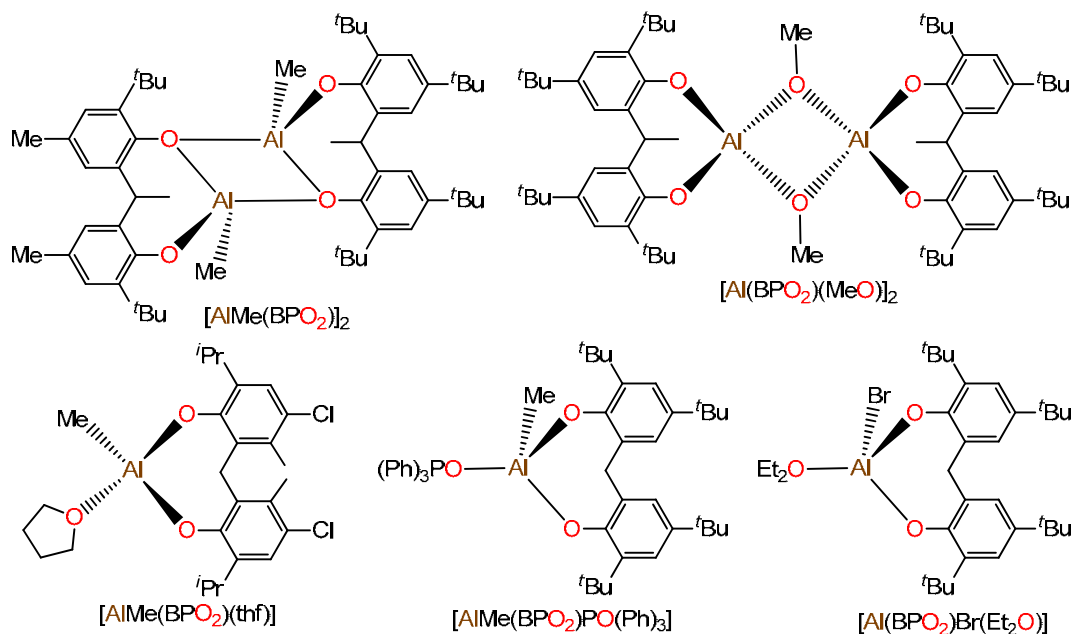
Figure 4.12 Known aluminium biphenolate structures of [AlMe(BPO$_2$)(thf)][15], [AlMe(BPO$_2$)PO(Ph$_3$)][37], [Al(BPO$_2$)Br(Et$_2$O)][36], [AlMe(BPO$_2$)]$_2$[35] and [Al(BPO$_2$)(MeO)]$_2$[38].

Table 4.13 Selected bond lengths and angles of [Al₂(BPO₂)₃(thf)₂], [AlMe(BPO₂)(thf)], [AlMe(BPO₂)(thf)][15] (BP(OH)₂ = 2,2′-methylene-bis(4-chloro-6-isopropyl-3-methylphenol) and [Al(BPO₂)Cl]₂[36] (BP(OH)₂ = 2,2′-methylene-bis-(4,6-di-*tert*-butylphenol).

Bond lengths (Å)	[Al₂(BPO₂)₃(thf)₂]	[Al(Me)(BPO₂)(thf)]	[AlMe(BPO₂)(thf)][15]	[Al(BPO₂)Cl]₂[35]
Al(1)–O(1)	1.714(4)	1.734(14)	1.728(3)	1.826(4)
Al(1)–O(2)	1.712(4)	1.718(14)	1.738(2)	1.637(4)
Al(1)–O(3)	1.846(5)	1.866(15)	1.885(3)	-
Al(1)–C(24)	-	1.940(2)	1.940(4)	-
Al(1)–O(4)	1.684(5)	-	-	-
Al(2)–O(5)	1.701(5)	-	-	-
Al(2)–O(6)	1.698(5)	-	-	-
Al(2)–O(7)	1.722(5)	-	-	-
Al(2)–O(8)	1.844(5)	-	-	-
Bond angles (°)				
O(1)–Al(1)–O(2)	114.10(2)	116.47(7)	108.11(12)	113.10(2)
O(1)–Al(1)–O(3)	-	101.44(7)	100.96(12)	-
O(2)–Al(1)–C(24)	-	113.95(8)	118.36(17)	-
O(3)–Al(1)–O(4)	101.30(2)	-	-	-
O(1)–Al(1)–O(4)	116.60(2)	-	-	-
O(2)–Al(1)–O(4)	118.30(2)	-	-	-
O(6)–Al(2)–O(7)	113.70(3)	-	-	-
O(5)–Al(2)–O(8)	98.70(3)	-	-	-
O(5)–Al(2)–O(6)	118.90(3)	-	-	-
O(5)−Al(2)−O(7)	117.00(3)	-	-	-

[Li₄(BPO₂)₂(thf)₄].thf (4.20)

Compound [Li₄(BPO₂)₂(thf)₄] crystallises in the trigonal space group $P3_1$ (Table 4.16).

Figure 4.17 exhibits a tetranuclear form bridged by four oxygen atoms of two biphenolate

ligands and four Li–C interactions to form a cage structure. The overall molecular

geometry around the terminal metals Li(1) and Li(4) is best described as distorted trigonal

planar. However, the overall molecular geometry around the interior metals Li(2) and

Li(3) is best described as a distorted tetrahedral. Each metal centre Li(1) and Li(4) are

three-coordinate, bound by two oxygen atoms of the (BPO₂) ligands and one oxygen atom

of thf molecule. Each metal centre Li(2) and Li(3) are four-coordinate, bound by three

oxygen atoms of the (BPO₂) ligands and one oxygen atom of thf molecule. Li(1) and Li(3)

have Li–C interactions with the same phenyl group, while Li(2) and Li(4) have Li–C

interactions with different phenyl group. The most interesting feature of this structure is

the diverse range of intramolecular interactions, such as, Li–C and Li–O.

Selected bond lengths Li–O, Li–C and the bond angles O–Li–O of [Li₄(BPO₂)₂(thf)₄] are

listed in Table 4.14. The average Li–O(phenolate) bond lengths of **4.20** were found to be 1.93

Å, which is in a agreement with the average Li–O bond lengths reported for

[Li₅(BPO₂)₂(BuO)(thf)₃] (1.94 Å).[39]

The bond lengths Li–C {Li(1), Li(4)} of **4.20** were found to be 2.476(12), 2.676(13) Å

respectively which are larger than the Li–C (2.45 Å, 2.53 Å) reported for

[Li₃(BPO₂)(BenO)]₂ (BenOH = Benzyl alcohol)[40] and [Li₃(TPO₃)(thf)₄] (TPOH = tris-

(3,5-t-butyl-2-hydroxyphenyl)methane)[41] respectively. The bond lengths Li–C {Li(2),

Li(3)} of **4.20** were found to be 2.743(12), 2.476(13) Å which are comparable to the Li–

C (2.79 Å, 2.66 Å) reported for [LiFe(Cp)L]₂ (L =

(C₅H₄CHCCH₃)N(CH₃CHCH₂OMe))[42] and [(H₂C=C(t-Bu)NPh)Li(OEt₂)]₂[41]

respectively. Figure 4.18 shows some known lithium biphenolate complexes.

178
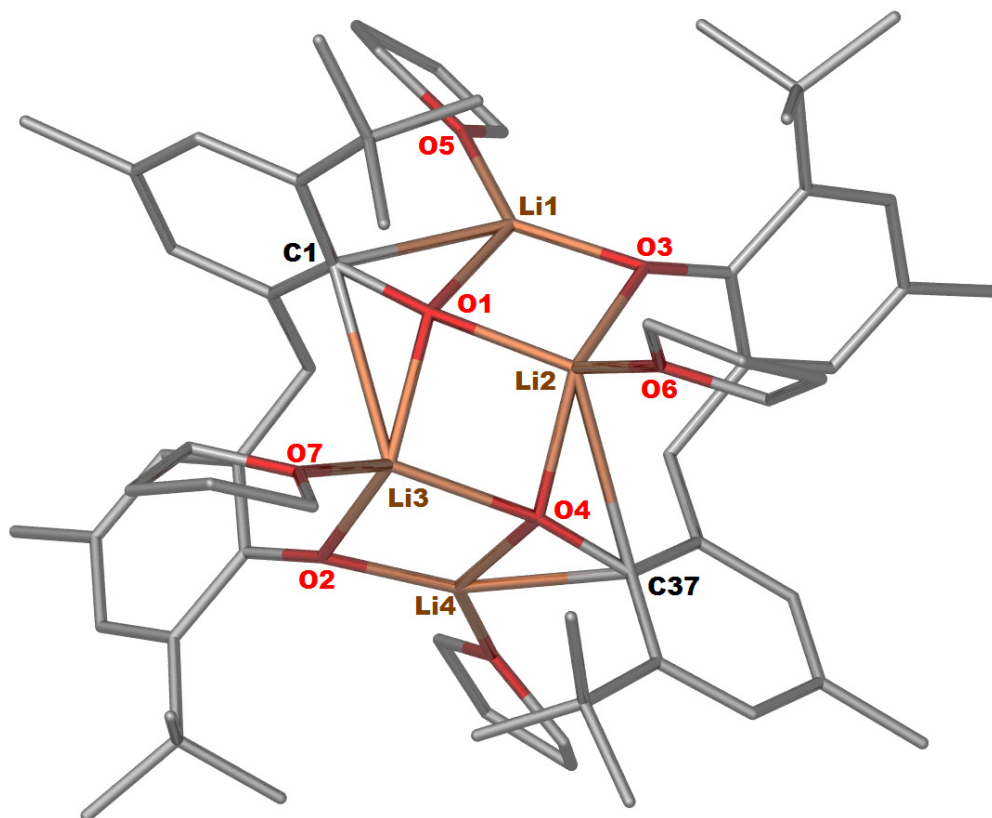
Figure 4.15 X-ray crystal structure of 4.20. Hydrogen atoms are omitted for clarity.

Table 4.14 Selected bond lengths and angles of [Li$_4$(BPO$_2$)$_2$(thf)$_4$].

Bond lengths (Å)	[Li$_4$(BPO$_2$)$_2$(thf)$_4$]	Bond lengths (Å)	[Li$_4$(BPO$_2$)$_2$(thf)$_4$]
Li(1)–O(1)	1.891(12)	Li(3)–O(4)	1.998(12)
Li(1)–O(3)	1.829(12)	Li(4)–O(2)	1.809(13)
Li(1)–O(5)	1.904(12)	Li(4)–O(4)	1.948(12)
Li(2)–O(3)	1.902(11)	Li(4)–O(8)	1.872(13)
Li(2)–O(4)	2.017(11)	Li(1)–C(1)	2.476(12)
Li(2)–O(6)	2.018(11)	Li(2)–C(37)	2.743(12)
Li(3)–O(1)	1.994(11)	Li(3)–C(1)	2.676(13)
Li(3)–O(2)	1.921(11)	Li(4)–C(37)	2.476(13)
Bond angles (°)			
O(1)–Li(1)–O(3)	100.80(6)	O(4)–Li(2)–O(6)	108.80(5)
Li(2)–Li(1)–O(5)	165.30(7)	Li(2)–C(37)-Li(4)	91.80(4)
Li(1)–C(1)–Li(3)	87.00(4)	O(2)–Li(3)–O(4)	95.30(5)
O(3)–Li(2)–O(4)	126.20(6)	O(4)–Li(3)–O(7)	128.70(6)
O(6)–Li(2)–O(1)	132.90(6)	Li(4)–Li(3)–C(1)	128.80(5)
O(3)–Li(2)–O(6)	104.20(5)		
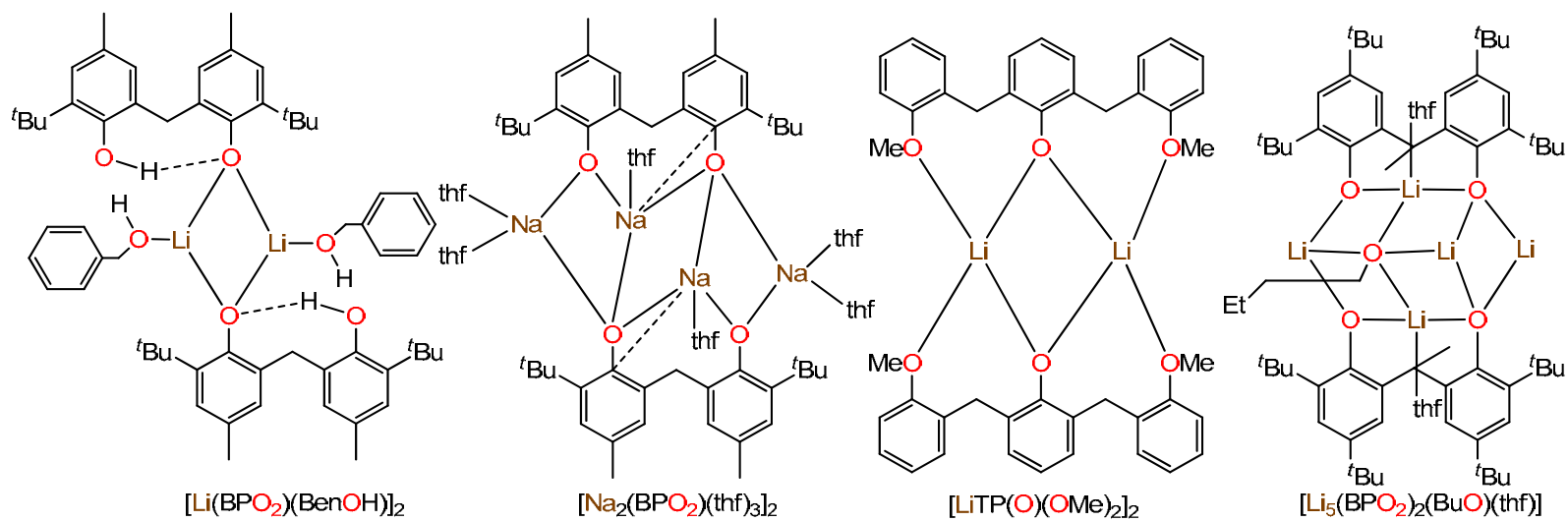
Figure 4.13 Known lithium biphenolate complexes [Na₂(BPO₂)(thf)₃]₂[43], [Li(BPO)(OH)(BenOH)]₂[44] (BenOH = Benzyl alcohol), [Li₅(BPO₂)₂(BuO)(thf)₃][39] and [LiTP(O)(OMe)₂}]₂[45].

[ZnEtYb(BPO$_2$)$_2$(thf)].2C$_6$D$_6$ (4.21)

Compound [ZnEtYb(BPO$_2$)$_2$(thf)] (Fig. 4.19) crystallises in the monoclinic space group *C*c (Table 4.16). The compound crystallises in a heterobimetallic form with Zn and Yb bridged by two oxygen atoms of two biphenolate ligands. The overall molecular geometry around the five coordinate Yb metal centre is best described as a distorted trigonal bipyramid and is coordinated by four oxygen atoms of the two (BPO$_2$) ligands and one oxygen atom of a thf molecule. Two oxygen atoms O(2) and O(5) occupy axial positions O(2)–Yb–O(5) 130.4(7)° with three other oxygen atoms O(1), O(3), O(4), are arranged in equatorial positions (Fig. 4.19). Zn has three coordination with two oxygen atoms of the biphenolate ligand and one ethyl group and the geometry around Zn is best described as distorted trigonal planar.

In the literature there are no reported examples of a heterobimetallic complex that contains both a lanthanoid and zinc. There is an example of a biphenolate ytterbium complex [Li(thf)$_2$Yb(BPO$_2$)$_2$(thf)][27] that contains Yb and has the same coordination number as Yb in [ZnEtYb(BPO$_2$)$_2$(thf)].

Selected bond lengths Yb–O$_{(phenolate)}$, Zn–O$_{(phenolate)}$ and the bond angles O–Yb–O, O–Zn–O of **4.21** are listed in Table 4.15. The average Yb–O$_{(phenolate)}$ bond lengths of [ZnEtYb(BPO$_2$)$_2$(thf)] were found to be 2.14 Å, which is slightly larger than the Yb–O$_{(phenolate)}$ average 2.12 Å obtained for [Li(thf)$_2$Yb(BPO$_2$)$_2$(thf)]. The average Zn–O$_{(phenolate)}$ bond lengths of [ZnEtYb(BPO$_2$)$_2$(thf)] were found to be 1.96 Å, which is in agreement the average Zn–O$_{(phenolate)}$ 1.97 Å reported for [EtZn(μ-OAr)]$_2$ (Ar = 2,6-(*t*-Bu)$_2$-4-Me-C$_6$H$_2$O).[46] The Zn–C bond length of [ZnEtYb(BPO$_2$)$_2$(thf)] was found to be 1.99(4) Å, which is larger than the Zn–C bond length 1.95(2) Å reported for [EtZn(μ-OAr)]$_2$ (Ar = 2,6-(*t*-Bu)$_2$-4-Me-C$_6$H$_2$O).[46]

Table 4.15 Selected bond lengths and angles of [ZnEtYb(BPO₂)₂(thf)].

Bond lengths (Å)	[ZnEtYb(BPO₂)₂(thf)]
Yb(1)–O(1)	2.053(4)
Yb(1)–O(2)	2.271(4)
Yb(1)–O(3)	2.207(4)
Yb(1)–O(4)	2.059(4)
Yb(1)–O(5)	2.285(4)
Zn(1)–O(2)	1.946(4)
Zn (1)–O(3)	1.977(4)
Zn (1)–C(100)	1.990(4)
Bond angles (°)	
O(1)–Yb(1)–O(2)	111.17(15)
O(3)–Yb(1)–O(4)	90.74(15)
O(1)–Yb(1)–O(4)	109.17(15)
O(3)–Yb(1)–O(5)	147.19(15)
O(3)–Zn(1)–O(2)	82.12(16)
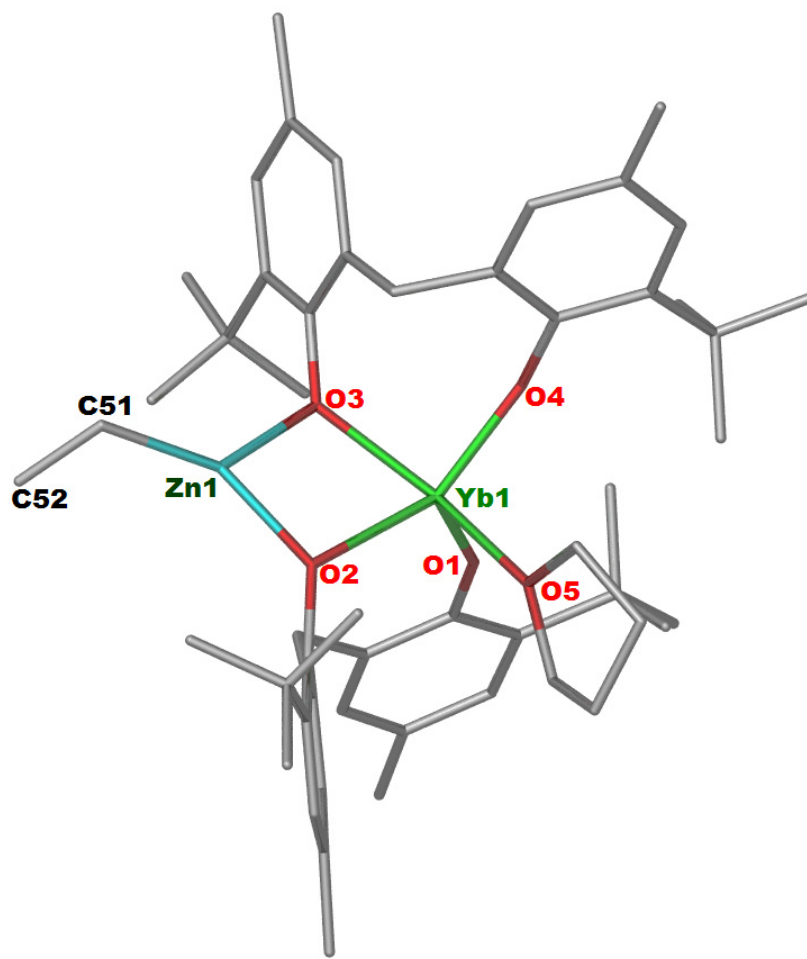
Figure 4.14 X-ray crystal structure of 4.21. Hydrogen atoms are omitted for clarity.

Table 4.16 Crystallographic data for compounds 4.18-4.21.

Compound	**4.18**	**4.19**	**4.20**	**4.21**
formula	$C_{81}H_{114}O_9Al_2$	$C_{34}H_{47}O_3Al$	$C_{66}H_{100}O_9Li_4$	$C_{64}H_{85}O_5YbZn$
fw	1285.73	530.72	1065.26	1172.79
crystal system	triclinic	monoclinic	trigonal	monoclinic
space group	P-1	$P2_1/c$	$P3_1$	Cc
a, Å	14.507(3)	25.068(5)	13.880(18)	22.938(5)
b, Å	17.952(4)	15.323(3)	13.880(18)	13.595(3)
c, Å	33.213(7)	16.825(3)	29.483(5)	19.431(4)
α, deg	104.99(3)	90	90	90
β, deg	90.25(3)	106.78(3)	90	106.54(3)
γ, deg	113.80(3)	90	120	90
V, Å^3	7587(3)	6188(2)	4919(16)	5809(2)
Z	4	8	3	4
T, K	173(2)	173(2)	298(2)	173(2)
no. of rflns collected	64058	90053	53607	31504
no. of indep rflns	22017	14713	14241	9449
R_{int}	0.076	0.043	0.135	0.047
Final R_1 values ($I > 2\sigma(I)$)	0.108	0.054	0.069	0.028
Final $wR_2(F^2)$ values ($I > 2\sigma(I)$)	0.307	0.138	0.149	0.070
Final R_1 values (all data)	0.159	0.068	0.221	0.028
Final $wR_2(F^2)$ values (all data)	0.353	0.155	0.207	0.070
$GooF$ (on F^2)	1.066	0.721	0.950	1.089

4.4 Conclusions

The reactivity of biphenolate lanthanoid complexes $[Ln(BPO_2)(BP(OH)O)(thf)_n]$ (n = 1, 2, 3) were determined with ^nBuLi and led to the isolation anionic $[Li(thf)_4][Ln(BPO_2)_2(thf)_2]$ (Ln = Y, Sm, Dy, Ho) and non-ionic $[Li(thf)_2Ln(BPO_2)_2(thf)_n]$ (Ln = La, Pr, Er, Yb, Lu; n = 1, 2) structures. Only the non-ionic structure $[K(thf)_3Gd(BPO_2)_2(thf)_2]$ was isolated with potassium (a larger alkali metal) in place of lithium. Using trimethyl aluminium as the metallating agent also gave two forms of structures as anionic $[Ln(BPO_2)(thf)_5][AlMe_2(BPO_2)]$ (Ln = La **4.11**) and non-ionic $[AlMe_2Ln(BPO_2)_2(thf)_2]$ (Ln = Y, Pr, Sm, Tb). Unexpected products $[(BPO_2)(thf)_3Ln(\mu-F)AlMe(BPO_2)]$ (Ln = Sm, Tb) were isolated from an attempt to synthesise $[AlMe_2Ln(BPO_2)_2(thf)_2]$ (Ln = Sm, Tb) and they are the only halogenated heterobimetallic complexes were isolated in this study. However, employing a transition metal $(ZnEt_2)$ as the metallating agent gave a non-ionic structure $[ZnEtYb(BPO_2)_2(thf)]$. The common feature of these ionic and non-ionic complexes is the lanthanoid coordination number. Lanthanoid metals involved in these structures have the same coordination number six-coordinate, except for lanthanum in $[La(BPO_2)(thf)_5][AlMe_2(BPO_2)]$, which has seven-coordinate. There was a five coordinate as well of $[Li(thf)_2Ln(BPO_2)_2(thf)]$ Ln (Ln = Er, Yb, Lu).

In conclusion, this study performed different directions of reactivity with biphenolate lanthanoid complexes $[Ln(BPO_2)(BP(OH)O)(thf)_n]$ (n = 1, 2, 3), which were initially prepared through a redox transmetallation reaction and were described in chapter three. Metallating biphenolate lanthanoid complexes $[Ln(BPO_2)(BP(OH)O)(thf)_n]$ (n = 1, 2, 3) with different metal alkyls/amides such as $(^nBuLi, KN(SiMe_3)_2, AlMe_3, ZnEt_2)$ can be used as a convenient method to synthesise heterobimetallic complexes, and provides a basis for future developments in a range of phenolic macrocyclic ligands.

[ZnEtYb(BPO$_2$)$_2$(thf)] **4.21** is the first type of heterobimetallic complex containing ytterbium and zinc. Also complex [(BPO$_2$)(thf)$_3$Ln(μ–F)AlMe(BPO$_2$)] (Ln = Sm, Tb) is the first type of heterobimetallic complexes containing a lanthanoid and aluminium bridged by a fluorine atom.

4.5 Experimental

Potassium bis(trimethylsilyl)amide, *n*-butyllithium, trimethyl aluminium, diethyl zinc and 2,2′-methylene-bis(6-*tert*-butyl-4-methylphenol) were purchased from Sigma Aldrich and used as received. $Hg(C_6F_5)_2$ was prepared by the literature method.[47] Further details regarding general considerations were described in Chapter two (experiment section 2.5). and Chapter three (experiment section 3.5).

$[Li(thf)_4][Ln(BPO_2)_2(thf)_2].thf$ (Ln = Y 4.1, Sm 4.2, Dy 4.3 and Ho 4.4)

Ln metal filings (Ln 2.00 mmol = Y 0.17 g, Sm 0.30 g, Dy 0.32 g, Ho 0.32 g), $BP(OH)_2$ (1.36 g; 4.00 mmol), $Hg(C_6F_5)_2$ (1.60 g; 3.00 mmol), and one drop of Hg were added to a Schlenk flask with dry thf (~20 ml), and stirred for two days. The resulting solution (yellow coloured for all Ln = Y, Sm, Dy, Ho) was filtered and (1.60 M, 1.00 mmol, 0.62 ml) ^{n}BuLi was added and stirred for one day. Crystallisation was achieved by concentrating the yellow solution under vacuum to (~5 ml). Small colourless crystals of **4.1-4.4** (0.70 g, 51 %; 0.54 g, 39 %; 0.65 g, 47 %; 0.63 g, 46 % respectively) grew upon standing overnight.

4.1: m. p. 132-134 °C. Elemental analysis calcd for $C_{74}H_{116}O_{11}YLi$ (1277.55 g.mol^{-1}): C 69.57, H 9.15, Y 6.96. Calcd for $C_{62}H_{92}O_8YLi$ (1061.24 g.mol^{-1} after lost of three solvation thf): C 70.17, H 8.74, Y 8.38. Found: C 69.83, H 8.11, Y 8.05. ^{1}H-NMR (400 MHz, C_6D_6, 25°C): δ = 7.03 (br, 8H, ArH), 4.02 (br, 4H, CH_2), 3.38 (br, 16H, OCH_2, thf), 2.18 (s, 12H, CH_3), 1.50 (s, 36H, $C(CH_3)_3$), 1.27 (br, 16H, CH_2, thf) ppm. IR (Nujol, cm^{-1}): 2370 w, 2275 w, 2049 w, 1883 w, 1741 s, 1605 s, 1381 s, 1254 s, 1204 m, 1172 m, 1139 m, 1025 s, 955 w, 865 s, 788 s, 722 m, 677 m.

4.2: m. p. 175-177 °C. Elemental analysis calcd for $C_{74}H_{116}O_{11}SmLi$ (1339.01 g.mol^{-1}): C 66.38, H 8.73, Sm 11.23. Calcd for $C_{70}H_{108}O_{10}SmLi$ (1266.90 g.mol^{-1} after lost of one thf

from lattice): C 66.36, H 8.59, Sm 11.87. Found: C 66.12, H 7.95, Sm 11.43. ^{1}H-NMR (400 MHz, C_6D_6, 25°C): δ = 5.42 (br, 8H, ArH), 4.68 (d, 2H, CH_2), 4.13 (d, 2H, CH_2), 1.42 (br, 24H, OCH_2, thf), 0.82 (s, 12H, CH_3), -0.73 (br, 24H, CH_2, thf), -1.43 (s, 36H, C(CH_3)$_3$) ppm. IR (Nujol, cm^{-1}): 2721 m, 2475 w, 2373 m, 2271 m, 2059 m, 1891 s, 1740 s, 1601 s, 1556 s, 1258 w, 1070 w, 874 w, 722 m, 673 s, 583 s.

4.3: m. p. 200-202 °C. Elemental analysis calcd for $C_{74}H_{116}O_{11}DyLi$ (1351.15 g.mol^{-1}): C 65.78, H 8.65, Dy 12.03. Calcd for $C_{70}H_{108}O_{10}DyLi$ (1279.04 g.mol^{-1} after lost of one thf from lattice): C 65.73, H 8.51, Dy 12.70. Found: C 65.08, H 7.95, Dy 12.19. IR (Nujol, cm^{-1}): 2484 w, 2373 w, 2279 w, 2063 m, 1891 m, 1728 s, 1601 s, 1376 s, 1262 s, 1204 w, 1139 m, 1025 s, 914 m, 861 s, 788 m, 677 m.

4.4: m. p. 182-184 °C. Elemental analysis calcd for $C_{74}H_{116}O_{11}HoLi$ (1353.58 g.mol^{-1}): C 65.66, H 8.64, Ho 12.18. Calcd for $C_{54}H_{76}O_6HoLi$ (993.05 g.mol^{-1} after lost four solvation thf and one thf in the lattice): C 65.31, H 7.71, Ho 16.61. Found: C 64.87, H 7.44, Ho 16.15. ^{1}H-NMR (400 MHz, C_6D_6, 25°C): δ = 7.00 (m, 8H, ArH), 5.74 (d, 2H, CH_2), 3.76 (d, 2H, CH_2), 2.09 (s, 12H, CH_3), 1.85 (br, 8H, OCH_2, thf), 1.40 (s, 36H, C(CH$_3$)$_3$), 0.29 (br, 8H, CH_2, thf) ppm. IR (Nujol, cm^{-1}): 2725 m, 2586 w, 2365 w, 2275 m, 1907 m, 1732 s, 1601 s, 1556 m, 1204 w, 1143 w, 1074 m, 1029 s, 861 m, 792 m, 722 m, 673 s, 587 s.

[Li(thf)$_2$Ln(BPO$_2$)$_2$(thf)$_2$] (Ln = La 4.5, Pr 4.6)

The synthesis of complexes **4.5** and **4.6** were carried out in an identical manner to that described for complex **4.1-4.4**. Crystallisation was achieved by concentrated the resulting solution under vacuum to (~5 ml). Small colourless crystals of **4.5** and **4.6** (0.34 g, 25 %, 0.43 g, 31 % respectively) grew upon standing overnight.

4.5: m. p. 228-230 °C. Elemental analysis calcd for $C_{62}H_{92}O_8LaLi$ (1111.24 g.mol^{-1}): C 67.01, H 8.34, La 12.50. Found: C 66.71, H 8.02, La 12.30. ^{1}H-NMR (400 MHz, C_6D_6,

25°C): δ = 6.82 (br, 8H, ArH), 4.70 (d, 2H, CH$_2$), 3.32 (d, 2H, CH$_2$), 2.97 (br, 16H, OCH$_2$, thf), 1.99 (s, 12H, CH$_3$), 1.26 (s, 36H, C(CH$_3$)$_3$), 0.78 (br, 16H, CH$_2$, thf) ppm. IR (Nujol, cm^{-1}): 2667 w, 2390 w, 2110 w, 1744 m, 1605 m, 11462 s, 1372 s, 1258 s, 1200 w, 1025 s, 914 m, 861 m, 808 s, 784 m, 730 s.

4.6: m. p. 168-170 °C. Elemental analysis calcd for C$_{62}$H$_{92}$O$_8$PrLi (1113.24 g.mol^{-1}): C 66.89, H 8.33, Pr 12.66. Found: C 66.17, H 7.69, Pr 12.27. IR (Nujol, cm^{-1}): 2377 w, 2271 w, 2050 m, 1891 m, 1744 s, 1568 s, 1225 s, 918 s, 861 s, 812 m, 722 m, 669 s.

[Li(thf)$_2$Ln(BPO$_2$)$_2$(thf)].sol (Ln = Er 4.7 sol = 2C$_6$D$_6$, Yb 4.8 sol = hexane, Lu 4.9 sol = 3C$_6$D$_6$)

The synthesis of complexes **4.7-4.9** were carried out similarly to that described for complexes **4.1-4.4**. Crystallisation was achieved by concentrated the resulting solutions under vacuum to (~5 ml). Small colourless crystals of **4.7** and **4.9** (0.53 g, 38 %; 0.54 g, 39 % respectively) grew upon standing overnight after recrystallised from C$_6$D$_6$, while large colourless crystals of **4.8** (0.34 g, 25 %) grew upon standing two days after recrystallised from hexane.

4.7: m. p. 170-172 °C. Elemental analysis calcd for C$_{70}$H$_{96}$O$_7$ErLi (1223.71 g.mol^{-1}): C 68.71, H 7.91, Er 13.67. Calcd for C$_{50}$H$_{68}$O$_5$ErLi (923.27 g.mol^{-1} after lost two solvation thf and two C$_6$D$_6$ from lattice): C 65.04, H 7.42, Er 18.12. Found: C 64.72, H 7.06, Er 17.84. ^{1}H-NMR (400 MHz, C$_6$D$_6$, 25°C): δ = 6.99 (br, 8H, ArH), 5.06 (d, 2H, CH$_2$), 4.31 (d, 2H, CH$_2$), 2.11 (br, 4H, OCH$_2$, thf), 1.34 (s, 12H, CH$_3$), 0.97 (br, 4H, CH$_2$, thf), 0.28 (s, 36H, C(C*H*$_3$)$_3$) ppm. IR (Nujol, cm^{-1}): 2724 s, 2536 w, 2479 w, 2373 w, 2279 w, 2066 m, 1890 m, 1735 s, 1600 s, 1563 m, 1204 w, 1016 m, 922 w, 856 m, 677 m.

4.9: m. p. 230-232 °C. Elemental analysis calcd for C$_{76}$H$_{102}$O$_7$LuLi (1309.53 g.mol^{-1}): C 69.71, H 7.85, Lu 13.36. Calcd for C$_{58}$H$_{84}$O$_7$LuLi (1075.19 g.mol^{-1}): C 64.79, H 7.87, Lu

16.27. Found: C 64.28, H 7.35, Lu 15.89. ^{1}H-NMR (400 MHz, C$_6$D$_6$, 25°C): δ = 6.98 (br, 8H, ArH), 4.49 (d, 2H, CH$_2$), 3.59 (d, 2H, CH$_2$), 2.96 (br, 12H, OCH$_2$, thf), 2.08 (s, 12H, CH$_3$), 0.42 (s, 36H, C(CH$_3$)$_3$), 0.87 (br, 12H, CH$_2$, thf) ppm. IR (Nujol, cm^{-1}): 2725 w, 2385 w, 2271 m, 1895 w, 1748 s, 1605 s, 1462 s, 1376 s, 1258 m, 1025 m, 861 w, 800 m, 722 m, 673 m.

[K(thf)$_3$Gd(BPO$_2$)$_2$(thf)$_2$].2thf (4.10)

The synthesis of complex **4.10** was carried out similarly to that described for complexes **4.1-4.4**, but (0.50 M, 1.00 mmol, 0.50 ml) KN(SiMe$_3$)$_2$ (potassium bis(trimethylsilyl)amide) was used instead of ^{n}BuLi. Crystallisation was achieved by concentrated the pale green solution under vacuum to (~5 ml). Small colourless crystals of **4.10** (0.65 g, 47 %) grew upon standing overnight.

4.10: m. p. 268-270 °C. Elemental analysis calcd for C$_{74}$H$_{116}$O$_{11}$GdK (1378.05 g.mol^{-1}): C 64.50, H 8.48, Gd 11.41. Calcd for C$_{66}$H$_{100}$O$_9$GdK (1233.84 g.mol^{-1} after lost of two thf of solvation): C 64.25, H 8.17, Gd 12.74. Found: C 63.79, H 7.82, Gd 12.36. IR (Nujol, cm^{-1}): 2549 m, 2410 w, 2369 w, 2283 w, 2079 m, 1891 m, 1744 s, 1609 s, 1560 m, 1233 m, 959 w, 681 s, 583 m.

[La(BPO$_2$)(thf)$_5$][AlMe$_2$(BPO$_2$)].thf (4.11), [(BPO$_2$)Ln(thf)$_3$(μ−F)AlMe(BPO$_2$)].thf (Ln = Sm 4.12, Tb 4.13), [AlMe$_2$Ln(BPO$_2$)$_2$(thf)$_2$].2C$_6$D$_6$ (Ln = Y 4.14, Pr 4.15, Sm 4.16, Tb 4.17)

The synthesis of complexes **4.11-4.17** were carried as per those described for complexes **4.1-4.4**, but (2.00 M, 1.00 mmol, 0.50 ml) AlMe$_3$ (trimethyl aluminium) was used instead of ^{n}BuLi. Crystallisation was achieved by concentrated the resulting solutions under vacuum to (~5 ml). Small colourless crystals of **4.11-4.13** (0.38 g, 27 %; 0.41 g, 30 %; 0.34 g, 25 % respectively) grew upon standing overnight. While very small colourless crystals of **4.14-4.17** unsuitable for X-ray analysis which were dried under vacuum and

recrystallisation from benzene (0.45 g, 33 %; 0.32 g, 23 %, 0.45 g, 33 %; 0.53 g, 38 % respectively).

4.11: m. p. 180-182 °C. Elemental analysis calcd for $C_{72}H_{114}O_{10}LaAl$ (1305.56 g.mol^{-1}): C 66.24, H 8.80, La 10.64. Calcd for $C_{60}H_{90}O_{7}LaAl$ (1089.24 g.mol^{-1} after lost three solvation thf): C 66.16, H 8.33, La 12.75. Found: C 66.04, H 8.21, La 12.34. ^{1}H-NMR (400 MHz, C_6D_6, 25°C): δ = 6.78 (br, 8H, ArH), 5.32 (s, 4H, CH_2), 3.34 (br, 12H, OCH_2, thf), 2.25 (s, 12H, CH_3), 1.36 (s, 36H, C(CH_3)$_3$), 0.12 (br, 12H, CH_2, thf), 0.26 (s, 6H, Al-CH_3) ppm. IR (Nujol, cm^{-1}): 2373 w, 2283 w, 2030 w, 1891 m, 1744 s, 1605 s, 1239 w, 1021 m, 865 m, 665 m.

4.12: m. p. 168-170 °C. Elemental analysis calcd for $C_{63}H_{95}O_{8}FSmAl$ (1176.76 g.mol^{-1}): C 64.30, H 8.14, Sm 12.78. Calcd for $C_{59}H_{87}O_{7}FSmAl$ (1104.66 g.mol^{-1}): C 64.15, H 7.94, Sm 13.61. Found: C 63.95, H 7.82, Sm 13.40. IR (Nujol, cm^{-1}): 2725 w, 2377 w, 2283 w, 2210 w, 2030 m, 1969 m, 1891 m, 1748 s, 1605 s, 1564 m, 1262 w, 1017 m, 796 m, 718 w, 669 w.

4.13: m. p. 158-160 °C; Elemental analysis calcd for $C_{63}H_{95}O_{8}FTbAl$ (1185.33 g.mol^{-1}): C 63.84, H 8.08, Tb 13.41. Calcd for $C_{55}H_{79}O_{6}FTbAl$ (1041.12 g.mol^{-1} after lost of two thf of solvation): C 63.45, H 7.65, Tb 15.26. Found: C 63.11, H 7.48, Tb 15.08. ^{1}H-NMR (400 MHz, C_6D_6, 25°C): δ = 7.08 (br, 8H, ArH), 5.70 (s, 4H, CH_2), 3.70 (br, 8H, OCH_2, thf), 2.13 (s, 12H, CH_3), 1.48 (s, 36H, C(CH_3)$_3$), 0.27 (br, 8H, CH_2, thf), -0.37 (s, 3H, Al-CH_3) ppm. IR (Nujol, cm^{-1}): 2733 w, 2586 w, 2377 s, 2218 m, 2153 w, 2059 m, 1895 s, 1744 s, 1634 m, 1576 m, 1258 w, 1008 w, 800 m, 722 m, 518 m.

4.14: m.p. 160-162 °C. Elemental analysis calcd for $C_{68}H_{94}O_{6}YAl$ (1123.36 g.mol^{-1}): C 72.70, H 8.43, Y 7.91. Calcd for $C_{56}H_{82}O_{6}YAl$ (967.13 g.mol^{-1} after lost of two molecules of C_6D_6 in the lattice): C 69.55, H 8.55, Y 9.19. Found: C 69.22, H 8.33, Y 9.03. IR (Nujol,

cm^{-1}): 2725 w, 2369 w, 2214 w, 1891 m, 1740 s, 1605 s, 1258 w, 1012 w, 800 w, 722 m, 669 m, 587 m, 518 m.

4.15: m. p. 130-132 °C. Elemental analysis calcd for $C_{68}H_{94}O_6PrAl$ (1175.36 g.mol^{-1}): C 69.49, H 8.06, Pr 11.99. Calcd for $C_{56}H_{82}O_6PrAl$ (1019.14 g.mol^{-1} after lost of the two C_6D_6 molecules in the lattice): C 66.00, H 8.11, Pr 13.83. Found: C 59.48, H 7.82, Pr 13.51. IR (Nujol, cm^{-1}): 2381 s, 2271 s, 2083 w, 2034 m, 1895 m, 1752 s, 1703 s, 1609 s, 1376 w, 1250 m, 1102 m, 1021 s, 967 w, 865 m, 788 s, 718 m, 692 s.

4.16: m. p. 130-132 °C. Elemental analysis calcd for $[AlMe_2Sm(BPO_2)_2(thf)_2].2C_6D_6$, thf, $C_{72}H_{102}O_7SmAl$ (1256.92 g.mol^{-1}): C 68.80, H 8.18, Sm 11.96. Calcd for $[AlMe_2Ln(BPO_2)_2(thf)_2].1/2(C_6D_6)$, $C_{59}H_{88}O_6SmAl$ (1070.67 g.mol^{-1} after lost one and half molecules of C_6D_6 and one thf in the lattice): C 66.19, H 8.28, Sm 14.04. Found: C 66.04, H 8.13, Sm 13.82. IR (Nujol, cm^{-1}): 2381 s, 2271 s, 2083 w, 2034 m, 1895 m, 1752 s, 1703 s, 1609 s, 1376 w, 1250 m, 1102 m, 1021 s, 967 w, 865 m, 788 s, 718 m, 692 s.

4.17: m. p. 175-177 °C. Elemental analysis calcd for $C_{68}H_{94}O_6TbAl$ (1193.38 g.mol^{-1}): C 68.44, H 7.94, Tb 13.32. Calcd for $C_{56}H_{82}O_6TbAl$ (1037.15 g.mol^{-1} after lost two molecules of C_6D_6 in the lattice): C 64.85, H 7.97, Tb 15.32. Found: C 64.57, H 7.63, Tb 15.08. ^{1}H-NMR (400 MHz, C_6D_6, 25°C): δ = 7.04 (br, 8H, ArH), 3.44 (br, 8H, OCH$_2$, thf), 2.17 (s, 12H, CH$_3$), 1.49 (s, 36H, C(C*H*$_3$)$_3$), 0.85 (s, 8H, CH$_2$, thf), 0.19 (s, 4H, CH$_2$), -0.38 (s, 6H, Al-CH$_3$) ppm. IR (Nujol, cm^{-1}): 2385 w, 2297 s, 1744 s, 1454 s, 1372 s, 1278 s, 1196 s, 1029 m, 996 s, 914 m, 895 s, 800 m.

[Al$_2$(BPO$_2$)$_3$(thf)$_2$].thf (4.18)

Following same stoichiometry that described for the synthesis of complexes **4.11**-**4.15** an attempt to synthesise [AlMe$_2$Yb(BPO$_2$)$_2$(thf)$_n$] led to isolation of [Al$_2$(BPO$_2$)$_3$(thf)$_2$] from

the mother liquor. Large colourless crystals of **4.18** which were suitable for X-ray (0.56 g, 15 %) grew upon standing for two days.

4.18: m. p. 132-134 °C. Elemental analysis calcd for $C_{81}H_{114}O_9Al_2$ (1285.73 g.mol^{-1}): C 75.67, H 8.94. Calcd for $C_{77}H_{106}O_8Al_2$ (1213.62 g.mol^{-1} after lost of one thf from lattice): C 76.20, H 8.80. Found: C 76.08, H 8.52. ^{1}H-NMR (400 MHz, C_6D_6, 25°C): δ = 7.08 (m, 12H, ArH), 3.90 (s, 6H, CH_2), 2.71 (br, 8H, OCH_2, thf), 1.96 (s, 18H, CH_3), 1.33 (s, 54H, C(CH_3)$_3$), 0.86 (br, 8H, CH_2, thf) ppm. IR (Nujol, cm^{-1}): 2725 m, 2377 w, 2148 w, 1932 w, 1748 s, 1638 m, 1605 m, 1204 m, 1147 s, 1047 s, 1014 m, 992 s, 800 m, 767 m, 722 s, 665 s, 612 m.

[AlMe(BPO$_2$)(thf)].C$_6$D$_6$ (4.19)

Following same stoichiometry that described for synthesise complexes **4.11**-**4.15** an attempt to synthesise [AlMe$_2$Gd(BPO$_2$)$_2$(thf)$_n$] led to isolate a large colourless crystals of [AlMe(BPO$_2$)(thf)] (0.30 g, 22 %) grew upon standing overnight after recrystallised from benzene.

4.19: m. p. 130-132 °C. Elemental analysis calcd for $C_{34}H_{47}O_3Al$ (530.72 g.mol^{-1}): C 76.95, H 8.93. Calcd for $C_{28}H_{41}O_3Al$ (452.60 g.mol^{-1} after lost one molecule of C_6D_6 in the lattice): C 74.30, H 9.13. Found: C 74.12, H 8.95. ^{1}H-NMR (400 MHz, C_6D_6, 25°C): δ = 6.98 (br, 4H, ArH), 3.86 (s, br, 4H, OCH_2, thf), 3.15 (s, 2H, CH_2), 2.28 (s, 6H, CH_3), 2.12 (s, 3H, Al–CH_3), 1.60 (s, 18H, C(CH_3)$_3$), 0.75 (br, 4H, CH_2, thf) ppm. IR (Nujol, cm^{-1}): 2377 m, 2214 w, 2054 w, 1940 w, 1854 m, 1744 m, 1638 s, 1462 m, 1255 m, 1074 s, 955 m, 804 w, 722 s.

[Li$_4$(BPO$_2$)$_2$(thf)$_4$].thf (4.20)

Following same stoichiometry that described for synthesise complexes **4.1**-**4.9** an attempt to synthesise [Li(thf)$_n$Gd(BPO$_2$)$_2$(thf)$_n$] led to isolate [Li$_4$(BPO$_2$)$_2$(thf)$_4$]. Complex

$[Li_4(BPO_2)_2(thf)_4]$ (**4.20**) was isolated from the mother liquor instead of the desired complex $[Li(thf)_nGd(BPO_2)_2(thf)_n]$, and grew upon standing for two days as large colourless crystals of **4.20** which were suitable for X-ray (0.25 g, 18 %).

4.20: m. p. 218-220 °C. Elemental analysis calcd for $C_{66}H_{100}O_9Li_4$ (1065.26 g.mol^{-1}): C 74.41, H 9.46. Calcd for $C_{62}H_{92}O_8Li_4$ (993.15 g.mol^{-1} after lost of one thf of solvation): C 74.98, H 9.34. Found: C 74.64, H 9.18. ^{1}H-NMR (400 MHz, C_6D_6, 25°C): δ = 6.88 (br, 8H, ArH), 3.96 (s, 4H, CH_2), 2.95 (br, 16H, OCH_2, thf), 2.06 (s, 12H, CH_3), 1.33 (s, 36H, $C(CH_3)_3$), 0.94 (br, 16H, CH_2, thf) ppm. IR (Nujol, cm^{-1}): 2496 w, 2369 w, 2279 w, 2071 w, 1920 m, 1748 s, 1380 s, 1230 m, 1147 w, 1041 s, 861 s, 780 s, 726 w.

$[ZnEtYb(BPO_2)_2(thf)].2C_6D_6$ (4.21)

The synthesis of complex **4.21** was carried out in the same way as that described for complexes **4.1-4.4**, but (1.00 M, 1.00 mmol, 0.50 ml) $ZnEt_2$ (diethyl zinc) was used instead of ^{n}BuLi. Crystallisation was achieved by evaporating the resulting solution under vacuum to dryness and then recrystallised from benzene. Small yellow crystals of **4.21** (0.70 g, 51 %) grew upon standing overnight.

4.21: m. p. 138-140 °C. Elemental analysis calcd for $C_{64}H_{85}O_5YbZn$ (1172.79 g.mol^{-1}): C 65.54, H 7.31, Yb 14.75. Calcd for $C_{55}H_{79}O_5YbZn$ (1058.64 g.mol^{-1} after lost one and half molecules of C_6D_6 in the lattice): C 62.40, H 7.52, Yb 16.35. Found: C 62.18, H 7.37, Yb 16.05. IR (Nujol, cm^{-1}): 2553 w, 2434 w, 2377 m, 2267 s, 2132 m, 2034 m, 1748 s, 1605 s, 1376 w, 1208 m, 628 m.

4.6 Crystal and refinement data

Crystalline samples were immersed in Paratone-N oil and mounted on a glass fibre. Data collection was done at 173(2) K using the MX1 beamline at the Australian Synchrotron. Data collection for **4.10**, **4.12** and **4.18**, were done on a Bruker APEX II diffractometer at 298(2) K using graphite-monochromate MoKα radiation, λ = 0.71073 Å. Further details regarding structure solutions and refinements were described in Chapter two (crystal and refinement data section 2.6). Crystal data and refinement parameters are compiled below.

[Li(thf)$_4$][Y(BPO$_2$)$_2$(thf)$_2$].thf (4.1)

$C_{74}H_{116}O_{11}YLi$, M = 1277.55, 0.10 × 0.08 × 0.05 mm^3, triclinic, space group P-1 (No. 2), a = 14.141(3), b = 17.116(3), c = 30.903(6), α = 105.04(3), β = 92.37(3), γ = 90.60(3), V = 7216(3) Å^3, Z = 4, ρ_c = 1.604 g/cm^3, μ = 5.223 mm^{-1}, F_{000} = 3588, λ = 0.71073 Å, T = 173(2) K, $2\theta_{max}$ = 50º, 46574 reflections collected, 23591 unique (R_{int} = 0.035). Final $GooF$ = 1.082, R_1 = 0.093, wR_2 = 0.250, R indices based on 19244 reflections with I > 2σ(I) (refinement on F^2), 1618 parameters, 20 restraints. Lp and absorption corrections applied.

[Li(thf)$_4$][Sm(BPO$_2$)$_2$(thf)$_2$].thf (4.2)

$C_{74}H_{116}O_{11}SmLi$, M = 1339.01, 0.12 × 0.04 × 0.09 mm^3, monoclinic, space group $P2_1$ (No. 4), a = 12.984(3), b = 37.320(8), c = 15.010(3), α = γ = 90, β = 106.79(3), V = 6963(3) Å^3, Z = 4, ρ_c = 1.891 g/cm^3, μ = 4.431 mm^{-1}, F_{000} = 3885, λ = 0.71073 Å, T = 173(2) K, $2\theta_{max}$ = 55º, 92998 reflections collected, 32648 unique (R_{int} = 0.046). Final $GooF$ = 0.998, R_1 = 0.034, wR_2 = 0.094, R indices based on 31020 reflections with I > 2σ(I) (refinement on F^2), 1554 parameters, 1 restraint. Lp and absorption corrections applied.

[Li(thf)₄][Dy(BPO₂)₂(thf)₂].thf (4.3)

$C_{74}H_{116}O_{11}DyLi$, $M = 1351.15$, $0.20 \times 0.05 \times 0.06$ mm³, monoclinic, space group $P2_1$ (No. 4), $a = 12.993(3)$, $b = 37.364(8)$, $c = 14.907(3)$, $\alpha = \gamma = 90$, $\beta = 106.44(3)$, $V = 6941(3)$ Å³, $Z = 4$, $\rho_c = 3.034$ g/cm³, $\mu = 7.334$ mm⁻¹, $F_{000} = 6183$, $\lambda = 0.71073$ Å, $T = 173(2)$ K, $2\theta_{max} = 55^\circ$, 110447 reflections collected, 31072 unique ($R_{int} = 0.030$). Final $GooF = 1.181$, $R_1 = 0.036$, $wR_2 = 0.128$, R indices based on 28850 reflections with $I > 2\sigma(I)$ (refinement on F^2), 1554 parameters, 1 restraint. Lp and absorption corrections applied.

[Li(thf)₄][Ho(BPO₂)₂(thf)₂].thf (4.4)

$C_{74}H_{116}O_{11}HoLi$, $M = 1353.58$, $0.09 \times 0.08 \times 0.15$ mm³, monoclinic, space group $P2_1$ (No. 4), $a = 12.997(3)$, $b = 37.232(7)$, $c = 14.912(3)$, $\alpha = \gamma = 90$, $\beta = 106.40(3)$, $V = 6922(3)$ Å³, $Z = 4$, $\rho_c = 1.981$ g/cm³, $\mu = 6.828$ mm⁻¹, $F_{000} = 3984$, $\lambda = 0.71073$ Å, $T = 173(2)$ K, $2\theta_{max} = 55^\circ$, 86174 reflections collected, 32278 unique ($R_{int} = 0.053$). Final $GooF = 1.037$, $R_1 = 0.037$, $wR_2 = 0.093$, R indices based on 29922 reflections with $I > 2\sigma(I)$ (refinement on F^2), 1549 parameters, 1 restraint. Lp and absorption corrections applied.

[Li(thf)₂La(BPO₂)₂(thf)₂] (4.5)

$C_{62}H_{92}O_{8}LaLi$, $M = 1111.24$, $0.05 \times 0.13 \times 0.09$ mm³, monoclinic, space group Cc (No. 9), $a = 18.153(4)$, $b = 17.589(4)$, $c = 18.005(4)$, $\alpha = \gamma = 90$, $\beta = 98.04(3)$, $V = 5693(2)$ Å³, $Z = 4$, $\rho_c = 2.115$ g/cm3, $\mu = 4.453$ mm⁻¹, $F_{000} = 3552$, $\lambda = 0.71073$ Å, $T = 173(2)$ K, $2\theta_{max} = 55^\circ$, 31367 reflections collected, 12776 unique ($R_{int} = 0.029$). Final $GooF = 0.932$, $R_1 = 0.026$, $wR_2 = 0.073$, R indices based on 12612 reflections with $I > 2\sigma(I)$ (refinement on F^2), 665 parameters, 2 restraints. Lp and absorption corrections applied.

[Li(thf)$_2$Pr(BPO$_2$)$_2$(thf)$_2$] (4.6)

C$_{62}$H$_{92}$O$_8$PrLi, M = 1113.24, 0.14 × 0.09 × 0.07 mm^3, monoclinic, space group Cc (No. 9), a = 18.145(4), b = 17. 484(4), c = 18.003(4), $\alpha = \gamma = 90$, $\beta = 97.45(3)$, V = 5663(2) Å^3, Z = 4, ρ_c = 2.140 g/cm^3, μ = 5.112 mm^{-1}, F_{000} = 3600, λ = 0.71073 Å, T = 173(2) K, $2\theta_{max}$ = 55°, 38831 reflections collected, 13383 unique (R_{int} = 0.044). Final $GooF$ = 1.114, R_1 = 0.054, wR_2 = 0.134, R indices based on 12879 reflections with I > 2σ(I) (refinement on F^2), 665 parameters, 2 restraints. Lp and absorption corrections applied.

[Li(thf)$_2$Er(BPO$_2$)$_2$(thf)].2C$_6$D$_6$ (4.7)

C$_{70}$H$_{96}$O$_7$ErLi, M = 1223.71, 0.12 × 0.11 × 0.05 mm^3, triclinic, space group P-1 (No. 2), a = 13.704(3), b = 15.874(3), c = 16.614(3), α = 71.89(3), β = 76.93(3), γ = 69.80(3), V = 3195 Å^3, Z = 2, ρ_c = 2.061 g/cm^3, μ = 7.835 mm^{-1}, F_{000} = 1908, λ = 0.71073 Å, T = 173(2) K, $2\theta_{max}$ = 55°, 43476 reflections collected, 13552 unique (R_{int} = 0.032). Final $GooF$ = 1.035, R_1 = 0.029, wR_2 = 0.081, R indices based on 13308 reflections with I > 2σ(I) (refinement on F^2), 728 parameters, 0 restraints. Lp and absorption corrections applied.

[Li(thf)$_2$Yb(BPO$_2$)$_2$(thf)].Hexane (4.8)

C$_{63}$H$_{96}$O$_7$YbLi, M = 1145.67, 0.16 × 0.08 × 0.13 mm^3, monoclinic, space group Pn (No. 7), a = 13.951(3), b = 30.577(6), c = 14.784(3), $\alpha = \gamma = 90$, $\beta = 101.09(3)$, V = 6189(2) Å^3, Z = 4, ρ_c = 2.079 g/cm^3, μ = 8.281 mm^{-1}, F_{000} = 3718, λ = 0.71073 Å, T = 173(2) K, $2\theta_{max}$ = 55°, 103588 reflections collected, 29272 unique (R_{int} = 0.043). Final $GooF$ = 1.059, R_1 = 0.033, wR_2 = 0.087, R indices based on 24931 reflections with I > 2σ(I) (refinement on F^2), 1351 parameters, 2 restraints. Lp and absorption corrections applied.

[Li(thf)$_2$Lu(BPO$_2$)(thf)].3C$_6$D$_6$ (4.9)

C$_{76}$H$_{102}$O$_7$LuLi, M = 1309.53, 0.04 × 0.06 × 0.12 mm^3, triclinic, space group P-1 (No. 2), a = 12.698(3), b = 14.857(3), c = 19.178(4), α = 79.95(3), β = 81.34(3), γ = 80.65(3), V = 3487(13) Å^3, Z = 2, ρ_c = 2.024 g/cm^3, μ = 8.463 mm^{-1}, F_{000} = 2040, λ = 0.71073 Å, T = 173(2) K, $2\theta_{max}$ = 55°, 56817 reflections collected, 14861 unique (R_{int} = 0.025). Final $GooF$ = 0.929, R_1 = 0.032, wR_2 = 0.086, R indices based on 14247 reflections with I > 2σ(I) (refinement on F^2), 782 parameters, 0 restraints. Lp and absorption corrections applied.

[K(thf)$_3$Gd(BPO$_2$)$_2$(thf)$_2$].2thf (4.10)

C$_{74}$H$_{116}$O$_{11}$GdK, M = 1378.05, 0.16 × 0.12 × 0.14 mm^3, monoclinic, space group $P2_1/c$ (No. 14), a = 15.065(5), b = 17.317(6), c = 28.544(9), α = γ = 90, β = 95.08(2), V = 7417(4) Å^3, Z = 4, ρ_c = 1.101 g/cm^3, μ = 0.997 mm^{-1}, F_{000} = 2396, λ = 0.71073 Å, T = 298(2) K, $2\theta_{max}$ = 54°, 123821 reflections collected, 17026 unique (R_{int} = 0.109). Final $GooF$ = 1.103, R_1 = 0.065, wR_2 = 0.183, R indices based on 9724 reflections with I > 2σ(I) (refinement on F^2), 739 parameters, 15 restraints. Lp and absorption corrections applied.

[La(BPO$_2$)(thf)$_5$][AlMe$_2$(BPO$_2$)].thf (4.11)

C$_{72}$H$_{114}$O$_{10}$LaAl, M = 1305.56, 0.06 × 0.21 × 0.04 mm^3, monoclinic, space group $C2/c$ (No. 15), a = 17.306(4), b = 20.132(4), c = 39.877(8), α = γ = 90, β = 94.87(3), V = 13843(5) Å^3, Z = 8, ρ_c = 1.853 g/cm^3, μ = 3.155 mm^{-1}, F_{000} = 7600, λ = 0.71073 Å, T = 173(2) K, $2\theta_{max}$ = 55°, 88149 reflections collected, 16560 unique (R_{int} = 0.035). Final $GooF$ = 1.388, R_1 = 0.042, wR_2 = 0.159, R indices based on 15062 reflections with I > 2σ(I) (refinement on F^2), 775 parameters, 0 restraints. Lp and absorption corrections applied.

[(BPO₂)Sm(thf)₃(μ–F)AlMe(BPO₂)].thf (4.12)

$C_{63}H_{95}O_8FSmAl$, M = 1176.76, 0.33 × 0.17 × 0.09 mm³, monoclinic, space group $P2_1/c$ (No. 14), a = 30.493(6), b = 14.633(3), c = 27.807(6), $\alpha = \gamma$ = 90, β = 90.30(3), V = 12407(4) Å³, Z = 8, ρ_c = 1.965 g/cm³, μ = 5.017 mm⁻¹, F_{000} = 7182, λ = 0.71073 Å, T = 173(2) K, $2\theta_{max}$ = 50º, 122736 reflections collected, 21604 unique (R_{int} = 0.045). Final $GooF$ = 1.206, R_1 = 0.082, wR_2 = 0.181, R indices based on 19747 reflections with I > 2σ(I) (refinement on F^2), 1369 parameters, 0 restraints. Lp and absorption corrections applied.

[(BPO₂)Tb(thf)₃(μ–F)AlMe(BPO₂)].thf (4.13)

$C_{63}H_{95}O_8FTbAl$, M = 1185.33, 0.05 × 0.26 × 0.14 mm³, monoclinic, space group $P2_1/c$ (No. 14), a = 14.585(3), b = 27.725(6), c = 30.613(6), $\alpha = \beta = \gamma$ = 90, V = 12379(4) Å³, Z = 8, ρ_c = 1.268 g/cm³, μ = 1.208 mm⁻¹, F_{000} = 4992, λ = 0.71073 Å, T = 173(2) K, $2\theta_{max}$ = 50º, 78907 reflections collected, 20549 unique (R_{int} = 0.059). Final $GooF$ = 1.052, R_1 = 0.056, wR_2 = 0.148, R indices based on 16545 reflections with I > 2σ(I) (refinement on F^2), 1369 parameters, 0 restraint. Lp and absorption corrections applied.

[AlMe₂Y(BPO₂)₂(thf)₂].2C₆D₆ (4.14)

$C_{68}H_{94}O_6YAl$, M = 1123.36, 0.09 × 0.18 × 0.13 mm³, monoclinic, space group $P2_1/n$ (No. 14), a = 9.845(2), b = 19.536(4), c = 32.429(7), $\alpha = \gamma$ = 90, β = 94.32(3), V = 6219(2) Å³, Z = 4, ρ_c = 1.200 g/cm³, μ = 1.001 mm⁻¹, F_{000} = 2408, λ = 0.71073 Å, T = 173(2) K, $2\theta_{max}$ = 50º, 76823 reflections collected, 10557 unique (R_{int} = 0.074). Final $GooF$ = 1.065, R_1 = 0.098, wR_2 = 0.259, R indices based on 8678 reflections with I > 2σ(I) (refinement on F^2), 703 parameters, 0 restraints. Lp and absorption corrections applied.

[AlMe₂Pr(BPO₂)₂(thf)₂].2C₆D₆ (4.15)

$C_{68}H_{94}O_6PrAl$, $M = 1175.36$, $0.14 \times 0.09 \times 0.06$ mm³, monoclinic, space group $P2_1/n$ (No. 14), $a = 10.009(10)$, $b = 19.875(2)$, $c = 32.781(3)$, $\alpha = \gamma = 90$, $\beta = 94.66(3)$, $V = 6500(11)$ Å³, $Z = 4$, $\rho_c = 1.201$ g/cm³, $\mu = 0.810$ mm⁻¹, $F_{000} = 2488$, $\lambda = 0.71073$ Å, $T = 298(2)$ K, $2\theta_{max} = 50°$, 54481 reflections collected, 11384 unique ($R_{int} = 0.084$). Final $GooF = 1.108$, $R_1 = 0.066$, $wR_2 = 0.169$, R indices based on 8716 reflections with I > 2σ(I) (refinement on F^2), 703 parameters, 0 restraints. Lp and absorption corrections applied.

[AlMe₂Sm(BPO₂)₂(thf)].2C₆D₆, thf (4.16)

$C_{72}H_{102}O_7SmAl$, $M = 1256.92$, $0.11 \times 0.08 \times 0.17$ mm³, monoclinic, space group $P2_1/n$ (No. 14), $a = 9.860(2)$, $b = 19.597(4)$, $c = 32.532(7)$, $\alpha = \gamma = 90$, $\beta = 94.70(3)$, $V = 6265(2)$ Å³, $Z = 4$, $\rho_c = 1.946$ g/cm³, $\mu = 4.968$ mm⁻¹, $F_{000} = 3591$, $\lambda = 0.71073$ Å, $T = 173(2)$ K, $2\theta_{max} = 50°$, 47064 reflections collected, 10455 unique ($R_{int} = 0.046$). Final $GooF = 1.085$, $R_1 = 0.052$, $wR_2 = 0.145$, R indices based on 9976 reflections with I > 2σ(I) (refinement on F^2), 703 parameters, 0 restraints. Lp and absorption corrections applied.

[AlMe₂Tb(BPO₂)₂(thf)₂].2C₆D₆ (4.17)

$C_{68}H_{94}O_6TbAl$, $M = 1193.38$, $0.24 \times 0.16 \times 0.05$ mm³, monoclinic, space group $P2_1/n$ (No. 14), $a = 10.004(10)$, $b = 19.930(2)$, $c = 32.763(3)$, $\alpha = \gamma = 90$, $\beta = 94.62(6)$, $V = 6511(11)$ Å³, $Z = 4$, $\rho_c = 1.217$ g/cm³, $\mu = 1.147$ mm⁻¹, $F_{000} = 2512$, $\lambda = 0.71073$ Å, $T = 298(2)$ K, $2\theta_{max} = 54°$, 81485 reflections collected, 14924 unique ($R_{int} = 0.281$). Final $GooF = 0.941$, $R_1 = 0.080$, $wR_2 = 0.185$, R indices based on 5567 reflections with I > 2σ(I) (refinement on F^2), 703 parameters, 0 restraints. Lp and absorption corrections applied.

[Al$_2$(BPO$_2$)$_3$(thf)$_2$].thf (4.18)

C$_{81}$H$_{114}$O$_9$Al$_2$, M = 1285.73, 0.08 × 0.12 × 0.19 mm^3, triclinic, space group P-1 (No. 2), a = 14.507(3), b = 17.952(4), c = 33.213(7), α = 104.99(3), β = 90.25(3), γ = 113.80(3), V = 7587(3) Å^3, Z = 8, ρ_c = 2.024 g/cm^3, μ = 6.849 mm^{-1}, F_{000} = 4466, λ = 0.71073 Å, T = 173(2) K, $2\theta_{max}$ = 47º, 64058 reflections collected, 22017 unique (R_{int} = 0.076). Final $GooF$ = 1.066, R_1 = 0.108, wR_2 = 0.307, R indices based on 13452 reflections with I > 2σ(I) (refinement on F^2), 1615 parameters, 0 restraints. Lp and absorption corrections applied.

[AlMe(BPO$_2$)(thf)].C$_6$D$_6$ (4.19)

C$_{34}$H$_{47}$O$_3$Al, M = 530.72, 0.18 × 0.04 × 0.16 mm^3, monoclinic, space group $P2_1$/c (No. 14), a = 25.068(5), b = 15.323(3), c = 16.825(3), α = γ = 90, β = 106.78(3), V = 6188(2) Å^3, Z = 8, ρ_c = 2.009 g/cm^3, μ = 5.675 mm^{-1}, F_{000} = 3633, λ = 0.71073 Å, T = 173(2) K, $2\theta_{max}$ = 55º, 90053 reflections collected, 14713 unique (R_{int} = 0.0438). Final $GooF$ = 0.721, R_1 = 0.054, wR_2 = 0.138, R indices based on 11914 reflections with I > 2σ(I) (refinement on F^2), 703 parameters, 0 restraints. Lp and absorption corrections applied.

[Li$_4$(BPO$_2$)$_2$(thf)$_4$].thf (4.20)

C$_{66}$H$_{100}$O$_9$Li$_4$, M = 1065.26, 0.13 × 0.25 × 0.16 mm^3, trigonal, space group $P3_1$ (No. 144), a = 13.880(18), b = 13.880(18), c = 29.483(5), α = β = 90, γ = 120, V = 4919(16) Å^3, Z = 3, ρ_c = 1.079 g/cm^3, μ = 0.068 mm^{-1}, F_{000} = 1740, λ = 0.71073 Å, T = 298(2) K, $2\theta_{max}$ = 55º, 53607 reflections collected, 14241 unique (R_{int} = 0.135). Final $GooF$ = 0.950, R_1 = 0.069, wR_2 = 0.149, R indices based on 5616 reflections with I > 2σ(I) (refinement on F^2), 728 parameters, 1 restraint. Lp and absorption corrections applied.

[ZnEtYb(BPO₂)₂(thf)].2C₆D₆ (4.21)

$C_{64}H_{85}O_5YbZn$, M = 1172.79, 0.31 × 0.14 × 0.07 mm³, monoclinic, space group Cc (No. 9), a = 22.938(5), b = 13.595(3), c = 19.431(4), α = γ = 90, β = 106.54(3), V = 5809(2) Å³, Z = 4, ρ_c = 1.349 g/cm³, μ = 1.978 mm⁻¹, F_{000} = 2580, λ = 0.71073 Å, T = 173(2) K, $2\theta_{max}$ = 54º, 31504 reflections collected, 9449 unique (R_{int} = 0.0476). Final $GooF$ = 1.089, R_1 = 0.0280, wR_2 = 0.0708, R indices based on 9429 reflections with I > 2σ(I) (refinement on F^2), 560 parameters, 181 restraints. Lp and absorption corrections applied.

4.7 References

[1]. Ling, J.; Shen, Z.; Huang, Q. *Macromolecules.* **2001**, *34*, 7613-7616.

[2]. Shen, Y.; Shen, Z.; Zhang, Y.; Yao, K. *Macromoleccules.* **1996**, *29*, 8289-8295.

[3]. Xu, X.; Ma, M.; Yao, Y.; Zhang, Y.; Shen, Q. *J. Mol. Struct.* **2005**, *743*, 163-168.

[4]. Xu, X.; Hu, M.; Yao, Y.; Qi, R.; Zhang, Y.; Shen, Q. *J. Mol. Struct.* **2007**, *829*, 189-194.

[5]. Tan, Y.; Xu, X.; Guo, K.; Yao, Y.; Zhang, Y.; Shen, Q. *Polyhedron.* **2013**, *61*, 218-224.

[6]. Xu, X.; Qi, R.; Xu, B.; Yao, Y.; Nie, K.; Zhang, Y.; Shen, Q. *Polyhedron*. **2009**, *28*, 574-578.

[7]. Shibasaki, M.; Yoshikawa, N. *Chem. Rev*. **2002**, *102*, 2187-2209.

[8]. Basolo, F.; Pearson, R. G. *Inorganic Reaction Mechanism, A Study of Metal Complexes in Solution*. 2nd ed. John Wiley and Sons: New York, **1968**.

[9]. Gonzalez, M.; Cuenca, T.; Frutos, L. M.; Castano, O.; Herdtweck, E. *Organometallics.* **2003**, *22*, 2694-2704.

[10]. Sernetz, F.; Mulhaupt, R.; Fokken, S.; Okuda, J. *Macromolecules*. **1997**, *30*, 1562-1569.

[11]. Linden, A.; Schaverien, C.; Meijboom, N.; Granter, C.; Orpen, A. *J. Am. Chem. Soc*. **1995**, *117*, 3008-3021.

[12]. Takeuchi, D.; Nakamura, T.; Aida, T. *Macromolecules.* **2000**, *33*, 725-729.

[13]. Okuda, J.; Fokken, S.; Kang, H.; Massa, W. *Chem. Ber*. **1995**, *128*, 221-227.

[14]. Braune, W.; Okuda, J. *Angew. Chem. Int. Ed.* **2003**, *42*, 64-68.

[15]. Chen, H.; Ko, B.; Huang, B.; Lin, C. *Organometallics.* **2001**, *20*, 5076-5083.

[16]. Liu, Y.; Ko, B.; Lin, C. *Macromolecules.* **2001**, *34*, 6196-6201.

[17]. Ko, B.; Wu, C.; Lin, C. *Organometallics.* **2000**, *19*, 1864-1869.

[18]. Amgoune, A.; Thomas, C. M.; Roisnel, T.; Carpentier, J. *Chem. Eur. J.* **2006**, *12*, 169-179.

[19]. Liu, X.; Shang, X.; Tang, T.; Hu, N.; Pei, F.; Cui, D.; Chen, X.; Jing, X. *Organometallics.* **2007**, *26*, 2747-2757.

[20]. Nie, K.; Gu, X.; Yao, Y.; Zhang, Y.; Shen, Q. *Dalton Trans.* **2010**, *39*, 6832-6840.

[21]. Schaverien, C. J.; Meijboom, N.; Orpen, A. G. *J. Chem. Soc. Chem. Commun.* **1992**, 124-126.

[22]. Gribkov, D. V.; Hultzsch, K. C.; Hampel, F. *Chem. Eur. J.* **2003**, *9*, 4796-4810.

[23]. Arnold, P. L.; Natrajan, L. S.; Hall, J. J.; Bird, S. J.; Wilson, C. *J. Organomet. Chem.* **2002**, *647*, 205-215.

[24]. Skinner, M. E.; Tyrell, B. R.; Ward, B. D.; Mountford, P. *J. Organomet. Chem.* **2002**, *647*, 145-150.

[25]. Xu, X.; Zhang, Z.; Yao, Y.; Zhang, Y.; Shen, Q. *Inorg. Chem.* **2007**, *46*, 9379-9388.

[26]. Mahoney, B. D.; Piro, N. A.; Carroll, P. J.; Schelter, E. J. *Inorg. Chem.* **2013**, *52*, 5970-5977.

[27]. Qi, R.; Liu, B.; Xu, X.; Yang, Z.; Yao, Y.; Zhang, Y.; Shen, Q. *Dalton Trans.* **2008**, 5016-5024.

[28]. Liang, Z.; Ni, X.; Li, X.; Shen, Z. *Inorg. Chem. Commun.* **2011**, *14*, 1948-1951.

[29]. Korobkov, I.; Gambarotta, S. *Organometallics.* **2009**, *28*, 4009-4019.

[30]. Wu, G.; Liu, J.; Sun, W.; Shen, Z.; Ni, X. *Polym. Int.* **2010**, *59*, 431-436.

[31]. Xu, X.; Ma, M.; Yao, Y.; Zhang, Y.; Shen, Q. *Eur. J. Inorg. Chem.* **2005**, 676-684.

[32]. Fang, Y.; Ming, W.; Jing, H.; Lin, S.; Quan, S. *Sci. China Ser. B-Chem.* **2009**, *52*, 1711-1714.

[33]. Xu, B.; Huang, L.; Yang, Z.; Yao, Y.; Zhang, Y.; Shen, Q. *Organometallics.* **2011**, *30*, 3588-3595.

[34]. Fang, L.; Yao, Y.; Zhang, Y.; Shen, Q.; Wang, Y. *Z. Anorg. Allg. Chem*. **2013**, *639*, 2324-2330.

[35]. Zhang, D. *Eur. J. Inorg. Chem*. **2007**, 3077-3082.

[36]. Lin, C.; Yan, L.; Wang, F.; Sun, Y.; Lin, C. *J. Organomet. Chem*. **1999**, *587*, 151-159.

[37]. Ko, B.; Chao, Y.; Lin, C. *Inorg. Chem.* **2000**, *39*, 1436-1469.

[38]. Liao, T.; Huang, Y.; Huang, B.; Lin C. *Macromol. Chem. Phys*. **2003**, *204*, 885-892.

[39]. Huang, B.; Ko, B.; Athar, T.; Lin, C. *Inorg. Chem.* **2006**, *45*, 7348-7356.

[40]. Ko, B.; Lin, C. *J. Am. Chem. Soc.* **2001**, *123,* 7973-7977.

[41]. Dietrich, H.; Mahdi, W.; Knorr, R. *J. Am. Chem. Soc.* **1986**, *108*, 2462-2464.

[42]. Hecht, E. *Z. Anorg. Allg. Chem.* **2001**, *627*, 2351-2358.

[43]. Zhang, J.; Wang, C.; Lu, M.; Yao, Y.; Zhang, Y.; Shen, Q. *Polyhedron.* **2011**, *30*, 1876-1883.

[44]. Hsueh, M.; Huang, B.; Wu, J.; Lin, C. *Macromolecules.* **2005**, *38*, 9482-9487.

[45]. Cole, M. L.; Junk, P. C.; Proctor, K. M.; Scottc, J. L.; Strauss, C. R. *Dalton Trans.* **2006**, 3338-3349.

[46]. Descour, C.; Sciarone, T. J.; Cavallo, D.; Macko, T.; Kelchtermans, M.; Korobkove, I.; Duchateau, R. *Polym. Chem.* **2013**, *4*, 4718-4729.

[47]. Edelmann, F. T. Lanthanides and Actinides. *In Synthesis Methods of Organometallic and Inorganic Chemistry*. Herrmann, W. A. Ed. Theime: Stuttgar, **1997**, Vol. 6, 48-51.

[48]. Shsnnon, R. D.; Prewitt, C. T. *Acta. Crystallogr. B.* **1969**, *B25*, 925-946.

[49]. Cole, M. L.; Junk, P. C. *Chem. Commun*. **2005**, 2695-2697.

[50]. Chen, MC.; Roberts, J. A.; Marks, T. J. *J. Am. Chem. Soc.* **2004**, *126,* 4605-4625.

Appendix 1: Copyright permission from Elsevier

Content has been removed

Appendix 2: Copyright permission from Wiley

Content has been removed